A STUDY OF WIDE BANDWIDTH DIRECTIONAL PATTERNS FROM CIRCULAR ARRAYS

by

MARTIN R. JONES

A thesis submitted to the University of London for the Degree of Doctor of Philosophy in Electronic Engineering

Department of Electronic and Electrical Engineering
University College London

APRIL 1990

Abstract

Passive radar warning receivers use amplitude comparison direction-finding to determine the angle of arrival of incoming signals. This type of direction-finding system requires wideband azimuth beams that do not change in shape with frequency. The subject of this thesis is the synthesis of wideband beams using a circular array.

In the first part of this thesis the excitation of the circular array is analysed using the concept of 'phase modes': the orthogonal terms of a spatial Fourier series. If the variations in phase and amplitude of these modes with frequency are corrected, azimuth patterns formed from these modes are instantaneously wideband. Pattern synthesis uses the principle of linear array equivalence, allowing us to apply low sidelobe techniques developed for linear arrays to the phase modes.

The design of the experimental system, operating over the frequency range 8 to 12 GHz, is subsequently presented. The characteristics of the phase modes excited on a four element monopoles array were evaluated, showing that the array could be used to form a low sidelobe beams. The initial beamformer design used a Butler matrix constructed from microwave directional couplers to excite the phase modes. By utilising microstrip compensation networks, the variation in phase and amplitude of these modes with frequency is corrected. Multiple beams are formed from the compensated modes by a second matrix. Both theoretical and measured results showed that the phase and amplitude errors introduced by this complicated network were unacceptable. Multiple beams were not demonstrated in this study. A simplified matrix design was developed to demonstrate a low sidelobe (-28 dB) beam at a single frequency.

A weighted corporate feed was developed to demonstrate instantaneously wideband pattern synthesis of a single beam. The element excitation required to form a low sidelobe pattern was calculated using phase mode theory. The frequency-dependent element excitation was practically realised using the microstrip networks. Anechoic chamber measurements of the synthesised wideband beam showed that the variation in the -3 dB beamwidth across the band 8 to 12 GHz was less than ±3°. The sidelobe level was below -20 dB. Theoretical calculations limit the frequency bandwidth for this synthesis technique to about one octave.

A wideband sin(Nx)/Nsin(x) pattern was also produced to demonstrate the versatility of this synthesis technique.

To my friends

Acknowledgements

My sincere thanks go to Dr H.D. Griffiths for his expert supervision, guidance and advice throughout the course of this work and during the compilation of this thesis.

Thanks are also due to Professor D.E.N. Davies, for his valuable advice and support, and to Mr L.W. Chua, of Racal-Decca Advanced Development, and Dr. K. Milne, for constructive discussions during the course of this project; also to Mr. A.D. Williams, for his technical expertise in the construction of much of the hardware relating to the work. Thanks go to Laura Wiles for proof-reading.

Finally I am especially grateful to Racal-Decca Advanced Development and the Science and Engineering Research Council for providing the necessary financial support, without which the research would not have been possible.

Contents

List of Figures

Chapter 3

Chapter 5

List of Tables

List of Principal Symbols

Symbol	Definition	Units
A_m	Excitation of m^{th} phase mode port	Volts
A'_m	Excitation of m^{th} phase mode port, including beamformer errors	Volts
BW	Beamwidth of radiation pattern	degrees
B_i	Fourier coefficient for element radiation pattern	none
C_m	Radiated amplitude of phase mode = $A_m K_m$	Volts
c	Speed of light in vacuum	ms^{-1}
D	Directivity	ratio
d	Separation of array elements	metres
d_n	Term in Schelkunoff's scalar representation of azimuth pattern	none
E	Efficiency	%
f	Frequency	Hz
$F(\phi,\theta)$	Amplitude of radiation pattern in azimuth direction ϕ, elevation direction θ	Volts
$F^*(\phi,\theta)$	Complex conjugate of $F(\phi,\theta)$	Volts
$G(\psi,\theta)$	Amplitude of radiation pattern for array element in azimuth direction ψ, elevation direction θ	Volts
G_i^E	Power gain of array element, relative to lossless isotropic source	ratio
G_i^m	Power gain of phase mode, relative to lossless isotropic source	ratio
Im	Imaginary part of function	none
I_n	Current exciting n^{th} element of linear array	Ampères
$J_n(x)$	The n^{th} order Bessel function of the first kind	none
K	The wave number, $2\pi/\lambda$	radians m^{-1}
K_m	Complex phase mode coefficient for the m^{th} mode	none

K_{Vm}	Vertically polarised component of the phase mode coefficient	none
K_{Hm}	Horizontally polarised component of the phase mode coefficient	none
l	Transmission line length	metres
L	Linear array length	metres
m	Numbering of phase modes	index term
M	Highest order phase mode	index term
n	Numbering of array elements	index term
N	Total number of array elements	index term
N_T	Total noise output of detector diode	Watts
$P(\phi,\theta)$	Power pattern of antenna on $\log_{10}$ scale	dB
r	Array radius	metres
R	Monopulse DF ratio (section 3.2)	dB
R_{max}	Maximum value of monopulse DF ratio	dB
R_{rad}	Radiation resistance of element	Ω
$\mathcal{R}$	The real part of a function	none
s_{kl}	Scattering parameters for k^{th} and l^{th} ports of electrical network	V/V
SLL	Sidelobe level	dB
S/N	Signal-to-noise power ratio	dB
T_n	n^{th} order Chebyshev polynomial	none
T	Temperature	K
t	Time	s
u	Kd sin(ϕ) azimuth variable	radians
V_g	Waveguide velocity	mS^{-1}
V_n	Excitation of n^{th} circular array element	Volts
$V_m{}^{out}$	Reflection from phase mode impedance mismatch seen at the m^{th} phase mode port	Volts
W_m	Amplitude taper applied to m^{th} phase mode	Volts
w	e^{ju} (see u above)	none
Z	Impedance	Ω
Z^m	Impedance of m^{th} phase mode	Ω
z_{kl}	Open circuit z parameter for k^{th} and l^{th} ports of electrical network	Ω

Z_0	Characteristic impedance of transmission line	Ω
α	Azimuth direction of steered beam	radians or degrees
β	The wave number $2\pi/\lambda$	radians m^{-1}
ΔA	Amplitude error	Volts
ΔP	Phase error	radians
$\zeta(\phi,\theta)$	Array factor	none
θ	Elevation angle	radians
λ	Free space wavelength	metres
λ_g	Wavelength in transmission line	metres
ϕ	Azimuth angle	radians or degrees
ϕ_0	-3 dB beamwidth of beam	radians or degrees
ϕ_s	Angular separation of circular array elements	radians
ψ	Azimuth angle of circular array elements	radians or degrees
φ	Azimuth angle, measured from -3 dB crossover point of overlapping beams	radians or degrees
φ_c	Calculated azimuth angle of incident signal	radians or degrees
ρ	Reflection coefficient	none
ω	Angular frequency	radians/s

Chapter 1

Introduction

1.1 Background

For many years phased array antennas have been used to form radiation patterns, with shapes tailored to fulfil a wide variety of roles. One advantage is that beams from a phased array can be scanned, without having to mechanically move the antenna. Many different physical layouts of the phased array elements have been used, the simplest being the linear array of elements equally spaced along a straight line. At the other end of the scale, the most complex physical layout is that of conformal arrays, where the physical layout fits a curved surface, for example the nose of an aircraft.

Many different beam shapes are required by system designers. For example, radar systems require a single high gain beam with low sidelobes, while monopulse DF (Direction-Finding) systems require a pattern with two main beams and a sharp null in between. For air traffic control a beam without nulls in the elevation plane is required, but it must be shaped so that returns from aircraft at the same horizontal distance are equal in amplitude. A great deal of work has been done on the synthesis of radiation patterns using linear arrays. By referring to standard texts, a system designer is able to determine the excitation of the linear array required to form the desired radiation pattern.

However, a major disadvantage of linear arrays is that they are limited in bandwidth. Few operate over a wide bandwidth because the shape of the synthesised beam changes greatly with frequency. As an example, consider a uniformly excited linear array of N isotropic elements. The radiation pattern formed has a sin(Nx)/Nsin(x) shape. The first sidelobe level (-13.46 dB) is largely independent of frequency, but the -3 dB beamwidth is given approximately by:

$$BW_{-3dB} \approx \frac{\lambda}{(N-1)d} \quad \text{(radians)} \tag{1.1}$$

where d is the inter-element spacing and N is the number of elements. For an octave drop in frequency, the -3 dB beamwidth of the main beam doubles.

Over the past fifteen years research has been carried out at University College London on the subject of circular phased arrays, where the array elements are located on the circumference of a circle, pointing radially outwards. The array excitation may be expressed in terms of a set of orthogonal modes, called phase modes. When a single mode is excited on the circular array, an omnidirectional radiation pattern is formed in the azimuth plane, with a linear phase change as a function of azimuth. For a mode of order m, there are m cycles of phase in one cycle of azimuth.

Davies and Rizk (1978) took advantage of the omnidirectional pattern of phase modes to use them in mobile VHF communications. Receivers in such systems can be susceptible to high powered interfering signals. This problem was overcome in this study by forming nulls in the patterns. The nulls were formed by combining two phase modes so they add destructively in the direction of the interference. This study showed that these nulls could easily be steered around 360° of azimuth using a phase shifter. Methods of varying the null width were investigated and the bandwidth of the nulls formed was measured, indicating a 60% operating bandwidth.

Guy and Davies (1983a) describe a technique for multiplexing radiocommunication antennas by taking advantage of the isolation between phase modes; even though they are omnidirectional, they are essentially orthogonal to each other.

Rahim and Davies (1982) made the important observation that using directional elements in a circular array (rather than omnidirectional elements) improves the potential for wideband performance. If the radiated amplitude of the phase modes (for an array of omnidirectional elements) is plotted as a function of frequency, there are periodic nulls that limit the operating bandwidth. For directional elements these nulls are filled in so the phase modes can be excited over a very wide bandwidth.

Guy and Davies (1983b) analysed the four-element Adcock Direction-Finder in terms of phase modes. They recommended this type of array as the basis for a wideband direction-finding system. Phase comparison DF is done by comparing the phase of a mode that cycles with azimuth to the constant phase (0^{th} order) mode. The DF calculations are complicated by the fact that the relative phases (and amplitudes) of the modes do change gradually with frequency, but this can be corrected using an (electronic) look-up table.

The Ph.D study of Karavassilis (1984) developed an HF direction-finding system based on a circular array using four antennas, each with a cardioid directional beam shape. This gave an operating bandwidth of 1.2 decades. However, there is a major problem with phase comparison DF: it operates on the strongest incident signal, and since the phase modes are omnidirectional, they are easily jammed. As explained earlier, nulls can be formed to eliminate a jammer. Using open loop techniques, however, the nulls were not deep enough and so Karavassilis developed a closed loop 'perturbation technique' that adaptively eliminated the jammer with a deep null.

Cvetkovic et al. (1988) developed the same four-element DF system still further. By combining three phase modes with adaptive control of their phase and amplitude, two jammers could be nulled out. Computer control allowed jammers to be nulled automatically without operator intervention. This DF system, now part of the C & S Antennas product range, is far smaller than most HF direction-finding systems and the latest version is easily portable.

There are many applications where the radiation patterns formed by linear phased arrays could prove useful, were it not for the limited bandwidth. From the phase mode analysis of these studies, the operating bandwidth of circular arrays appears to be much greater. Directional patterns can be formed using phase modes, forming nulls is a simple example of this. The subject of this thesis is the application of the wide operating bandwidth of circular arrays to pattern synthesis.

1.2 Amplitude comparison direction-finding

The most accurate microwave DF systems currently available are phase comparison direction finding systems. A good example is the wideband system described by Rehnmark (1984). This system performs DF from 2 to 18 GHz with an accuracy of 2° RMS. Again this is done by comparing the phases of modes excited on circular arrays.

Phase comparison DF systems are complex and expensive. Most DF systems in use today use amplitude comparison. These employ a set of wideband antennas with beams that overlap. Cavity-backed spiral antennas are commonly used, as shown in figure 1.1. In a simple wideband system, RF detector diodes are connected to the antenna outputs. The coarse angle of arrival is determined by the output giving the strongest signal. The precise angle of arrival is calculated from the ratio of the signal amplitudes received in adjacent antennas. A good example of an amplitude comparison DF system is the AN/SLR-21, used by the United States Navy. This system, described by Moncrief (1978), can perform DF from 2 to 18 GHz with an accuracy of 10° RMS. Amplitude comparison DF

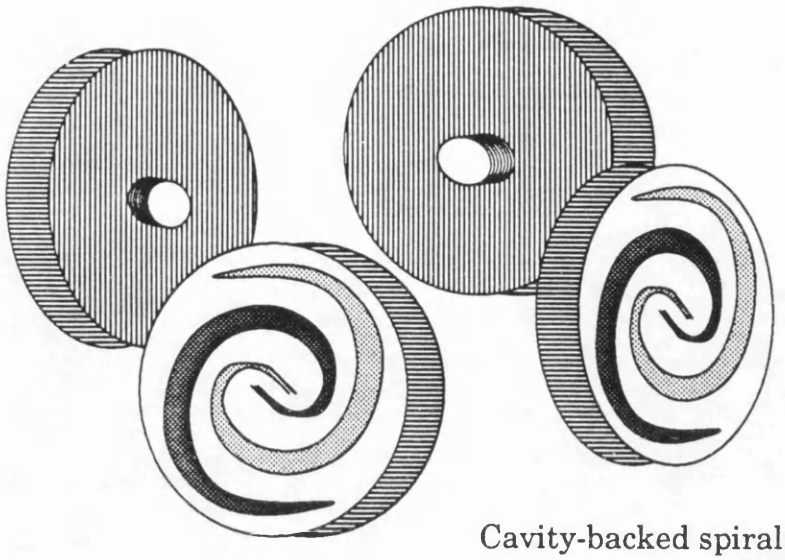

Cavity-backed spirals

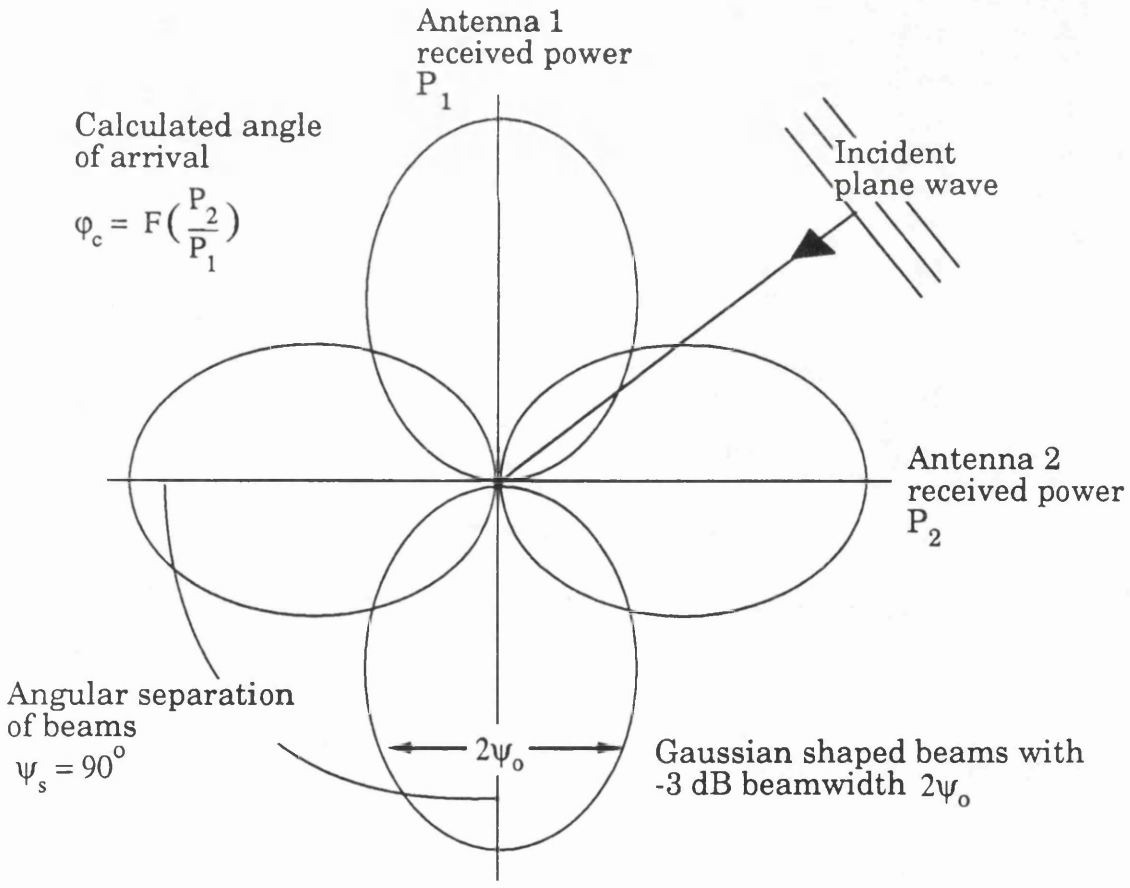

Figure 1.1 Amplitude comparison DF using four wideband antennas for 360° coverage.

is cheaper than phase comparison DF, but less accurate.

For accurate amplitude comparison DF wideband antennas with a beam that does not change shape with frequency are required - changes in the beamwidth produce DF errors. Most existing amplitude comparison DF systems use cavity-backed spiral antennas, chosen for their wide operating bandwidth. These have a -3 dB beamwidth that typically changes by 25% over a decade bandwidth, as described by Lipsky (1987b). Beams with low sidelobes are required, mainly to prevent jammers 'swamping' the DF system: cavity-backed spirals typically have sidelobe levels of the order of -20 dB. The next section shows that the phase mode analysis of circular arrays can provide beams suitable for an amplitude comparison DF rôle, beams that are potentially better than those of cavity-backed spirals.

1.3 Pattern synthesis using circular arrays

As an introduction to pattern synthesis using arrays, let us first consider pattern synthesis with a linear array. For isotropic array elements the radiation pattern is the spatial Fourier transform of the array excitation. This pattern is called the 'array factor' $\zeta(\phi,\theta)$. Practical array elements are not isotropic, but have a directional radiation pattern $G(\phi,\theta)$. For the common case where all the elements are identical and are similarly oriented in space, the far field radiation pattern $F(\phi,\theta)$ is simply the product of the array factor and the element pattern. The array factor for a linear array of N equally spaced isotropic elements in the azimuth plane ($\theta = 0°$) is given by:

$$\zeta(\phi) = \sum_{n=0}^{N-1} \frac{I_n}{I_0} e^{jn\frac{2\pi d}{\lambda}\sin(\phi)} \qquad (1.2)$$

where ϕ is the azimuth angle

d is the inter-element spacing

λ is the wavelength

I_n is the excitation current of the n^{th} element

As an example, the array factor formed by exciting the elements with uniform amplitude and equal phase can be expressed in the form:

$$\zeta(\phi) = \frac{\sin\left(\frac{N\frac{2\pi d}{\lambda}\sin\phi}{2}\right)}{N\sin\left(\frac{\frac{2\pi d}{\lambda}\sin\phi}{2}\right)} \qquad (1.3)$$

To form different beam shapes with linear arrays, theoretical analyses calculate the element currents required to form the desired pattern. Much of the theory centres on the correct positioning of the (N-1) nulls in the radiation pattern. For the pattern of (1.3), the -3 dB beamwidth of this radiation pattern is half the distance between the first nulls. If a reduction in the -3 dB beamwidth is required, the nulls on each side of the main beam should be moved closer together. Sidelobe levels are reduced by clustering nulls closer together, inevitably increasing the beamwidth of the mainlobe. Even null-free radiation patterns may be formed by careful placement of the nulls - in imaginary space.

Let us now consider pattern synthesis with a circular array. The simplest way of exciting phase modes on a circular array is to use an electrical network called a Butler matrix. This network has N outputs (each connected to a circular array element) and N inputs. Exciting one of these inputs with an RF (Radio Frequency) source excites a single phase mode on the circular array. The Butler matrix was originally developed for beamforming with linear arrays. Connecting one to a linear array excites an orthogonal set of beams, but these have a narrowband sin(Nx)/Nsin(x) radiation pattern.

Exciting a single phase mode on a circular array with a Butler matrix forms an omnidirectional radiation pattern, with m cycles of phase change in one cycle of azimuth. This radiation pattern can be expressed in the form:

$$F(\phi) = A_m K_m(f)\, e^{jm\phi} \tag{1.4}$$

A_m is the amplitude of the RF source exciting the m^{th} phase mode port of the Butler matrix. $K_m(f)$ is a dimensionless complex term, called the 'phase mode coefficient'. The coefficient is a function of the mode order m, and generally changes with frequency. The magnitude of this coefficient is determined by factors such as the array radius, the directional pattern of the element and mutual coupling. Suppose N coherent RF sources are used to excite the other phase mode ports of the Butler matrix. The radiation pattern produced by exciting all the phase modes up to the order ±M is the superposition (sum) of the separate patterns:

$$F(\phi) = \sum_{m=-M}^{M} A_m K_m(f) e^{jm\phi} \tag{1.5}$$

As practical circular arrays have a finite number of elements N, only a finite number of phase modes can be excited. The highest order modes that can be excited are the M = +N/2 and M = -N/2 modes. This is a manifestation of the Nyquist sampling theorem. To receive (or excite) a spatially periodic mode of order M, it must be sampled 2M times by the array in one cycle of azimuth, so N = 2M elements are required for the M^{th} mode.

Since the phase mode coefficient (K_m) for each mode changes as a function of frequency, the shape of the beam changes as the source frequency changes. However, if the RF excitation A_m of each of the modes is weighted to correct for the change in the phase mode coefficient with frequency:

$$A_m = \frac{1}{K_m(f)} \tag{1.6}$$

then the radiation pattern of (1.5) can be written:

$$F(\phi) = \sum_{m=-M}^{M} e^{jm\phi}$$

This radiation pattern can be expressed in the form:

$$F(\phi) = \frac{\sin\left(\{2M+1\}\frac{\phi}{2}\right)}{(2M+1)\sin\left(\frac{\phi}{2}\right)} \tag{1.7}$$

This is the same shape as the pattern formed by uniformly exciting an N element linear array (where $d = \lambda/2$), except for a change of scale. While the pattern is formed by a linear array in 180° of sin(ϕ) space, the radiation pattern of a circular array is formed directly in ϕ space.

There is no frequency dependent term in (1.7), unlike the linear array equation of (1.3) where λ is present. The radiation pattern remains the same over the frequency band for which the phase mode excitation meets the requirement of (1.6). Patterns with a perfectly constant -3 dB beamwidth can theoretically be formed with a circular array. This is exactly what is required for an accurate amplitude comparison DF system.

The pattern of (1.7) is formed from 2M + 1 modes and has 2M nulls. All the weighting functions developed for linear arrays can be applied to the placement of these nulls. By applying an amplitude taper to the excitation

of the phase modes, radiation patterns with sidelobes lower than the -20 dB level of cavity- backed spirals can theoretically be formed with a circular array.

For linear arrays, mutual coupling between elements changes the array excitation, often increasing sidelobe levels and generally degrading the shape of the radiation pattern. Well known effects of this include active impedance, where the apparent impedance of an element changes as a function of the beam scan angle, as described by Hansen (1983). Even 'blind spots' can occur, directions in which the beam cannot be formed because the real part of the array impedance drops to zero. Since phase modes are orthogonal terms, these problems do not arise. The excitation of one mode in no way affects the excitation of the other modes. Mutual coupling between circular array elements does, however, modify the impedance of each element. This study investigates the impedance characteristics of modally excited arrays.

Clearly for wideband patterns it is desirable that the phase mode coefficients (the K_ms) do not change with frequency or, if this is unavoidable, that the changes are easy to compensate. This study investigates the circular array structures needed to achieve this. The design of RF networks to compensate for changes in K_m with frequency is also considered.

Very wide bandwidth RF components and measuring equipment are expensive. At UCL, however, microwave components and measurement systems operating in the frequency range 8 to 12 GHz are available, so the study concentrates on this particular frequency range. The potential for wider bandwidth operation is investigated by determining the upper and lower limits on the bandwidth of this synthesis technique.

Practical circular arrays have a finite number of elements. When a single phase mode is excited on such an array, the radiation pattern given by equation (1.4) is not exact. Why is this ? The reason is that as well as the fundamental modes with an order m between -N/2 and +N/2, higher order

harmonics are also excited as well. They manifest themselves as a periodic amplitude ripple superimposed on the azimuth pattern of the fundamental mode. The effect of these spatial harmonic terms on directional radiation patterns is investigated in this study.

Since a fan of overlapping azimuth beams is required for amplitude comparison DF, beamformers that can synthesise multiple beams from circular arrays are investigated. The orthogonal properties of multiple beams formed from phase modes is also studied.

A schematic diagram of the proposed system is shown in figure 1.2. The practical side of the project can be divided into five main areas.

- A circular array that operates over the band 8 to 12 GHz.
- A microwave Butler matrix to form the set of phase modes.
- Microwave frequency compensation networks.
- Weighting networks to apply an amplitude taper.
- A beamformer to synthesise multiple beams from the phase modes.

The proposed beamforming network of figure 1.2 is very complex. It contains a long chain of passive devices, each of which contribute significant errors. Some components have errors in their transmission amplitude and phase. Others are not a perfect match, introducing reflections, and yet the beamformer must operate over a wide bandwidth. The effect of beamformer errors on synthesised beams is evaluated. In this study the design of less complex RF networks to perform wideband pattern synthesis is considered.

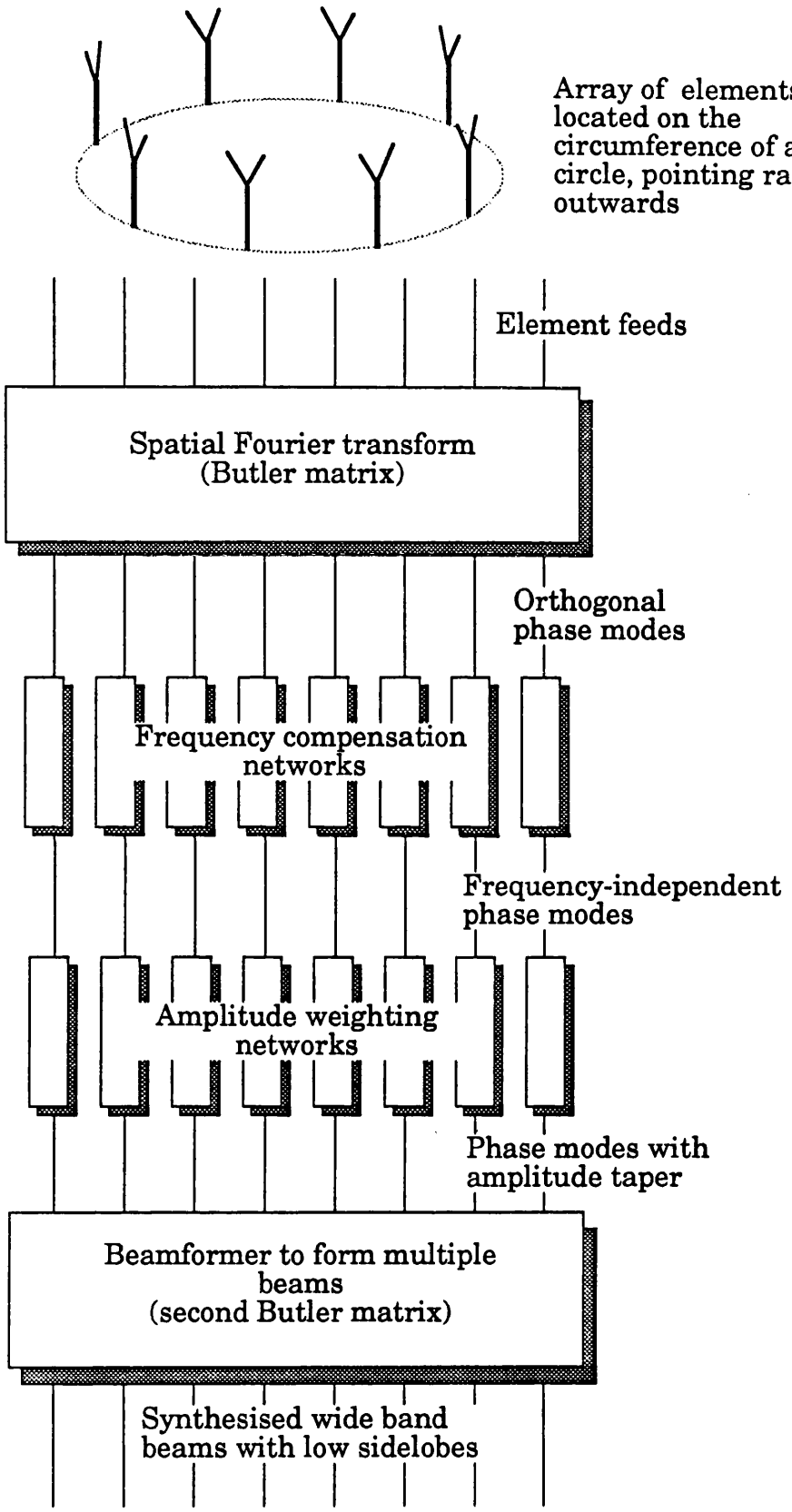

Figure 1.2 Block diagram of the proposed wideband pattern synthesis system.

1.4 Thesis structure

Chapter 2 looks at the theory of pattern synthesis using linear arrays, and considers how this may be applied to the synthesis of wideband radiation patterns using the phase modes of circular arrays.

The results of this study lead to the design, in chapter 3, of a circular array that operates over the frequency range 8 to 12 GHz. The measured phase mode characteristics for a four-element array constructed at UCL are compared to theoretical values.

Chapter 4 investigates the design of the microwave beamforming networks used to form instantaneously wideband beams. The evolution of the beamformer design during the course of this study is described, illustrating a move towards simpler networks which is necessary to realise low sidelobe beams.

The results of measurements on beams synthesised using wideband beamformers are presented in chapter 5. Reducing the sidelobe levels of wideband beams by applying an amplitude taper is demonstrated. The effect of beamformer errors, and changing the elevation angle on the shape of the wideband beam are determined. The results are compared to the theoretical performance.

Chapter 6, the concluding chapter of this thesis summarises the results of this study. This pattern synthesis technique is compared with alternative approaches. Ideas and proposals for future work are presented. The last section draws the conclusions of this study.

Chapter 2

The application of phase mode theory to pattern synthesis

2.1 Pattern synthesis using linear arrays

2.1.1 Introduction

Linear arrays of discrete elements have been used in the synthesis of directional radiation patterns for many years, and the theory behind this has been developed to a high level of sophistication. This review section follows the analysis of Elliott (1981a).

The radiated fields of a discrete linear array are the sum (superposition) of the fields radiated by each element. The field of an element is determined by an excitation parameter, for example the current on a dipole. In the notation used here, the excitation vector is given as an amplitude and phase at each element of the array, with the excitation of one element defined as a phase reference.

For isotropic array elements the radiation pattern is the spatial Fourier transform of the array excitation. This pattern is called the 'array factor' $\zeta(\phi,\theta)$. Most discrete elements have a directional radiation pattern $G(\phi,\theta)$. For the case where all the elements are identical and are similarly oriented in space, the far field radiation pattern $F(\phi,\theta)$ is the product of the array factor and the element pattern:

$$F(\phi,\theta) = \zeta(\phi,\theta)\, G(\phi,\theta)$$

In this section, the radiation pattern of a linear array of isotropic elements is considered.

Most feeds produce a 'free excitation' of the linear array, where the drive voltages are fixed and the excitation currents are determined by the element self and mutual impedances. In this case the element has an 'active' impedance. For example, the element impedance changes with angle as a synthesised beam is scanned. In this section only a 'forced' excitation of a linear array is considered, where the drive voltages are individually adjusted so that each excitation current is exactly the value required. As we shall see later on in this chapter, the concept of a forced excitation is applicable to pattern synthesis using circular arrays.

2.1.2 The radiation pattern of a linear array

Figure 2.1 shows the array factor for a five element array. The array factor for a linear array of N equally spaced isotropic elements is given by:

$$\zeta(\phi) = \sum_{n=0}^{N-1} \frac{I_n}{I_0} e^{jnKd \sin(\phi)} \qquad (2.1.1)$$

where ϕ is the azimuth angle

d is the inter-element spacing

$K = 2\pi/\lambda$

I_n is the excitation current of the n^{th} element

For a linear array, peak directivity of the main beam is obtained by exciting the array elements with uniform amplitude and equal phase. The array factor is then:

$$\zeta(\phi) = \sum_{n=0}^{N-1} e^{jnKd \sin(\phi)} \qquad (2.1.2)$$

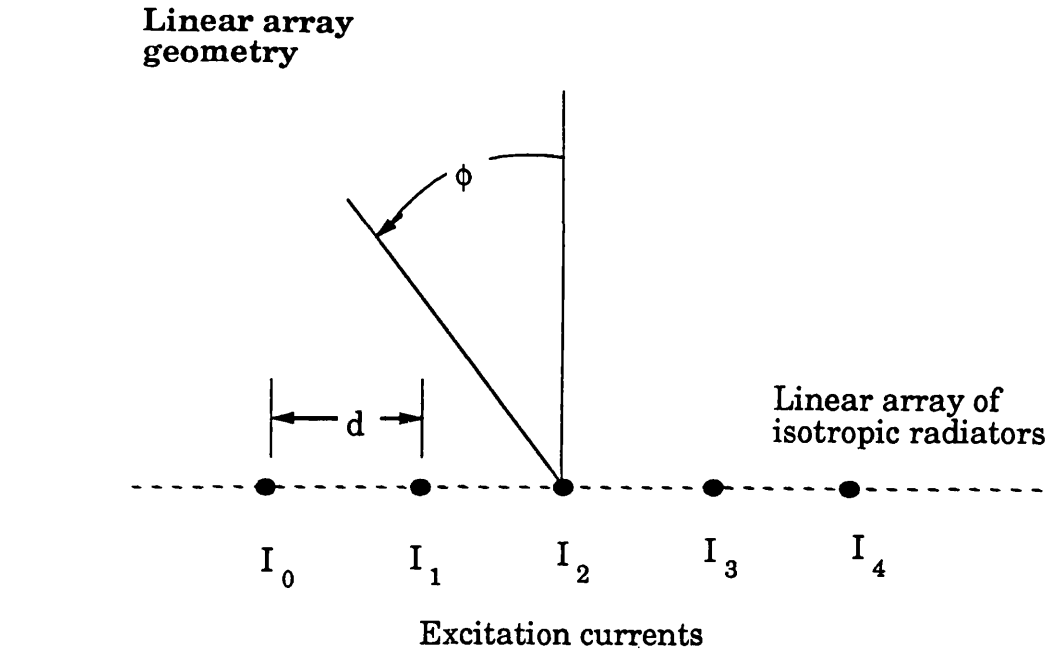

Uniform excitation

Sin(Nx)/Nsin(x) beam formed by the uniform excitation of a five-element linear array (d = λ/2)

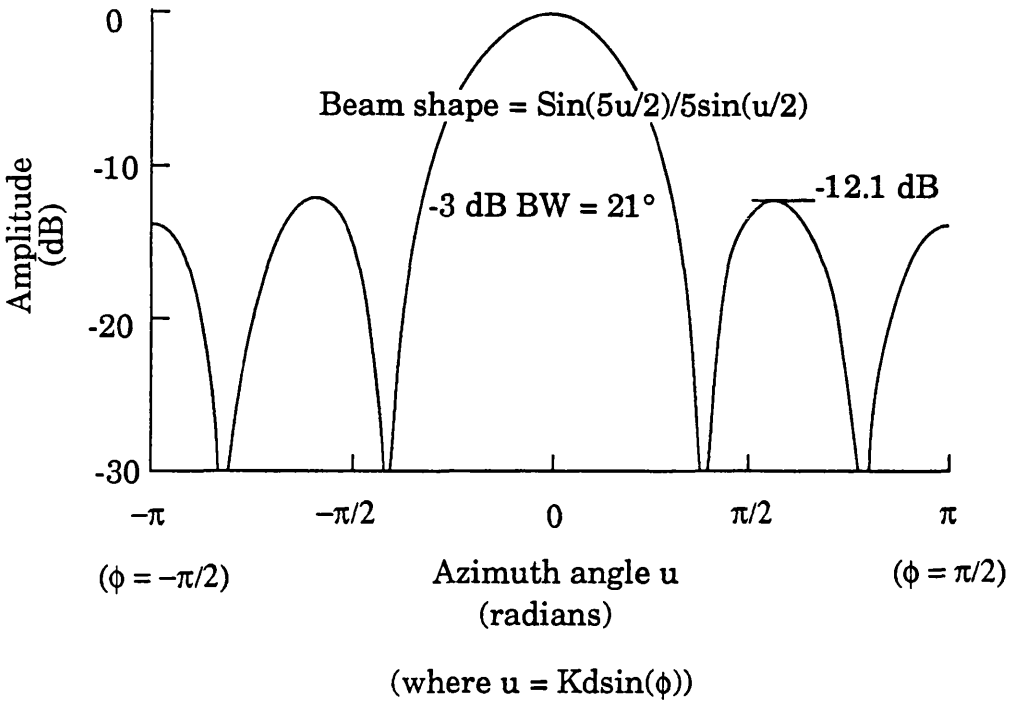

Figure 2.1 Geometry of a linear array of isotropic radiators, showing the array factor for a uniformly excited five-element array.

Putting $u = Kd\sin(\phi)$ and $w = e^{ju}$:

$$\zeta(\phi) = \sum_{n=0}^{N-1} w^n = \frac{w^N - 1}{w - 1} = w^{\frac{(N-1)}{2}} \left\{ \frac{w^{\frac{N}{2}} - w^{-\frac{N}{2}}}{w^{\frac{1}{2}} - w^{-\frac{1}{2}}} \right\}$$

Extracting the constant amplitude factor $w^{(N-1)/2}$:

$$\zeta(\phi) = \frac{\sin\left(\frac{Nu}{2}\right)}{N \sin\left(\frac{u}{2}\right)} \qquad (2.1.3)$$

As an example, consider the radiation pattern formed by a linear array of five uniformly excited elements where the inter-element spacing is $\lambda/2$. Figure 2.1 plots the power pattern:

$$P(\phi) = 10 \log_{10} \left\{ \frac{F(\phi) . F^*(\phi)}{[F(\phi) . F^*(\phi)]^{max}} \right\} \qquad (2.1.4)$$

where the denominator $[F(\phi).F^*(\phi)]^{max}$ is the peak power of the beam, in the direction $\phi = 0°$. The gain relative to isotropic in the direction $\phi = 0°$ is given by the directivity of the beam, $2Nd/\lambda$. Throughout this thesis, radiation patterns are plotted using the normalised power pattern of (2.1.4).

The 21° half power beamwidth is calculated by inserting $\zeta(\phi) = 1/(\sqrt{2})$ into (2.1.3). For a uniformly excited array the -3 dB beamwidth of the mainlobe can be plotted as a function of N, as shown figure 2.2. The level of the first sidelobe level in figure 2.1 is -12.1 dB. As the number of elements in the linear array increases, the first sidelobe level reaches a limiting value of -13.26 dB, as shown in figure 2.2.

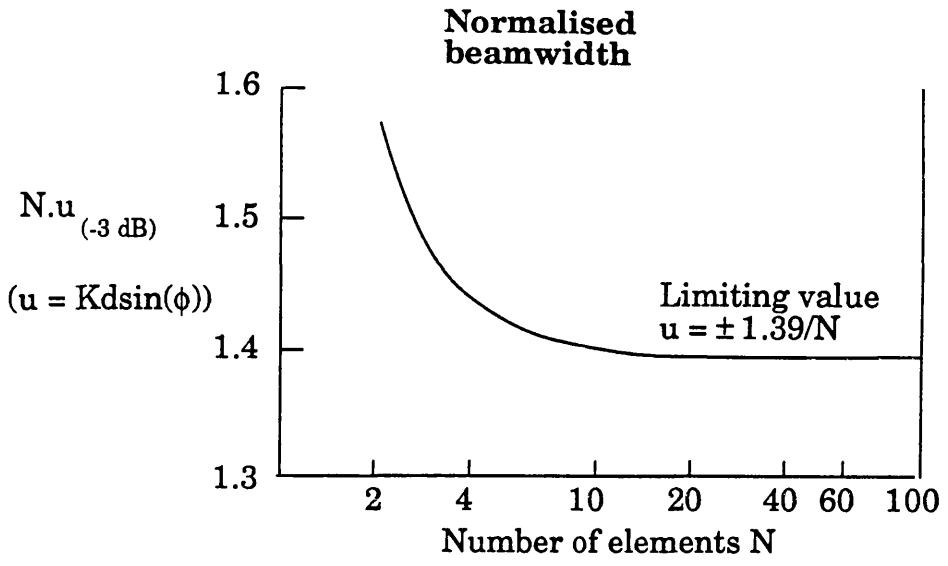

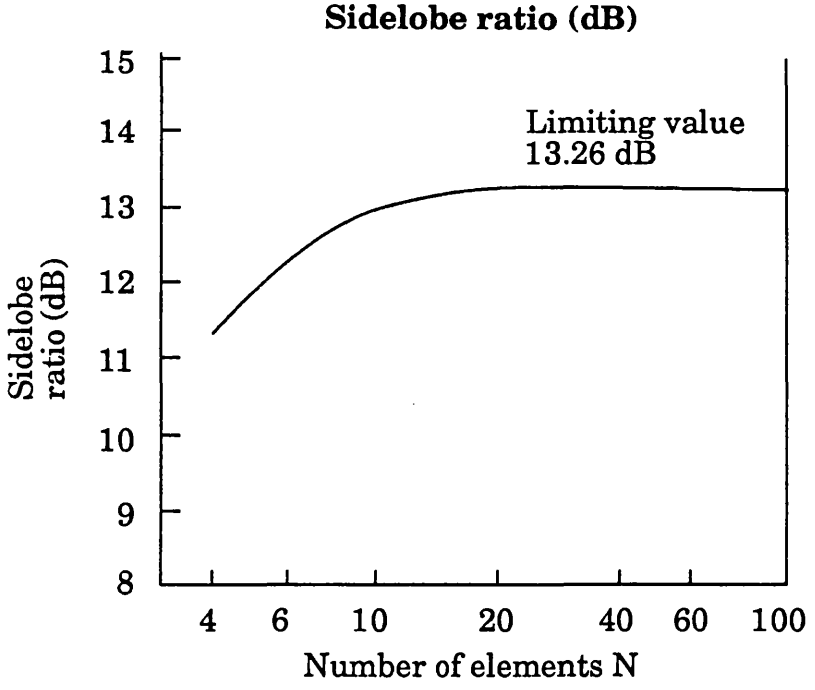

Figure 2.2 Plots used to calculate the -3 dB beamwidth and sidelobe ratio for a uniformly excited linear array of N isotropic elements.

The beam formed by the cophasal excitation of (2.1.2) is a broadside beam. A beam is steered by applying a linear progressive phase slope to the linear array elements. If the element amplitudes are equal then the excitation has the form:

$$I_n = I_0 e^{-jn\alpha}$$

where α is the progressive phase factor. The array factor now becomes:

$$\zeta(\phi) = \sum_{n=0}^{N-1} e^{jn\{Kd \sin(\phi) - \alpha\}}$$

$$\zeta(\phi) = \frac{\sin\left(\frac{N(u-\alpha)}{2}\right)}{N \sin\left(\frac{(u-\alpha)}{2}\right)}$$

The mainlobe of this pattern is oriented in the direction $\phi = \alpha$. The sidelobe levels of this pattern are the same as those of a broadside beam (α=0). The mainlobe increases in width as the beam is scanned off broadside, the beamwidth between nulls being determined by the projected length of the array in the plane at right angles to the beam direction.

Large inter-element spacings ($d > \lambda/2$) produce additional main beams, called grating lobes. The mainlobe peaks are located where $(u - \alpha) = n\pi$. If d/λ and α are chosen properly, only the mainlobe ($n = 0$) will be in the visible range $-90° \leq \phi \leq 90°$. If the beam is to be scanned close to end-fire, the inter-element spacing must be less than $\lambda/2$.

2.1.3 **Schelkunoff's unit circle representation**

A useful representation of the linear array excitation was given by Schelkunoff (1943). If $w = e^{ju}$ (where $u = Kd\sin(\phi)$) is inserted into (2.1.1), then the array factor can be written:

$$\zeta(\phi) = \sum_{n=0}^{N-1} \frac{I_n}{I_0} w^n$$

$$= \frac{I_{N-1}}{I_0} w^{N-1} + \frac{I_{N-2}}{I_0} w^{N-2} + \ldots\ldots + \frac{I_0}{I_0}$$

where I_n is complex. This polynomial can be factorised to give the array factor in the form:

$$\zeta(w) = (w - w_1)(w - w_2)(w - w_3) \ldots\ldots (w - w_{(N-1)}) \qquad (2.1.5)$$

The (N - 1) roots of this polynomial can be plotted on the complex w plane, as shown in figure 2.3. Real space corresponds to the function $w = e^{ju}$ traversing a sector of the unit circle given by:

$$-Kd \leq u \leq Kd$$

Thus a $\lambda/2$ spacing allows us to traverse the unit circle once. If the (N - 1) roots are placed on the unit circle (within the range $w = e^{ju}$) a pattern with (N - 1) nulls will result. If all the roots are placed off the unit circle, then a pattern devoid of nulls will be formed. As an example figure 2.3 shows the root positions for a uniformly excited five-element array with an inter-element spacing of $\lambda/2$. The roots are found on the unit circle at the positions $\pm 2\pi/5$ and $\pm 4\pi/5$. The magnitude of F(w) at a point w on the unit circle (that is, real space) is given by the product of the four distances d_1, d_2, d_3 and d_4, as shown in figure 2.3. As w moves along the unit circle this product changes, mapping out the array factor in u space. At the root

Schelkunoff unit
circle representation

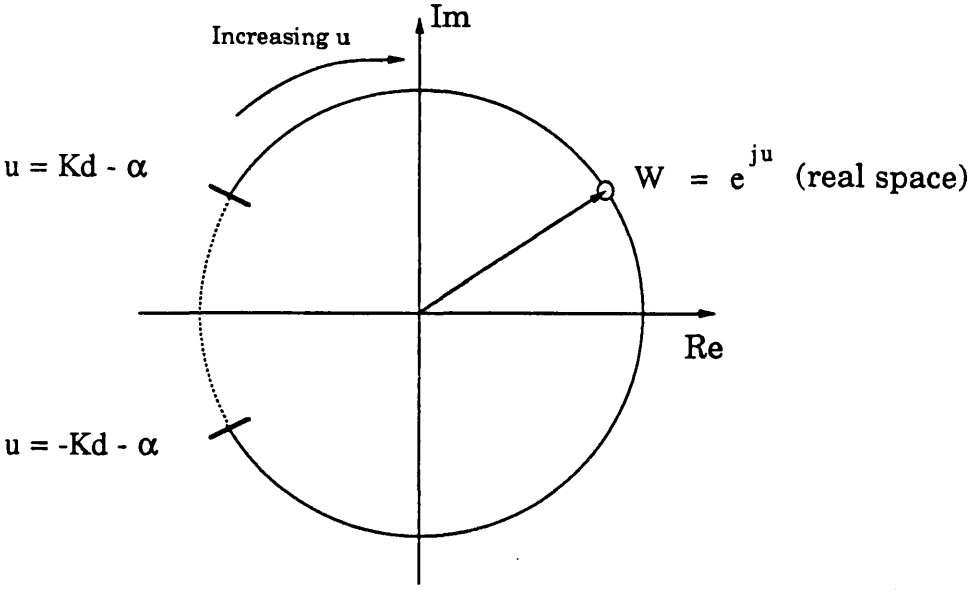

Representation of the array factor
for the uniform excitation of a five-
element linear array (d = λ/2)

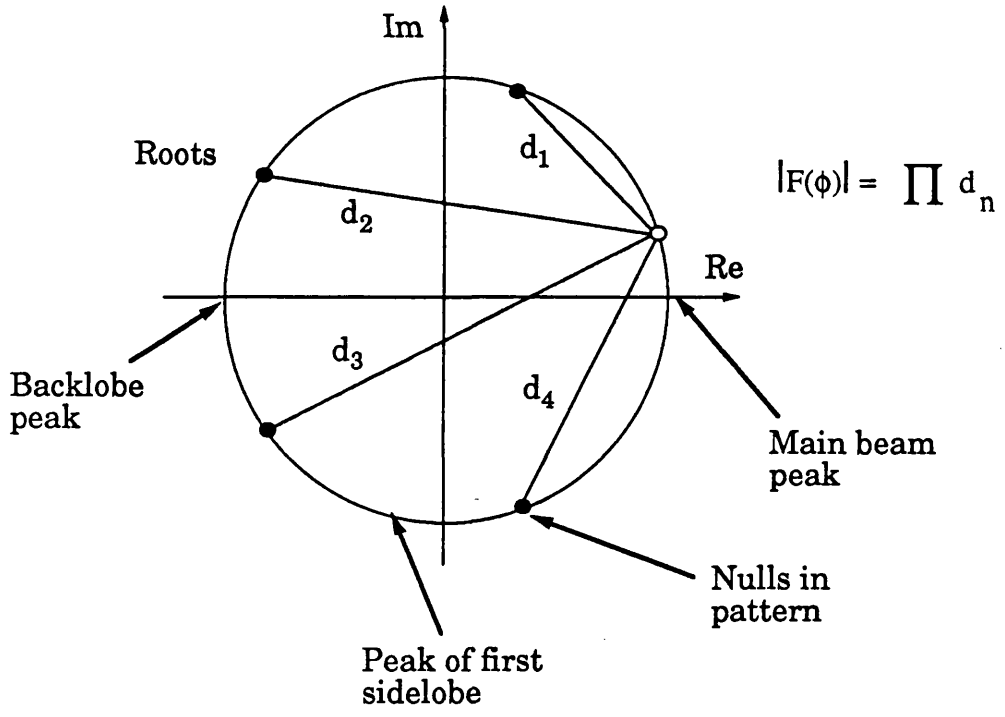

Figure 2.3 Schelkunoff unit circle representation of the array factor for a linear array.

locations there will be nulls in the pattern. In this plot the product is a maximum for u = 0; the peak of the mainlobe. The height of a sidelobe is calculated from the product when w is about half way between adjacent zeros.

2.1.4 **Dolph-Chebyshev synthesis of low sidelobe patterns**

For many applications, such as radar and communications, radiation patterns with sidelobes considerably below -13 dB are required. The Schelkunoff unit circle representation is a useful tool in the synthesis of low sidelobe patterns. For a linear array with 2N + 1 elements, the 2N roots can be placed on the unit circle in complex conjugate pairs, forming a symmetrical beam pattern. The sidelobe level is reduced by clustering the roots close to u = π, although this will result in a widening of the main beam. For many applications the suppression of all sidelobes is equally important, so the optimum design is one where the sidelobes are of equal height. Further reduction in the sidelobe level can only be done by increasing the width of the main beam. The problem of seeking the proper root positions to give uniform sidelobes at a specified height was solved by Dolph (1946). This solution uses the Chebyshev polynomials, which can be expressed in the form:

$$T_n(x) = \begin{cases} (-1)^n \cosh(n \text{ arc } \cosh |x|) & x < 1 \\ \cos(n \text{ arc } \cos(x)) & |x| \leq 1 \\ \cosh(n \text{ arc } \cosh(x)) & x \geq 1 \end{cases} \qquad (2.1.6)$$

Within the range x = ±1 there are oscillations of unit amplitude, while outside this range the polynomial increases monotonically (figure 2.4). If the variable x can be made to correspond to the angle variable u, then a pattern with uniform sidelobes can be formed. A direct correspondence cannot be made, however, as the main beam must have zero slope at the centre. The asymptotic response is therefore mapped onto the side of the mainlobe, while the oscillatory portion covers the sidelobe region. A linear

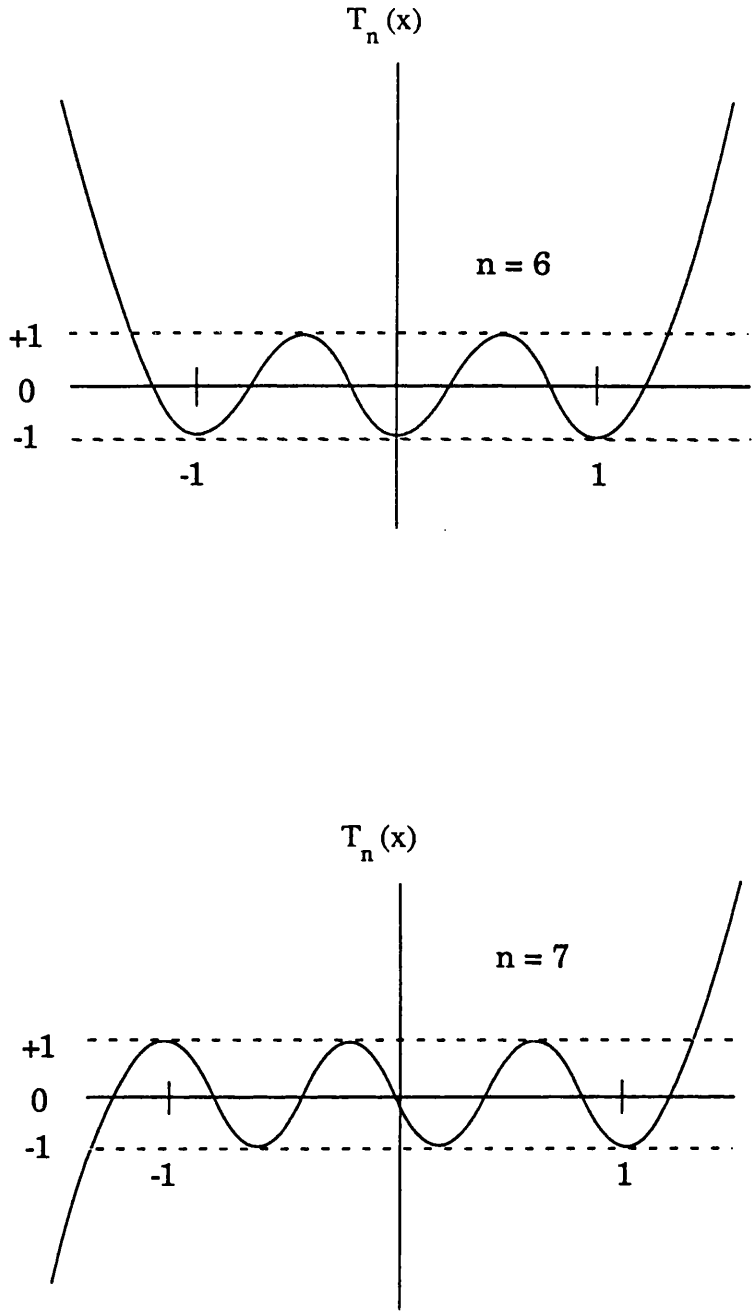

Figure 2.4 Chebyshev functions of order n = 6 and n = 7.

array with N elements produces a pattern with N - 1 zeros, so an N - 1 degree Chebyshev polynomial is used. The transformation from the Chebyshev function $T_{N-1}(x)$ to the array factor F(u), with $u = Kd\sin(\phi)$ is:

$$x = x_0 \cos(u/2) \tag{2.1.7}$$

The voltage sidelobe ratio SLR is given by:

$$SLR = T_{N-1}(x_0)$$

from which x_0 is calculated. Inserting x_0 into (2.1.6) allows us to determine the location of the roots on the unit circle. As an example, consider the excitation of a five-element array with an inter-element spacing of $\lambda/2$, where a pattern with sidelobe levels of -20 dB is required. x_0 is calculated to be 1.2933. From (2.1.7) the roots on the unit circle are at the positions:

$$u = \pm 88.82°, \pm 145.16°$$

These roots are plotted on the w plane in figure 2.5. Taking the product of the roots using (2.1.5), the tapered element excitation is:

Element	1	2	3	4	5
I_n (A)	0.517	0.833	1	0.833	0.517

The array factor for this excitation is depicted in figure 2.5. As for a uniform distribution, the beam is steered by applying a uniform progressive phase α to the amplitude distribution. As for a uniform excitation, large element spacings ($d \geq \lambda/2$) will produce one or more additional main beams (grating lobes). Again only the mainlobe will be in the visible range of u if d/λ and α are chosen properly.

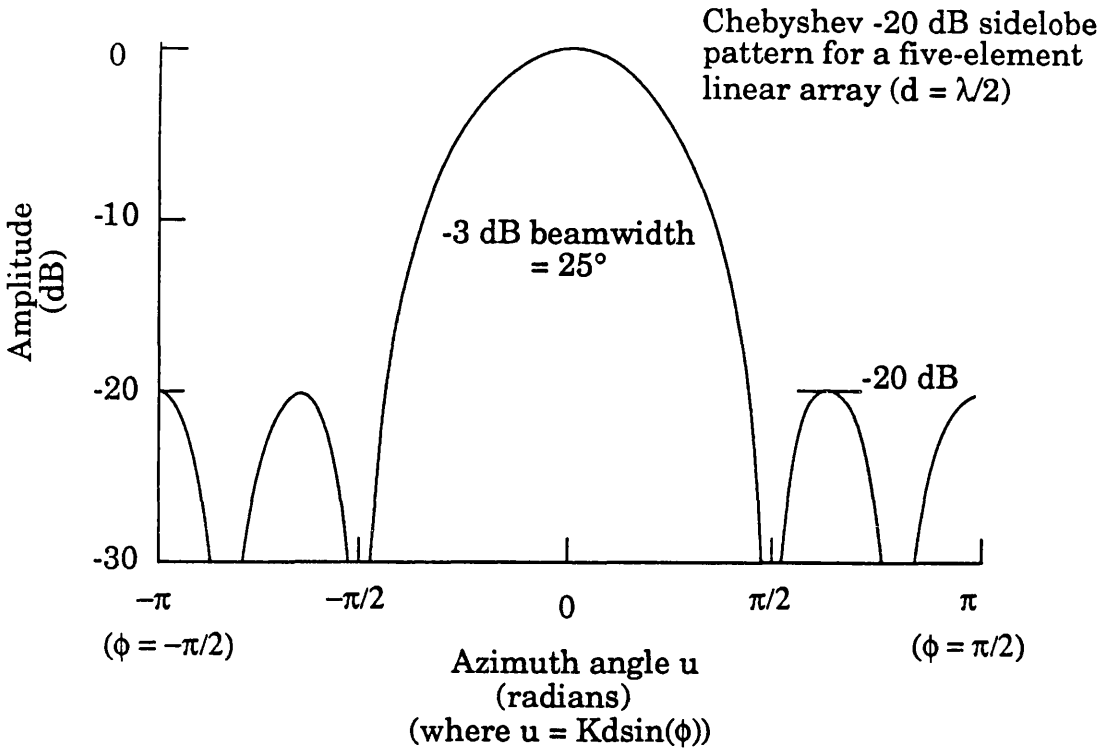

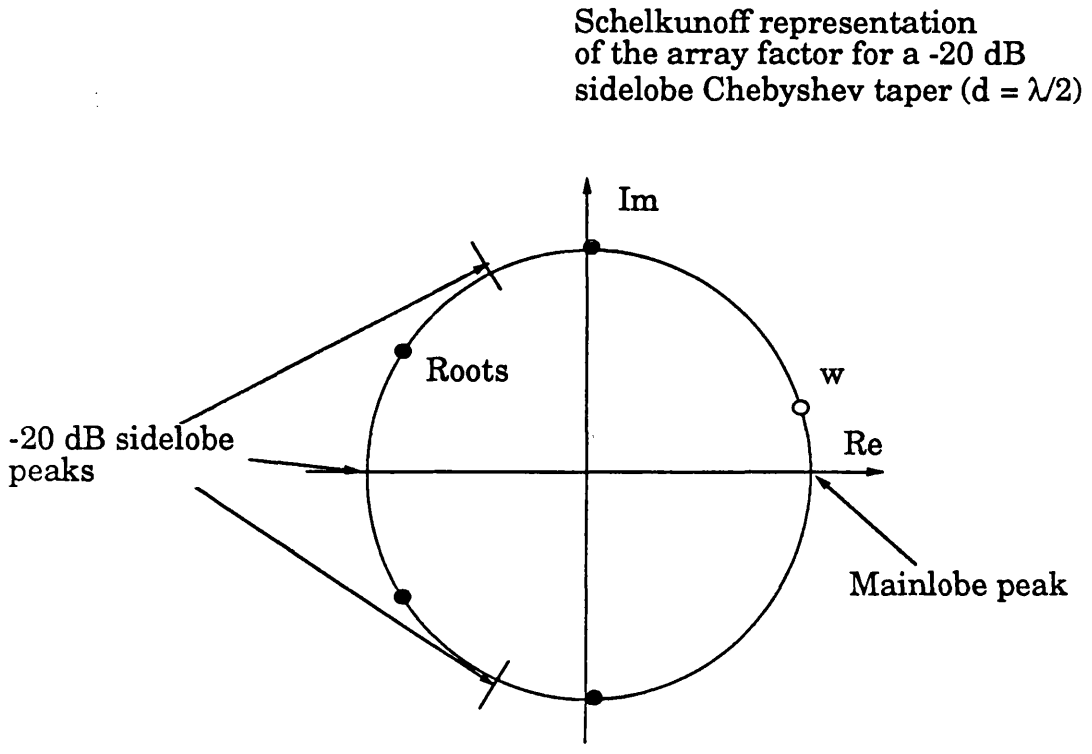

Figure 2.5 Theoretical array factor for a five-element linear array, excited with a Chebyshev taper to give a -20 dB sidelobe pattern.

A novel application of the Chebyshev polynomial to pattern synthesis is described by Milne (1987), where it is used as a 'scanning function' that is convolved with the desired pattern shape to give low sidelobes. The resulting linear array excitation has a non-linear phase progression - the phasing of the elements is employed as an additional degree of freedom.

The equivalent of the Dolph-Chebyshev array factor for a continuous line source was developed by Taylor (1955). The procedure determines the aperture distribution for a pattern with a single main beam and sidelobes at a specified level. For a uniformly excited line source, a pattern with the first sidelobes at -13 dB is formed, with the outer sidelobes dropping off according to the function u^{-1}. Taylor devised a synthesis technique that suppressed the levels of the innermost sidelobes, while leaving the outer (low level) sidelobes unchanged. As an example figure 2.6 depicts a Taylor pattern with a -20 dB sidelobe level. This continuous excitation can be sampled and applied to a discrete linear array. The excitation specified using this technique is generally easier to realise than a Dolph excitation with the same sidelobe level.

2.1.7 **Difference patterns**

Difference patterns used for monopulse DF systems can be synthesised using linear arrays. This pattern has two lobes symmetrically oriented on either side of a central null, as shown in figure 2.7. To form this pattern the two halves of the array are excited in antiphase. Arrays with an odd number of elements are not suitable for forming difference patterns because of the presence of a centre element. In the case where all the elements are excited with equal amplitudes the pattern has the form:

$$\zeta(\phi) = \frac{\sin^2\left(\frac{\pi L}{2\lambda}\cos(\phi)\right)}{\sin\left(\frac{\pi d}{2\lambda}\cos(\phi)\right)} \qquad (2.1.9)$$

where L is the array length. The high sidelobe level of -9.5 dB is due to the

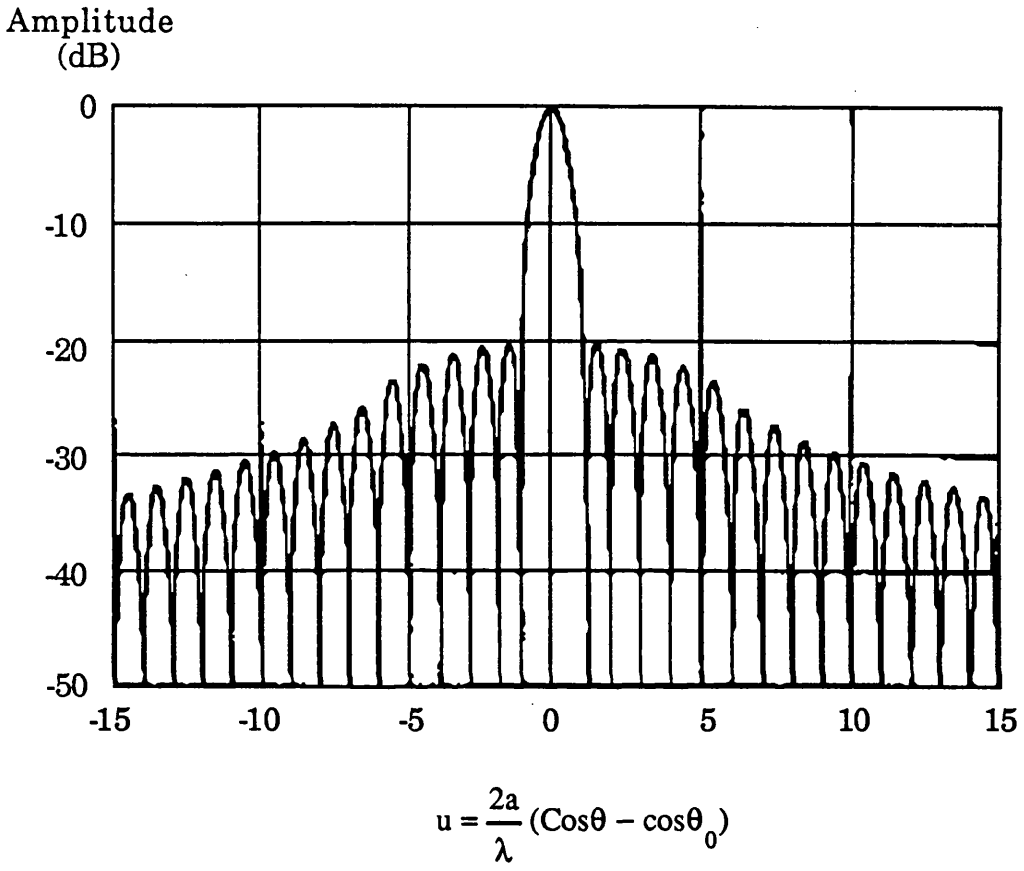

Figure 2.6 Taylor sum pattern for continuous line source, n = 6 with -20 dB Sidelobe level (after Elliot (1981a)).

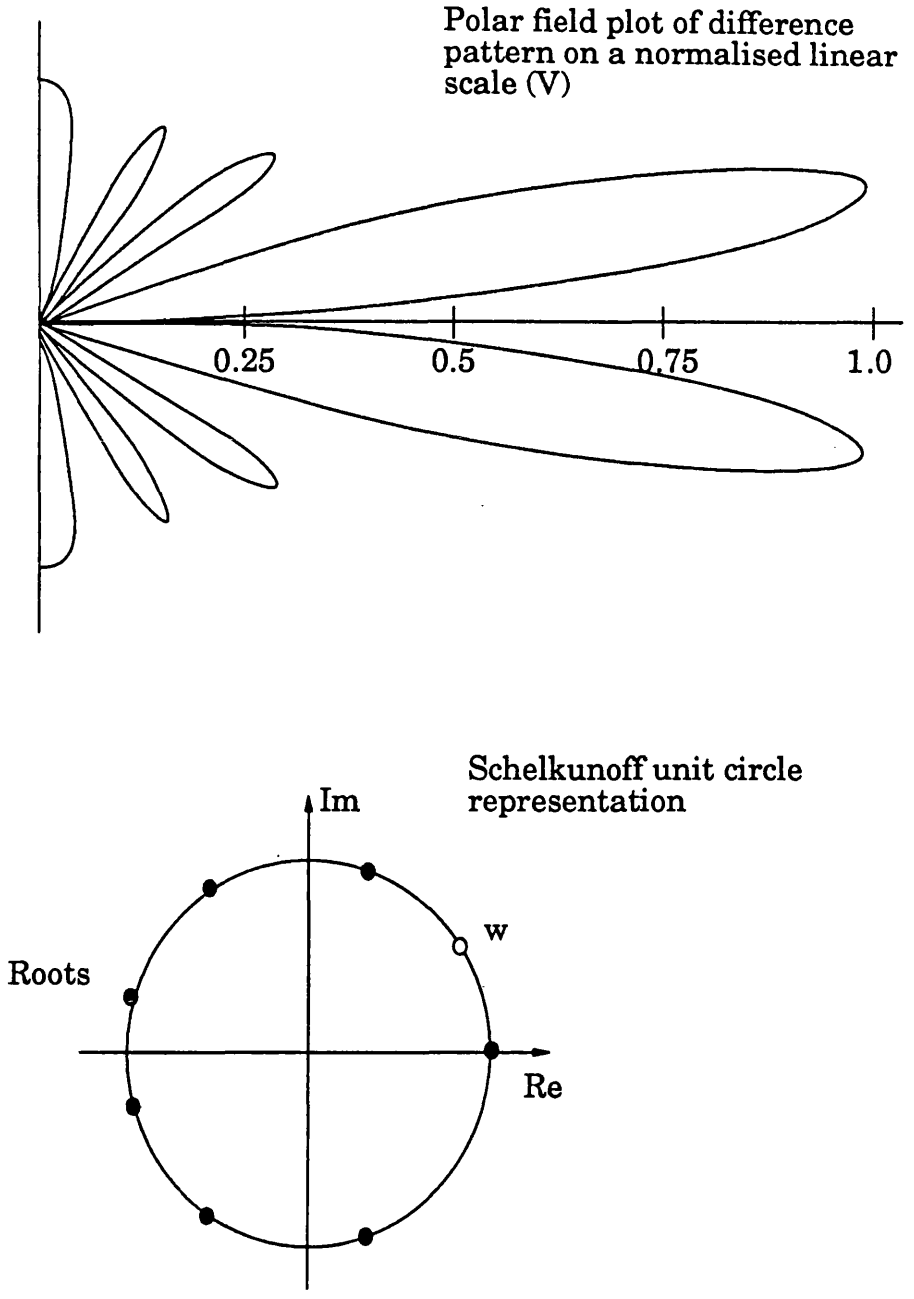

Figure 2.7 Theoretical difference pattern formed using a fourteen-element linear array excited with uniform amplitude and antisymmetric phase (d = $\lambda/2$). Plot taken from Elliot (1981a).

choice of equal amplitudes on the elements. Figure 2.7 shows the excitation of (2.1.9) depicted using the Schelkunoff unit circle representation. One root is located on the unit circle at $\phi = 0°$, while the others form complex conjugate pairs equispaced on the unit circle. All the roots are double roots, except the single root at $\phi = 0°$ - a very inefficient root placement. If a tapered distribution is applied to the amplitudes, then the sidelobe levels can be reduced. Bayliss (1968) describes a technique for synthesizing low sidelobe difference patterns. As for patterns with a single mainlobe a uniform progressive phase $e^{-jn\alpha}$ can be applied to steer the null pattern, but with the two halves of the array still in phase opposition, .

2.1.8 **Null-free patterns**

Some antenna applications require radiation patterns that are free of nulls. For air traffic control a beam without nulls in the elevation plane is required, but with a cosecant shape so that returns from aircraft at the same horizontal distance are equal in amplitude. The Woodward synthesis technique (1947) can be used to produce null-free patterns with a linear array. The pattern is formed from a fan of overlapping orthogonal beams. Each beam is formed from a uniform amplitude and linear phase distribution, producing a sin(Nu)/Nsin(u) type beam. For a linear array of N elements, if the beams are spaced by $2\pi/N$ in u space then the first null in each beam is filled by the peak of the adjacent beam. If the n^{th} beam is excited with an amplitude F_n then the pattern is simply:

$$H(u) = \sum_{n=1}^{N} F_n \left[\frac{\sin\{N(u-\alpha_n)\}}{N \sin\{(u-\alpha_n)\}} \right]$$

An example of this (showing only the mainlobes of the overlapping beams) is depicted in figure 2.8. The amount of ripple on the null-free pattern is controlled by the element spacing.

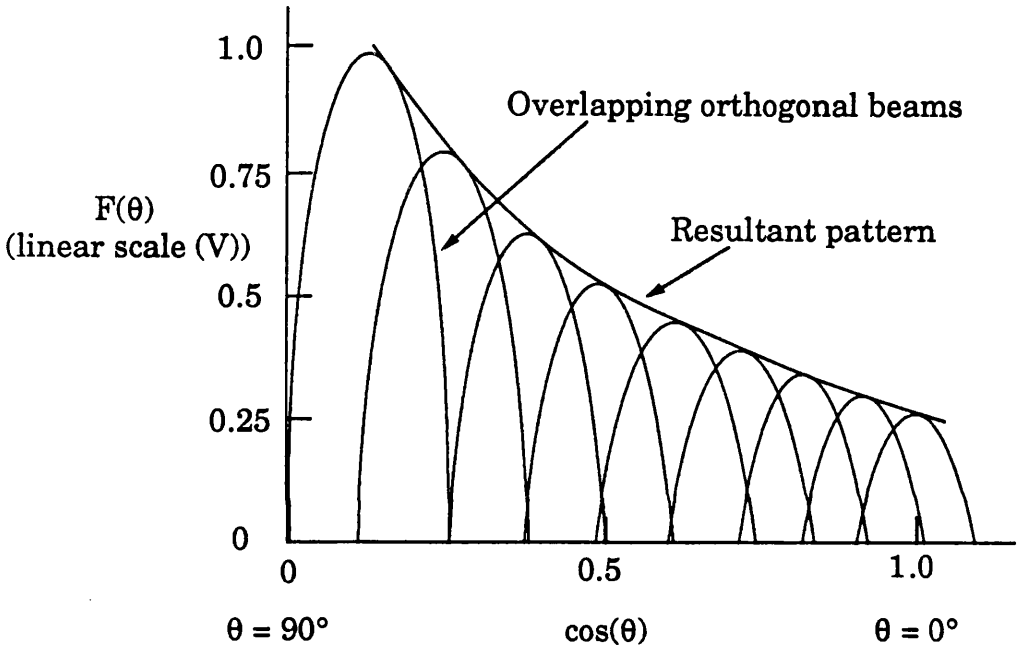

Figure 2.8 The synthesis of a null-free pattern using the Woodward synthesis technique (after Elliot (1981a)). For clarity only the mainlobes are shown.

2.1.9 **Superdirective arrays**

A uniform excitation of a linear array with equal phase gives the maximum mainlobe gain. While excitations that produce a higher directivity can be realised, in practice the absolute gain is reduced by losses. This type of excitation is termed a superdirective excitation. Using the Schelkunoff unit circle analysis, consider a linear array with a very small inter-element spacing, so the excursion of w on the unit circle is small. The (N - 1) roots of an N element array can still be placed within the range of w so a pattern with a prescribed beamwidth and sidelobe level can be formed. The current distribution will not be uniform, because for a uniformly excited array, the -3 dB beamwidth is approximately λ/Nd. If the impedance of the array elements is calculated for this excitation, a major reduction in the radiation resistance is observed. If the loss resistance of the element becomes significant, in comparison to the radiation resistance, the efficiency drops. As an example, Elliott (1981b) considers the case of a five-element array, uniformly excited to produce a -13 dB sidelobe pattern. Let us assume that the loss resistance results in a 1% reduction in efficiency for an inter-element spacing of $\lambda/2$. If the spacing is reduced to $\lambda/4$ and the excitation adjusted to form the same array factor, the same loss resistance results in the dissipation of 80% of the input power. For a spacing of $\lambda/144$ ($u = 1°$) the losses are over a million times as large as the radiated power. In addition the radiation patterns of superdirective arrays are sensitive to errors in the excitation and the positioning of elements.

2.1.10 **The orthogonality of overlapping beams**

Multiple beams can be formed using a single linear array. An N element array can generate up to N independent beams. RF networks to form multiple beams include the beamformer developed by Blass (1960) and the well-known matrix of Butler and Lowe (1961). It is desirable for reasons of efficiency that the overlapping beams of a multiple beam antenna should be independent: the radiation pattern resulting from exciting two or more of the input ports should be a linear superposition of the radiation pattern

obtained when the ports are excited separately. Additionally, applying power to one of the beam ports should not result in any power output at the other beam ports. White (1962) explains that this condition can only be fulfilled if the individual beam patterns are orthogonal in space. The orthogonality relation can be expressed:

$$\int_0^{2\pi} d\phi \int_{-\pi/2}^{\pi/2} F_j(\phi,\theta) \cdot F_k^*(\phi,\theta) \cos\theta \, d\theta = 0 \qquad (2.1.10)$$

where ϕ is the azimuth angle.

θ is the elevation angle.

$F_j(\phi,\theta)$ is the radiation pattern associated with the j^{th} input terminal.

$F_k^*(\phi,\theta)$ is the complex conjugate of $F_k(\phi,\theta)$.

A pattern with well defined orthogonal properties is the sin(Nu)/Nsin(u) pattern. A pair of these beams produced by a linear array are orthogonal provided the azimuth spacing in u space is:

$$K d \sin(\phi) = 2\pi/N, \qquad \sin(\phi) \approx \lambda/Nd \qquad (2.1.11)$$

For this spacing the mainlobes are at the same angle as the first nulls of the adjacent beams and the crossover level between adjacent beams is about -4 dB. If an amplitude taper is applied to the array excitation to lower the sidelobes, then the beam spacing for orthogonality increases. For example, if a cosine shaped amplitude taper is applied to the excitation, the orthogonal spacing is given by $u = 4\pi/N$. For some excitations the radiation patterns do not have an orthogonal spacing, for example an excitation that linearly tapers to zero at the ends of the array.

Before applying linear array theory to pattern synthesis with circular arrays, the 'phase mode' analysis of circular array excitations must be discussed.

2.2 The phase mode excitation of a circular array

2.2.1 The theoretical characteristics of phase modes

This theoretical analysis considers the excitation of a circular array required to form a desired radiation pattern in the far field. By the reciprocity theorem, the synthesis results obtained here are equally valid for receiving arrays, such as amplitude comparison DF systems. The array excitation is expressed as a series of spatial Fourier terms. Davies (1983) examines the properties of these orthogonal terms, called 'phase modes'.

First consider a continuous circular array. If ψ represents the angle around the array, then the function $F(\psi)$ represents the excitation of the array. $F(\psi)$ is periodic in ψ with an angular period of 2π radians so it can be expressed as the sum of a series of Fourier terms:

$$F(\psi) = \sum_{m=-\infty}^{+\infty} A_m e^{jm\psi} \qquad (2.2.1)$$

where

$$A_m = \frac{1}{2\pi} \int_0^{2\pi} F(\psi) e^{-jm\psi} \, d\psi$$

If a single term of the first equation is considered, such as $A_m e^{jm\psi}$, it can be seen that it represents an excitation of constant amplitude, with a linear phase change of m cycles of phase around the array.

Let us consider the radiation pattern formed if a single phase mode is excited around a circular array, for the case where the array elements have omnidirectional radiation patterns. The array excitation is of the form:

$$F(\psi) = A_m \, e^{jm\psi}$$

where A_m is the excitation amplitude. If the distance P from the centre of the array to a point in the far field (at an angle ϕ) is used as a reference, there is a path difference Δr from an element at an angle ψ to this point. This path difference modifies the phase of the element excitation in the far field by ΔP:

$$\Delta P = e^{j\beta r \cos(\psi - \phi)}$$

where $\beta = 2\pi/\lambda$. and r is the array radius. The far field excitation at an angle ϕ is given by summing contributions from all parts of the array:

$$F(\psi) = \frac{1}{2\pi} \int_0^{2\pi} A_m e^{j\beta r \cos(\psi - \phi)} e^{jm\psi} \, d\psi$$

This expression can be evaluated using the integral identity:

$$\int_0^{2\pi} e^{j\beta r \cos(\psi - \phi)} e^{jm\psi} \, d\psi = 2\pi j^m J_m(\beta r) e^{jm\phi}$$

where $J_m(\beta r)$ is a Bessel function of order m and argument βr. Hence:

$$F(\phi) = A_m j^m J_m(\beta r) e^{jm\phi}$$

$$\equiv A_m K_m e^{jm\phi} \qquad (2.2.2)$$

The radiation pattern is also a phase mode of order m, but weighted by K_m, a dimensionless complex number called the 'phase mode coefficient'. For a given array radius r, the amplitude of the m^{th} phase mode coefficient can be determined from a plot of the Bessel functions (figure 2.9). As a general rule, $J_m(\beta r)$ is small for arrays where $m > \beta r$. For an array of radius r, the amplitude of the m^{th} phase mode coefficient is zero for the wavelengths where $J_m(\beta r) = 0$, so the mode cannot be excited at those frequencies.

The use of directional elements in an array can be incorporated in the analysis by including the directional pattern, $G(\psi)$ of the elements in the phase mode expression. Here we consider the case where the boresight direction of the elements point radially outwards. Since the element pattern is also spatially periodic with a period 2π, it too can be expressed as a Fourier series:

$$G(\psi) = \sum_{i=-p}^{+p} B_i e^{ji\psi}$$

where

$$B_i = \frac{1}{2\pi} \int_0^{2\pi} G(\psi) e^{-ji\psi} \, d\psi$$

Bach and Hansen (1969) show that if this array is excited by a single mode of order m, the radiation pattern again has the phase mode form:

$$F(\phi) = A_m K_m e^{jm\phi} \qquad (2.2.3)$$

where K_m is now given by;

$$K_m = \sum_{i=-p}^{+p} B_i j^{m-i} J_{m-i}(\beta r) \qquad (2.2.4)$$

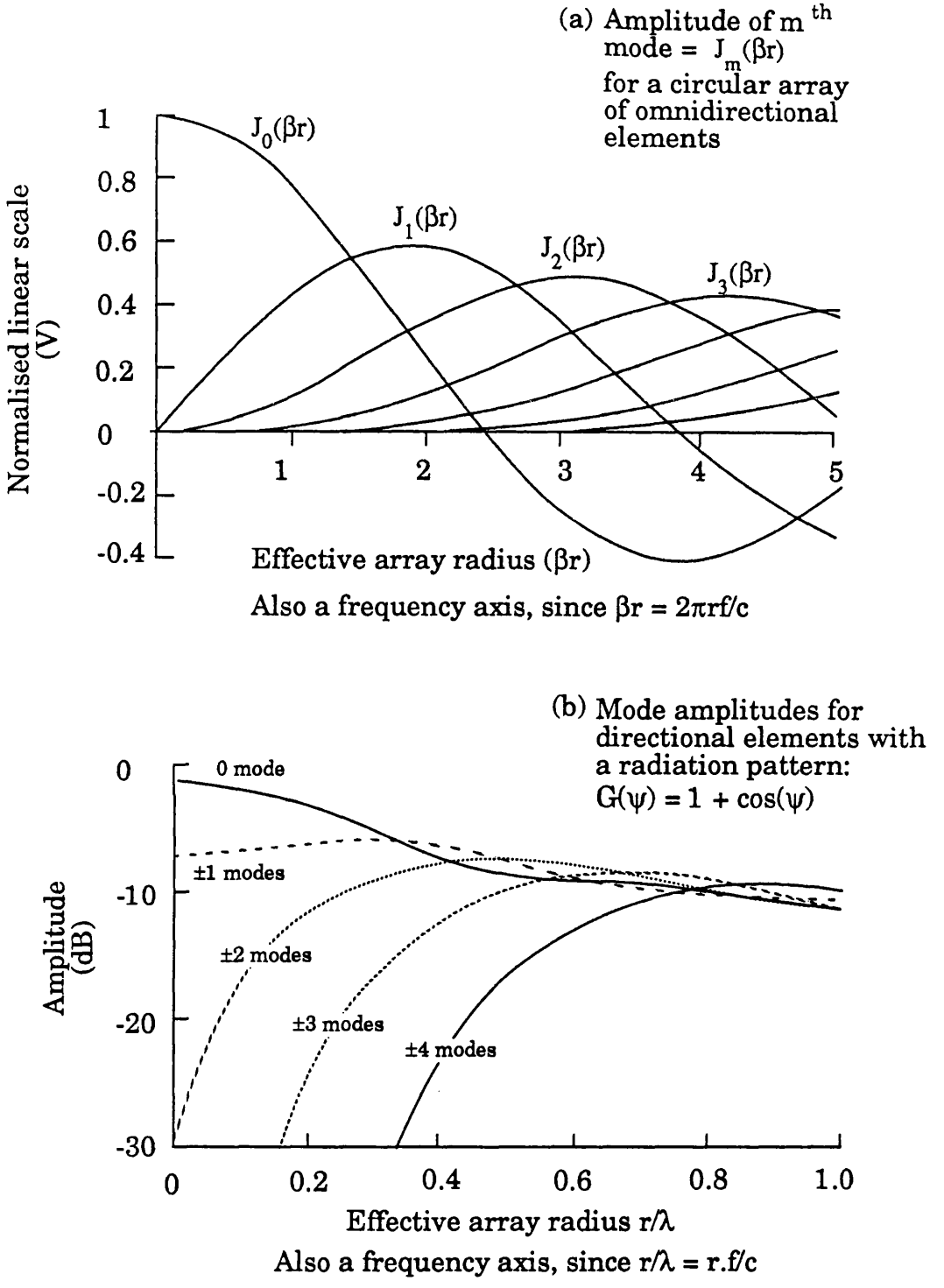

Figure 2.9 The change in the phase mode amplitude as a function of the array radius for arrays composed of:

(a) Omnidirectional elements.

(b) Directional elements with a radiation pattern: $G(\psi) = 1 + \cos(\psi)$.

The complex phase mode coefficient K_m is no longer proportional to a single Bessel function, but to a sum of Bessel functions. Rahim and Davies (1982) showed that for some directional elements the mode amplitudes change much less with frequency compared with an array of omnidirectional elements. As an example of this, figure 2.9(b) shows the amplitude of the phase mode coefficients (in dB) for an array of elements with a directional pattern: $G(\psi) = 1 + \cos(\psi)$.

If the directional pattern of the antenna elements has reflective symmetry in the boresight direction, i.e. $G(\psi) = G(-\psi)$, then $B_{+i} = B_{-i}$ and it can be shown that $K_{+m} = K_{-m}$.

2.2.2 Amplitude modes

If we excite two phase modes of order +m and -m with equal amplitude $A_m/2$, and the same phase, from (2.2.3) the radiation pattern is the superposition (sum) of the orthogonal excitations:

$$F(\phi) = \frac{A_m}{2} K_m e^{jm\phi} + \frac{A_m}{2} K_m e^{-jm\phi}$$

$$= A_m K_m \cos(m\phi) \qquad (2.2.5)$$

This cosine function is periodic in angle with m cycles of amplitude variation in 2π radians. This term is called an amplitude mode and is a term of a cosine/sine Fourier series. If we excite two phase modes of order +m and -m with equal amplitude A/2 and in antiphase, the radiation pattern has the form:

$$F(\phi) = \frac{A_m}{2} K_m e^{jm\phi} - \frac{A_m}{2} K_m e^{-jm\phi}$$

$$= jA_m K_m \sin(m\phi) \qquad (2.2.6)$$

This amplitude mode is the m^{th} order sine term. The 'cosine type'

amplitude modes are used to synthesise symmetrical patterns with a single mainlobe. The 'sine type' amplitude modes are used in the synthesis of odd patterns, like the monopulse difference pattern. Throughout this thesis the $\cos(\phi)$ mode is called the C1 mode, $\cos(2\phi)$ the C2 mode and so on. Correspondingly, S1 is the $\sin(\phi)$ mode and S2 is the $\sin(2\phi)$ mode.

2.2.3 Phase modes formed by discrete element circular arrays

Practical designs for circular arrays have a finite number of elements equally spaced around the circumference of a circle. The excitation of a discrete array can be analysed as a sampled continuous array. Let $S(\psi)$ represent a series of uniformly spaced delta functions at those values of ψ where the elements are located. The modal excitation of an N element discrete array can be expressed as:

$$F(\psi)\,S(\psi) = \sum_{m=-\infty}^{\infty} C_m e^{jm\psi} \sum_{n=0}^{N-1} \delta\left(\psi - \frac{2n\pi}{N}\right) \qquad (2.2.7)$$

where $\delta(\psi - 2n\pi/N)$ is periodic with period 2π. Bach and Hansen (1969) show that for this discrete excitation by a mode of order m the radiation pattern $F(\phi)$ has the form:

$$F(\phi) = A_m N \sum_{n=-\infty}^{\infty} K_{(m-nN)} e^{j(m-nN)\phi}$$

$$= A_m N \left[\ldots + K_{(m-2N)} e^{j(m-2N)\phi} + K_{(m-N)} e^{j(m-N)\phi} \right.$$

$$\left. + K_{(m)} e^{j(m)\phi} + K_{(m+N)} e^{j(m+N)\phi} + K_{(m+2N)} e^{j(m+2N)\phi} + \ldots \right]$$

(2.2.8)

For a discrete array, a phase mode has the same phase mode coefficient as the corresponding phase mode of a continuous array, but higher order harmonics are also excited. The order of the harmonic terms is determined by the number of elements in the array.

2.2.4 The Butler matrix

The RF matrix of Butler and Lowe (1961) was developed to generate multiple beams with linear arrays. It can also be used to excite the phase modes of a discrete circular array. A Butler matrix is a network with N input ports (the mode ports) and N output ports, that are connected to the element feeds. Figure 2.10 shows a 4 x 4 Butler matrix. While the early matrix designs were narrowband, Withers (1969) developed designs for wideband matrices. Butler matrices can excite circular arrays with any number of elements in the series 1, 2, 4, 8, 16, ...2^n. Generally matrices are constructed from a network of directional couplers and fixed wideband phase shifts. For an N element array, at least $\{(N/2)\log_2(N)\}$ couplers are required. If the m^{th} mode port is excited by a source of amplitude A_m the output at the n^{th} element port is given by:

$$V_n = \frac{A_m}{\sqrt{N}} e^{j\frac{2\pi(n-1)}{N}} \qquad (2.2.9)$$

Figure 2.10 plots the transmission phase characteristics of a 4 x 4 matrix. When an array is excited using a Butler matrix, the currents excited on the elements are determined by the element impedance, which is considered in the next section.

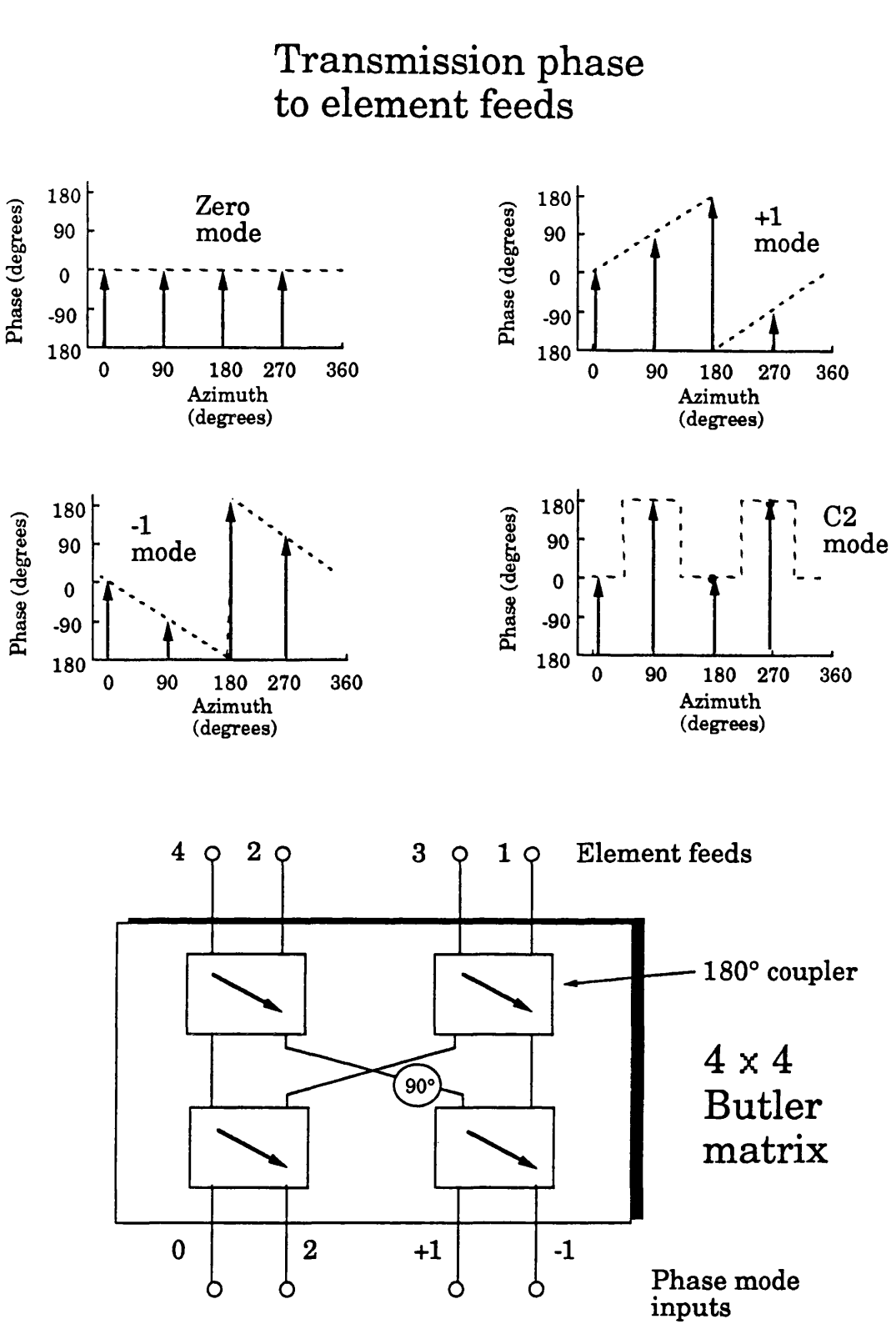

Figure 2.10 The transmission phase characteristics of an ideal 4 x 4 Butler matrix.

2.2.5 The phase mode impedance of circular array elements

As with linear arrays, mutual coupling between the array elements modifies the driving point impedance of the elements. King, Mack and Sandler (1968) show that for a circular array of dipoles excited by a single phase mode the driving point impedance of all the elements is identical. The element has an impedance that is a function of the mode order, termed the 'phase mode impedance' and calculated using:

$$Z^m = \sum_{k=1}^{N} z_{1k} e^{j\left(\frac{2\pi(k-1)m}{N}\right)} \qquad (2.2.10)$$

where z_{1k} is the mutual impedance between element 1 and the k^{th} element of an N element array. As an example, let us consider the phase mode impedances of the four-element array depicted in figure 2.11. From (2.2.10) the phase mode impedances are:

$$Z^0 = z_{11} + 2z_{12} + z_{13}$$

$$Z^{+1} = Z^{-1} = z_{11} - z_{13}$$

$$Z^{+2} = Z^{-2} = z_{11} - 2z_{12} + z_{13} \qquad (2.2.11)$$

Since the modes are orthogonal, exciting (for example) the 2^{nd} order mode has no effect on the impedance of the 0^{th} or 1^{st} order modes. Phase mode impedances are fixed, unlike linear array elements that have 'active' impedances, that are a function of the array excitation. The power radiated by a circular array element is given by:

$$P_{rad} = I^2 R_{rad}$$

I is the current at the input terminal of the element and R_{rad} is the radiation resistance of the (modally excited) element. The radiation

Four-element circular array

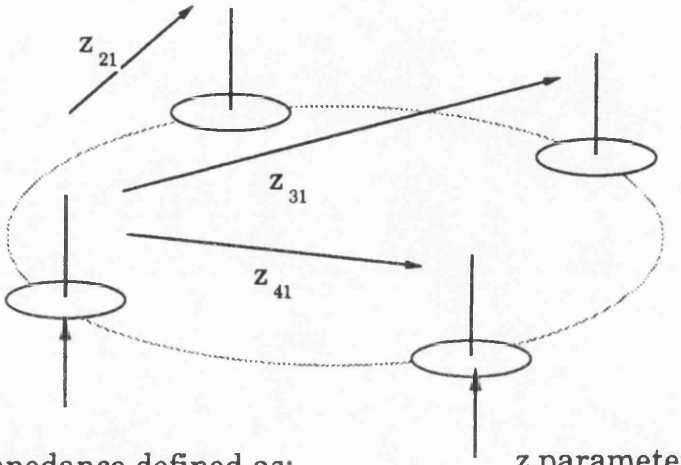

Element self impedance defined as:

$$z_{11} = \left.\frac{V_1}{I_1}\right|_{I_2, I_3, I_4 = 0}$$

z parameters measured at element drive points

Mutual impedance between elements 1 and 2:

$$z_{21} = \left.\frac{V_2}{I_1}\right|_{I_2, I_3, I_4 = 0}$$

Calculation of the phase mode impedance:

$$V_1 = z_{11}I_1 + z_{12}I_2 + z_{13}I_3 + z_{14}I_4$$

For example, for the zero order mode $I_1 = I_2 = I_3 = I_4$ (by symmetry), so:

$$Z_1^0 = \frac{V_1}{I_1} = z_{11} + 2z_{12} + z_{13}$$

Figure 2.11 The relationship between the mutual impedances and the phase mode impedances for a four-element circular array of vertical dipoles or monopoles.

resistance of an element is the real part of the phase mode impedance $\mathcal{R}(z^m)$. For dipoles and monopoles the values of the self and mutual impedances have been extensively tabulated, for example by King (1956). For close-spaced dipoles ($<\lambda/2$) the real part of the mutual impedance is positive, and increases as the element spacing becomes smaller (or as the frequency decreases). At a minimum frequency f_{min} the array will not be able to support the higher order modes. For the 2nd order mode excited on a four-element array this occurs when (from (2.2.11)):

$$\mathcal{R}(z_{11} + z_{13}) - \mathcal{R}(2z_{12}) = 0$$

In this case the real part of the 2nd order phase mode impedance tends to zero - i.e the mode cannot be radiated. If only the 0th and 1st order modes are required, f_{min} for a four-element array occurs when:

$$\mathcal{R}(z_{11}) - \mathcal{R}(z_{13}) = 0$$

For the 0th order mode alone there is no f_{min} - the radiation resistance does not drop to zero as the frequency decreases.

To conclude, the phase mode impedance determines the lowest operating frequency for an array with a fixed radius r. If we wish to excite modes up to the order m = M, then as the frequency decreases, the real part of the Mth phase mode impedance drops, until the array cannot adequately support this mode. These results are equivalent to those for a linear array with a superdirective excitation; there is a rapid change in phase of the excitation across the (discrete) aperture, resulting in a low radiation resistance and a corresponding loss of efficiency.

2.3 Pattern synthesis using phase modes

2.3.1 **Linear array equivalence.**

The phase mode analysis of a circular array is ideally suited for synthesising directional radiation patterns. Any directional radiation pattern (which is a periodic function with period 2π) can be expressed in terms of a series of phase modes. Using a Butler matrix-fed circular array, the orthogonal modes are excited at the appropriate phase mode port. The amplitude and phase of each mode excitation is chosen to realise the desired directional pattern. The radiation pattern produced by exciting modes up to the order $\pm M$ is given by:

$$F(\phi) = \sum_{m=-M}^{M} A_m K_m e^{jm\phi} \qquad (2.3.1)$$

where A_m is the excitation of the m^{th} mode port and K_m is the m^{th} phase mode coefficient.

The use of this Fourier technique means that the pattern synthesis techniques developed for linear arrays can be applied to circular arrays. In section 2.1 it was noted that exciting an N element linear array with uniform amplitude produces a sin(Nu)/Nsin(u) type pattern. Davies (1983) shows that this type of pattern can be produced in ϕ space with a continuous circular array of omnidirectional elements. Suppose that (2M + 1) phase modes are excited on the array with an excitation:

$$A_m = \frac{1}{j^m J_m(\beta r)} \qquad (-M < m < M)$$

This corresponds to exciting all the modes to the same level in the far field, resulting (from (2.1.3)) in a directional pattern:

$$F(\phi) = \sum_{m=-M}^{M} A_m j_m J^m(\beta r) e^{jm\phi} = \sum_{m=-M}^{M} e^{jm\phi} = \frac{\sin\left(\{2M+1\}\frac{\phi}{2}\right)}{(2M+1)\sin\left(\frac{\phi}{2}\right)} \quad (2.3.2)$$

This produces a directional pattern with a beamwidth $\phi \approx 2\pi/M$, as for a uniform linear array, but the pattern now extends over 360° and relates to a ϕ variable. As an example, figure 2.12 shows the radiation pattern formed when a continuous circular array is excited with five phase modes from -2 to +2.

It is useful to visualise the modes as the 'elements' of a linear array, radiating into ϕ space, also depicted in figure 2.12. Let us consider the properties of this linear array:

- Phase modes are omnidirectional in azimuth, so the 'elements' are also omnidirectional. The radiation pattern corresponds to the array factor for this 'linear array'.

- If the m^{th} phase mode port is excited by a source of amplitude A_m, the radiated phase mode is weighted by a complex term K_m. As shown in figure 2.12 this can be represented by a two-port network in the feed of the m^{th} linear array 'element', with a transmission amplitude and phase corresponding to K_m.

- Phase modes are orthogonal functions, so there is no mutual coupling between the 'elements' of this linear array. The input impedance at the two-port network of the m^{th} 'element' has a fixed value (the m^{th} phase mode impedance, Z^m) whatever the array excitation.

- The radiation patterns formed from phase modes have the same shape (in ϕ space) as those formed by a true linear array (in u space) with an

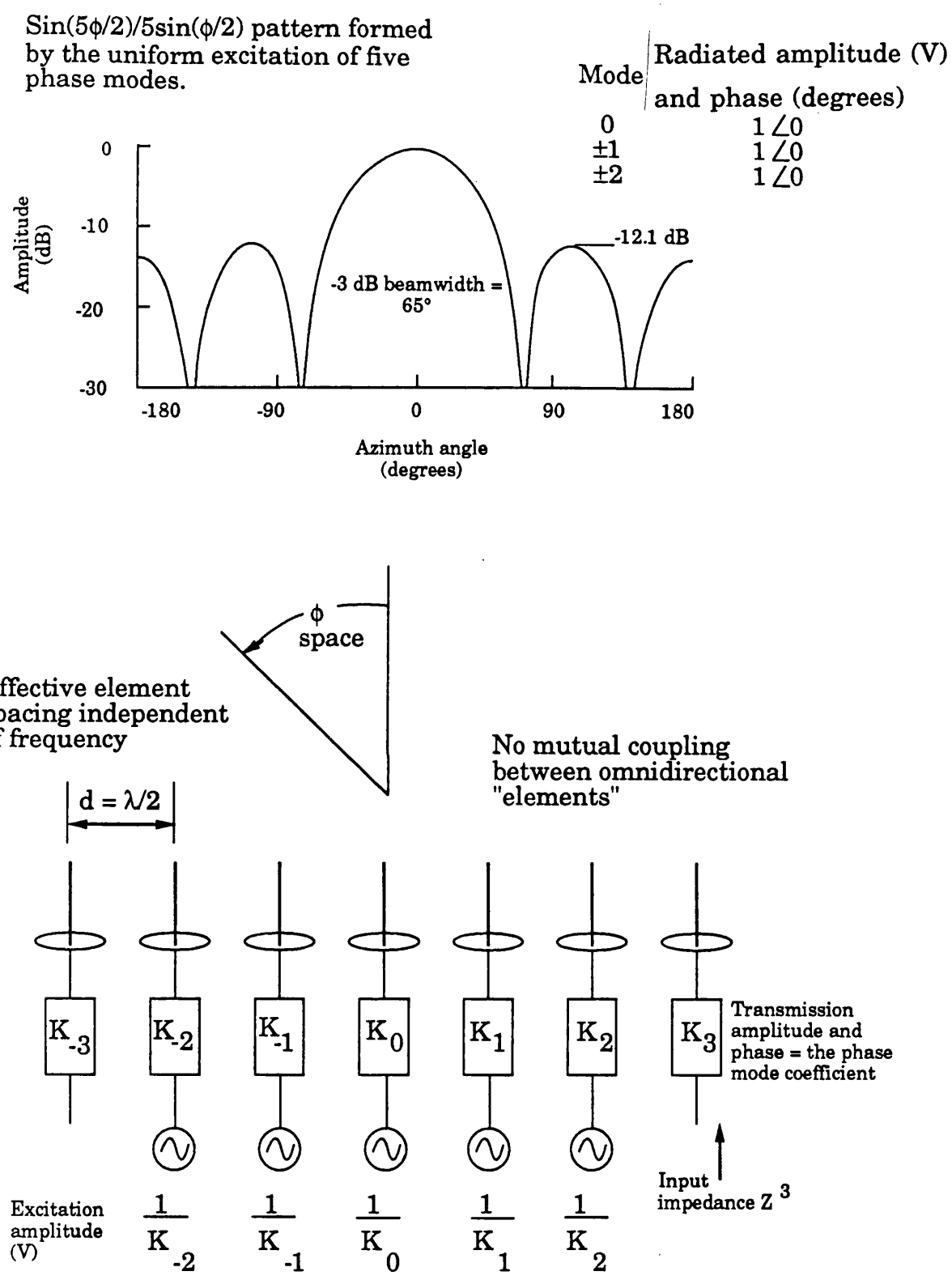

Figure 2.12 Representation of phase modes as the "elements" of a linear array, showing the radiation pattern formed when the mode excitation is chosen so the "elements" are uniformly excited.

inter-element spacing of $\lambda/2$. This is illustrated by comparing figure 2.1 and figure 2.12, which show the radiation patterns for a uniformly illuminated linear array and for uniformly excited modes of a circular array respectively. The -3 dB beamwidth for the pattern of figure 2.12 is found by reference to figure 2.2 for the beamwidth of an N (= 2M + 1) element linear array, giving a figure of 65°. The first sidelobe level of -12.1 dB is also found by reference to figure 2.2, giving the sidelobe levels for an N element linear array.

- For a linear array $u = Kdsin(\phi)$ changes with frequency (that is, the effective inter-element spacing changes). For the modes of a circular array the function $u = \phi$ is independent of frequency, so the effective spacing of the 'elements' of figure 2.12 is $\lambda/2$ - whatever the frequency.

- Davies (1965) has shown that any directional pattern synthesised from phase modes can be electronically rotated by applying a phase slope to the phase mode inputs of the Butler matrix. To form an azimuth beam in a direction α, the phase applied to the m^{th} mode is $e^{-jm\alpha}$. Unlike linear arrays the effective 'element' spacing is independent of angle, so the radiation pattern does not deform as the beam are steered. Grating lobes do not appear, and there is no change in the -3 dB beamwidth.

2.3.2 Applying an amplitude taper to phase modes

While a uniform excitation of the modes gives the maximum directivity in ϕ space, it has rather high (-13 dB) sidelobe levels. Referring again to the linear array theory of section 2.1, lower sidelobes are formed by applying a taper to the mode excitation:

$$A_m = \frac{W_m}{K_m} \qquad (2.3.4)$$

where W_m is the amplitude taper applied to the m^{th} mode.
As for a linear array, radiation patterns with equal level sidelobes can be formed by applying the Dolph Chebyshev amplitude taper of section 2.1.

Consider a continuous circular array with modes up to M = ±2 excited. The taper required for a beam with -20 dB sidelobes is:

Mode order	-2	-1	0	+1	+2
Taper (V)	0.517	0.833	1	0.833	0.517

(2.3.5)

This -20 dB sidelobe pattern, plotted using (2.3.1), is depicted in figure 2.13. The -3 dB beamwidth is wider than that of a uniform excitation; as for linear arrays, there is a trade-off between sidelobe levels and mainlobe beamwidth.

For small radius arrays the higher order modes are excited with reduced amplitudes, providing an inherent amplitude taper. The array radius can be selected to produce the desired taper on the modes. For example, inspection of figure 2.9 gives the amplitudes of the phase mode coefficients (in dB) for a continuous array of elements with a 1 + cos(ψ) directional pattern. Considering the 0^{th} order mode as a reference, the relative amplitudes (K_m) of the modes for $\beta r = 2.75$ are:

Mode order	-2	-1	0	+1	+2
Relative mode amplitude	0.545	0.837	1	0.837	0.545
Required taper (V)	0.517	0.833	1	0.833	0.517

So by choosing the array radius carefully, the amplitude taper of (2.3.5) required for a Chebyshev -20 dB sidelobe pattern is (almost) realised.The array radius can be chosen to realise the 1^{st} order mode taper exactly, or the 2^{nd} order mode taper exactly, but not both.
The main aim of this study is to form wideband low sidelobe patterns. However, to illustrate another application of linear array theory let us

Chebyshev -20 dB sidelobe pattern

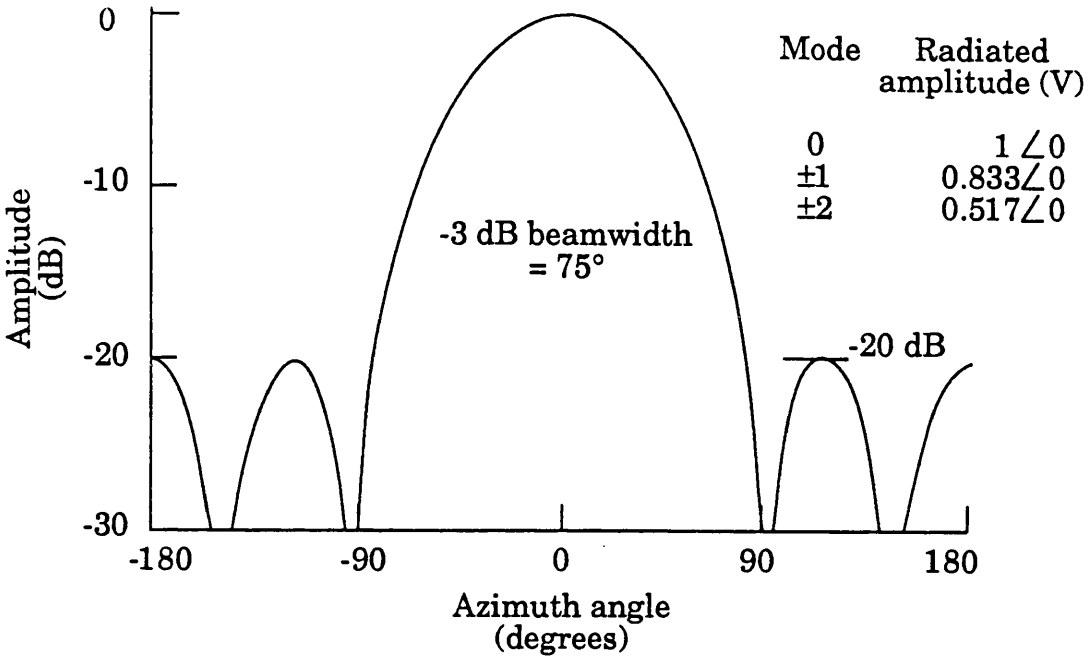

Linear array representation

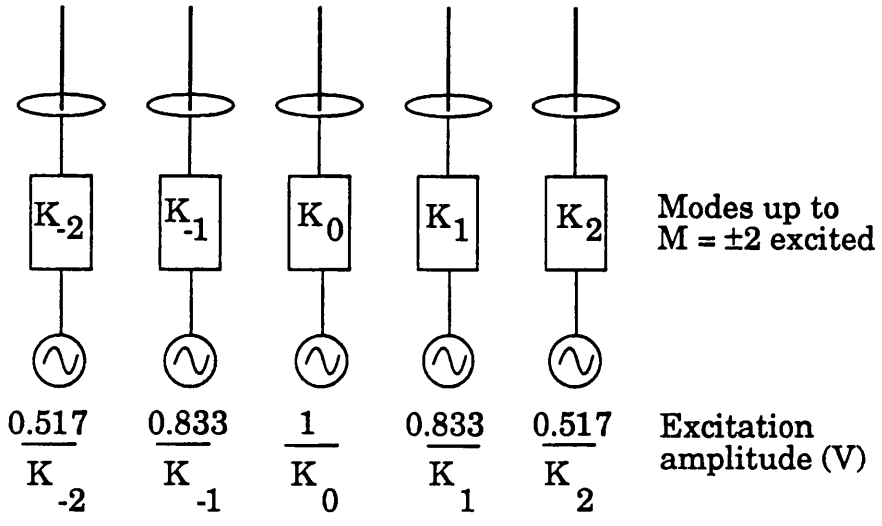

Figure 2.13 Theoretical synthesis of a -20 dB sidelobe pattern formed by applying a Chebyshev taper to the phase modes of a circular array.

consider the synthesis of difference patterns using phase modes. For a linear array, the two halves of the array are excited in antiphase, so the modes of order -m are excited in antiphase to the modes of order +m. The 0^{th} order mode corresponds to the centre 'element' of a linear array and cannot be used in the synthesis of difference patterns. As an example, the theoretical excitation:

Mode order	-2	-1	0	+1	+2
$\lvert A_m K_m \rvert$ (V)	-1	-1	0	+1	+1

produces the difference pattern of figure 2.14.

2.3.3 The orthogonality of overlapping beams formed from phase modes

Multiple beams can be formed from the phase modes of a circular array. As for a linear array, an N element circular array can generate up to N independent beams. A second N x N Butler matrix provides the linear phase progressions required to form N beams. Figure 2.15 illustrates this for a 4 x 4 matrix. With a four element array four identical beams, spaced 90° apart in azimuth can be formed. As explained in section 2.1.10, it is desirable that the overlapping beams of any multiple beam antenna should be orthogonal. The coupling between beams may be determined from equation (2.1.10). $\mathrm{Sin}(N\phi/2)/N\sin(\phi/2)$ beams produced by uniformly exciting N phase modes have an orthogonal spacing of $\phi = 2\pi/N$, calculated using (2.1.11). As for linear arrays the mainlobes are at the same angle as the first nulls of the adjacent beams, and the crossover level between adjacent beams is about -4 dB. For the pattern of figure 2.12 (formed with a uniform excitation of modes up to the order $M = \pm 2$) the orthogonal spacing is $5\pi/2$ (72°). Beams with lower sidelobe levels have wider orthogonal spacings, again calculated using (2.1.11).

Difference pattern

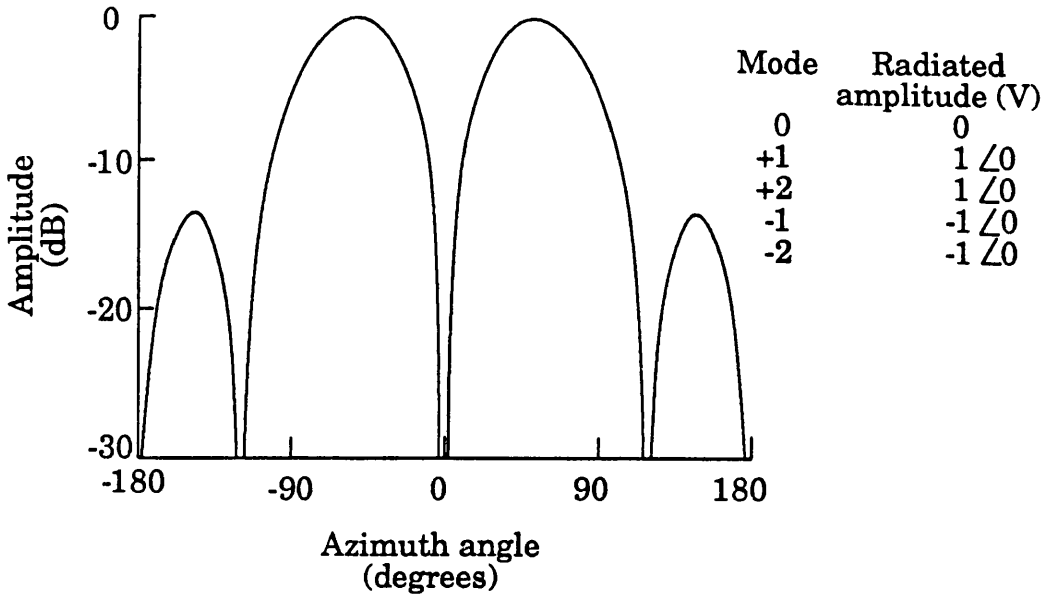

Linear array representation

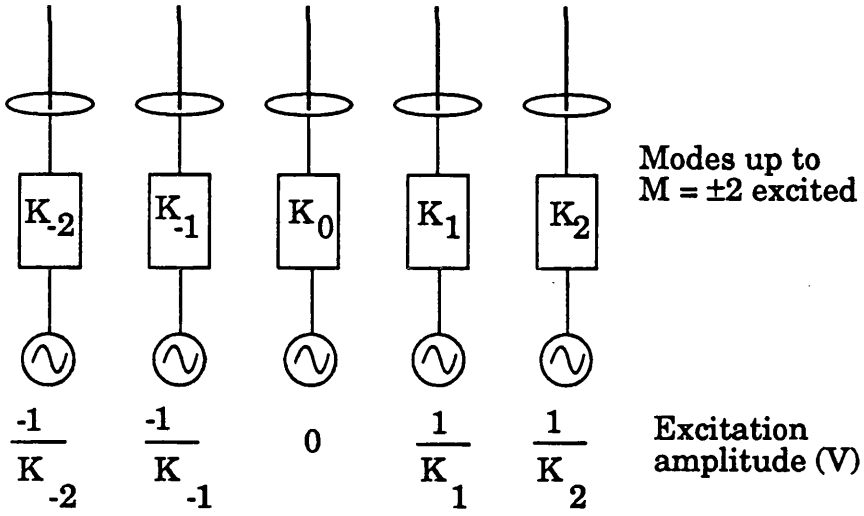

Figure 2.14 Theoretical synthesis of a difference pattern using a circular array. The phase modes are excited with uniform amplitude and antisymmetric phase.

Linear phase progression applied to modes by a second 4x4 Butler matrix

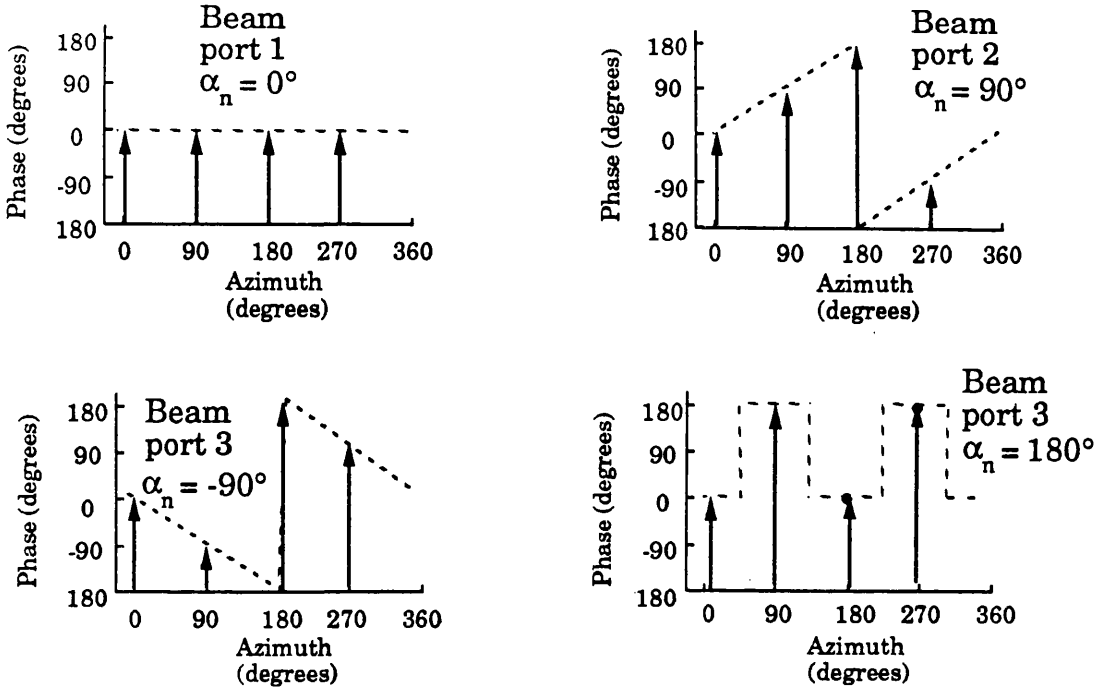

Linear array representation of the phase mode excitation to form a beam in the direction α_n

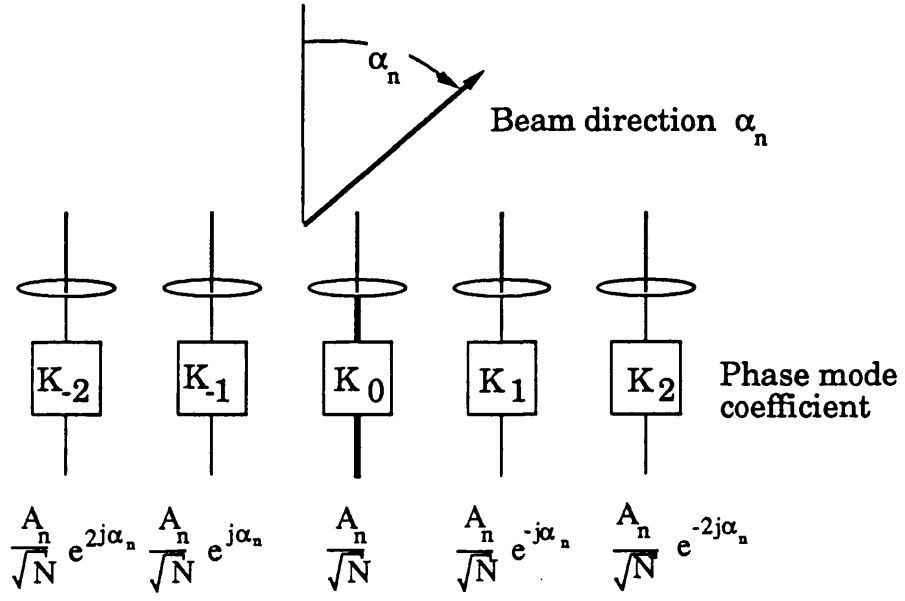

Figure 2.15 The synthesis of a fan of beams using a second Butler matrix to supply the linear progressive phase slope.

If N orthogonal beams are formed using a second Butler matrix, these beams could in principle be used to synthesise null-free patterns, in a manner analogous to the Woodward synthesis technique described in section 2.1.8 for linear arrays. However, such a technique is beyond the scope of this study.

The Schelkunoff unit circle analysis can also be applied to circular arrays. This technique is useful in considering the effect of higher order harmonics on the synthesised pattern, considered in the next section.

2.3.4 Pattern synthesis using the phase modes of a discrete circular array

Phase modes up to the order $M = \pm N/2$ can be excited using a discrete circular array with N elements. By considering figure 2.12, it is clear that the patterns formed from these modes are equivalent to those formed by a linear array with N + 1 elements. When a mode is excited on a discrete array, higher order harmonics are also excited, as discussed in section 2.2.3. Let us consider the effect of these harmonics on pattern synthesis:

- For a discrete array, exciting a single mode port excites a periodic sequence of modes. If we consider the modes as the 'elements' of a linear array, the harmonics correspond to additional 'elements', as shown in figure 2.16. The effect of these additional elements on the synthesised patterns can be predicted by extending M in (2.3.1) to include the harmonic terms. The radiated amplitude and phase of the m^{th} order harmonic is determined by the m^{th} phase mode coefficient. For small radius arrays, only the lower order harmonics will be of significant amplitude.

- The N phase mode excitations of an N element circular array form a set of orthogonal functions, even with the harmonics present. Inspection of (2.2.8) shows that each harmonic 'element' is excited by just one fundamental. Every phase mode excited by a continuous circular array is excited by a discrete array of the same radius, only not independently.

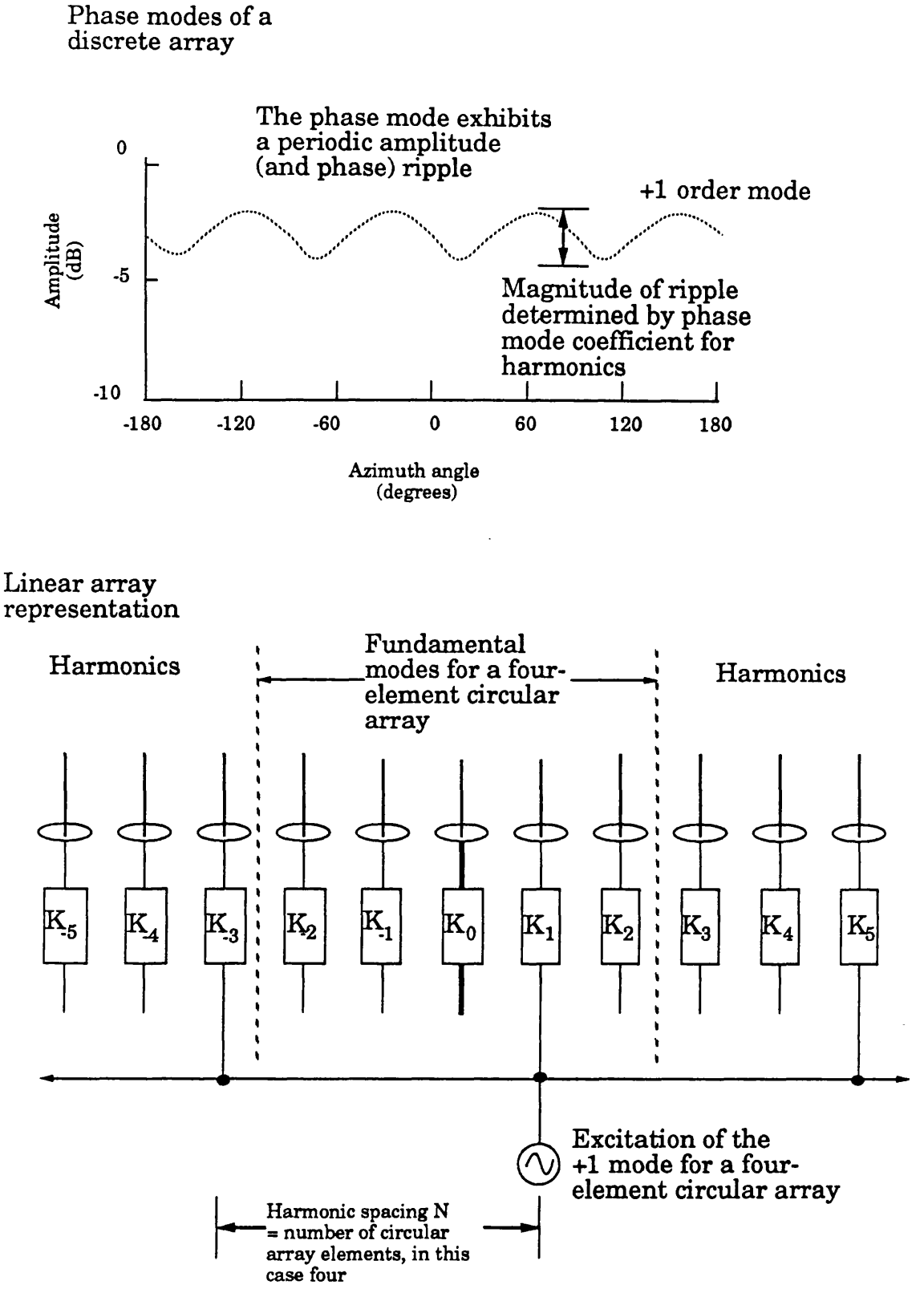

Figure 2.16 The excitation of harmonic modes by a discrete circular array with four elements. The harmonics are represented as additional "elements" of a linear array.

- An N element circular array can form radiation patterns with the same shape as a linear array with N + 1 elements. This is illustrated in figure 2.15, where a four-element circular array excites five modes, from -2 to +2.

- The highest order fundamental mode (M = N/2) is a cosine type amplitude mode, formed by exciting the +N/2 and -N/2 modes from the same port. Ignoring higher harmonics, inserting M = N/2 into (2.2.8) gives a radiation pattern of the form:

$$F(\phi) = A_m N \left[K_{\left(\frac{N}{2} - N\right)} e^{j\left(\frac{N}{2} - N\right)\phi} + K_{\left(\frac{N}{2}\right)} e^{j\left(\frac{N}{2}\right)\phi} \right]$$

$$= 2 A_m N \left[K_{\left(\frac{N}{2}\right)} \cos\left\{\left(\frac{N}{2}\right)\phi\right\} \right] \qquad (2.3.6)$$

This amplitude mode cannot be used in steered beams. It can be used to form beams in fixed directions, where the linear progressive phase $\alpha = \pm 2\pi/N, \pm 4\pi/N$. This corresponds to the angular locations of the N array elements.

- The corresponding sine mode of order M = N/2 cannot be excited on an N element circular array, as the array elements are located at the angular positions of the nulls in this pattern. Although the sine term is missing, the cosine term can be used to form difference patterns in the directions where $\phi = \pi/2M$. For example, the difference pattern of figure 2.14 can be formed using a four-element discrete array in the fixed directions ϕ = +45°,-45°,+135° and -135°.

- All the phase modes lower in order than the M = N/2 mode can be used in steered beams. The harmonic terms deform the azimuth pattern as the beam is steered, because the uniform progressive phase ($e^{-jm\alpha}$) applied to the m^{th} 'element' is also applied to the harmonics of (2.2.8). The deformation of the synthesised pattern can be predicted using (2.3.1).

Karavassilis (1984) and Cvetkovic et al. (1988) developed a phase comparison DF system using a discrete circular array. In this type of system the harmonics can introduce errors in the measured DF bearing. They concluded that the effect of the harmonic ripple could be taken into account with the aid of electronic look-up tables provided the inter-element spacing was less than $\lambda/2$ at the highest operating frequency.

For pattern synthesis these harmonics can, in principle, be used to improve the synthesised pattern. The harmonics can be thought of as additional elements in a wider effective aperture, so they could be employed to provide a narrower beam or reduce sidelobe levels, particularly as the reduced amplitude of the harmonics provides a taper. In practice, this is very difficult. As an example, let us consider a four-element array of omnidirectional elements with an array radius of $\beta r = 1.88$ - an inter-element spacing just below $\lambda/2$. If a Chebyshev taper is used to produce a pattern with -30 dB sidelobes, figure 2.17a depicts the radiation pattern formed by the fundamental modes. The effect of harmonics on the pattern can be predicted using (2.3.1), as shown in figure 2.17b. This shows that the mainlobe is severely deformed, and the sidelobe levels are increased to -15 dB.

To contribute to a low sidelobe beam oriented in the direction $\phi=0$ the modes should have equal phase. For the direction $\phi = 0°$ the two 3rd order modes are in antiphase with the two 1st order modes. While there are directions for which the 1st and 3rd order modes are cophasal ($\phi = \pm 45°, \pm 135°$), to make use of the 2nd order amplitude mode as well the beam must be formed in different azimuth directions ($\phi = 0°, \pm 90°$ or $180°$).

The Schelkunoff unit circle analysis of (2.1.2) can be used to depict the radiation patterns formed by a modal excitation, using the variable $w = e^{j\phi}$. Again the unit circle corresponds to real space, and one traverse of the unit circle corresponds to a single revolution in ϕ space. Harmonics are represented as additional roots. As an example figure 2.18 depicts a -20 dB sidelobe pattern synthesised using a four-element array of omnidirectional

(a) Chebyshev beam with
-30 dB sidelobes

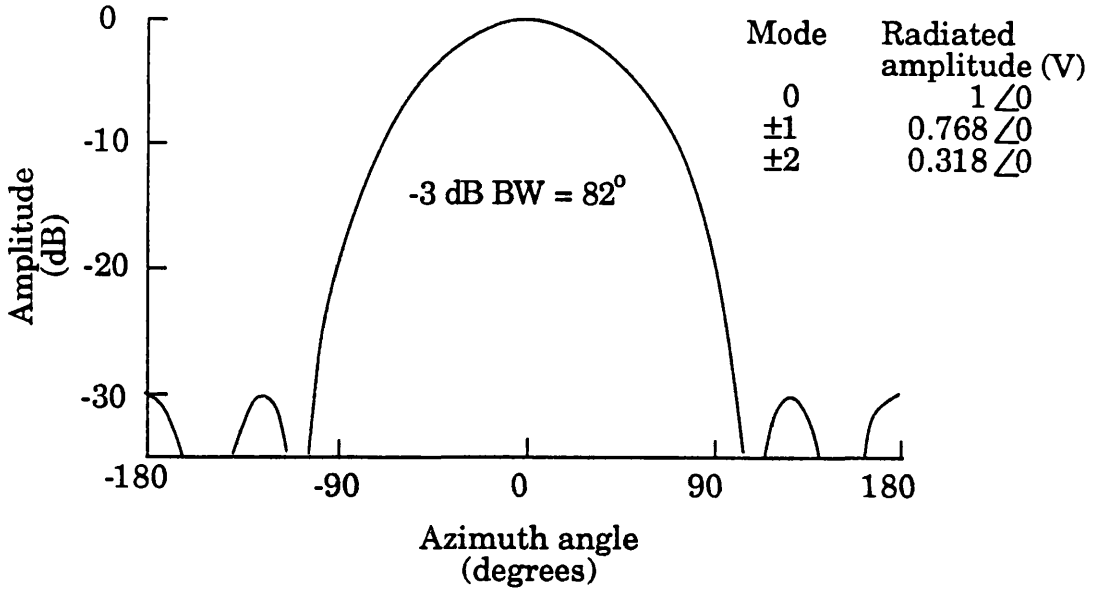

(b) Effect of harmonic
modes on the radiation pattern

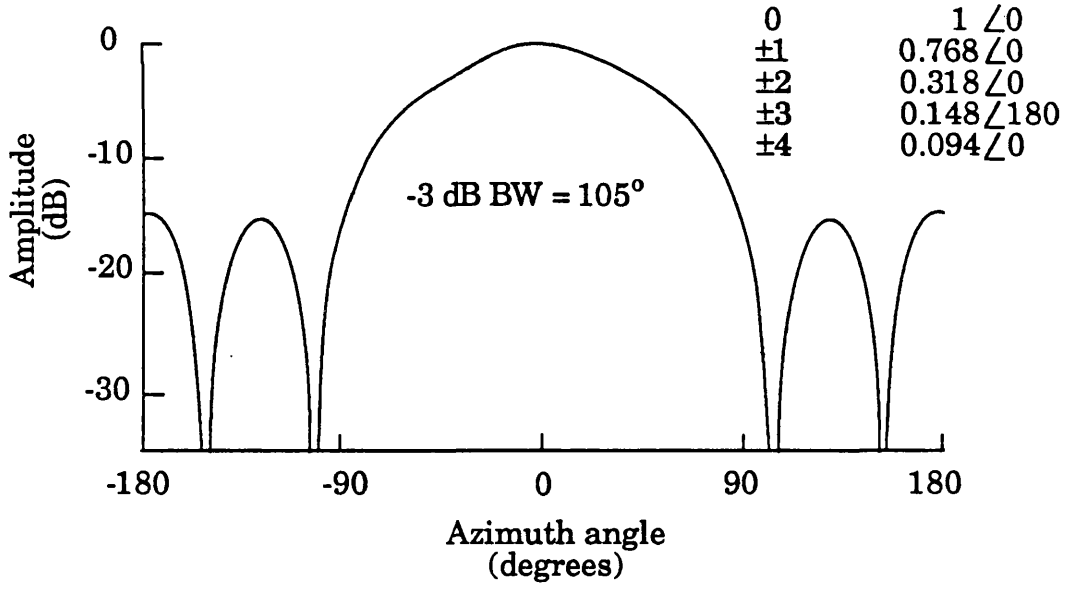

Figure 2.17 Theoretical calculation of the effect of harmonic modes on a -30 dB Chebyshev pattern for a four-element circular array of omnidirectional elements $\beta r = 1.88$, an inter-element spacing slightly less than $\lambda/2$.

Effect of low amplitude harmonics on a Chebyshev beam with -20 dB sidelobes

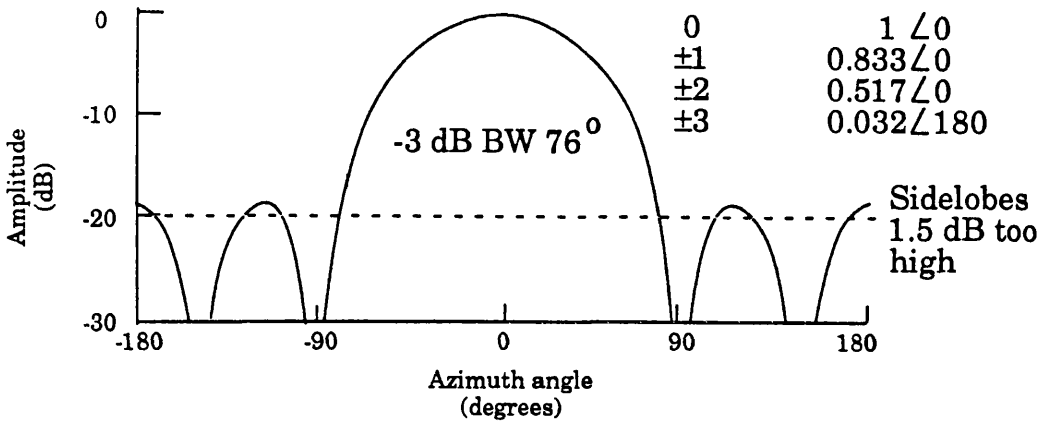

Schelkunoff unit circle representation

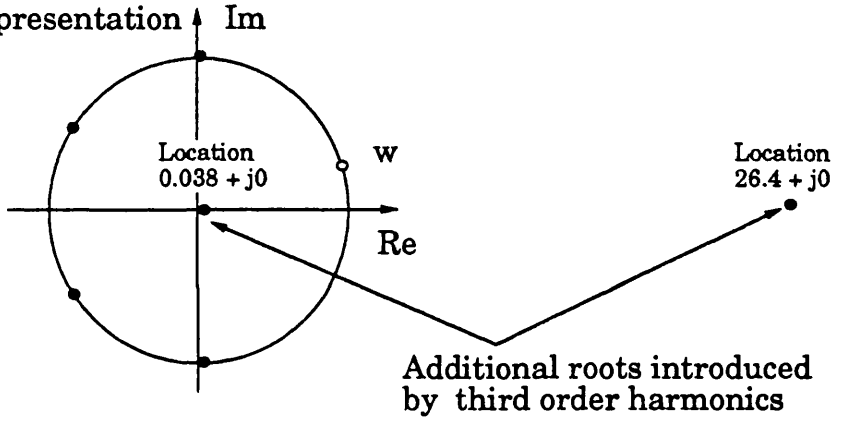

Corrected excitation using the Schelkunoff unit circle analysis

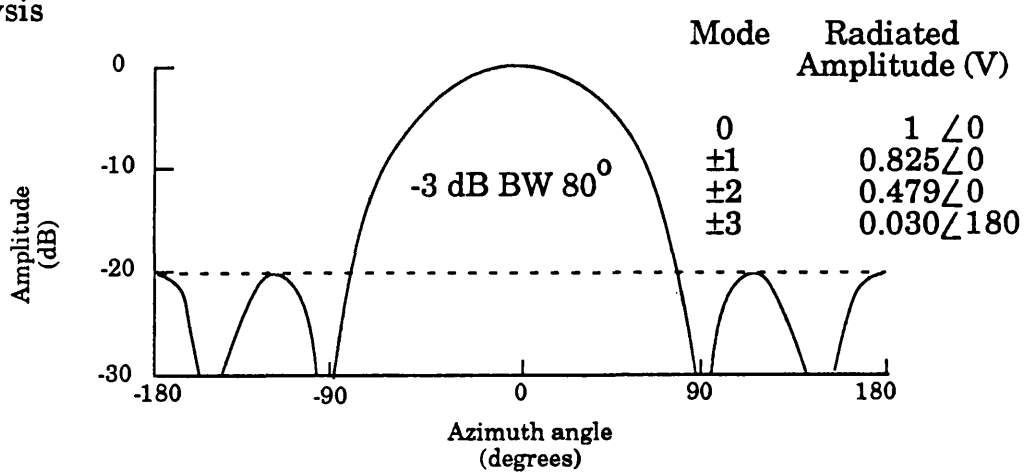

Figure 2.18 A theoretical illustration of the use of the Schelkunoff analysis on circular arrays. In this example the effect of harmonics on sidelobe levels is corrected.

elements, this time on a smaller array radius ($\beta r = 0.63$). The 3rd harmonic level of -29.8 dB increases the sidelobe level by 1.5 dB. If the excitation is factorised using (2.1.5), and the roots plotted on the w plane, two of the roots are placed well off the unit circle. By adjusting the position of the roots that are on the unit circle, using an iterative technique, the sidelobes can be reduced to -20 dB, at the expense of a small increase in the mainlobe beamwidth (figure 2.18).

In addition to degrading the pattern, any solution that includes the harmonics will be narrowband. In the case of a four-element array of omnidirectional elements, the amplitude of the third harmonic $|J_3(\beta r)|$ relative to the first order fundamental $|J_1(\beta r)|$ changes greatly with frequency, as shown in figure 2.9. This cannot be corrected, as they are excited at the same phase mode port.

To conclude, if the amplitude of the harmonic is the same as the sidelobe level, there will be a large increase (up to 6 dB) in the sidelobe level. The harmonics must be considerably lower in amplitude than the desired sidelobe level. As the theoretical phase mode coefficients for the harmonics are known, equation (2.3.1) can be used to calculate their effect on a synthesised pattern.

2.3.5 Wideband pattern synthesis with phase modes

To form patterns instantaneously across a wide frequency band requires a mode excitation A_m that changes as a function of frequency to correct for the change in the phase mode coefficient $K_m(f)$. From (2.3.4):

$$A_m = \frac{W_m}{K_m(f)} \qquad (2.3.7)$$

where W_m is the amplitude taper applied to the mth mode. As an example, consider the theoretical synthesis of the pattern of figure 2.12 using a four-element array of omnidirectional elements over the frequency range 8 to 12 GHz. The array radius chosen is 5.25 mm. The theoretical

mode amplitudes are plotted in figure 2.19, showing that the harmonics of order three and above are negligible in magnitude. For the pattern of figure 2.12 modes up to the order M = ±2 are excited with uniform amplitude in the far field. From (2.3.5) the required excitation of the modes is plotted in figure 2.19 as a function of frequency. The synthesised pattern has a constant beamwidth of 65°. By comparison, for a uniformly excited linear array there is a large change in the -3 dB beamwidth. For a five-element linear array, with an inter-element spacing of $\lambda/2$ at 10 GHz, the -3 dB beamwidth changes by 50%, from 17° at 12 GHz to 26° at 8 GHz.

2.4 Polarisation and elevation characteristics of phase modes

2.4.1 The polarisation of phase modes

In the previous analysis we have assumed that the radiation pattern produced by exciting a single phase mode is a scalar quantity. In fact the radiation pattern is a vector quantity with a certain polarisation. Any polarisation can be expressed as an orthogonal pair of polarisations, commonly vertical and horizontal.

Suppose an array element has a measured directional pattern $G_H(\psi)$ when illuminated by horizontally polarised radiation, and a pattern $G_V(\psi)$ when illuminated by vertically polarised radiation. For a given array radius r, the phase mode coefficients K_{Hm} and K_{Vm} for these orthogonal polarisations can be determined from (2.2.4). From (2.2.3), when the phase mode is excited by a source of amplitude A_m the radiation pattern has the form:

$$F(\phi) = A_m\left(K_{Vm}e^{jm\phi} + K_{Hm}e^{jm\phi}\right) \qquad (2.4.1)$$

For an amplitude comparison DF system the radiation patterns formed should ideally be the same for both vertical and horizontal polarisations (that is, $K_{Hm} = K_{Vm}$).

Phase mode coefficients for four element monopole array, radius = 5.25mm

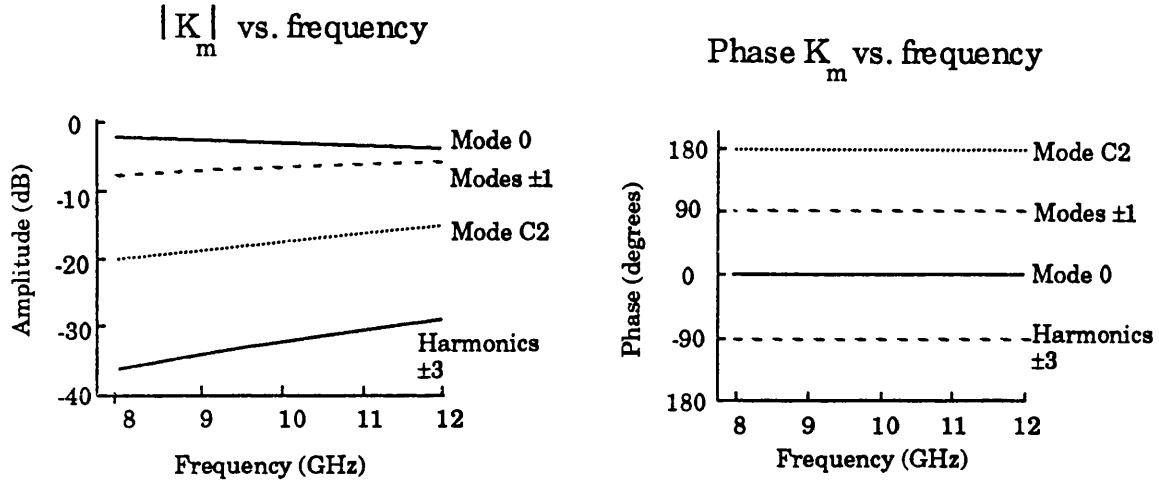

Phase mode excitation for wideband synthesis of sin(Nx)/Nsin(x) beam i.e. uniformly excited phase modes

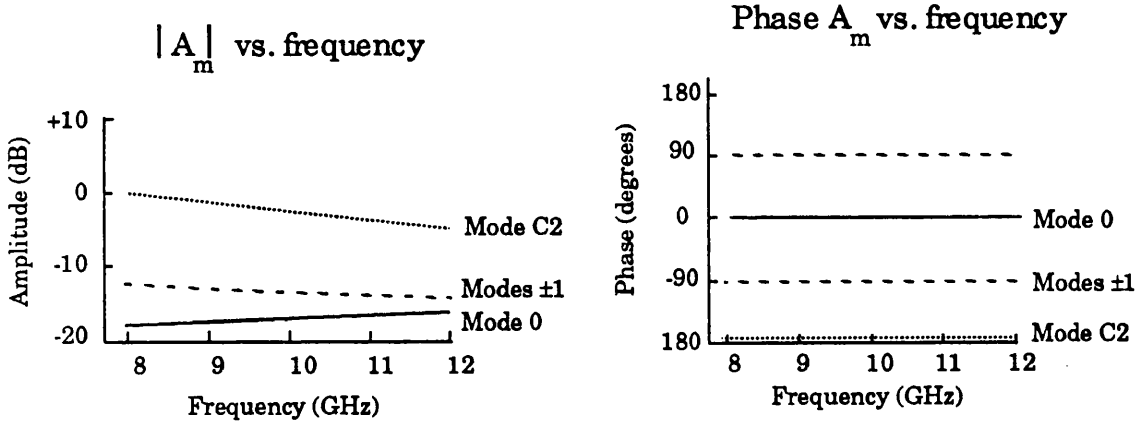

Figure 2.19 Excitation of phase modes required for the synthesis of a wideband sin(Nx)/Nsin(x) beam. The pattern has -12.1 dB sidelobes and a -3 dB beamwidth of 65°.

For many elements, for example cavity-backed spirals, the gain pattern is the same for vertical and horizontal polarisations. For the circular array proposed here, the inter-element spacing is less than $\lambda/2$, so the effect of mutual coupling on polarisation must also be considered. As an example, consider a circular array of dipoles, mounted at 45° to the vertical. The radiation pattern of a lone dipole at 45° of tilt is the same for both horizontal and vertically polarised radiation. Since the radiation pattern is the same, the phase mode coefficients K_{Hm} and K_{Vm} should be the same. However, when the element is located in the array it couples to the adjacent elements. There are electric and magnetic modes of coupling for slant dipoles. These different modes of coupling make the element radiation pattern different for vertical and horizontal polarisations. Borgiotti (1983) discusses the 'modes of coupling' between elements on cylindrical surfaces, although calculation of the changes in the radiation pattern is beyond the scope of this study.

Since array elements for which $K_{Hm} = K_{Vm}$ are not realisable, the solution adopted here is to use linear elements that are sensitive only to vertically polarised signals (that is, $K_{Hm} = 0$). The reason for selecting vertically polarised elements, rather than horizontally polarised elements becomes clear when we consider the effect of the elevation angle on polarisation. This is done in the next section.

2.4.2 The elevation characteristics of phase modes

Horizontal dipole elements are sensitive only to the horizontally polarised component of an incident signal at 0° elevation. However, as the elevation angle increases, these elements detect a component of the vertically polarised component, as shown in figure 2.20. As described above, elements sensitive to two polarisations are undesirable. Conversely, figure 2.20 shows that vertical dipole elements are insensitive to horizontally polarised incident signals, whatever the elevation angle. Elements sensitive to vertically polarised signals were adopted for this study.

For horizontally oriented dipoles the vertically polarised signal is detected at elevation angles above 0°

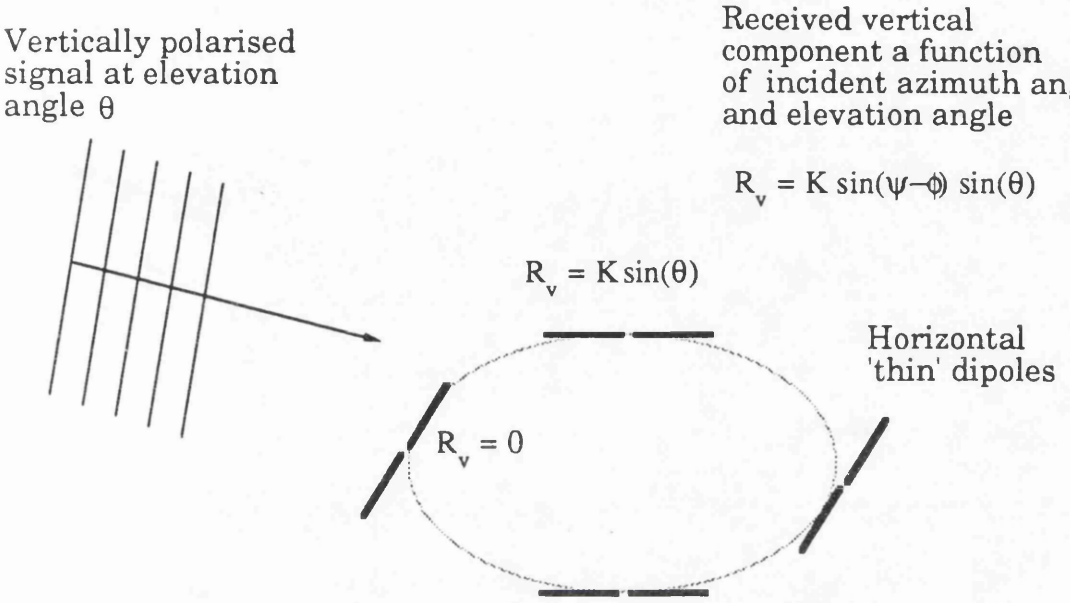

For vertically oriented dipoles there is no reception of a horizontally polarised signal

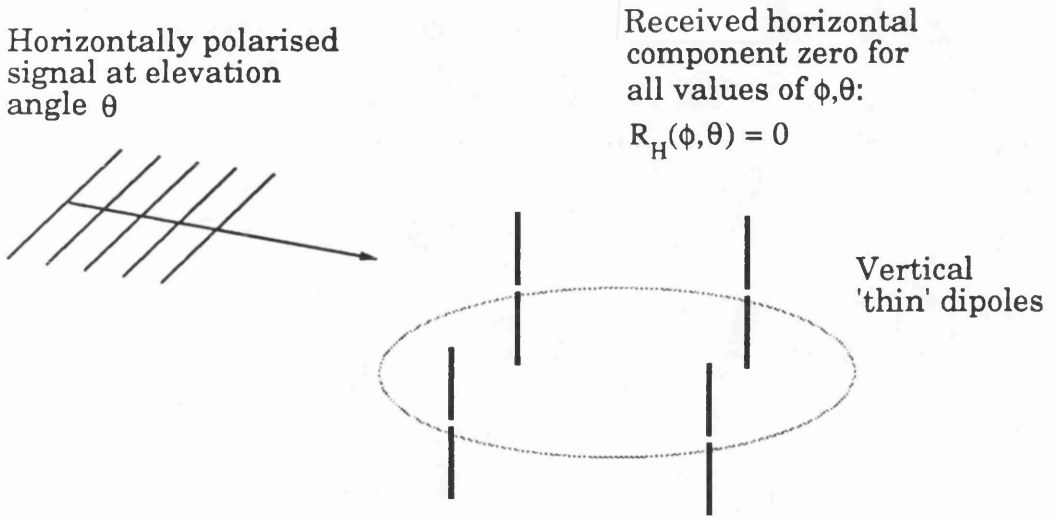

Figure 2.20 A comparision of the cross-polar performance of horizontally and vertically oriented dipoles.

When a single phase mode is excited on a circular array, the phase mode coefficients calculated in section 2.2.1 are for 0° elevation. If the azimuth pattern is measured at an elevation angle θ the radiation pattern is still a phase mode, but the phase mode coefficient K_m will have changed. For isotropic circular array elements the phase mode coefficient at an elevation angle θ is given by Davies (1983):

$$K_m(\theta) = j^m J_m(\beta r \cos\theta) \qquad (2.4.2)$$

For our DF application, directional azmuth patterns that do not change shape with elevation are required. If the modes are excited with the weights required to form a pattern at 0° elevation, the changes in K_m with elevation alter the pattern shape. As an example, consider the -20 dB sidelobe pattern of figure 2.13, formed at 0° of elevation using a four-element array where $r/\lambda = 0.175$ - sufficiently small for the effect of harmonics to be neglected. If the changes in the mode coefficients are calculated using (2.4.2) the changes in the pattern with elevation can be predicted. Figure 2.21 shows the azimuth pattern measured at elevation angles of +20° and +40°. While $J_0(\beta r \cos\theta)$ increases in amplitude with elevation, the amplitudes of the higher order modes decrease, producing a steeper amplitude taper. This produces a gradual increase in the -3 dB beamwidth, from 77° at 0° elevation to 83° at +40° elevation. The average sidelobe level initially drops, because of the increased taper, but at +40° elevation one sidelobe becomes dominant, with an amplitude of -17 dB. If directional elements are adopted, the changes in the phase mode coefficients with elevation will be less pronounced. Inspection of figure 2.9 show that the variations in K_m with the effective radius are smaller for elements with a directional pattern of the form $(1 + \cos(\psi))$.

Most practical elements have a radiation pattern $G(\phi,\theta)$ that changes in gain with elevation. Let us consider the effect of this on the phase modes. Most antennas used in DF applications have higher directivity for low elevation angles (below 40°) and reduced directivity at high elevation angles. The gain of the phase modes will change correspondingly, with higher gain

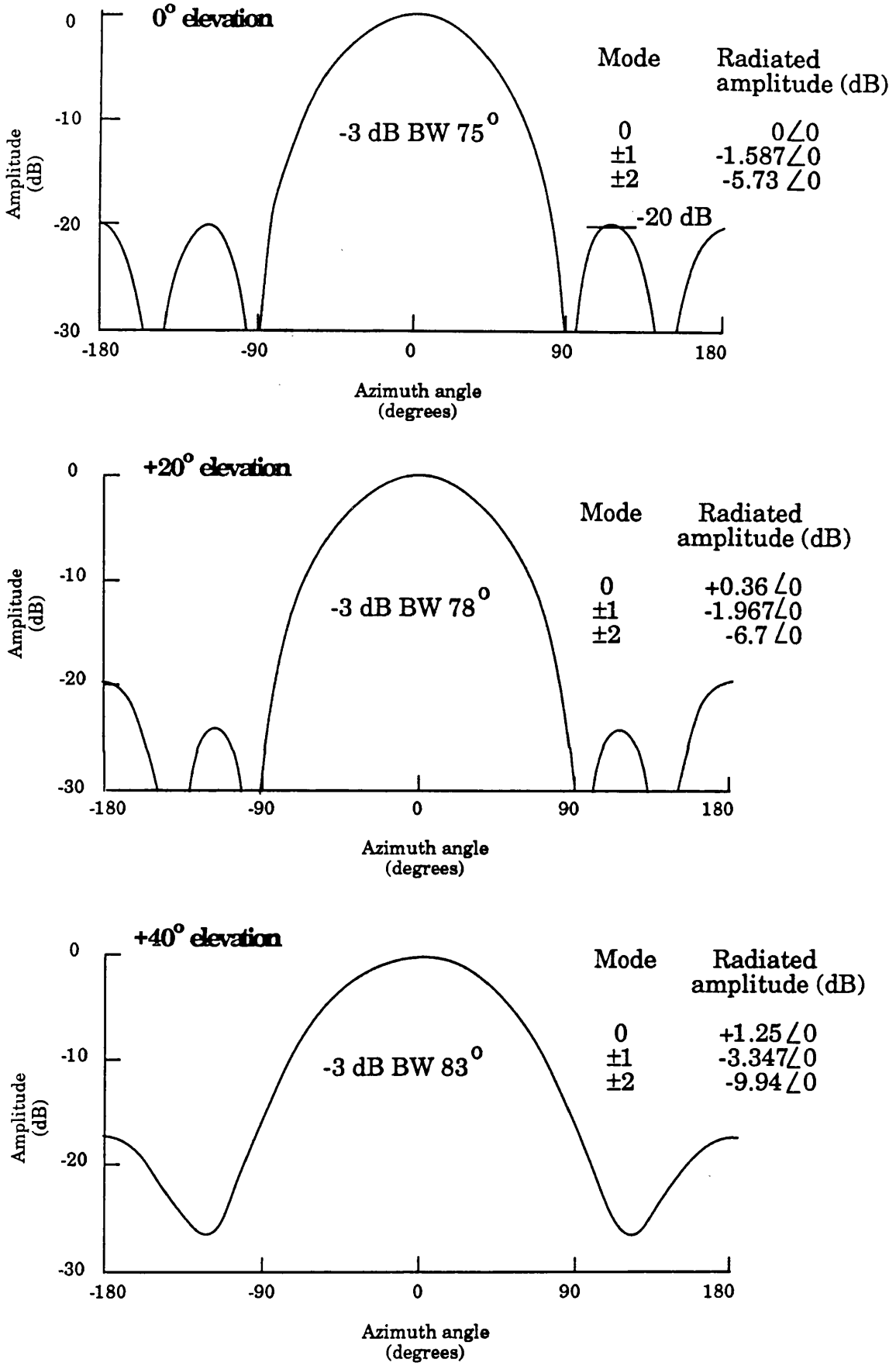

Figure 2.21 Prediction of changes in a -20dB sidelobe Chebyshev pattern with elevation. Pattern synthesised with a circular four-element circular array ($\beta r = 1.1$).

at low elevation angles. Since the gain of all the phase modes is affected equally, this does not affect the azimuth shape of the synthesised patterns, only the variation in the gain with elevation.

As an example, if vertical dipoles are used as the array elements (rather than isotropic elements) then at 0° of elevation the gain of all the modes is increased by the directivity of the dipole: 2.1 dB. Vertically above the array (90° of elevation) all the modes have zero amplitude, because the elements do not radiate in this direction. The change in gain of a phase mode G_i^m with elevation is now given by:

$$G_i^m(\theta) = G_i^E(\theta) J_m(\beta r \cos(\theta)) \qquad (2.4.3)$$

where G_i^E is the gain of the element at an elevation angle θ and J_m is the corresponding Bessel function.

Chapter 3

Circular array design and analysis

3.1 Introduction

In section 3.2 the properties of antennas used in existing DF systems are reviewed. In particular the main sources of DF error are identified, since any reduction in the DF errors is commercially desirable. This information is used to specify the beam shape to be formed for the amplitude comparison DF rôle. The number of phase modes needed to form the wideband beam is determined.

Section 3.3 considers the design of the circular array required to excite these phase modes. The array radius and array element type to be used are chosen to produce a circular array that can excite the phase modes across the frequency band 8 to 12 GHz.

Because the beams used in amplitude comparison DF are wide, their directive gain is low. Matching the feed impedance to that of the (modally excited) elements can potentially improve the gain. Section 3.4 investigates how the impedance of the circular array elements changes with frequency. A technique for calculating the phase mode impedances is compared to directly measured values. Measurements of the bandwidth over which the mode impedances can be matched are made.

As explained in chapter 2, the relative amplitudes and phase of the modes change with frequency, and accurate information about these changes is essential, so that the compensation required can be evaluated. In section 3.5 the measured radiation patterns for the array elements are compared to theory, both in the azimuth and elevation planes. A technique for calculating the amplitude and phase of the radiated phase modes is compared to directly measured results.

3.2 The use of directional beams in amplitude comparison DF

3.2.1 **An introduction to amplitude comparison DF**

The aim of this study is to synthesise wideband beams for an amplitude comparison DF system. This is done using a circular array in place of the wideband antennas used in existing systems. This type of DF system was first described by Watson-Watt and Herd (1926). Consider two vertical loop antennas, A and B, oriented at right angles to each other, both having a beam pattern with a cosine amplitude variation with azimuth angle. A plane wave, amplitude E incident from a direction ϕ, produces voltages at the element feeds:

$$V_A \propto E \cos(\phi)\cos(\theta)$$
$$V_B \propto E \cos(90 + \phi)\cos(\theta) = -E \sin(\phi)\cos(\theta)$$

where θ is the elevation angle. Comparison of these voltages (using an oscilloscope X-Y display) gives an indication of the azimuth bearing. With simple loop elements there is an ambiguity of 180° that can be eliminated by adopting unidirectional elements. Developments of this basic system are used by most of the current radar warning systems, as described by Baron, Davis, and Hofmann (1982). A typical system consists of four wideband antennas covering 360° of azimuth, as shown in figure 3.1. Gross angle of arrival is determined by the antenna receiving the strongest signal. The precise angle of arrival is calculated from the ratio of the signal amplitudes received by adjacent antennas.

3.2.2 **Amplitude comparison DF using Gaussian-shaped beams**

Lipsky (1987a) analyses the relation between the signal amplitudes received by adjacent antennas and the calculated bearing. Many modern amplitude comparison DF systems use wide bandwidth cavity-backed spiral antennas. The gain and beamwidth of a typical cavity-backed spiral antenna is illustrated in figure 3.2. These antennas can operate over a bandwidth of

Calculated angle of arrival

$$\varphi_c = F\left(\frac{P_2}{P_1}\right)$$

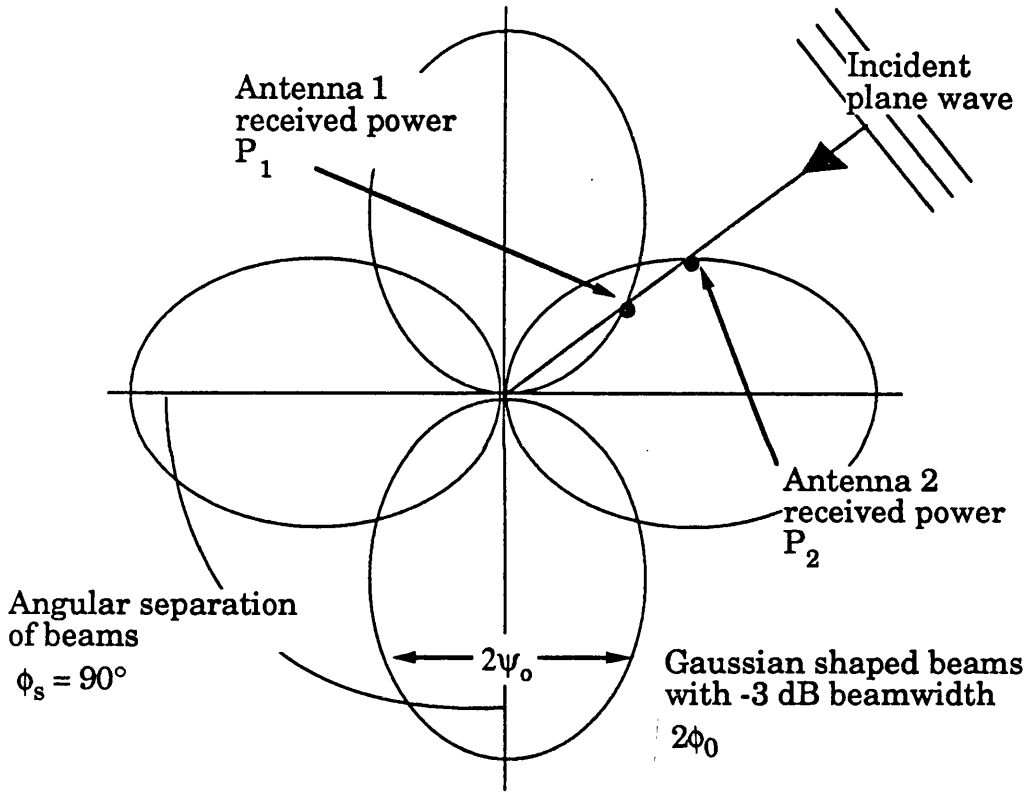

Figure 3.1 Amplitude comparison DF using four wideband antennas for 360° coverage.

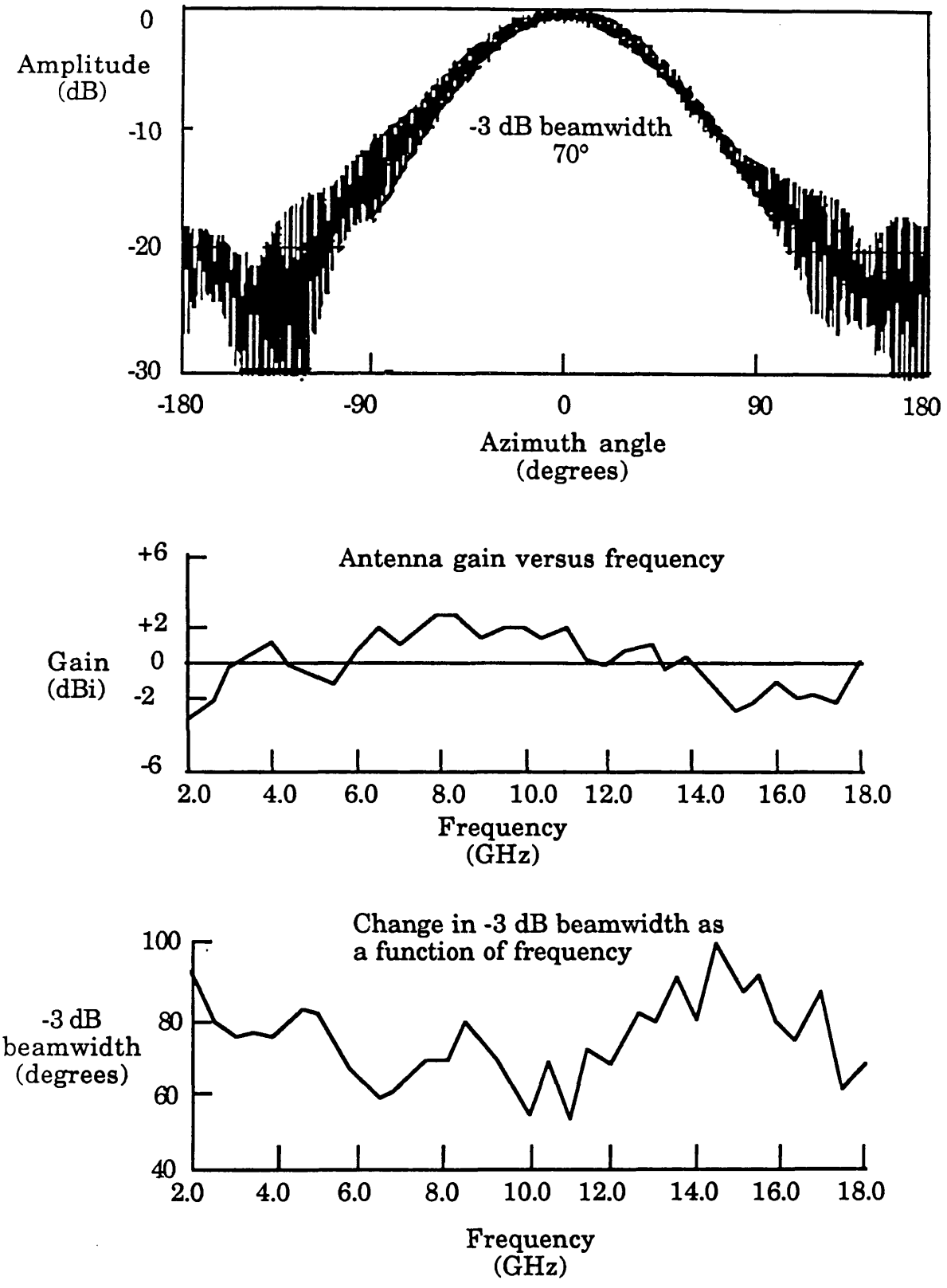

Figure 3.2 Typical gain and beamwidth characteristics for a cavity backed spiral antenna (after Lipsky (1987b)).

close to a decade. The beam of a cavity-backed spiral antenna is approximately Gaussian in shape, with a power pattern of the form:

$$P(\phi) = \exp\left[-K\left(\frac{\phi}{\phi_0}\right)^2\right]$$

where ϕ_0 is half the antenna -3 dB beamwidth (in radians) and K is a constant of proportionality (typically K = 0.69). The power received by antenna 1 is:

$$P_1 = \exp\left[-K\left(\frac{\phi_s/2 + \varphi}{\phi_0}\right)^2\right] \qquad (3.2.1)$$

Here the azimuth angle of arrival φ is measured from the crossover point between adjacent beams, and ϕ_s is the angular separation between the antenna beams. The amplitude ratio R, also called the monopulse ratio, is given by the ratio of the received amplitudes in dB:

$$R = 10\log_{10}\frac{P_2}{P_1}$$

$$= \frac{10K\log_{10}}{\phi_0^2}\left[\exp\left\{\left(\frac{\phi_s}{2} + \varphi\right)^2 - \left(\frac{\phi_s}{2} - \varphi\right)^2\right\}\right]$$

$$= \frac{20K\phi_s\log_{10}(e)}{\phi_0^2}\varphi \qquad (3.2.2)$$

For Gaussian beams the amplitude ratio (in dB) is therefore a linear function of the azimuth angle φ. For a measured value of R the calculated azimuth angle φ_C is given by:

$$\varphi_C = \frac{\phi_0^2}{6\phi_s} R = CR \tag{3.2.3}$$

The linear slope C is determined by the angular separation ϕ_s and the antenna -3 dB beamwidth ($2\phi_0$) alone. Using a look-up table the calculated angle of arrival φ_C can readily be determined from the amplitude ratio R. If the antenna has a constant beamwidth over the operating frequency band, and the boresight direction of the beams does not change with frequency, just one look-up table is required. In an ideal system $\varphi_C = \varphi$. Let us consider the main sources of error in a practical amplitude comparison DF system.

3.2.3 DF errors in an amplitude comparison system

The effect of amplitude imbalance between channels on DF accuracy

If there is a difference in gain between the two channels that give the amplitude ratio, the DF error $\Delta\varphi_C$ is determined by calculating the partial derivative of φ_C with respect to R. From (3.2.3):

$$\frac{\partial \varphi_C}{\partial R} = \frac{\phi_0^2}{6\phi_s}$$

and

$$\Delta\varphi_C = \left(\frac{\phi_0^2}{6\phi_s}\right) \Delta R \tag{3.2.4}$$

The effect of an imbalance ΔR on DF accuracy is plotted in figure 3.3 for a four-antenna DF system, showing that imbalance errors can be greatly reduced by using beams with a narrower -3 dB beamwidth. The beams must, of course, be wide enough to overlap with the adjacent beams.

The effect of changes in the angular separation of beams on DF accuracy

The boresight direction of wideband beams can squint with frequency, resulting in changes in the angular separation between beams. The resulting DF error is determined by calculating the partial derivative of φ_C with respect to ϕ_s from (3.2.3):

$$\frac{\partial \varphi_C}{\partial \phi_s} = -\frac{R\phi_0^2}{6\phi_s^2} = -\frac{\varphi_C}{\phi_s}$$

so the magnitude of the DF error $\Delta\varphi_C$ is a function of the incident angle:

$$\Delta\varphi_C = -\left(\frac{\varphi}{\phi_s}\right)\Delta\phi_s \qquad (3.2.5)$$

Figure 3.3 shows a plot of the DF error as a function of the error in the angular separation for antennas with a 90° -3 dB beamwidth Gaussian beam.

The effect of changes in the antenna beamwidth on DF accuracy

Changes in the -3 dB beamwidth ($2\phi_0$) with frequency introduce a DF error that is calculated from the partial derivative of φ_C with respect to ϕ_0. From (3.2.3):

$$\frac{\partial \varphi_C}{\partial \Psi_0} = \frac{2\phi_0 R}{6\phi_s}$$

DF error as a function of the channel imbalance

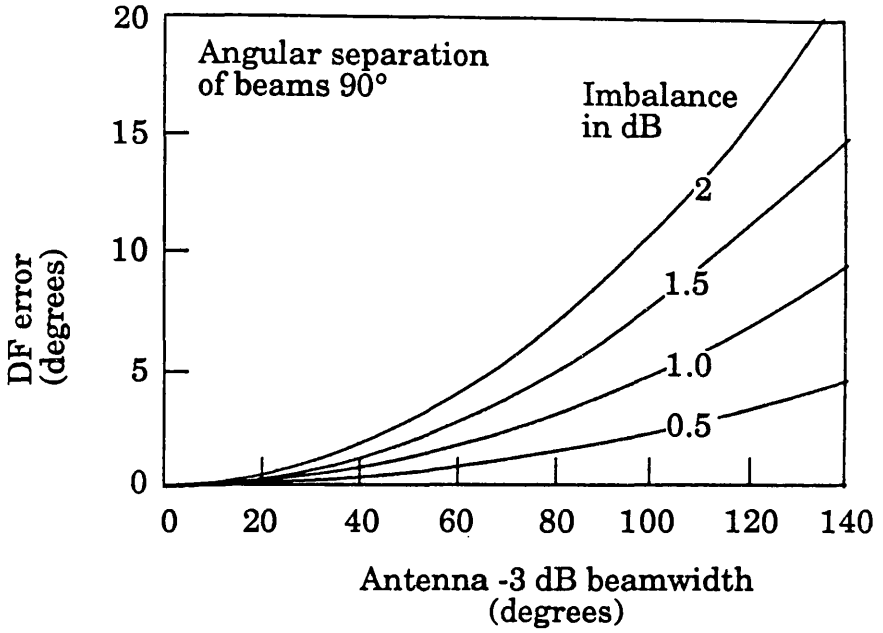

DF error as a function of the beam squint error $\Delta\phi_s$

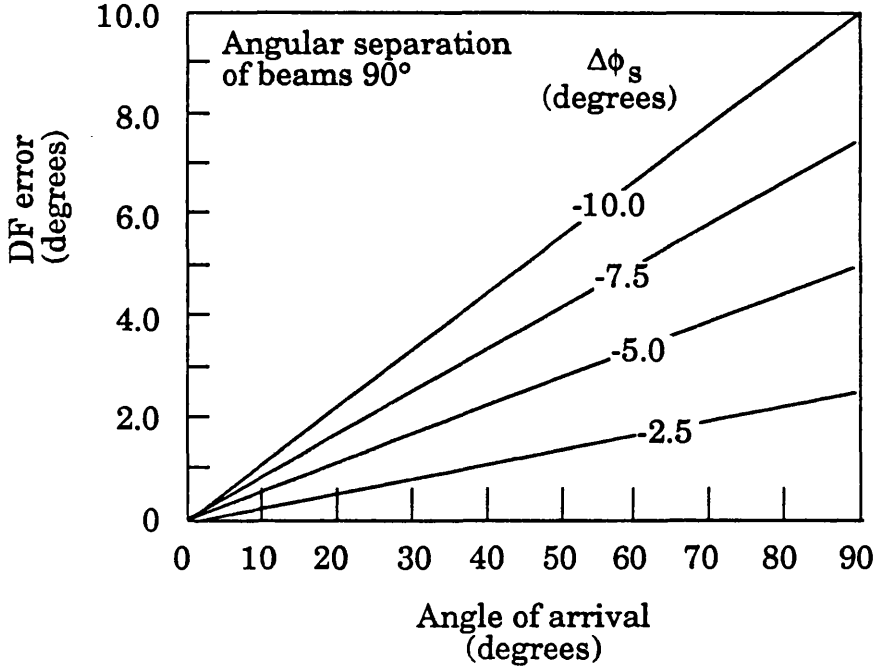

Figure 3.3 DF errors introduced by channel imbalance and squint errors in a four-element amplitude comparison DF system (after Lipsky (1987a)).

Substituting for R gives:

$$\Delta\varphi_C = 2\frac{\varphi}{\phi_0}\Delta\phi_0 \qquad (3.2.6)$$

The DF error introduced by a variation in the -3 dB beamwidth ($\Delta\phi_0/2\phi_0$) is plotted in figure 3.4 for a four-antenna DF system.

In the boresight direction of antenna 2 the the ratio P_2/P_1 is at a maximum R_{max} so from (3.2.2):

$$R_{max} = \frac{3\phi_s^2}{\phi_0^2} \qquad (3.2.7)$$

For Gaussian beams with a -3 dB beamwidth of 90°, where $\phi_s = 90°$, R_{max} is 12 dB. For narrow beams the change in the ratio R with azimuth $dR/d\varphi$ is large. This reduces the effect of imbalance errors, as depicted in figure 3.2. So from accuracy considerations the -3 dB beamwidth should be small. However, this does mean that more beams are required to cover 360° of azimuth.

Signal processing on weak signals suffers from two problems: first it may be buried in noise, a problem considered in the next section. Secondly, signals picked up in sidelobes may disturb the DF operation. Signals incident from azimuth angles outside the mainlobes are received on sidelobes. This is analogous to active radar systems, where jammers 'inject' signals into sidelobes after the main radar beam has passed, introducing an error into the azimuth angle. The same problem affects amplitude comparison DF systems.

As an example consider an amplitude comparison system of using four beams with a -3 dB beamwidth of 90° and a sidelobe level of -20 dB. Suppose a weak signal is incident from a direction of 0°, the boresight direction of

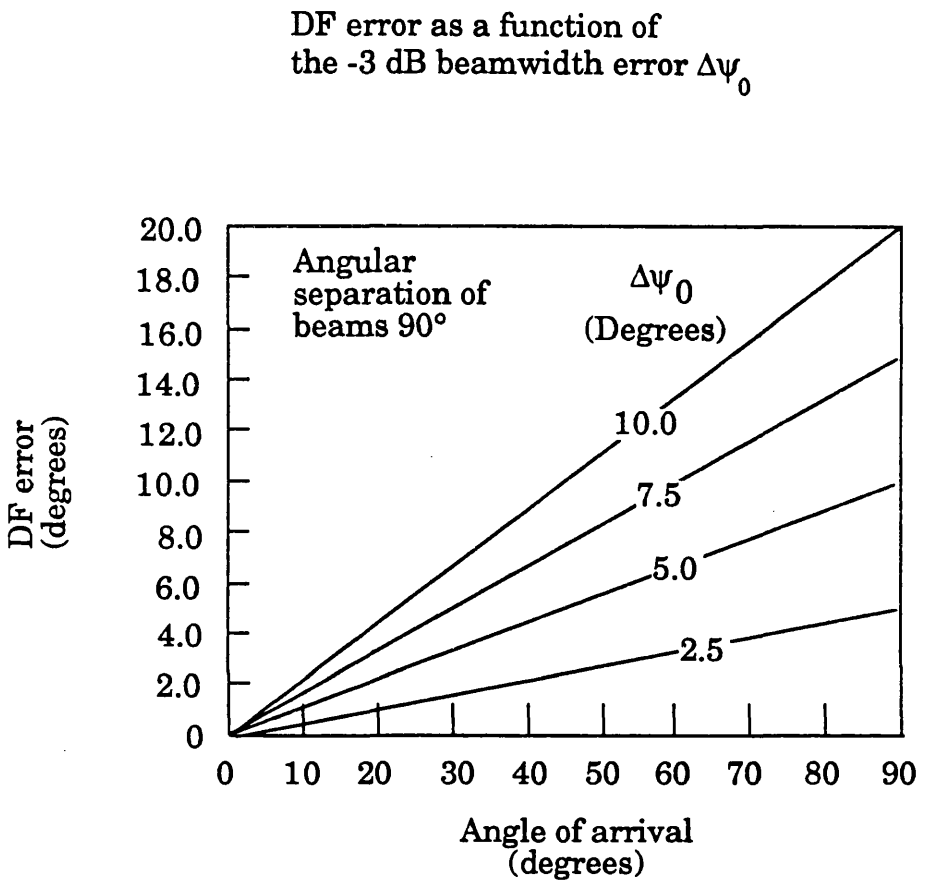

Figure 3.4 DF errors introduced by changes in the -3 dB beamwidth in a four-element amplitude comparison DF system (after Lipsky (1987a)).

element 1, with a received amplitude x dBm. The amplitude received by beam 2 is $(x - R_{max})$ dBm. This ratio R_{max} accurately indicates the signal to be in the 0° direction. Suppose a jamming signal with an intensity of y dBm is received by element 4 from the $\phi = 180°$ direction and this signal is picked up by a -20 dB sidelobe of element 2, with an amplitude (y - 20) dBm. The output of the receiver connected to element 2 is increased, shifting the indicated bearing of the signal from 0° towards +90°. If the jamming signal is strong i.e. if $(y - 20) \geq (x - R_{max})$, gross DF errors will occur. This problem can be alleviated by the use of thresholds to detect when strong signals are present. For larger values of R_{max}, the DF accuracy is more susceptible to jammers. Reducing sidelobe levels, one of the main aims of this study, is clearly beneficial.

A jammer incident from an angle within adjacent mainlobes does not affect amplitude comparison DF - the system provides an accurate indication of the jammer bearing. If both signal and jammer are incident on adjacent beams, the indicated DF bearing will lie between the angles of the two signals, at an angle closer to the stronger signal.

The effect of noise on DF accuracy

In an instantaneous amplitude comparison DF system each channel has its own dedicated intercept receiver. Noise introduced by the receiver components limits the DF accuracy for low amplitude signals. The noise characteristics of receivers is beyond the scope of this study. However, we will briefly consider the effect of noise on DF for the simplest receiver; the wideband video detector diode with the equivalent circuit of figure 3.5. There are three main types of noise generated by a diode. If the diode is unbiased, the output is just thermal noise, $4KT\Delta f$, where K is Bolzmann's constant, T is the temperature in degrees Kelvins and Δf is the noise bandwidth of the detector diode. If the diode is biased, shot noise proportional to the bias current is generated. This simple analysis will neglect the third type of noise; flicker (or 1/f noise). Torrey and Whitner (1948) calculate the noise output from thermal and shot noise. The shot

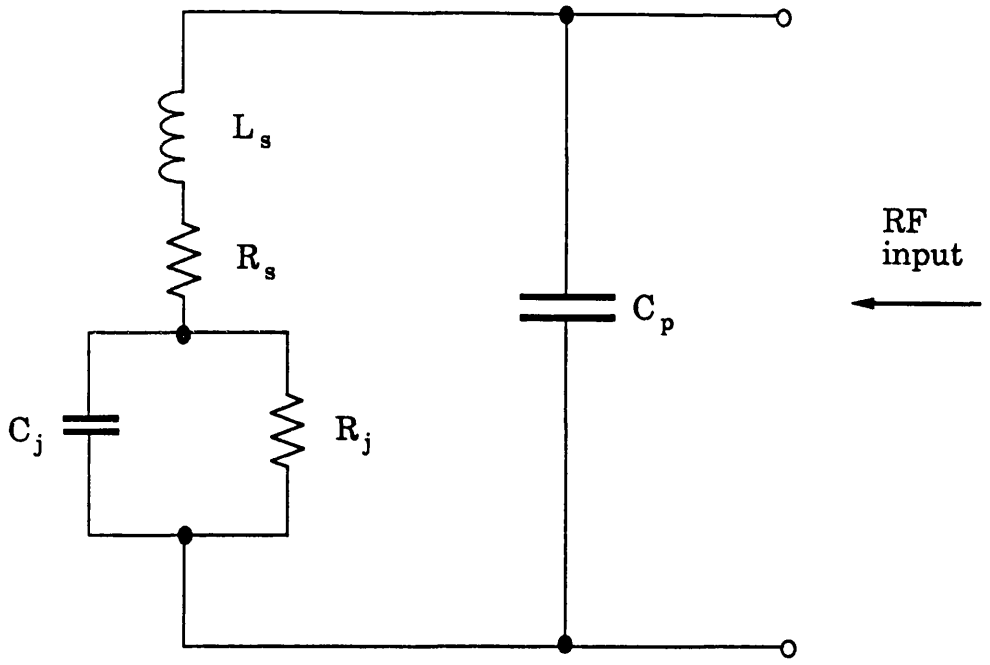

C_j is the diode junction capacitance

R_j is the diode junction resistance

R_s is the base spreading resistance

L_s is the lead inductance

C_p is the mount capacitance

Figure 3.5 The equivalent circuit of a detector diode (after Lipsky (1987c)).

noise power N_S introduced by the junction resistance is defined as:

$$N_S = 2 e I R_j \Delta f$$

where I is the total diode current

e is the charge on an electron, 1.6×10^{-19} C

Δf is the noise bandwidth of the detector diode

R_j is the diode junction resistance of figure 3.5

The total thermal and shot noise power output N_T for the equivalent circuit of figure 3.5 is:

$$N_T = \frac{R_j N_S + R_s K T \Delta f}{R_s + R_J} \qquad (3.2.8)$$

where R_s is the base spreading resistance of figure 3.5

One measure of the sensitivity of a detector diode is the 'Tangential Sensitivity', defined as the RF input required so that the amplitude of the signal plus noise just exceeds the peak noise level. Typically an RF input of -50 dBm is required for a video bandwidth of 2 MHz.

Lipsky (1987d) computes the DF error produced by a given noise level. Expressing the error in the calculated azimuth angle in terms of the signal-to-noise ratios in the two DF channels:

$$\Delta\varphi_{RMS} = \frac{1.446\,\phi_0^2}{\phi_s} \sqrt{\frac{N_T}{S_1} + \frac{N_T}{S_2}}$$

The diode noise power N_T is the same for both channels. The DF error is a minimum at the crossover point where $S_2 = S_1 = S$ and is a maximum in the boresight direction of an antenna. The signal-to-noise ratio is also a function of the incident field strength. For a given signal-to-noise ratio (S/N_T) the DF error can be plotted as a function of azimuth. Figure 3.6 plots

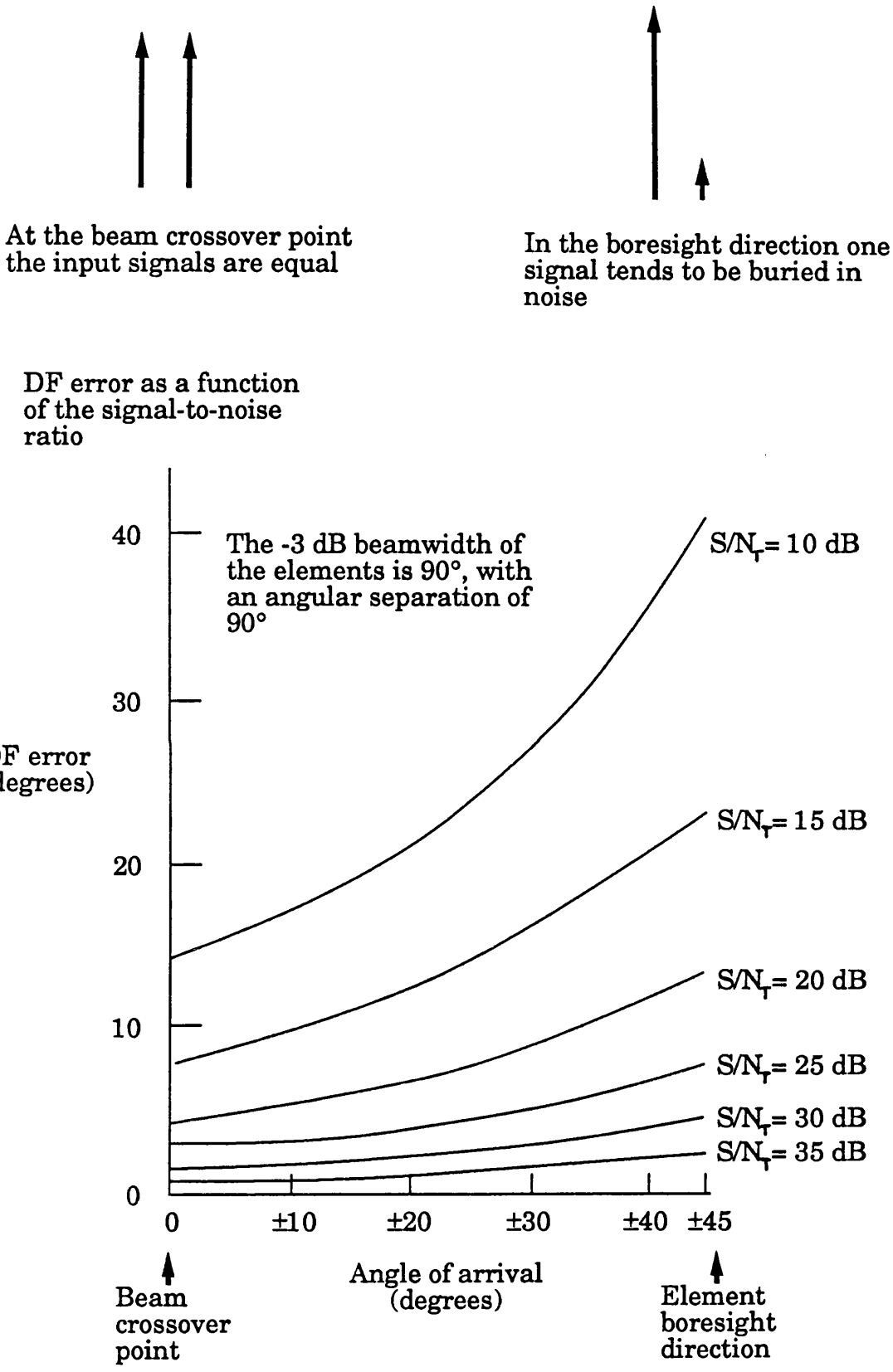

Figure 3.6 DF error introduced by noise in a four-element amplitude comparison DF system.

the effect of noise on DF error, for a selection of signal-to-noise ratios, for a four-beam system where the -3 dB beamwidth of the elements is 90°. Clearly for larger values of R_{max}, the DF accuracy is more susceptible to noise.

3.2.5 The synthesis of beams for amplitude comparison DF using phase modes

From this analysis of amplitude comparison DF systems the required radiation pattern can be specified. For this study to have a practical application to amplitude comparison DF, the synthesised beams should have wideband properties significantly better than the cavity-backed spiral antennas currently used:

- The phase comparison DF system of Karavassilis (1984) demonstrated a four-element circular array operating over an HF bandwidth of 1.2 decades; wider than the (decade) bandwidth of a cavity-backed spiral. The microwave components available for this study operate over the frequency range 8 to 12 GHz, so pattern synthesis can only be demonstrated over half an octave bandwidth. Nevertheless, the potential for wider bandwidth operation can be analysed in this study.

- The mainlobe of the synthesised pattern should have a Gaussian shape so (from (3.2.2)) the change in the amplitude ratio with azimuth is a linear function. This allows us to adopt the intercept receivers and signal processing components of existing amplitude comparison DF systems. The mainlobe does not have to be perfectly Gaussian. Minor deviations mean that the change in the DF ratio with azimuth will not be perfectly linear. This can be corrected by a modified look-up table. The boresight direction of the synthesised beams should not change with frequency.

- The absolute gain of the beam should be better than that of existing DF elements such as cavity-backed spirals - see figure 3.2. A figure of 0 dBi is acceptable. A degree of variation in the absolute gain with frequency is

acceptable, since this does not affect the amplitude ratio of (3.2.3).

- The maximum value of the DF ratio R_{max} occurs for signals incident from the boresight beam direction. For the cavity-backed spiral R_{max} is about 14 dB. This is a good compromise between good DF accuracy on strong signals and sensitivity to noise on weak signals. For a Gaussian beam this corresponds to a beamwidth of about 360°/N, where N is the number of beams.

- The synthesised beams should have a constant -3 dB beamwidth as a function of frequency. Any change will seriously affect DF accuracy. Inspection of figure 3.2 shows that for a cavity-backed spiral the -3 dB beamwidth changes typically by ±10° over the frequency range 8 to 12 GHz. In theory radiation patterns with a perfectly constant beamwidth can be formed with a circular array, provided changes in the phase mode coefficients with frequency are compensated - see section 2.3.5.

- The synthesised beam should have an azimuth beamwidth that does not change when a cut of the azimuth beam is measured at elevation angles above $\theta = 0°$. In this case a single wideband look-up table of indicated angle φ_c against amplitude ratio R will suffice. The theoretical variation in the azimuth -3 dB beamwidth with elevation of Chebyshev beams synthesised from phase modes is analysed in section 2.4.2. This predicted a variation of less than ±4° on a -3 dB beamwidth of 79°, over the elevation range from 0° to +40°.

- The synthesised pattern should have low sidelobes. This reduces the susceptibility of the system to jamming by high powered wideband sources. Typically cavity-backed spiral antennas have sidelobes of about -20 dB. By applying linear array equivalence to phase modes any desired sidelobe level can be realised, albeit at the expense of an increase in beamwidth. A sidelobe level of -30 dB will be aimed for in this study, 10 dB lower than that of cavity-backed spirals. The reason for this choice of sidelobe level becomes clearer later; both spatial harmonics and errors in the excitation of the array by the beamformer set this sidelobe level.

- Cavity-backed spiral antennas are circular polarised. As explained in section 2.4.1 the circular array will use elements that are sensitive to vertically polarised signals only, so the horizontally polarised component of an incoming signal is not detected.

The beam of figure 3.7 can be formed using a four-element circular array. Applying a Chebyshev amplitude taper gives equal level -30 dB sidelobes, as described in section 2.1.4. This plot shows that the mainlobe of the Chebyshev mainlobe is approximately Gaussian in shape. The DF calculations of section 3.2 remain valid, although the wideband look-up table of indicated angle φ_c against amplitude ratio R will not be perfectly linear. If four overlapping beams are used, the -3 dB beamwidth of 82° gives a maximum DF ratio R_{max} of 15 dB. The theoretical study of section 2.4.1 predicted that beams formed from compensated phase modes do not squint, either as a function of frequency or elevation. The absolute gain will depend on the gain of the array elements selected, considered in the next section.

3.3 Circular array design

3.3.1 **The number of elements**

Butler matrices excite circular arrays with a number of elements N in the series 1, 2, 4, 8, 16, ...2^n. For an N-element array, the highest order phase mode that can be excited independently is M = N/2. Since the complexity of the Butler matrix increases rapidly as the number of elements increases, the number should be kept to a minimum. The simplest circular array uses just two elements connected to a single 180° coupler. This forms the 0^{th} order mode and one amplitude mode with a cos(ϕ) azimuth pattern. This array can form radiation patterns with two (non independent) nulls, insufficient for this study. A four-element circular array connected to a 4 x 4 Butler matrix can excite the 0^{th}, ±1 and ±2 order phase modes, forming patterns with four nulls. The -30 dB sidelobe pattern of figure 3.7 can be formed with these modes. Since a second 4 x 4 Butler matrix can form four beams with the required

Mode	Radiated amplitude (dB)
0	0∠0
±1	-2.29 ∠0
±2	-9.94 ∠0

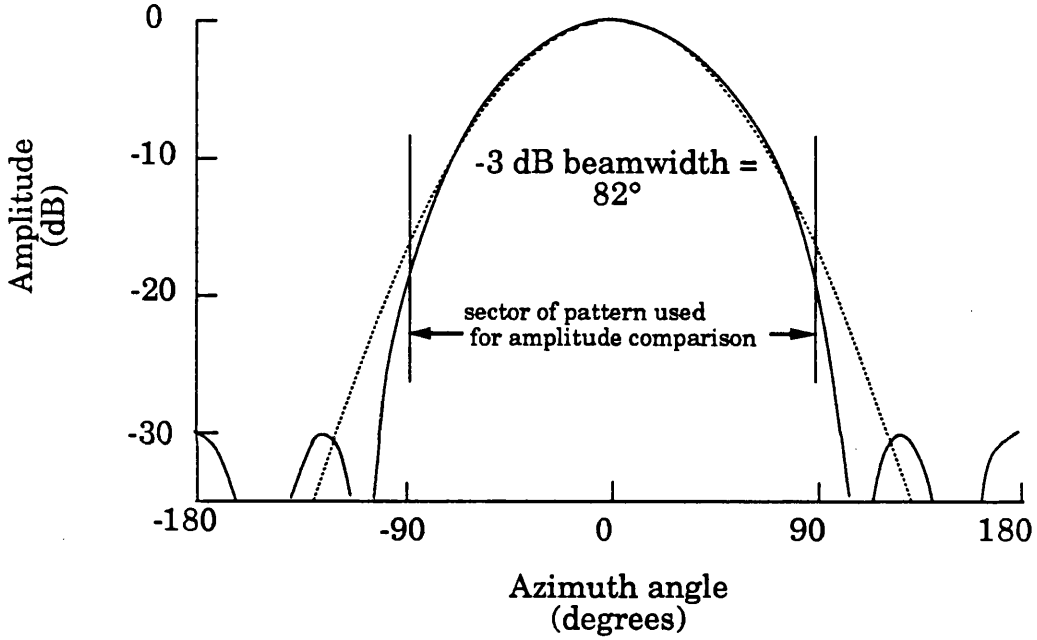

Chebyshev -30 dB sidelobe pattern

Gaussian pattern with same -3 dB beamwidth

Figure 3.7 Comparison of the mainlobe shape for a Chebyshev beam to a Gaussian curve.

separation of 90°, all the requirements for an amplitude comparison DF system are fulfilled.

An eight-element circular array connected to an 8 x 8 Butler matrix can excite phase modes up to the 4th order. These can be used to form a narrower (~45°) beamwidth Chebyshev beam suitable for an eight-beam DF system. With narrower beams greater DF accuracy is possible and tolerance to jammers is improved. A second 8 x 8 Butler matrix can form eight beams, spaced 45° apart in azimuth. This system would require two 8 x 8 matrices with (N/2) $\log_2(N)$ couplers, 24 altogether. A four-element circular array was chosen for this study for two reasons. First, the cost of 24 couplers was prohibitive. Secondly, considerable difficulty was encountered in building microwave 4 x 4 Butler matrices, simple RF networks compared with 8 x 8 matrices. The problems encountered in the construction of beamforming networks will be discussed in chapter 4.

3.3.2 **The array radius**

As described in section 2.3.4, the upper limit on the array radius is determined by the magnitude of the harmonic terms. The magnitude of the harmonic, relative to the fundamental, should be less than the specified sidelobe level, -30 dB in this case. For a four-element circular array the 3rd order mode is the most significant harmonic, as it has the highest amplitude. The amplitude of the 3rd harmonic is determined by its phase mode coefficient. The amplitude of this harmonics is plotted in figure 2.9 for both arrays of omnidirectional elements and elements with a $(1 + \cos(\psi))$ directional pattern. In either case the effective array radius (r/λ) must be less than 0.15 for the 3rd harmonic to be below -30 dB in amplitude. So at the top of the band (12 GHz):

$$r/\lambda < 0.15 \qquad (3.3.1)$$

giving a radius below 3.75 mm and an inter-element spacing of 5 mm. For this small inter-element spacing the phase mode coefficient for the second

order mode is low in amplitude (~ -15 dB) relative to the 0^{th} order mode. This is because the real part of the phase mode impedance for this mode (calculated in section 2.2.5) is small for close-spaced elements. As the frequency drops, this mode becomes a superdirective excitation of the circular array, with a rapid change of phase (π radians) between elements less than $\lambda/4$ apart. While a large amplitude taper on the 2^{nd} order mode is actually needed for the Chebyshev beam, the problem of exciting the mode with the strict tolerance required for a superdirective excitation remains.

Increasing the number of elements in the array does little to reduce the problem of harmonics. Theoretical synthesis studies based on equation (2.3.1) showed that the effect of the 5^{th} order harmonics on Chebyshev beams formed by an eight-element array were very similar to the effect of 3^{rd} order harmonics on Chebyshev beams formed by a four-element circular array. The eight element system has a small advantage because the narrower mainlobe has a higher directive gain, and consequently the relative level of sidelobes caused by harmonics is lower.

Let us briefly consider the circular array design for a different application. Suppose a sin(Nx)/Nsin(x) pattern was required, by exciting the phase modes with equal amplitudes. If four omnidirectional elements are used, an array radius of about $r/\lambda \approx 0.3$ is suitable. For this radius the 0^{th}, 1^{st} and 2^{nd} order modes have theoretical amplitudes (figure 2.9a) within 5 dB of one another. For this radius the 3^{rd} order mode has an amplitude of about -23 dB, but the effect on -13 dB sidelobes of this harmonic would be small. The gain could be improved by adopting elements with a directional pattern, possibly by using a pillar at the centre of the array to act as a simple reflector. With a shallow $\{1 + \cos(\phi)\}$ element pattern the 0^{th}, 1^{st} and 2^{nd} order modes have theoretical amplitudes (figure 2.9b) within 2 dB of one another, for an array radius of $r/\lambda = 0.353$. The 3^{rd} order mode, at an amplitude of -15 dB increases the first sidelobes by about 2 dB to -10.2 dB, calculated using (2.3.1).

3.3.3 Selection of the element type

As explained in section 2.4.1, elements with a single linear polarisation are required. The microwave antennas considered included horns, slots, dipoles, monopoles and the 'Vivaldi Aerial' of Gibson (1979). The separation of the element phase centres needed is just 5 mm. This small inter-element spacing severely limits the choice of elements. Most of the elements considered were physically too large to meet this criterion. Since the element aperture is small the elements will have radiation patterns that are omnidirectional, or with low directivity.

For an antenna facing an infinite flat reflector, the phase centre of the image lies behind the plane of the reflector. The possibility of using elements such as horns, but facing a central reflector was considered, but rejected because of its complexity. This idea is discussed further in chapter 6.

The only elements small enough to fit 5mm apart were vertically oriented dipoles or monopoles. Even with dipoles, the semi-rigid coaxial feeds were very large relative to the size of the array, causing location problems. An array with four vertical monopoles located on a ground plane 50 cm in diameter was finally adopted. The monopoles were fed from under the ground plane by the 0.3 mm wide centre conductor of a semi-rigid cable, with the outer soldered to the ground plane. Monopoles 7.5 mm long, resonant at the centre of the band (10 GHz), were chosen to maximise the gain. Elliott (1981c) notes that the real part of the monopole impedance is largely independent of the monopole thickness, but the change in the reactive component with frequency is less for thick monopoles. For this study 1 mm diameter monopoles were used. Figure 3.8 is a photograph of this array (constructed at UCL).

Rahim and Davies (1982) recommend the use of directional elements, rather than omnidirectional elements for wideband performance. To make the elements directional, the use of a central pillar as a reflector was

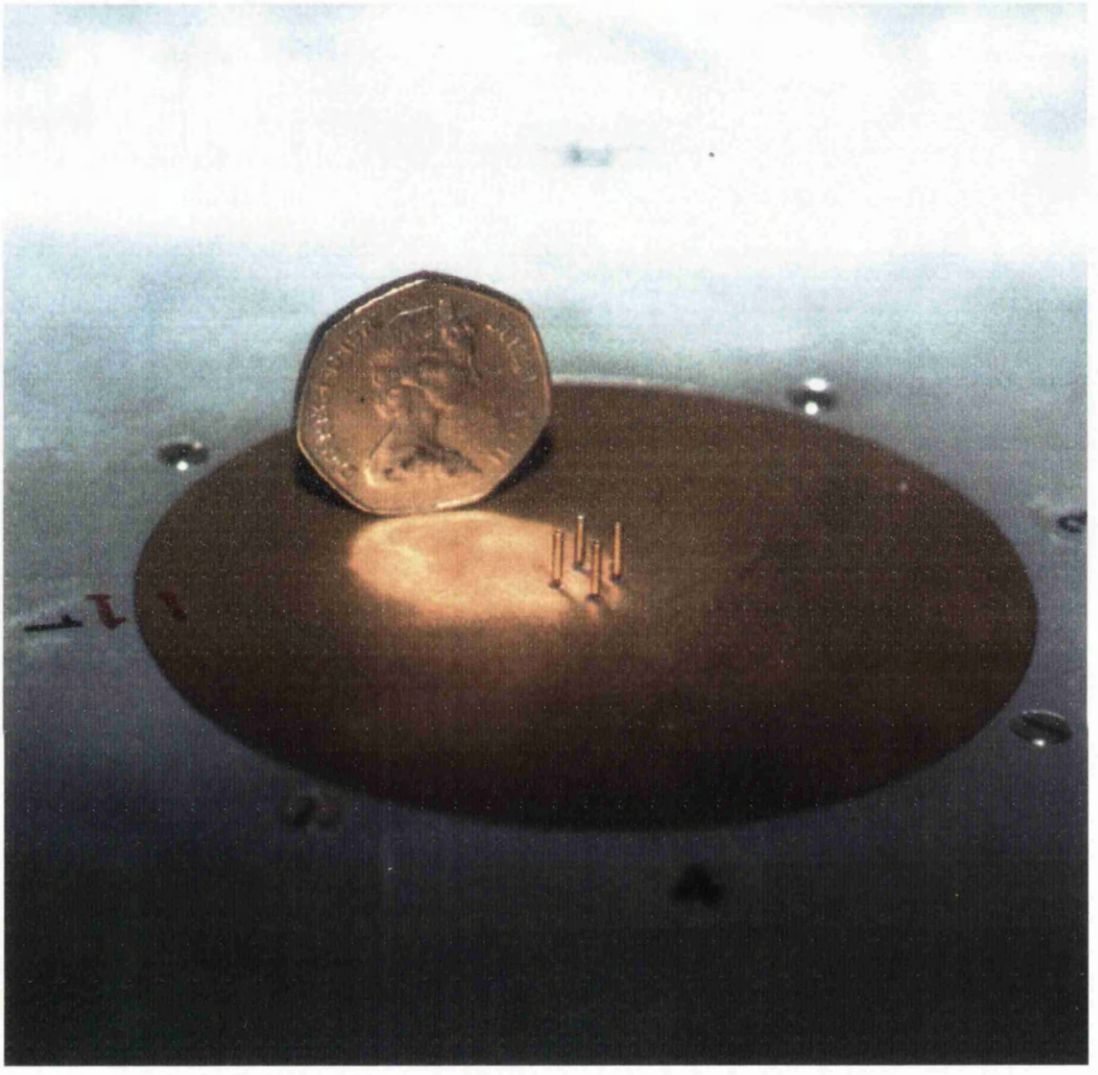

Figure 3.8 A photograph of the four element circular array of monopoles.

investigated. The image of the element in the reflector acts as a second monopole, excited in anti-phase. The close spacing of the primary element and the image results in an inefficient element with a low radiation resistance. This drastically increased the measured mismatch of the element to the feed. The calculated reduction in gain was unacceptable. In any case the measured element patterns of section 3.5 show that additional directivity is not needed.

3.4 The phase mode impedance of the array elements

3.4.1 **Calculation of the phase mode impedance**

When a circular array is excited by a single phase mode the element impedance is a function of the mode order m. In section 2.2.5 the phase mode impedance is calculated from the self- and mutual-impedances of the array elements, expressed in terms of the open circuit z parameters. For a four-element array:

$$Z^{0} = z_{11} + 2z_{12} + z_{13}$$

$$Z^{+1} = Z^{-1} = z_{11} - z_{13}$$

$$Z^{C2} = z_{11} - 2z_{12} + z_{13} \qquad (3.4.1)$$

At microwave frequencies, measuring the open circuit z parameters directly is impractical. However, z parameters can be derived from measurements of scattering parameters using the matrix transformation:

$$[z] = z_0[1+s][1-s]^{-1}$$

Measurements were made of the s parameters at the semi-rigid feeds for the four elements using an HP 8410B network analyser over the frequency range 8 to 12 GHz, as shown in figure 3.9(a). Unused element ports were terminated in 50 Ω loads. To correct for the length of the element feed cables, the element drive points were shorted to the ground plane and the reflection measurements repeated to provide a phase reference plane. The z parameters were calculated using a Fortran matrix solution routine, and are plotted in figure 3.10. The theoretical self-impedance of a monopole is also plotted, using the equation of Tai (1961) for calculating the input impedance of a centre fed dipole. The monopole impedance is half that of a dipole of corresponding length. At the centre of the band the measured real part of the element self-impedance $\mathcal{R}(z_{11})$ is close to the theoretical value of 36.5Ω for a λ/4 monopole, while the imaginary part crosses through zero at about 9 GHz.

The theoretical mutual-impedances of closely spaced monopoles are also plotted, calculated using the technique of Brown and King (1934) for two coupled linear parallel antennas. For both the self- and mutual-impedances there are quite large differences between the theoretical and measured results, particularly at the ends of the frequency band. These differences can be attributed to several factors:

- Neither of the theoretical techniques take account of the feed structure. The monopoles used here were fed by the 0.3 mm wide centre conductor of a semi-rigid cable, with the outer soldered flush to the top of the ground plane.

- The calculations of Brown and King used here to determine the mutual-impedances of monopoles assume that 'thin' monopoles are used. The monopoles used here have a diameter of λ/30 at 10 GHz. While the self-impedance calculations do take account of the diameter, λ/30 is close to the limit for these equations.

(a)

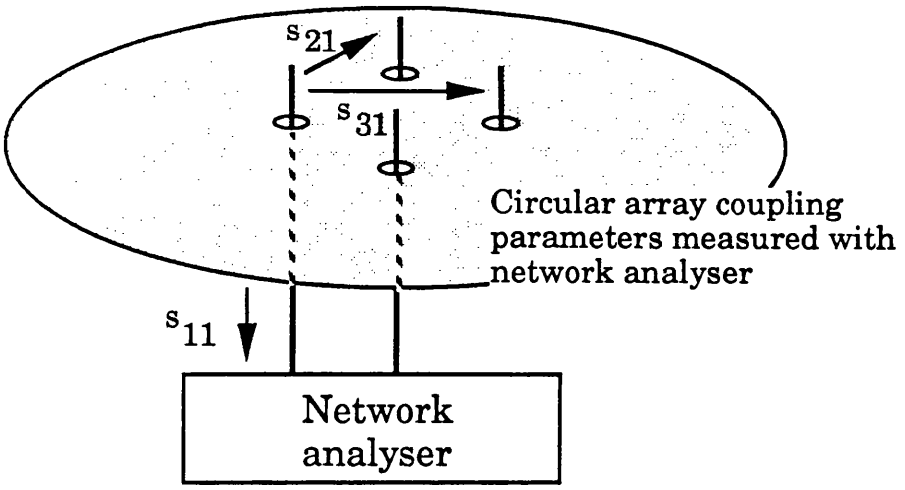

(b) For direct phase mode impedance measurements a 4 x 4 amplitude mode matrix is connected to the array

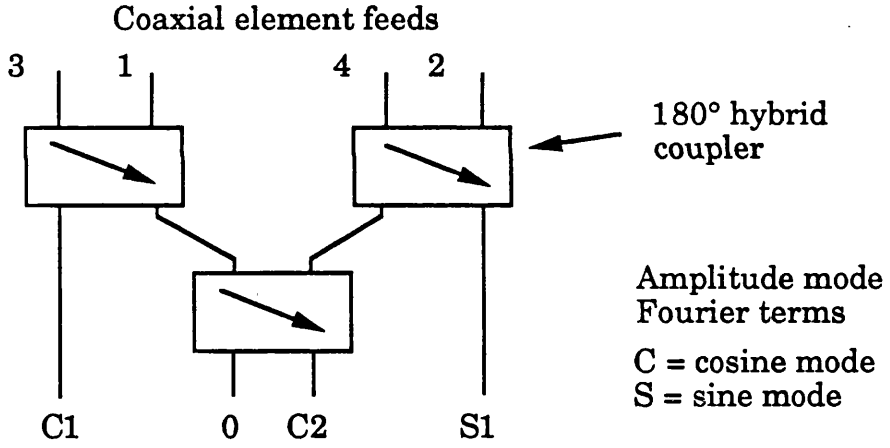

One port measurement of mode impedance:

$$z_m = z_0 (1 + \rho_m)/(1 - \rho_m)$$

Figure 3.9 Measurement of:
(a) Scattering parameters for the circular array elements.
(b) The modal impedances of array elements.

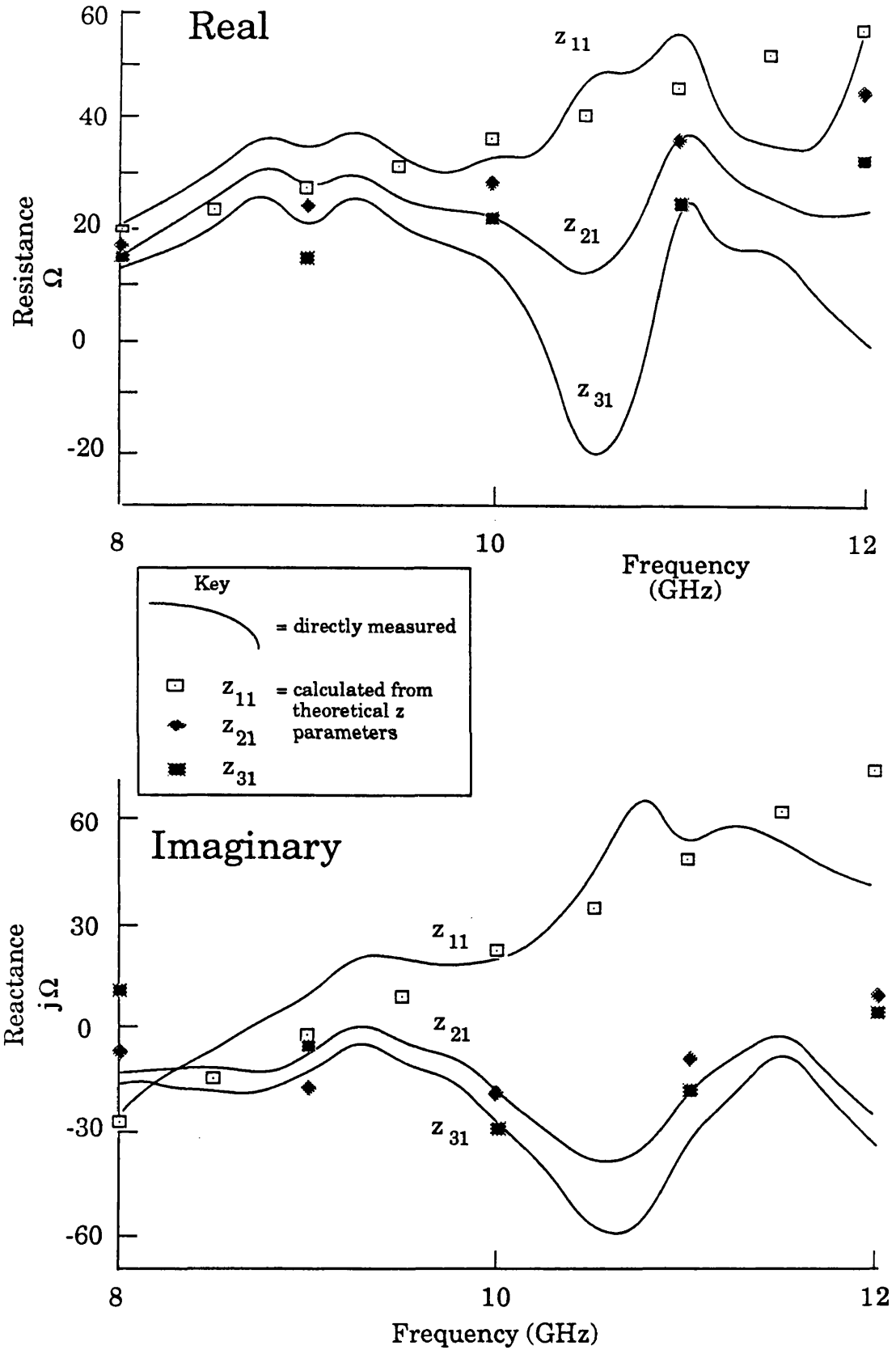

Figure 3.10 Open circuit z parameters calculated from measured scattering parameters for the four-element circular array of figure 3.8.

- The theoretical results assume that the current distribution along the elements is sinusoidal. The elements are in close proximity, just $\lambda/6$ apart, and this will disturb the current distribution. Changes in the current distribution may explain the rapid changes in the impedance close to 11 GHz.

Alternative theoretical techniques might improve the agreement between the theoretical and measured impedances. For thick monopoles the current distribution is not sinusoidal, although this is a good approximation. To find the current distribution an integral equation is derived and solved, usually by Moment Method techniques, as described by Balanis (1982a). Applying these theoretical techniques is time consuming and beyond the scope of this study. Nevertheless, the approximate equations used here provided a useful prediction of the element impedances, and hence the phase mode impedance. For elements with a more complex structure, such as spiral antennas, little theoretical information is available about the self- and mutual-impedances, so measured results must be used.

The phase mode impedances calculated from the measurements of the scattering parameters using (3.4.1) are plotted in figure 3.11. This technique for calculating the phase mode impedance can be applied to circular arrays with more elements by inserting the required value of N into (2.2.10). This technique can also be applied to arrays of elements with a directional radiation pattern. This technique may not work with elements where there are different 'modes of coupling' between adjacent elements, as discussed in section 2.4.1 on the polarisation of phase modes. To check the calculated phase mode impedances, a technique for the direct measurement of the phase mode impedance was devised.

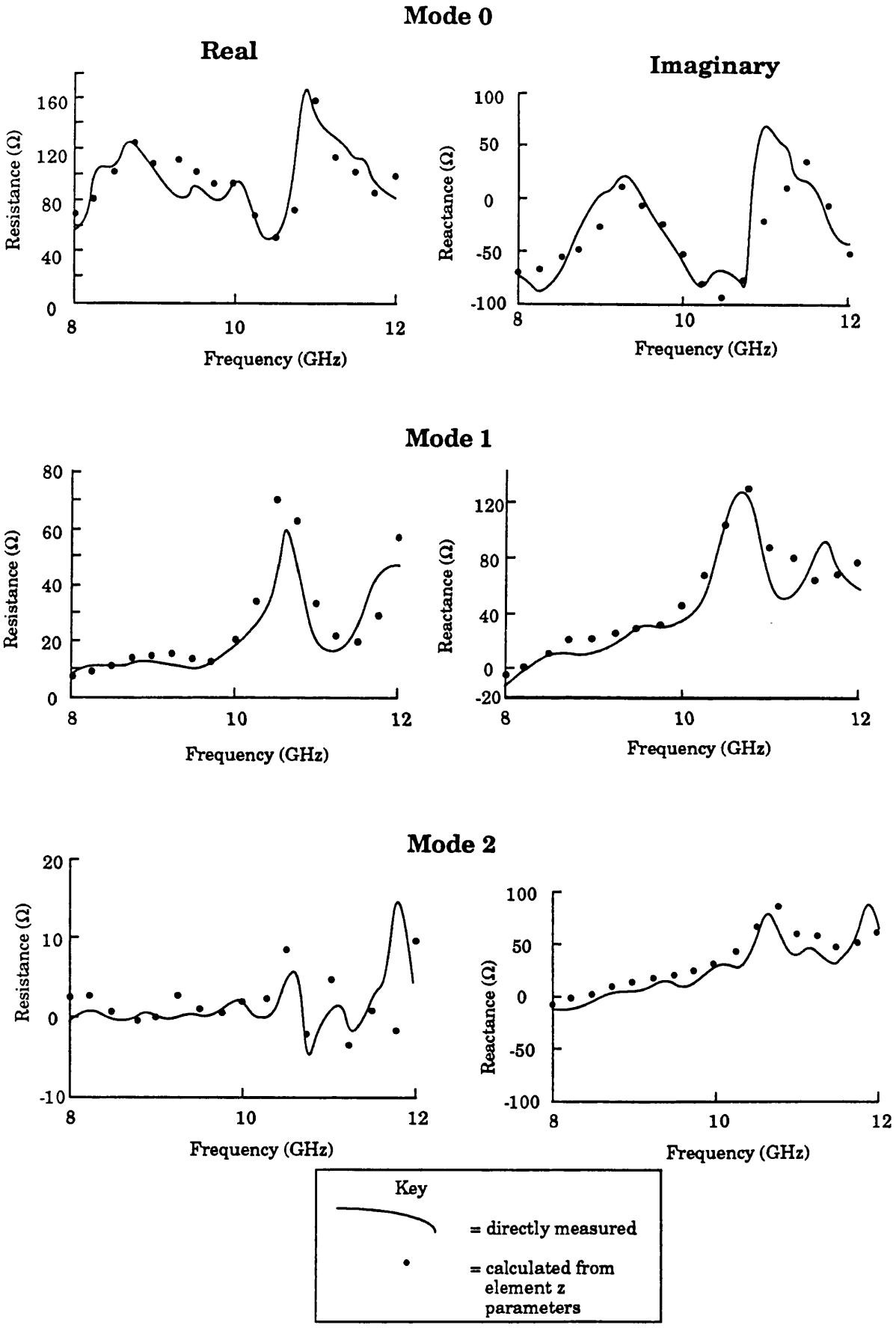

Figure 3.11 Comparison of the directly measured phase mode impedance and that calculated from the self and mutual impedances of the array elements.

3.4.2 **Direct measurement of the phase mode impedance**

If a Butler matrix is used to excite a circular array, there is a mismatch between the characteristic impedance of the feed (50 Ω) and the phase mode impedance of the array elements Z^m. This results in a reflection. If the array is excited by a single mode of order m the amplitude and phase of the reflection from the array element is given by the equation:

$$V_m^{out} = A_m \left(\frac{Z^m - Z_0}{Z^m + Z_0} \right) \tag{3.4.2}$$

where Z_0 is the characteristic impedance of the matrix feed. By symmetry the magnitude and phase of the reflection from all of the array elements is identical. The reflection from the four elements appears at a single output port of the Butler matrix. Taking into account the electrical length of the matrix:

$$V_m^{out} = A_m \left(\frac{Z^m - Z_0}{Z^m + Z_0} \right) e^{-2j\beta l}$$

$2\beta l$ is the two-way propagation phase of the matrix. In practical layouts the length of the element feeds should also be included in the calculations.

If the +1 phase mode port of a 4 x 4 Butler matrix is excited, analysis of the matrix transmission phases show that the reflection appears at the conjugate -1 phase mode port. This conjugate reflection is true for any phase mode. In the case of the 2nd order amplitude mode (C2) formed by a 4 x 4 Butler matrix, the reflection returns to the same input port (C2). This is true for all amplitude modes, including the 0th order mode. The mode impedances of the m^{th} amplitude mode and the m^{th} phase modes are identical

To perform measurements of the phase mode impedance for the four-element array a 4 x 4 'amplitude mode matrix' was connected to the circular array, as shown in figure 3.9. This matrix, described in greater detail in chapter 4, is very similar to the familiar wideband Butler matrix, but is made from just one type of hybrid coupler, and uses fewer components. This matrix forms the 1st order cosine and sine (C1 and S1) amplitude modes, rather than the +1 and -1 phase modes formed by a Butler matrix. The mode impedances were calculated from reflection (s_{11}) measurements using an HP 8410B network analyser. Short circuits at the element drive points were used to define a phase reference plane, enabling the length of the matrix and element feed cables to be calculated. The measurements were performed over the band 8 to 12 GHz, the operating band of the amplitude mode matrix. The calculated phase mode impedances are plotted in figure 3.11, allowing comparison with those calculated from the self- and mutual-impedances of the array elements. Agreement is generally very good. Differences can be attributed to component errors in the matrix feed. The (two-way) transmission amplitude and phase errors of the hybrid couplers change the amplitude and phase of the signal returned to the mode port. The Butler matrix was set up to have the correct transmission amplitude and phase at the centre of the band, so the results close to 10 GHz are very good. Of course, these errors do not affect the impedances calculated from the element self- and mutual-impedances, where the network analyser was connected directly to the element feeds.

For the 0th order phase mode excitation, $\mathcal{R}(z^0)$ is about 90Ω - mutual coupling increases the real part of the element impedance. For the 1st order phase mode $\mathcal{R}(z^{+1})$ is reduced by mutual coupling to about 12Ω. For the 2nd order mode $\mathcal{R}(z^{C2})$ is very low, only 1 or 2Ω. The small negative real impedances registered at 10.75 GHz for $\mathcal{R}(z^{C2})$ are attributable to an imperfect calibration short. The reference short was applied by using a loop of malleable wire to short the bottom of the array element to the ground plane. This short may have been imperfect at microwave frequencies, resulting in the erroneous negative impedance of the 2nd order mode.

3.4.3 Phase mode impedance matching

The magnitude of the reflection from the element mismatch is given by (3.4.2). Ideally, if the characteristic impedance of the feed is matched to the phase mode impedance, then there is no reflection at the element feed. This gives the maximum transfer of power from the feed to the array elements. For a feed with a given characteristic impedance, the loss of efficiency (in %) caused by the mismatch can be calculated using:

$$E = \frac{P_{rad}}{P_{in}} x100$$

$$= \left(1 - \frac{\left(V_m^{out}\right)^2}{\left(A_m\right)^2} \right) x\,100 \qquad (3.4.3)$$

A_m is the input voltage at the m^{th} mode port, and $V^{out}{}_m$ is the voltage of the reflection from the element/feed mismatch, seen at the same mode port. For the 2^{nd} order mode the efficiency will be low, as there is a large mismatch between the real phase mode impedance of 1 Ω to 2 Ω and the 50 Ω feed, as well as the reactive mismatch. Davies (1983) considered impedance matching at the phase mode port as a technique for reducing the mismatch loss. For maximum efficiency, the input impedance at the mode port should be matched to the complex conjugate of the phase mode impedance Z^{m*}. In this case the voltage at the element drive point V^E is given by:

$$V^E = A_m \left(\frac{Z^m}{Z^m + Z^{m*}} \right)$$

and there is no reflected signal. The electrical length of the Butler matrix feed must also be taken into account. Unless the length is small compared with a wavelength, this will act as an impedance transformer, so the input

impedance of the matching network should be matched to the transformed phase mode impedance:

$$Z^m(l) = \frac{Z^m + jZ_0 \tan(\beta l)}{Z_0 + jZ^m \tan(\beta l)} \qquad (3.4.4)$$

where Z_0 is the characteristic impedance of the Butler matrix and βl is the effective electrical length of the matrix. Table 3.1 below compares the electrical lengths of microwave matrices with the lengths of VHF and UHF matrices (all constructed at UCL).

Electrical length in wavelengths		
X band @ 10 GHz	UHF @ 300 MHz	VHF @ 60 MHz
7.33 λ	0.615 λ	0.26 λ

Table 3.1 The electrical length of 4 x 4 Butler matrices.

The microwave matrix is very long in terms of wavelengths. Titze (1988) measured the change in the match with frequency caused by the electrical length of the matrix. The mode ports of the 4 x 4 amplitude mode matrix were matched using a triple stub tuner, as depicted in figure 3.12. The tuner input impedance at 10 GHz was the conjugate of the (transformed) mode impedance. Figure 3.12 depicts the measured change in the reflection coefficient with frequency, showing that the magnitude of the reflection coefficient increases to -3 dB within just 50 MHz of 10 GHz. This is in good agreement with theoretical calculations of the change in match with frequency, also plotted in figure 3.12. The theoretical plot used equations based on (3.4.4).

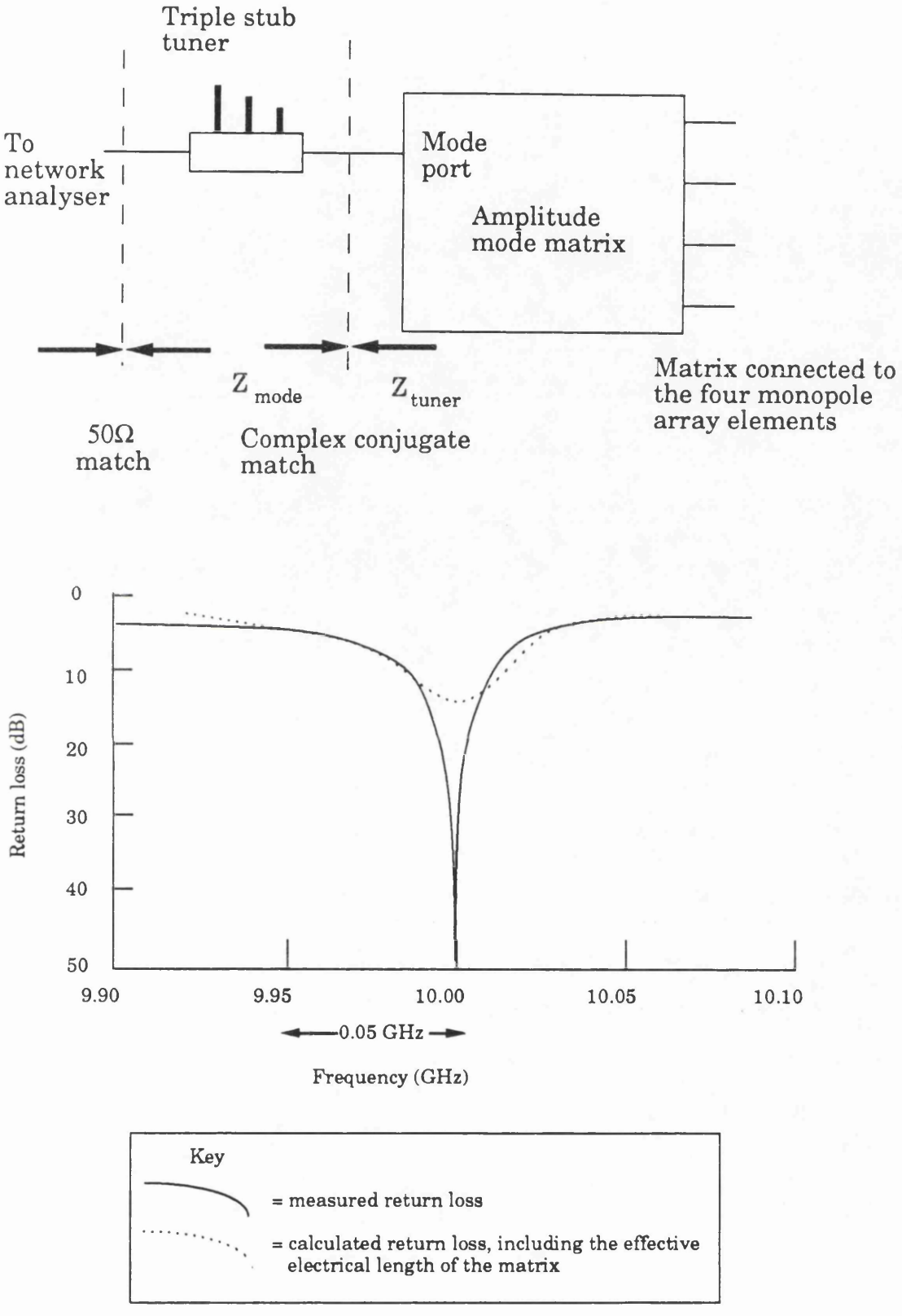

Figure 3.12 Impedance matching at an amplitude mode port, showing the match bandwidth produced by a triple stub tuner at the C2 amplitude mode port (after Titze, 1988).

These measurements show that amplitude mode impedance-matching is narrowband at microwave frequencies. The amplitude mode impedance seen at the mode port changes very rapidly with frequency, transformed by the long electrical length of the matrix. Over this small frequency range, changes in the true phase mode impedance, as seen at the element port, were small by comparison. Another disadvantage of this matching technique is the presence of standing wave fields in the transmission paths of the matrix, leading to greater transmission losses.

As stated by Guy and Davies (1983a) it is attractive to have full orthogonality between phase modes. He suggested a technique for eliminating the reflection of signals at the conjugate port using circulators. The loss of orthogonality can also be corrected by impedance matching. If the 1^{st} order C1 and S1 amplitude modes, formed by a amplitude mode matrix, are matched using stub tuners, they can then be combined using a quadrature coupler. This produces the familiar 4 x 4 Butler matrix layout. The +1 and -1 phase modes will now be (narrowband) matched, so for an input at the +1 phase mode port, there is no reflection seen at the conjugate -1 phase mode port. At lower operating frequencies, wide bandwidth operation might also be feasible.

3.5 Characteristics of the of the radiated phase modes

3.5.1 The radiation pattern and gain of the monopole elements

Measurements of radiation patterns were made using the anechoic chamber facilities at UCL. Full details of the measurement system are given in section 5.1 of chapter 5. First the azimuth pattern of the monopole element was measured. For these measurements a 50 Ω impedance feed was used, and the three unused elements were terminated in 50 Ω loads; the characteristic impedance of the Butler matrix. For an array located on a finite ground plane the peak gain is located above the horizon, so the azimuth radiation pattern of the monopole element was measured at a fixed elevation angle of +8°. Plots of the azimuth radiation patterns at 1 GHz intervals across the frequency band are plotted in figure 3.13. An isolated vertical monopole is theoretically omnidirectional in azimuth. The measured radiation pattern is not perfectly omnidirectional; at 10 GHz the pattern has a front-to-back ratio of 2.5 dB. The -3 dB beamwidth of the low gain mainlobe changes by about 20° across the band. At 8 GHz the gain is actually slightly higher in the $\phi = 180°$ direction, compared with the $\phi = 0°$ direction.

The elevation pattern of the monopole is plotted in figure 3.14, for a frequency of 10 GHz. Also plotted is the theoretical radiation pattern of a $\lambda/4$ monopole element:

$$F(\theta) = \frac{\cos\left\{\frac{\pi}{2}\cos(\theta)\right\}}{\sin(\theta)} \qquad (3.5.1)$$

Agreement between the two patterns is fair, although there is a ripple on the measured elevation pattern, with a periodic spacing in elevation of about 9°. This is a result of using a finite ground plane 50 cm in diameter (16 wavelengths). Storer (1952) predicts that for a ground plane of this size, an amplitude ripple with a periodic spacing of about 8° in elevation will be produced. The measured mainlobe peak is at about +13° of elevation,

Radiation pattern of monopole elements, other array elements terminated in 50 Ω loads

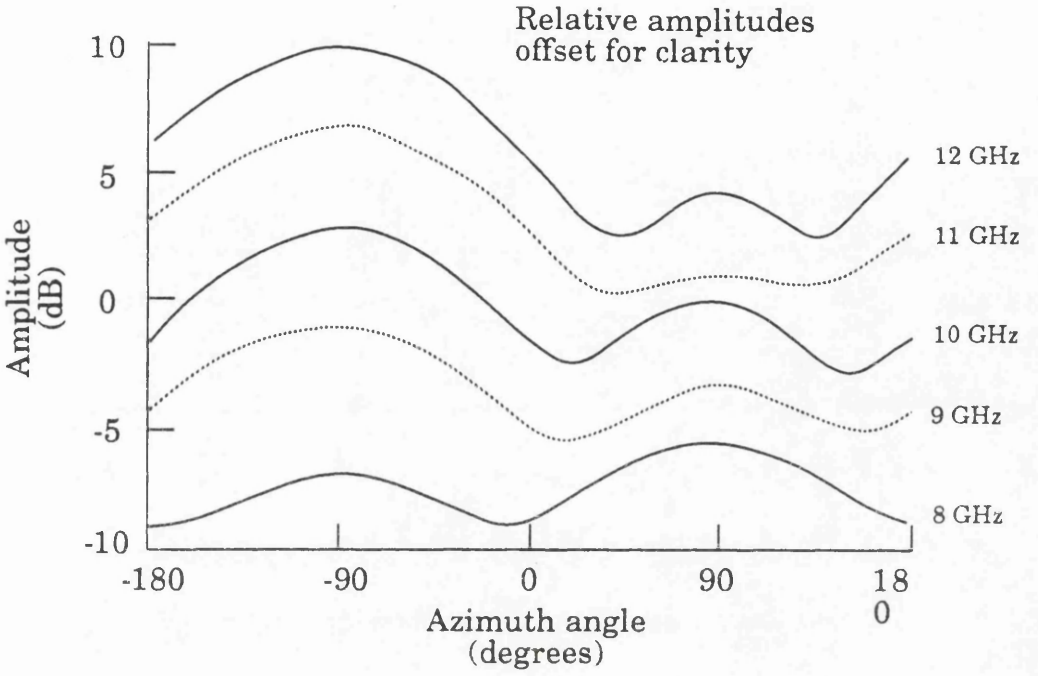

Far field phase (referred to centre of array)

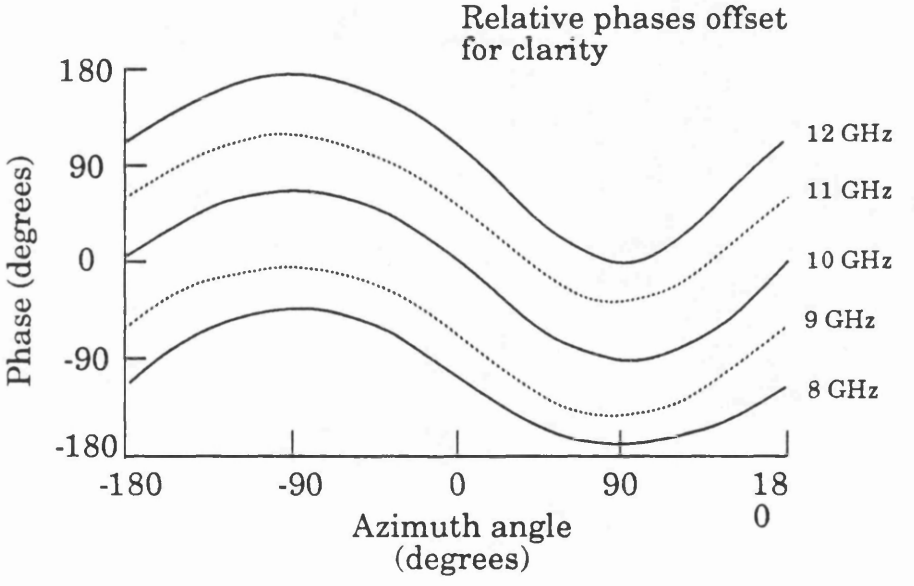

Figure 3.13 Anechoic chamber measurements of monopole radiation patterns across the band 8 to 12 GHz.

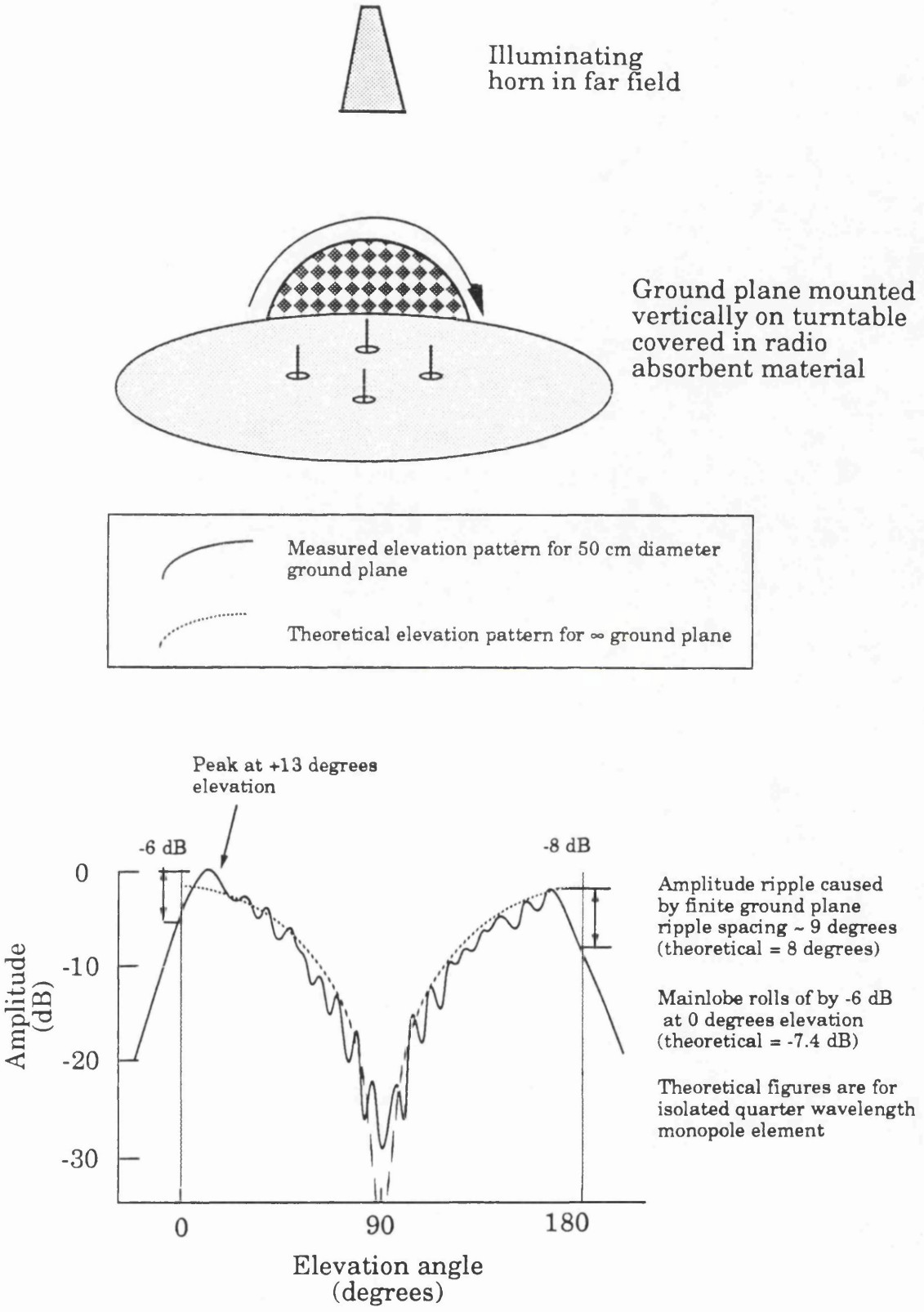

Figure 3.14 Measured elevation pattern of a monopole element at 10 GHz, with the other array elements terminated in 50 Ω loads.

rolling off by -6.5 dB at 0° elevation. This can be compared to the theoretical drop of -7.4 dB for an isolated monopole, given by Tai (1961). These measurements were repeated across the band 8 to 12 GHz, revealing only minor changes in the elevation pattern with frequency.

The theoretical directivity D of a $\lambda/4$ monopole on an infinite ground plane is 1.64, relative to an isotropic antenna. This is the same directivity as that of a half wavelength dipole in free space. The directivity changes with frequency, as the effective length of the monopole changes, but over the (half octave) operating bandwidth used here the change is small. Even for an infinitesimal dipole the directivity is only 0.3 dB lower than that of a half wavelength dipole. For a lossless monopole element the gain over isotropic G_i^E is the same as the directivity, but in practice losses reduce the gain:

$$G_i^E(\phi,\theta) = e_t \, D(\phi,\theta)$$

where e_t is the total antenna efficiency. This contains three main components:

- Conduction losses, due to the finite resistance of the element.
- Dielectric losses, for elements using dielectric materials.
- The mismatch between the element impedance and the feed impedance (50Ω).

Since the monopoles are not matched to the 50Ω feed the most significant loss is the mismatch loss. The other losses are very difficult to calculate theoretically and are in any case small (< 1%) for short copper monopoles (or dipoles), as calculated by Balanis (1982b). The reduction in gain due to the mismatch is calculated using:

$$G_i^E(\theta,\phi) = (1 - |\rho|^{2)}) \, D(\theta,\phi)$$

where ρ is the mismatch between the element self-impedance and the 50Ω

impedance of the network. Figure 3.15 plots the theoretical monopole gain, using the theoretical element self-impedance of figure 3.10 to calculate the mismatch. The theoretical gain is plotted at two elevation angles, 0° and +13°. This is to allow comparison with the measured peak gain, at +13° of elevation because a finite ground plane was used (figure 3.14).

Figure 3.15 also plots the change in the measured monopole gain with frequency. This was measured in an anechoic chamber using the techniques described in section 5.1. A standard gain horn was substituted in place of the array to provide a gain reference. The monopole gain is greatest at the centre of the band, where it is resonant. The results are in fair agreement, except at the top of the band where the measured gain is lower by 1.5 dB. Theoretical results do not take into account the presence of the other three monopoles, terminated in 50 Ω loads for this measurement. Coupling to the other elements will result in a loss of gain and the radiation pattern is no longer omnidirectional, as shown in figure 3.13. Determining the changes in the theoretical gain caused by the presence of the other monopoles is a complex task, and would have contributed little to the main aim of this study.

3.5.2 Calculation of the phase mode coefficients

Inspection of equation (2.4.3) shows that the directivity of a phase mode is the same as that of the array element, but weighted by a complex term, called the phase mode coefficient. The peak directivity is at the same elevation angle as that of the element, +13° for the monopoles used here due to the finite ground plane. Figure 3.16 plots the theoretical gain of the 0^{th} order mode across the frequency band 8 to 12 GHz calculated using the equation:

$$G_i^m(\theta) = G_i^E(\theta) J_m(\beta r \cos(\theta))$$

G_i^E is the theoretical gain of the monopole element, including mismatch losses. For comparison the measured gain of the 0^{th} order mode

Monopole gain relative to isotropic

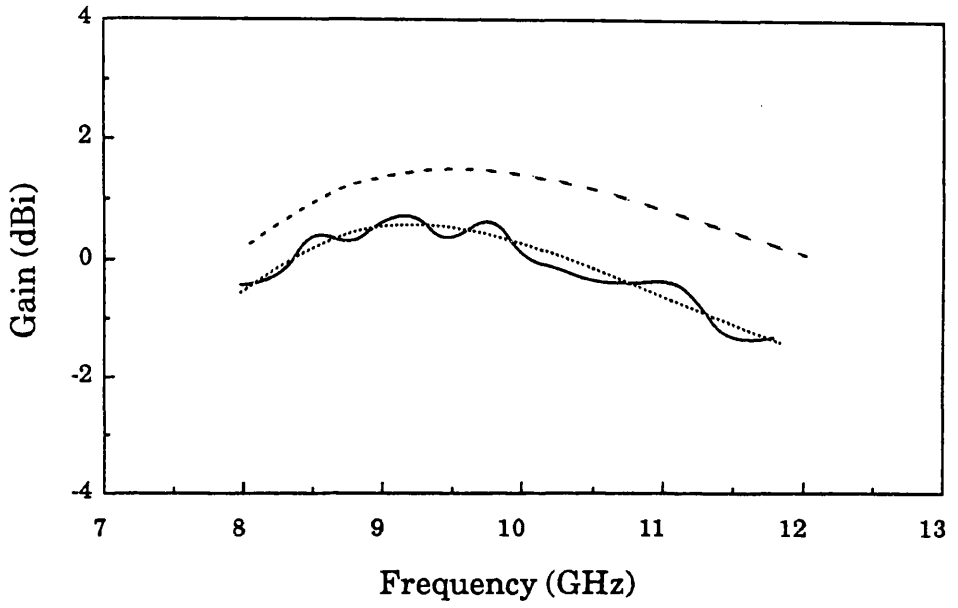

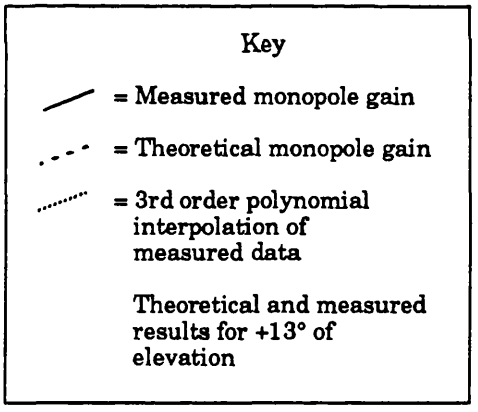

Reasons for differences between theoretical and measured results:

- The theoretical results for single monopole, while the measured results are for a monopole in a circular array with 50 Ω terminated monopoles in close proximity, increasing losses.

- The ±0.25 dB ripple is due to mismatches in UT.085 feed cable and connectors.

Figure 3.15 A comparison between the measured gain of a monopole element, and the theoretical gain.

Gain of the zero order phase mode relative to isotropic

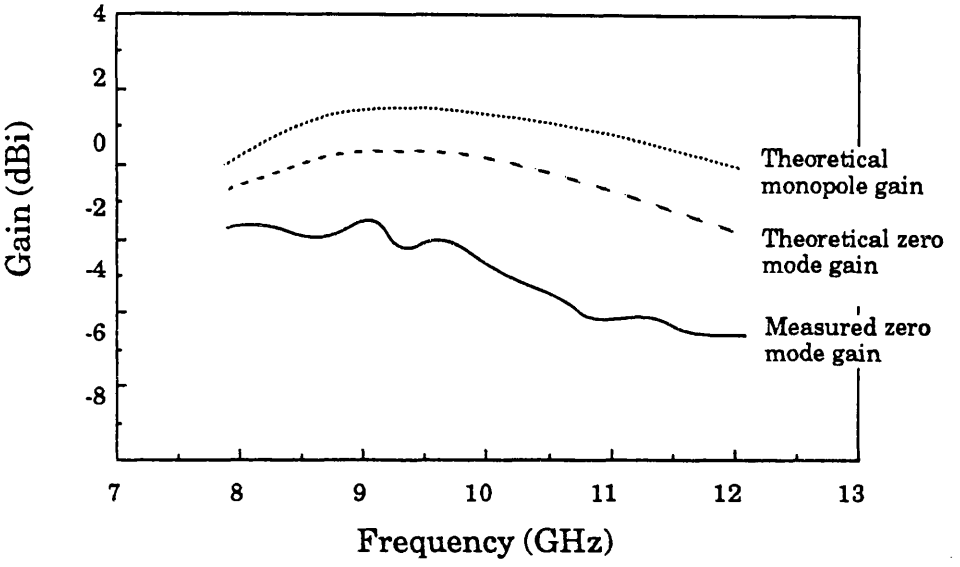

Theoretical and measured results for an elevation angle of +13°

Reasons for differences between theoretical and measured results:

- Each directional coupler in the matrix has 0.5 dB of loss, resulting in 1 dB of loss in total.
- The measured monopole gain is lower than the theoretical gain - see figure 3.15.
- The ±0.75 dB ripple is due to mismatches in the Butler matrix.

Figure 3.16 A comparison between the measured gain of the zero order phase mode, and the theoretical gain.

is also plotted in figure 3.16. There is a discrepancy between the two results, with the measured results low by 1 dB (at 8 GHz) and 2 dB (at 12 GHz). Two reasons for this can be identified. First there are losses in the matrix feed, each hybrid coupler introduces a loss of 0.8 dB maximum. Secondly, the measured gain of the monopole is about 1.5 dB lower than the theoretical value at 12 GHz, hence the 2 dB of loss at the top of the band, compared to the theoretical result.

Let us now consider the gain of the higher order modes. To perform pattern synthesis with a circular array, the phase mode coefficients for our array must be known, as these determine the relative amplitudes and phases of the modes. As monopoles are omnidirectional in azimuth the phase mode coefficients for the array should be those depicted in figure 2.9, for an array where r = 3.53 mm. However, as shown in figure 3.13 earlier, the radiation pattern of an element 'embedded' in a circular array is different to that of an isolated element, due to mutual coupling. King, Mack and Sandler (1968) calculate the effect of mutual coupling on the current distribution for a circular array of thin dipole elements. For directional element types, the mode coefficients have been measured experimentally, using a Butler matrix feed to excite the array. For example Rahim, Guy and Davies (1981) give the measured mode amplitudes for a UHF circular array with directional elements.

The technique of Jones and Griffiths (1988) calculates the phase mode coefficients from measurements of the radiation pattern of an array element, located in the array environment. Any excitation of a circular array can be expressed in terms of a series of phase mode terms, so exciting a single array element with an RF source is also a modal excitation of the array. Appendix 1 proves that exciting a single element of a four-element circular array can be expressed modally:

$$F(\phi) = \sum_{m=-\infty}^{m=+\infty} K_m e^{jm\phi} \qquad (3.5.2)$$

This is the phase mode expression for the measured monopole radiation

pattern of figure 3.13. This radiation pattern is the same as that formed by connecting a Butler matrix to the array, and exciting the four phase mode ports with equal amplitude. As the radiation pattern of (3.5.2) is the sum of a Fourier series, the complex coefficient K_{+m} for the +m order mode can be calculated using the standard integration:

$$K_{+m} = \frac{1}{2\pi} \int_0^{2\pi} F(\phi)\, e^{-jm\phi}\, d\phi \qquad (3.5.3)$$

Both phase and amplitude information is required for this calculation. By repeating this integration for all values of m the mode coefficients for all the fundamental and harmonic terms can be calculated from this single azimuth measurement. For element patterns that exhibit symmetry about the radial boresight axis (which is generally the case) the mode coefficients for the -m modes are the same as those of the +m modes. The integration was done on the data of figure 3.13 using an HP 85 desktop computer with a BASIC program using Simpson's rule. By repeating the calculations at 1 GHz intervals across the frequency band, changes in the mode coefficients as a function of frequency were calculated, and are plotted in figure 3.17.

3.5.3 **Direct measurement of the mode coefficients**

To verify these results the phase mode coefficients were measured directly by exciting the amplitude modes using a 4 x 4 amplitude mode matrix, as described in section 3.4.2. The 0^{th}, 1^{st} and 2^{nd} order amplitude modes were excited in turn, and the radiated mode characteristics were measured in an anechoic chamber, again at 1 GHz intervals across the band. Figure 3.18 depicts the radiated amplitude modes at 10 GHz. From this figure the direct plot of the mode coefficients (figure 3.17) is taken. There is good agreement between the coefficients calculated from the monopole measurements and those measured directly, within ±1 dB and ±5° for the 0^{th}, 1^{st} and 2^{nd} order modes. Differences are mainly due to component errors in the matrix feed. These affect the directly measured coefficients, but not those calculated from measurements of the element patterns.

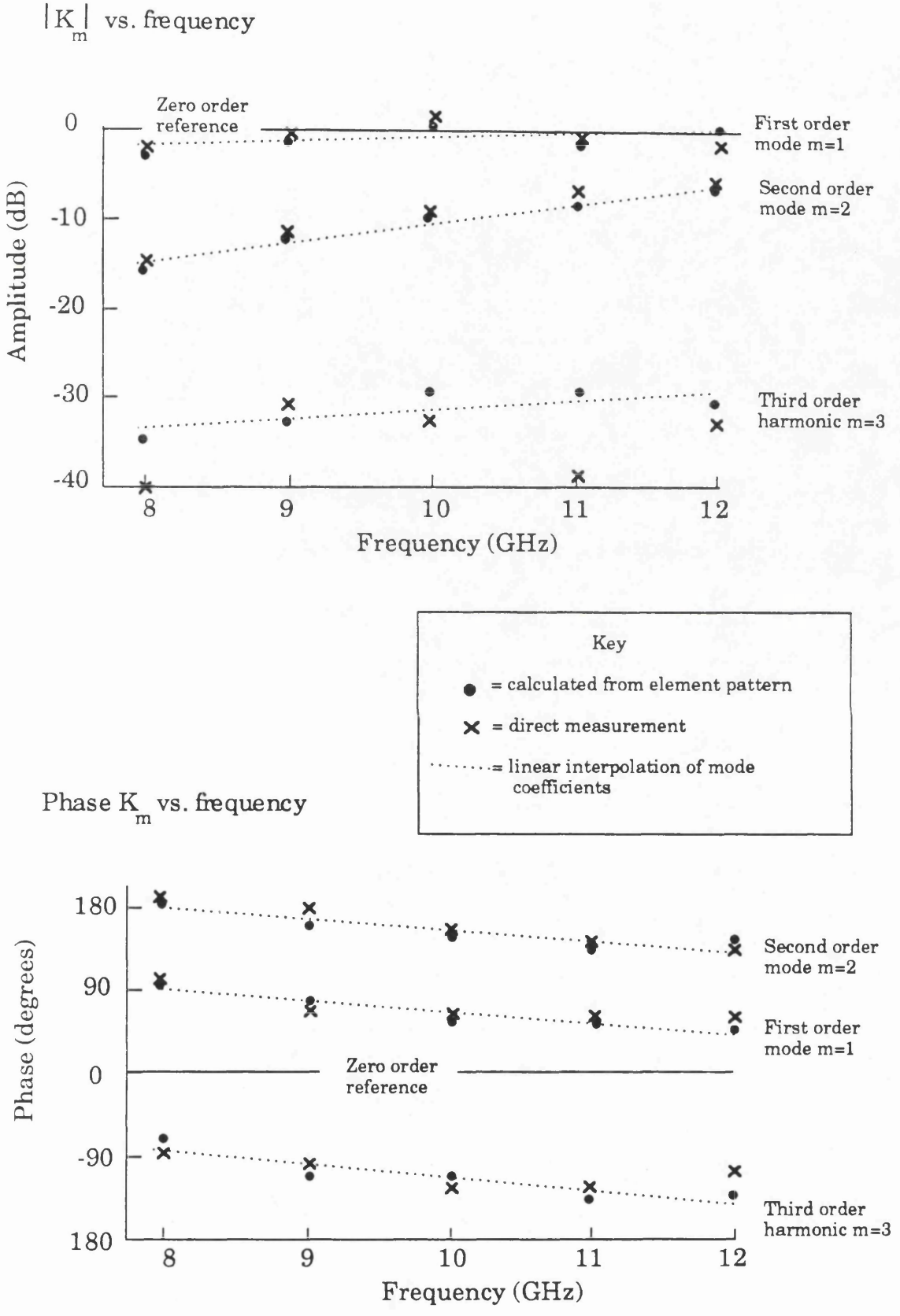

Figure 3.17 A comparison between phase mode coefficients measured directly, and those calculated from measurements of the element pattern.

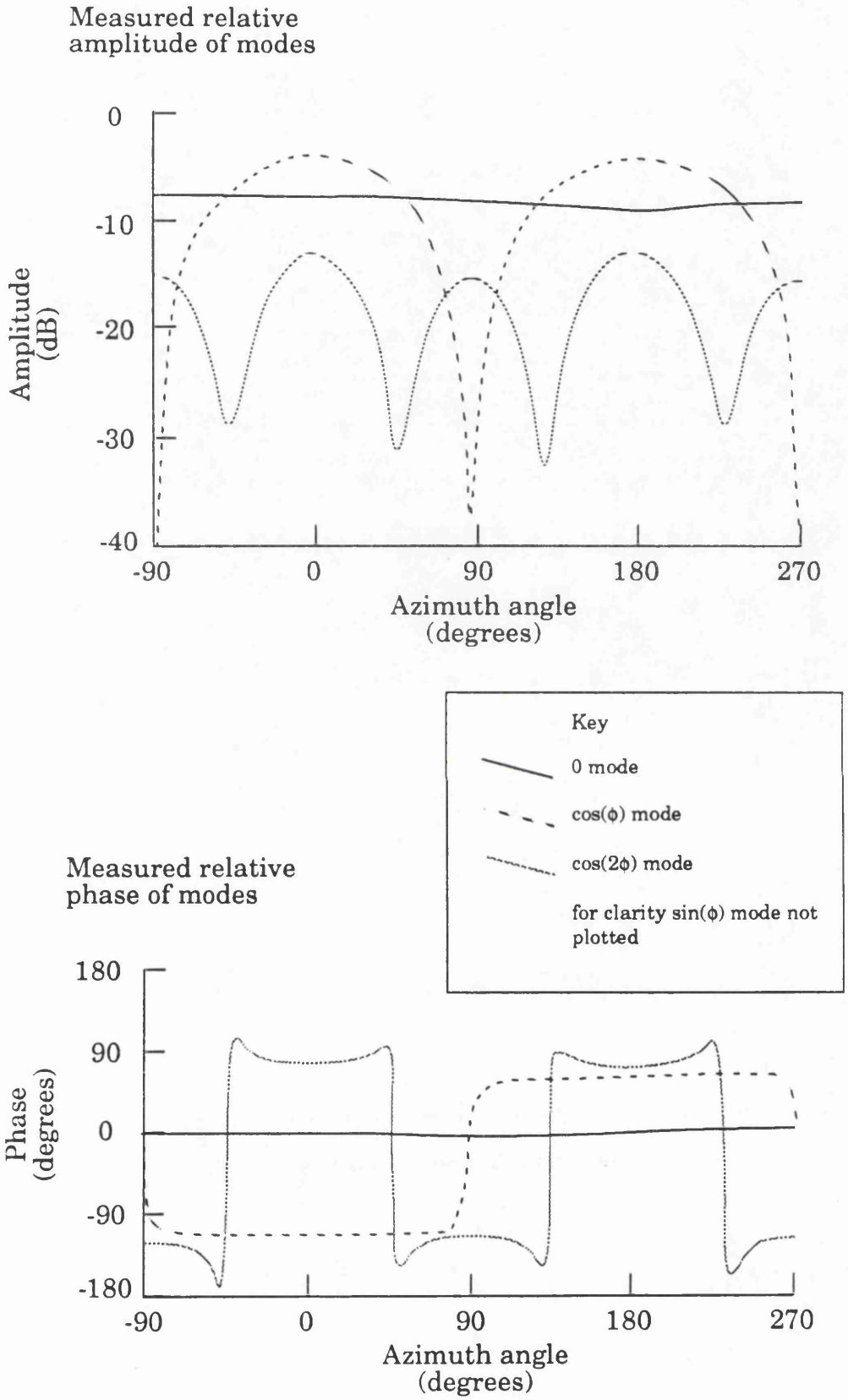

Figure 3.18 Anechoic chamber measurements of amplitude modes at 10 GHz.

The 3rd order ripple on the 1st order mode was not immediately apparent. Numerical integration of the 1st order C1 amplitude mode pattern using (3.5.3) showed that there was a third order harmonic component with an amplitude of about -30 dB, as predicted. Both sets of measurements showed that the mode coefficients for harmonics of order four and above were of negligible magnitude (< -40 dB below the 0th order mode). For $\phi = 0°$ the measured phase of the C1 mode is -114° (figure 3.18), while the plotted phase is +66° in figure 3.17. This -180° discrepancy is explained by the amplitude mode matrix transmission phase (see table 4.7 in chapter 4). This effect also explains the -90° discrepancy for the C2 mode.

The measured mode coefficients are not the same as those expected for a circular array composed of elements that are, in isolation, omnidirectional. For example, the magnitude of the 2nd order mode relative to the 0th order mode is about 10 dB higher than that theoretically calculated for omnidirectional elements with an inter-element spacing of $\lambda/6$. Clearly mutual coupling plays a major role in determining the mode coefficients.

Let us consider the theoretical gain of directional beams formed from phase modes. The directive gain of beams is higher than that of the omnidirectional modes. From Balanis (1982c) for a uniformly excited linear array of N isotropic elements, the directivity is:

$$2\,N\,(d/\lambda) \qquad (3.5.4)$$

so for a five-element linear array with an inter-element spacing of $\lambda/2$ the directivity is 7 dB. For a circular array where five phase modes are excited with equal amplitude the directivity D is the same, despite the change in scale from sine(ϕ) space to ϕ space. The absolute gain, however must take into account the gain of the phase modes. For a uniform excitation of the modes $G_i^0 = G_i^1 = G_i^2 = G_i^m$. The gain of the beam is the product of the directive gain of the beam D and the gain of the phase modes:

$$G_i^b = D_i\, G_i^m \qquad (3.5.5)$$

For linear arrays, applying a taper reduces the directivity. Balanis (1982d) calculates the directivity for a Chebyshev beam. For a five-element linear array, with an inter-element spacing of $\lambda/2$ and a -30 dB sidelobe level the directivity D is 3.5 dB. This is also the directivity of the Chebyshev beam formed by the five phase modes of a four-element circular array. The theoretical gain of the Chebyshev beam will be 3.5 dB higher than that of the 0^{th} order mode, plotted in figure 3.16.

One final factor must be taken into account in predicting the gain; the amplitudes of the higher order modes. At 8 GHz the 2^{nd} order mode is -15 dB in amplitude, relative to the 0^{th} order mode, but the Chebyshev taper requires the 2^{nd} order mode to be -9.94 dB in amplitude. Since the use of wideband amplifiers was not planned, the 0^{th} order phase mode must be attenuated by 5 dB to realise the correct taper, with a corresponding loss in the gain of the synthesised beam. Thus the gain of the beam G_b becomes:

$$G_b(dB) = D(dB) + G_i^0(dB) - A_0\,(dB) \qquad (3.5.6)$$

where A_0 is the attenuation applied to the 0^{th} order phase mode, in dB. At 8 GHz the absolute gain of the Chebyshev beam is reduced to -3 dBi. Attenuation of the 0^{th} order mode is not necessary above 10 GHz , as the 2^{nd} order amplitude mode is above -9.94 dB in amplitude. This problem does not arise with the 1^{st} order mode, since the mode amplitude is higher than the specified taper across the band

To conclude, the monopole array is suitable for pattern synthesis over the frequency range 8 to 12 GHz. The relative amplitudes of the 0^{th}, 1^{st} and 2^{nd} order modes have approximately the right taper for a -30 dB Chebyshev pattern. The amplitude of the 2^{nd} order mode is rather low (-15 dB) at the bottom of the band. This could be altered by increasing the array radius, but the 3^{rd} order harmonic is already rather high (at -30 dB) and increasing the radius increases the amplitude of this harmonic. Changes in the relative amplitudes and phases of the modes across the band are monotonic and smooth, and should prove amenable to compensation, as has been considered in the next chapter.

Chapter 4

Wideband beamformer design

4.1 Introduction

This chapter considers the design of wideband beamformers to form radiation patterns using a phased circular array. Section 4.2 is a theoretical study of the effect of beamformer errors on the synthesised beams. This information is used to evaluate the beamformer designs in the rest of this chapter.

Section 4.3 describes the evolution of the beamformer design over the course of this study, the prime aim being to reduce excitation errors to acceptable levels, as defined in section 4.2.

As explained in chapter 2, the array excitation required to form a wideband radiation pattern changes as a function of frequency. This is necessary to compensate for changes in the phase mode coefficient. Section 4.4 considers the design of RF networks to compensate for these changes.

4.2 The effect of theoretical beamformer errors on synthesised beams

4.2.1 Beamformer parameters that degrade the shape of the synthesised beam

The theoretical study of chapter 2 showed that radiation patterns that do not change shape with frequency can be formed using a circular array. However, errors in the excitation of the array change the synthesised pattern. Beamformer errors can alter the beam in five ways:

- The peak gain of the beam is changed.
- The -3 dB beamwidth is changed.
- Sidelobe levels are increased.
- Nulls are filled in.
- The beam squints.

Changes in the peak gain, compared with that of overlapping beams reduces the DF accuracy of an amplitude comparison DF system, as calculated in section 3.2. Changes in the -3 dB beamwidth also reduces the accuracy. Increased sidelobe levels and filled-in nulls increase the susceptibility of the system to interfering signals.

Figure 4.1 illustrates the beamformer design initially chosen to form wideband beams using the four-element monopole array, based on the general design of figure 1.1. The network can be divided into three sections (overleaf):

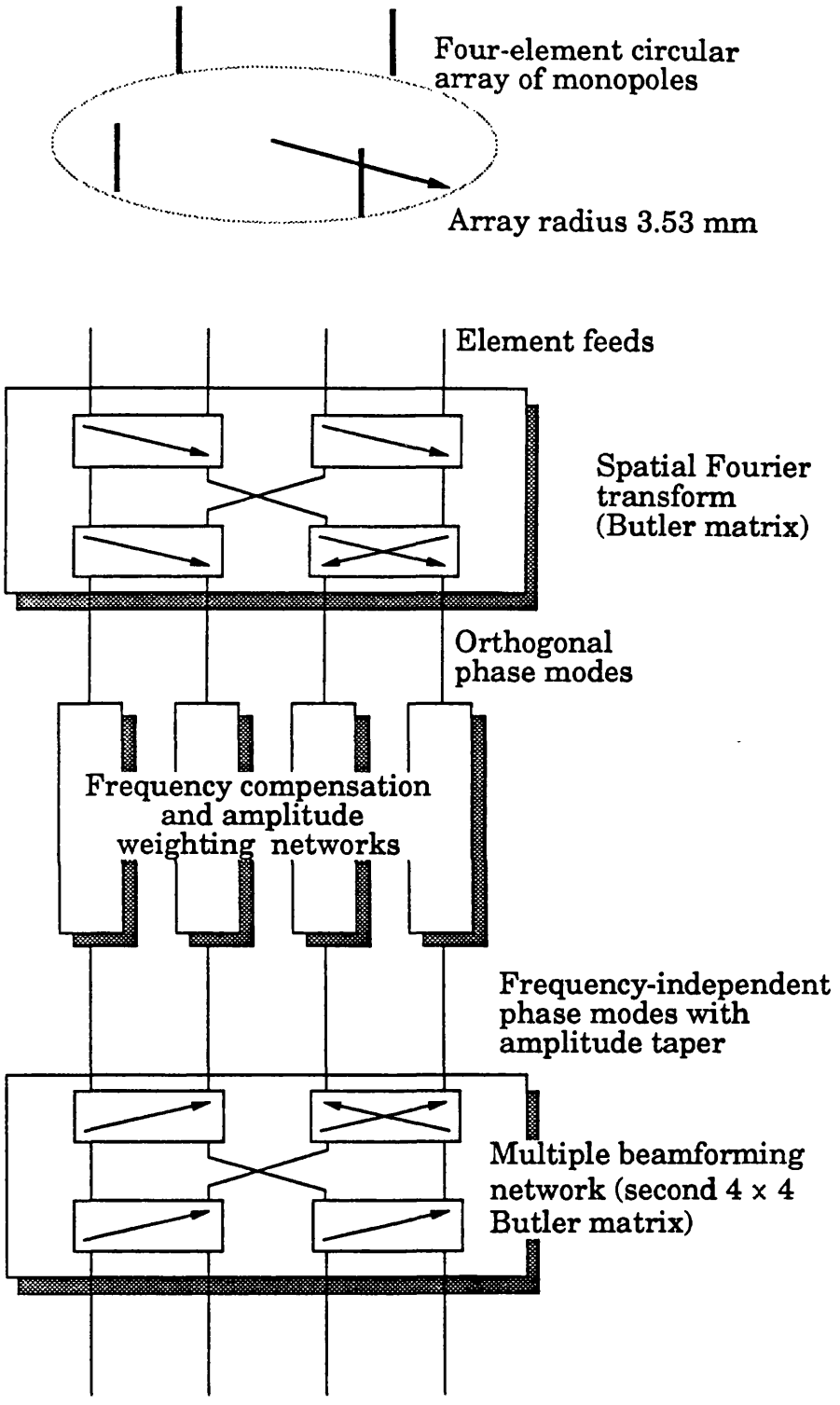

Figure 4.1 Block diagram of the proposed wideband pattern synthesis system.

- A wideband 4 x 4 Butler matrix used to form the orthogonal phase modes.

- Two-port frequency compensation networks connected to each of the phase mode ports. These correct changes in the amplitude and phase of each of the modes with frequency. These also apply the taper to form a low sidelobe pattern.

- A second wideband 4 x 4 Butler matrix used to form four overlapping beams from the compensated modes.

Figure 4.1 shows a wideband Butler matrix design containing three 180° couplers and one 90° coupler. Omni Spectra 180° couplers type 2031-6335-00, were purchased for this matrix. The manufacturers specification for this device is given in given in table 4.1 below.

Frequency range	8.0 to 12.4 GHz
Coupler amplitude imbalance	±0.5 dB
Phase error	±6°
Insertion loss	+0.8 dB
Isolation between inputs	17 dB
Input VSWR (Max)	1.40

Table 4.1 The manufacturers specification for Omni-Spectra 180° couplers type 2031-6335-00.

The formation of wideband Chebyshev beams is one aim of this study. Errors in the hybrid couplers degrade the wideband pattern. Three main sources of error can be identified from this specification (overleaf):

- Errors in the transmission amplitude and phase of the device.

- Imperfect matching of the device to the 50 Ω characteristic impedance of the beamformer

- Imperfect isolation between input ports.

The insertion loss reduces the absolute gain of the synthesised beam, but does not affect the shape. This was observed in figure 3.16, where the gain of the zero order mode was reduced by 1 dB due to this loss. In this chapter an insertion loss of +x dB is commonly called a transmission amplitude of -x dB.

4.2.2 The effect of compensation network errors on synthesised beams

Let us first consider transmission phase and amplitude errors. The simplest errors to analyse are transmission errors in the compensation networks, as opposed to those in the matrix. The specified (complex) compensation required is calculated using (2.3.7):

$$A_m = \frac{W_m}{K_m(f)} \tag{4.2.1}$$

$K_m(f)$ is the phase mode coefficient for the circular array. W_m is the amplitude taper applied to the m^{th} order phase mode. The theoretical radiation pattern at a frequency f is calculated using:

$$F(\phi) = \sum_{m=-M}^{M} A_m K_m(f)\, e^{jm\phi} \tag{4.2.2}$$

The amplitude of the compensation can be specified in polar form, with an amplitude 20 log($|A_m|$), and a phase arg(A_m). Suppose that the specified compensation of one of the modes is -2.5 dB, while only a -3 dB wideband

attenuator is available. The modified radiation pattern is given by the equation:

$$F(\phi) = \sum_{m=-M}^{M} A'_m(f) K_m e^{jm\phi} \qquad (4.2.3)$$

where $A'_m(f)$ includes the errors in the transmission amplitude and phase of the compensation. Let us consider the effect on a radiation pattern of an amplitude error ΔA, and a phase error ΔP. While the equations above are general, this analysis will concentrate on patterns formed from the 0^{th}, 1^{st} and 2^{nd} order phase modes; the modes of a four-element circular array. In this analysis it is assumed the four phase modes are of equal amplitude, rather than tapered - this is the worst case for vector errors. Equation (4.2.3) can easily be adapted to include amplitude tapers.

The effect of transmission errors on nulls

At azimuth angles ϕ where there is a null in the ideal radiation pattern the vector sum of the terms in (4.2.2) adds up to zero. The effect of phase and amplitude errors is to leave a resultant R that fills in the nulls. For a given amplitude error ΔA, and phase error ΔP the magnitude of the resultant R is calculated using (4.2.3). Figure 4.2 shows the amplitude of the resultant relative to the mainlobe peak gain. Clearly, if sidelobes below -30 dB are required, the nulls between them must also be below -30 dB, placing a limit on the tolerable amplitude and phase errors.

The effect of transmission errors on sidelobe levels

At the peaks of sidelobes the vector sum of the terms in the exact equation (4.2.2) adds up to a (small) finite vector value. Phase and amplitude errors in the compensation change this value. The changes in amplitude can be considered as the vector sum of the sidelobe vector and the error resultant R, plotted in figure 4.2. Let us consider the case where the vector R has the same magnitude as the sidelobe level. In some cases the two vectors will

(a) Magnitude of resultant for four phase modes combined together with given phase and amplitude errors

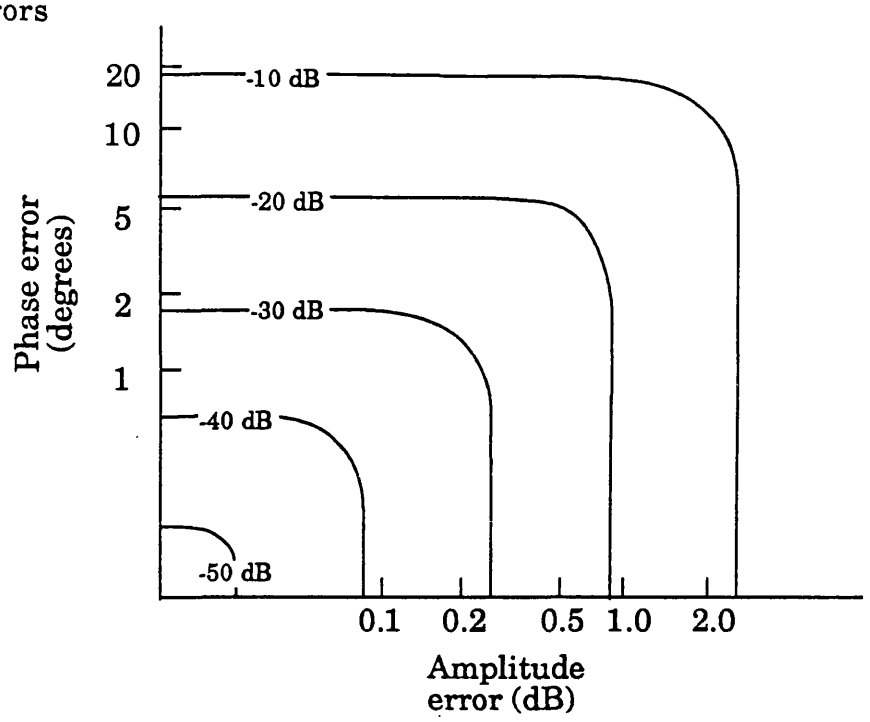

(b) Peak increase in sidelobe level for a resultant of amplitude R

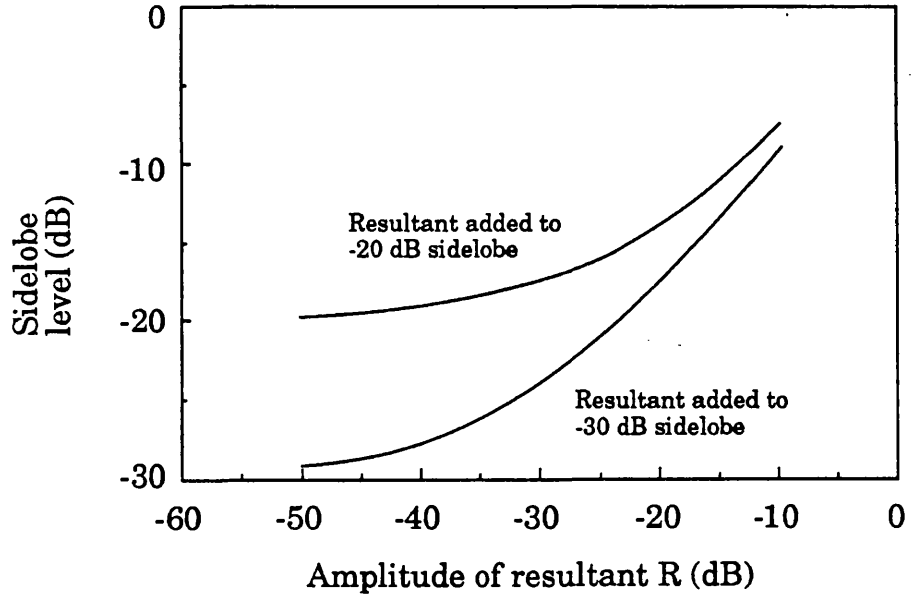

Figure 4.2 Effect of amplitude and phase errors in the compensation on:

(a) Pattern nulls.

(b) Sidelobe levels.

cancel, turning the sidelobe into a null, or at least reducing the sidelobe level. In other cases the two vectors will add, increasing the sidelobe level by 6 dB. On average, the sidelobe level will increase by 3 dB - the result of quadrature addition of the two vectors. Figure 4.2 plots the increase in sidelobe levels as a function of the resultant amplitude R, showing that small phase and amplitude errors can greatly increase the sidelobe level. As an example, consider a phase error of 2° in the mode compensation. The produces a -30 dB resultant. If the beam has a theoretical -30 dB sidelobe level, in the worst case this small phase error will increase the peak sidelobe level by 6 dB to -24 dB.

The effect of transmission errors on peak gain

At the peak of the mainlobe, the phase modes of (4.2.2) are in phase, so the vector sum is a maximum. An error ΔP in the phase compensation of (4.2.3) reduces the peak gain, as the modes are not then exactly in phase. Figure 4.3 depicts the reduction in gain as a function of the phase error. The reduction in gain may be different for adjacent beams, giving rise to a channel imbalance error. This reduces the DF accuracy of an amplitude comparison DF system, as calculated in section 3.2. As an example, a phase error of 15° in the compensation introduces a peak loss of -0.5 dB, so the worst case variation in gain will be ±0.25 dB, introducing a DF error of about 1°.

The effect of transmission errors on the -3 dB beamwidth

Phase and amplitude errors in the compensation change the -3 dB beamwidth. In the worst case, the effect of an amplitude error ΔA on the -3 dB beamwidth is to change the amplitude taper applied to the higher modes, relative to the zero order mode. If the taper is reduced, the beam becomes narrower, while if it is increased, the beam becomes wider. Again the change can be calculated using (4.2.3). Figure 4.3 shows the change in the -3 dB beamwidth as a function of the amplitude error ΔA, for a -30 dB sidelobe Chebyshev pattern formed from the 0^{th}, 1^{st} and 2^{nd} order phase

Effect of compensation network errors on the mainlobe gain

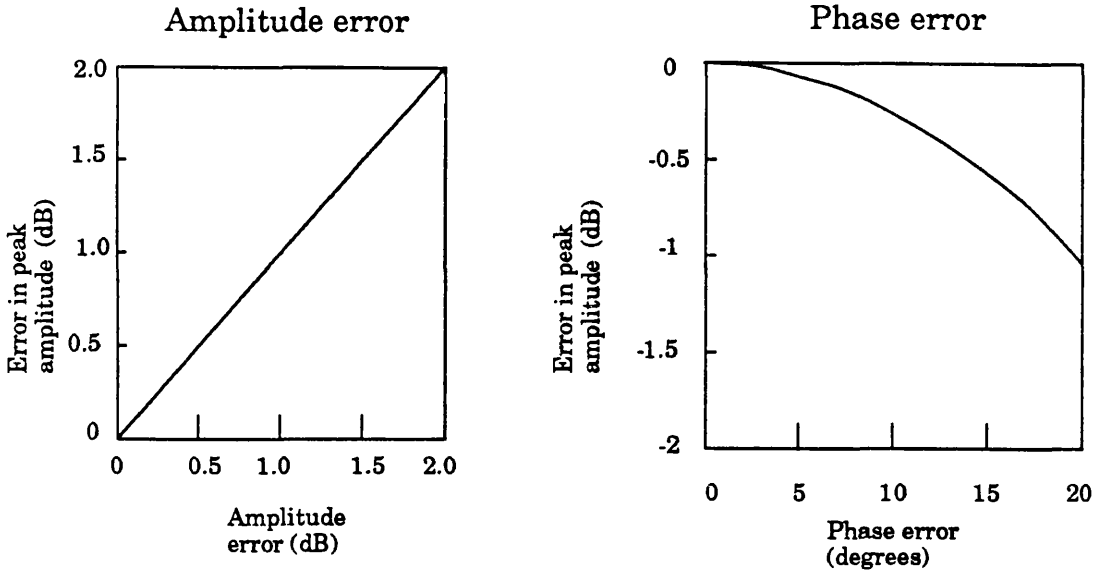

Effect of compensation network errors on the -3 dB beamwidth (Chebyshev pattern)

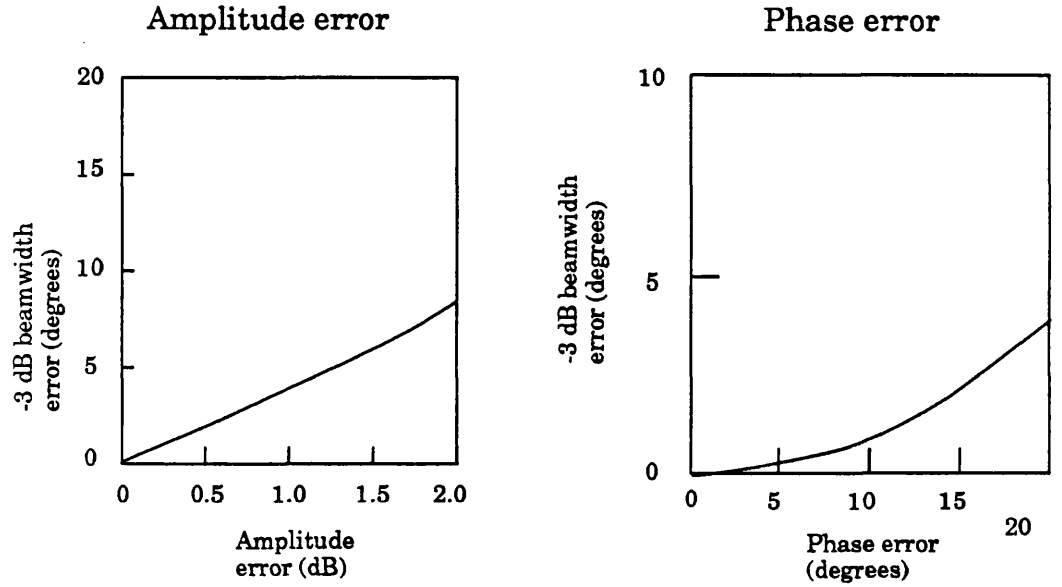

Figure 4.3 The effect of compensation network errors on the peak gain and -3 dB beamwidth of the synthesised beam.

modes. As an example, in the worst case an amplitude error in the compensation of 0.5 dB introduces a 2° change in the -3 dB beamwidth. This in turn introduces a DF error close to 2°, calculated using the equations of section 3.2.

Phase errors increase the -3 dB beamwidth of the mainlobe. Again the change can be calculated using (4.2.3). Figure 4.3 predicts the change in the -3 dB beamwidth as a function of the phase error ΔP for a Chebyshev -30 dB sidelobe pattern. The effect of the change in the -3 dB beamwidth on DF accuracy can be calculated using the equations of section 3.2.

4.2.3 **The effect of Butler matrix transmission errors**

Let us now consider the effect of an error in the transmission paths of a Butler matrix. For a perfect matrix, exciting the 0^{th} order phase mode port excites the four array elements with equal amplitude and phase. Now suppose that the path between the 0^{th} order phase mode port, and element 3 is +10° in error, compared with the other three paths at 0°. The radiation pattern formed by exciting the 0^{th} order mode will not be a perfectly omnidirectional pattern, with constant phase. Nystrom (1987) proposed an analysis of this type of error that assumes the matrix is perfect, and the matrix error alters the mode excitation i.e. the compensation weights. Clearly in the excitation discussed here with a 10° phase error, the zero order mode is dominant, but small components of other modes are present as well.

This study used computer modelling to calculate the transmission scattering parameters for the complete beamformer. Figure 4.1 depicts the matrix beamforming network, with the phase mode compensation in place. Consider the excitation of a single beam port, to form a single wideband azimuth beam. If a signal V_p is applied to the p^{th} beam port, the output at the n^{th} element port is calculated as:

$$V_n^- = V_p^+ \sum_{m=-M}^{M} s^{M2}_{mp}\, s^{m}_{21}\, s^{M1}_{nm} \qquad (4.2.4)$$

s^{M2}_{mp} is the transmission amplitude and phase for the second matrix between the p^{th} element port and the m^{th} mode port.

$s^{m}_{21} = A_m(f)$ - the transmission amplitude and phase for the compensation network connected between the m^{th} mode port of the first matrix, and the corresponding mode port of the second matrix (including the amplitude taper).

s^{M1}_{nm} is the transmission amplitude and phase for the first matrix between the m^{th} mode port and the n^{th} element port.

The element excitation can now be expressed as:

$$V_n^- = V_p^+ s_{np}$$

where

$$s_{np} = \sum_{m=-M}^{M} s^{M2}_{mp} s^{m}_{21} s^{M1}_{nm} \qquad (4.2.5)$$

For a four-element circular array, the excitation is now expressed in terms of four scattering parameters, defining the transmission amplitude and phase between the beam port and the four element ports. Errors in the transmission parameters for either of the matrices can be inserted into

(4.2.4) and the changes in the scattering parameters calculated using the computer program. Either theoretical or measured data can be used.

Once the errors in the amplitude and phase of the transmission parameters are known, the change to the radiation pattern is determined by calculating the excitation of the phase modes required to generate this set of scattering parameters, in effect performing (4.2.4) in reverse, and assuming that the matrices are perfect:

$$A'_m(f) = \sum_{n=1}^{N} s'_{np}(f)\, e^{j2\pi(n-1)m/N} \qquad (4.2.6)$$

The 'effective' mode compensation of the beamformer calculated here can be compared to that theoretically specified by 4.2.1. The effect of compensation amplitude and phase errors ΔA and ΔP on the radiation pattern are predicted by repeating the analysis of section 4.2.2. Alternatively the change in the pattern can be plotted using (4.2.3).

If sidelobe levels below -30 dB are required, the error in the phase mode excitation (whatever the source) must be less than ±2° and ±0.3 dB. For these errors, the peak DF error introduced by changes to the mainlobe is calculated as ±4°. If sidelobes of -20 dB are required, the mode compensation must be realised to better than ±6° and ±0.8 dB. The peak DF error introduced by changes to the mainlobe is ±20°. An individual 180° coupler has the phase and amplitude errors of table 4.1. Since each signal passes through four couplers in total, the cumulative peak errors will be large - transmission errors of 20° and 2 dB can be expected, without even considering the compensation network errors. Inspection of figures 4.2 and 4.3 show that this level of error is unacceptable. Design changes that reduce transmission errors are described in section 4.3.

4.2.4 **Isolation and mismatch errors**

The computer simulation of section 4.2.3 assumes that the input ports of the 180° couplers are isolated and matched. The manufacturer's figures (table 4.1) give an isolation of 17 dB, while the input VSWR is 1.35:1.

Ideally a signal entering from element 1 is isolated from element 3. Imperfect isolation transmits a signal between the two, as shown in figure 4.4. If the transmission between the input ports of the coupler is given by $s_{21} = s_{isol}$, the amplitude of the signal leaving element port 3 will be:

$$V_3^- = V_1^+ s_{isol}$$

If this signal was simply re-radiated by element 3 the synthesised beam would be unaffected, but there is a large mismatch between the monopole element and the 50Ω characteristic impedance of the matrix system, particularly at the ends of the frequency band. If the self-impedance of the monopole element is represented by the scattering parameter s^E_{11} Then the signal reflected back to element port 3 is given by:

$$V_3^+ = V_1 s_{isol} s^E_{11}$$

This signal is now transmitted to the output ports with an amplitude given by the scattering parameters of (4.2.6) for the coupling of the input port 1 to to the output ports. For the p^{th} port:

$$V_p^- = V_3^+ s_{isol} s^E_{11} s_{p1}$$

So in addition to the signal transmitted directly from element port 1 to the beam ports, there is an error signal A_p transmitted from element port 1 to the beam ports via element port 3. This signal will modify the transmission scattering parameters. Let us calculate the approximate magnitude of this error signal. From table 4.1 the isolation between the inputs of a hybrid

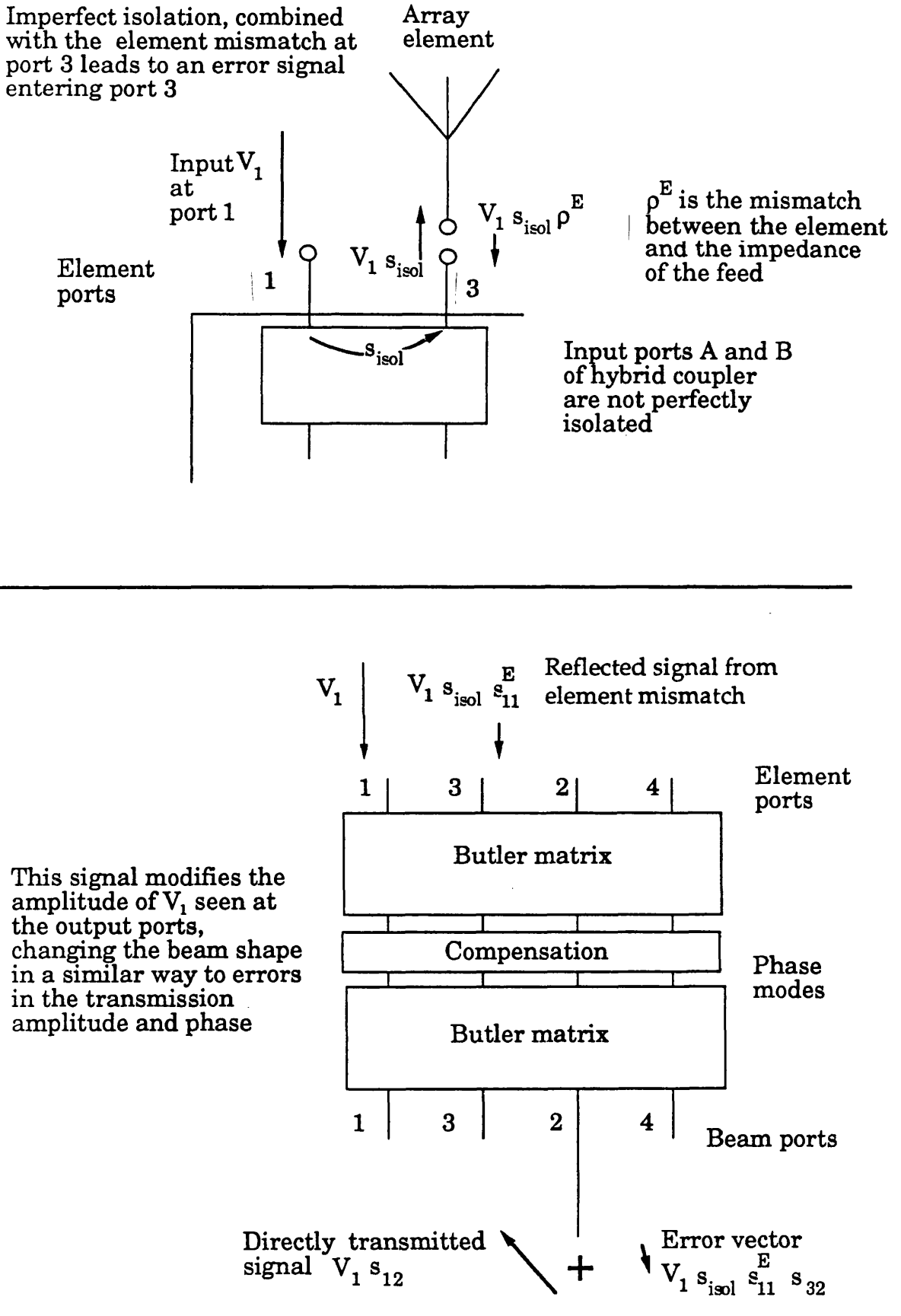

Figure 4.4 An illustration showing how the imperfect isolation of the input ports degrades the transmission amplitude and phase of the network.

coupler is 17 dB. The impedance measurements of section 3.4 show that the return loss of the element (s^E_{11}) is as high as 3 dB. So relative to the main transmission path, the isolation error is -20 dB in amplitude. This will modify the transmission parameters by as much as 0.9 dB, in amplitude, or 5.7° in phase, depending on the relative orientation of the two vectors. The effect of this error on the synthesised pattern can be calculated using the analysis of section 4.2, where the effect of transmission amplitude and phase errors on the synthesised pattern is calculated.

The predicted effect of imperfect isolation on the synthesised pattern was unacceptable. To reduce this, isolators operating over the band 8 to 12 GHz were installed in the element feeds. Omni-Spectra isolators type ML 3221, with a peak return loss of 17 dB were used. This reduced the return loss of the elements from 3 dB to 17 dB, giving an error signal amplitude of -34 dB - acceptable for this study.

The match at the input port of a hybrid coupler is not perfect. From table 4.1 the VSWR (max) for a hybrid coupler is 1.35, corresponding to a return loss of 17 dB. For a signal entering the hybrid coupler from the element port, a significant proportion of the signal is reflected back to the element, and then reflected again by the element, which does not present a good match across the frequency band. The effect of this is to change the transmission parameters in exactly the same way as the isolation error. This error manifests itself as a ripple on the amplitude and phase response, when plotted as a function of frequency. At certain frequencies the main signal and the reflected signal add in phase and the transmission amplitude is increased. At other frequencies the main signal and the reflected signal are in antiphase and the transmission amplitude is reduced. In between these frequencies the amplitude error is reduced but the phase error is a maximum. Indeed, the physical distance between the mismatches can be calculated from the period of the amplitude ripple in the frequency domain. As for isolation errors, the effect of mismatch errors is largely eliminated by using isolators in the element feeds.

4.3 The evolution of the beamformer design

4.3.1 The design and evaluation of a microwave wideband Butler matrix

To form the phase modes a 4 x 4 Butler matrix operating over the frequency band 8 to 12 GHz was required. The matrix design of Butler and Lowe (1961) is depicted in figure 2.10. This matrix is a narrowband design, unless the single 90° phase shift is also wideband. The wideband design of figure 4.5 eliminates the single 90° phase shift by substituting a 90° (quadrature) coupler for one of the 180° couplers. This wideband matrix was developed to operate in the UHF frequency range by Chow and Davies (1967). This design was adopted for this study, using microwave directional couplers. Figure 4.5 also depicts the 8 x 8 wideband Butler matrix for feeding eight-element arrays.

Three Omni-Spectra 180° couplers type 2031-6335-00, with the specification of table 4.1 were used in the matrix. One Anaren 10018-3 quadrature coupler was used, with the specification of table 4.2 below.

Frequency range	8.0 to 12.4 GHz
Coupler amplitude imbalance	±0.5 dB
Phase error	±6°
Insertion loss	+0.5 dB
Isolation between inputs	18 dB
Input VSWR (Max)	1.40

Table 4.2 The manufacturers specification for Anaren quadrature couplers type 10018-3 operating over the frequency band 8 to 12.4 GHz.

There is a significant difference in the transmission phases of microwave 180° couplers, compared with HF 180° couplers, illustrated by table 4.3 overleaf.

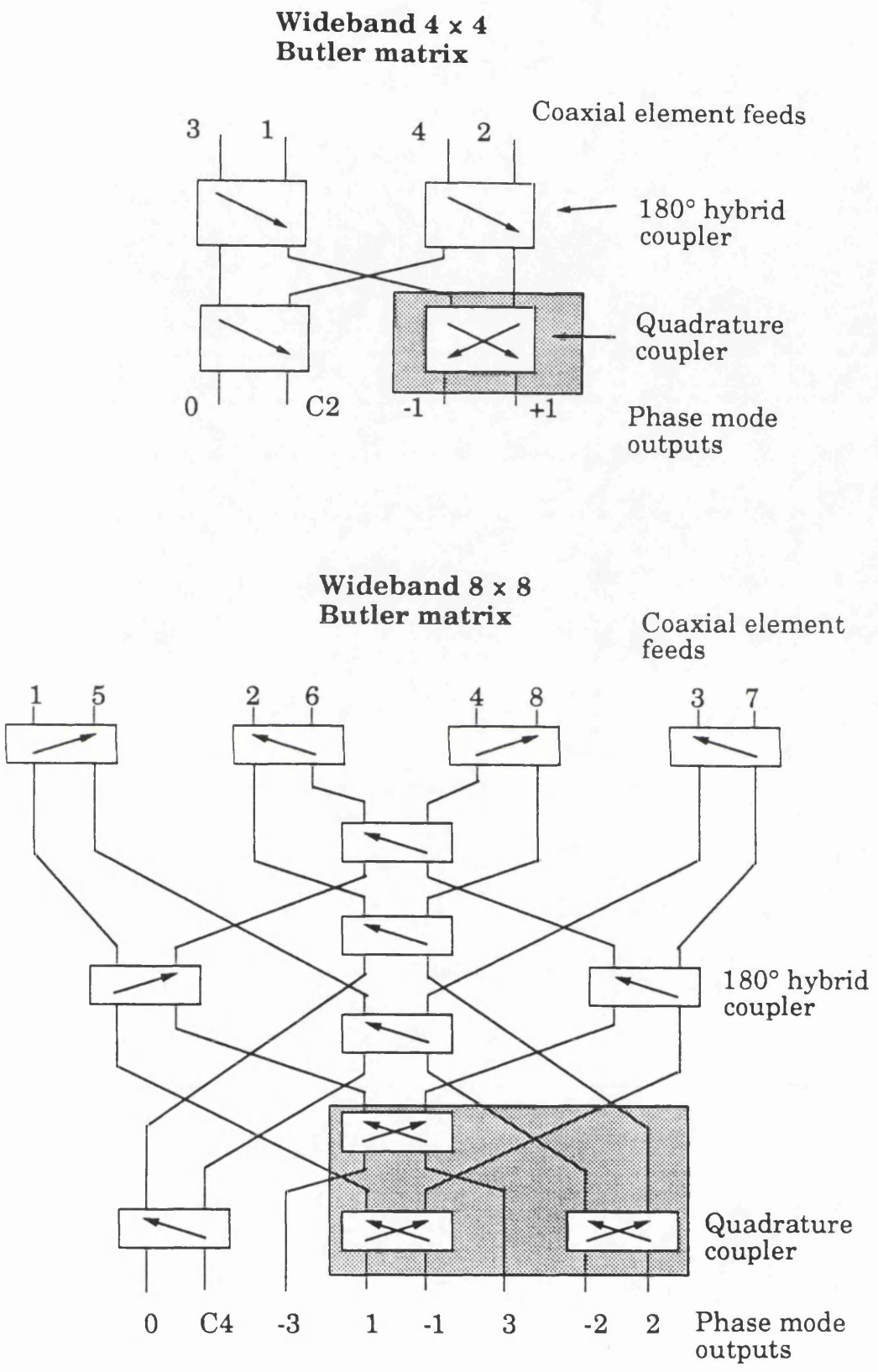

Figure 4.5 Schematic diagrams of 4 x 4 and 8 x 8 Butler matrices. If the couplers in the shaded areas are removed, the matrices are turned into wideband amplitude mode matrices.

	C	D
A	0	180
B	0	0

Transmission phases for HF "magic tee" coupler

	3 (0)	4 (0180)
1 (Δ)	+90	-90
2 (Σ)	0	0

Transmission phases for microwave hybrid coupler

Table 4.3 A comparison between the transmission phases of HF and microwave 180° couplers.

At HF frequencies the 180° coupler is based on a transformer with a centre-tapped secondary. At microwave frequencies the 180° coupler is a quadrature (90°) coupler with an additional +90° wideband phase shift in the line to output three (0°). The +90° wideband phase shift is supplied by a second coupled $\lambda/4$ section, developed by Schiffmann (1958). Both the coupler and phase shift are built on stripline. The phase transfer characteristics of a microwave matrix is compared with that of an HF matrix in table 4.4 overleaf.

Transmission phases for 4 x 4 HF wideband matrix

Element No.	Phase mode 0	+1	2	-1
1	0	0	0	0
2	0	+90	180	-90
3	0	180	0	-180
4	0	-90	180	+90

Transmission phases for 4 x 4 microwave wideband matrix

Element No.	Phase mode 0	+1	2	-1
1	0	+90	-90	0
2	0	180	+90	-90
3	0	-90	-90	-180
4	0	0	+90	+90

Table 4.4 A comparison between the transmission phases of HF and microwave wideband Butler matrices.

The only difference these phase shifts make is to alter the wideband phases of the +1 and C2 modes, relative to the zero order mode. Wideband phase shifts of -90° and +90° are now required in the mode compensation to bring them back into phase alignment. The transmission amplitude of HF and microwave matrices is the same, barring errors. For an input of 0 dBm at an element port, there is an output of -6 dBm at each of the mode ports.

Figure 4.6 is a photograph of a 4 x 4 matrix constructed for this study. Sealectro semi-rigid cable type AA50141 of 0.141 inch diameter was used to connect the couplers together. All 16 paths through the matrix must be the same electrical length, to preserve the wideband phases of the modes. Fine adjustments were done using four Midisco 1089-1 line stretchers with screw adjusters. The change in length was accommodated by loops of semi-rigid cable, visible in the photograph. The completed matrix was enclosed in a die-cast box. The (-6 dB) transmission amplitude to the mode ports was realised to within ±1 dB. The phase transmission characteristics of table 4.4 were realised to within ±10° across the frequency band. Since the individual couplers contributed ±0.5 dB and ±6° of transmission error,

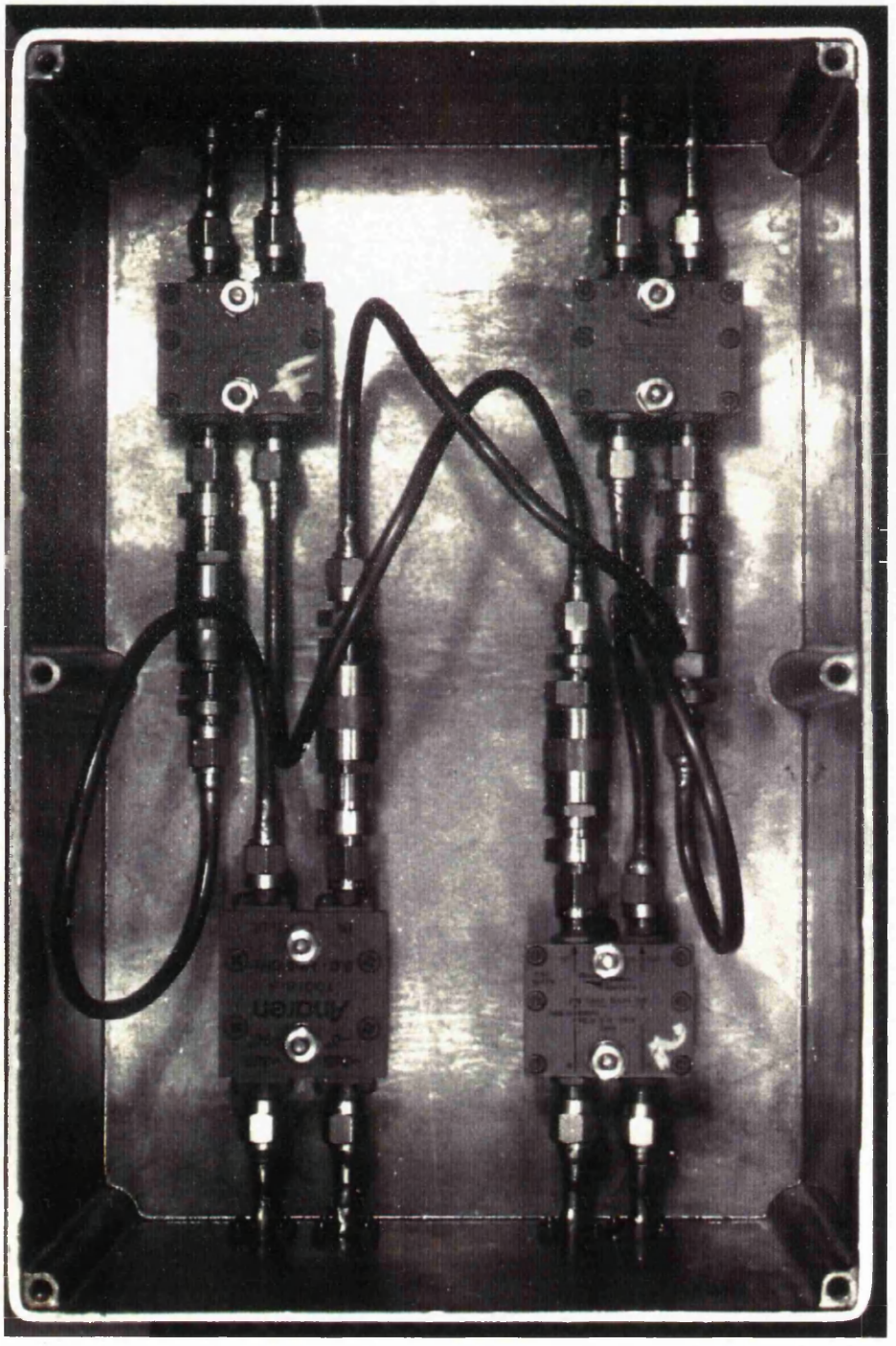

Figure 4.6 A photograph of a 4 x 4 wideband Butler matrix that operates over the band 8 to 12.4 GHz. This was turned into an amplitude mode matrix by removing the single quadrature coupler and replacing it with longer semi-rigid cables.

these figures were expected. The isolation and mismatch performance will be considered later in this section.

A second 4 x 4 matrix identical to the first was built to form the four beams from the compensated phase modes, as shown in figure 4.1.

Section 4.2 describes a technique for comparing the measured beamformer transmission amplitude and phase to the theoretical transmission parameters. This allowed the performance of the complete beamformer to be evaluated. At this stage of the project the frequency compensation networks were not ready. Rather than wait, the matrices were connected together without any compensation networks, as shown in figure 4.7. The transmission scattering parameters were measured using a network analyser. These results were compared to those predicted by the computer model based on equation (4.2.4). In the computer model the figures:

$$|A_m(f)| = 1$$
$$\text{Arg}\{A_m(f)\} = 0° \qquad (4.3.1)$$

were inserted in place of the theoretical frequency compensation. The computer program showed that this beamformer has unusual transmission characteristics. Consider a signal of 0 dBm fed into element port 1 of the first matrix. The theoretical output amplitude at each of the output beam ports is given in table 4.5 overleaf.

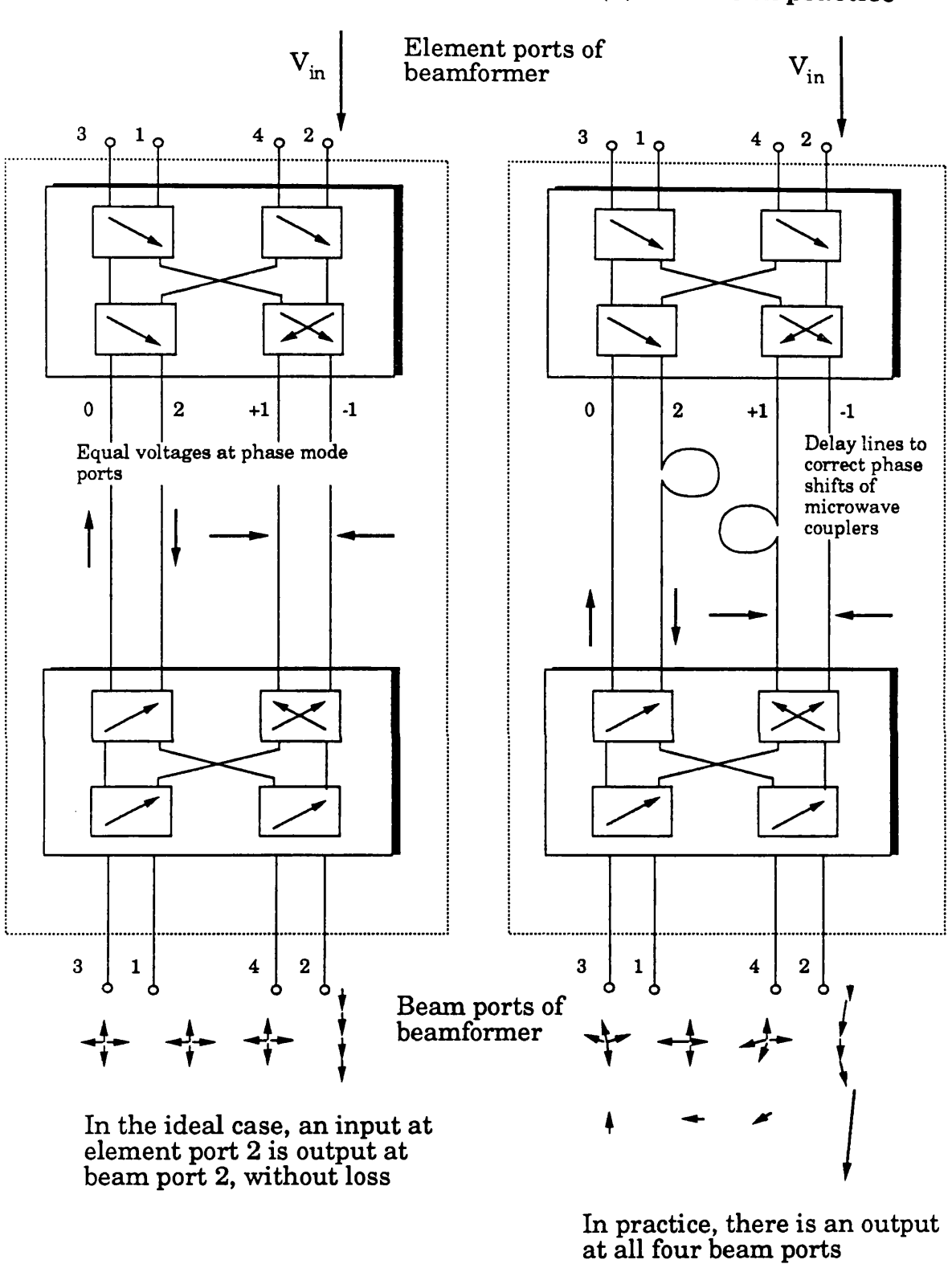

Figure 4.7 The transmission amplitude and phase of a pair of Butler matrices connected together:
(a) The ideal case.
(b) Measured results.

Output port number	Ideal transmission response	
	|s|(dB)	∠(s)
1	0 dBm	$e^{-2jb\|m}$
2	-∞ dB	-
3	-∞ dB	-
4	-∞ dB	-

Table 4.5 The theoretical wideband transmission parameters for a pair of Butler matrices, connected together without compensation.

At beam port 1 there is an output of 0 dBm, while the other three outputs ports are quiescent; there is no output. This is illustrated graphically in figure 4.7. Equally, if a 0 dBm signal is fed to element port 2, there is a 0 dBm output at beam port 2, and ports 1, 3 and 4 are quiescent. The phase of the output signal is determined by the electrical length of the two matrices, $2\beta l_m$. This system is effectively a spatial Fourier transform immediately followed by an inverse Fourier transform. If this beamformer was connected to a monopole array, the beams 'synthesised' from the phase modes would have a shape identical to the radiation pattern of the monopole elements - a remarkably pointless exercise.

Table 4.6 (overleaf) gives the results of network analyser measurements for the beamformer. Delay lines were used to correct the wideband phase shifts of the +1 and C2 modes (table 4.5) so these result are narrowband. By adjusting the delay line length, measurements were made at 8, 9, 10, 11 and 12 GHz. Worst case results are given in each case, with the frequency at which it occurred. The ideal figures, supplied by the computer program, are in brackets

Matrix parameter	Theoretical parameters for ideal system	Measured parameter
Transmission amplitude	0 dB	-4.0 dB @ 12 GHz
Output at quiescent ports	-∞ dB	-14 dB @ 11 & 12 GHz
Isolation between element ports (dB)	-∞ dB	15 dB @ 12 GHz
Return loss at element ports	-∞ dB	14 dB @ 12 GHz
Electrical length of matrix	e^{-2jblm}	2 x 7.33λ @ 10 GHz including line stretchers

Table 4.6 Network analyser measurements of the Butler matrix pair.

The isolation between beam ports was 15 dB. Table 4.1 shows that the worst isolation between coupler ports is 17 dB. However, added to this is a second signal, reflected from the mismatch of the next coupler down the line. This reflection is -23 dB in amplitude (peak) at the isolated element port. If this reflection adds in phase with the (-17 dB) isolation, the isolation between the element ports is reduced by as much 3.5 dB.

The return loss was 14 dB. This compares with 17 dB for a single coupler. Again, the 3 dB increase was due to secondary reflections adding to that of the first coupler.

The peak beamformer loss of -4.0 dB is to be expected. The peak loss introduced by each hybrid coupler is about 0.5 dB, so each matrix had a measured loss of about 1.5 dB, including the connectors. Another 0.5 dB can be attributed to the line stretches and coaxial lines connecting the two matrices. The transmission phase and amplitude errors sent -14 dB

(maximum) to the other beam ports, reducing the main signal by about 0.5 dB.

The peak amplitude at the quiescent port was -14 dB, attributable to imperfect phase and amplitude transmission errors. While the isolation and mismatch errors can be eliminated with isolators, transmission errors present a greater problem. Referring to figure 4.2, a resultant of -14 dB will grossly increase sidelobe levels and distort the shape of the main lobe. The -14 dB result at 12 GHz was actually at beam port 3, for an input at element port 1. By 'tweaking' the length of the connecting lines (i.e. adjusting the transmission phase of the compensation) this was reduced to -20 dB. Unfortunately the output at beam port 2 then increased to -13.5 dB at 12 GHz. Similar difficulties were encountered in chapter 5, where these matrices were used for pattern synthesis. Optimising the output at one beam port made the other three worse.

These results show that the beamformer of figure 4.1 cannot synthesise low sidelobe beams for an amplitude comparison DF system, due to the transmission errors. For this reason, the design of beamformers with smaller transmission errors was investigated.

4.3.2 **The design and evaluation of a microwave amplitude mode matrix**

For the pair of Butler matrices, connected as shown in figure 4.7, the systematic errors in the transmission amplitude and phase of the directional couplers add cumulatively. Thus at the ends of the frequency band some of the 16 paths between the four inputs and four outputs have errors close to ±2 dB and ±24°. Mosko (1984) looked at the design of 'symmetrical' beamformers, where the errors introduced by the couplers of the beam forming network cancel the errors introduced by the couplers of the mode forming network. The Butler matrix is clearly asymmetrical, with just one 90° coupler. If this 90° coupler is removed the resulting matrix can be drawn as shown in figure 4.8. While the 0^{th} and 2^{nd} order modes remain unchanged, the other two outputs are clearly not phase

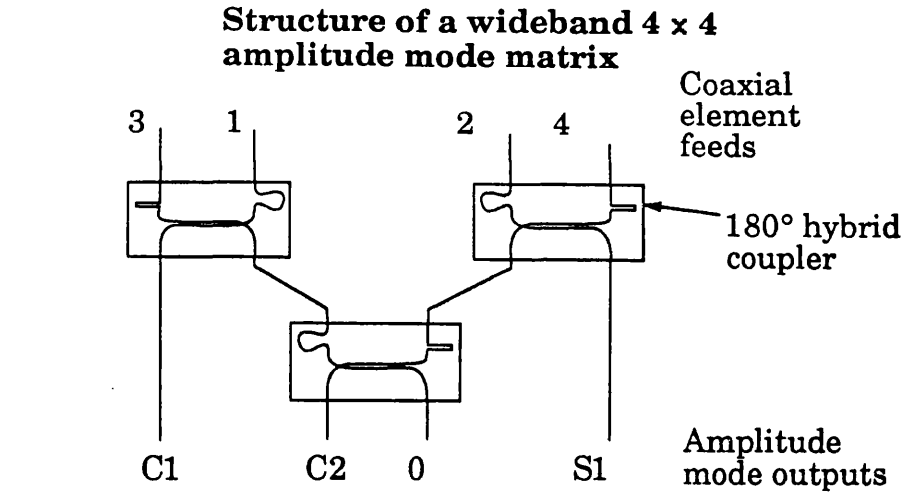

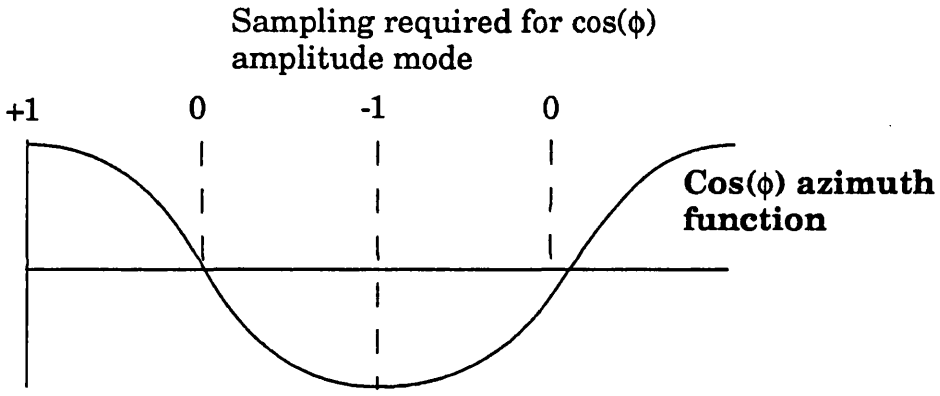

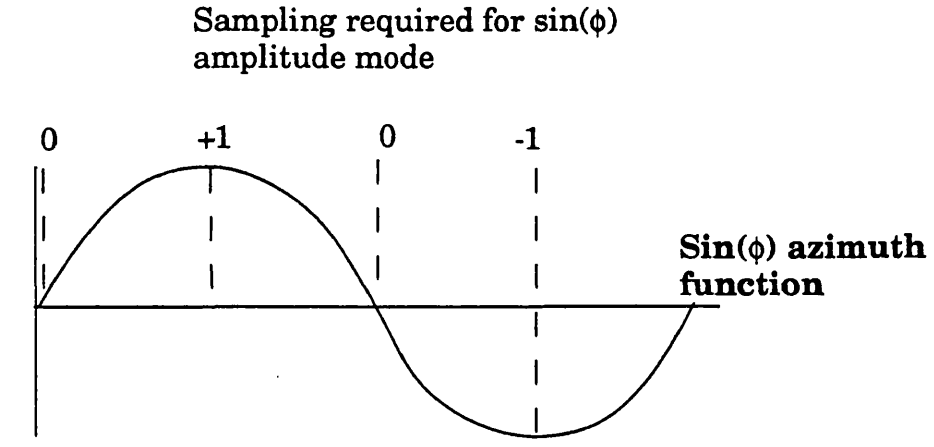

Figure 4.8 Transmission amplitude and phase for a microwave 4 x 4 amplitude mode matrix

modes; they combine signals from opposing array elements in antiphase. Figure 4.8 shows that this is the sampling of the four-element array required to excite the 1st order sine and cosine amplitude modes. Since every mode excited by this matrix is an amplitude mode, the name 'amplitude mode matrix' was chosen for this design. (N.B. the zero order mode is a special case, as it is both an amplitude mode and a phase mode). The transmission amplitude and phase for this device is given in table 4.7 below.

		Phase mode			
		0	C1	C2	S1
Element No.	1	-6	-3	-6	-∞
	2	-6	-∞	-6	-3
	3	-6	-3	-6	-∞
	4	-6	-∞	-6	-3

Amplitude (dB)

		Phase mode			
		0	C1	C2	S1
Element No.	1	0	180	-90	-
	2	0	-	+90	180
	3	0	0	-90	-
	4	0	-	+90	0

Phase (degrees)

Table 4.7 Wideband transmission amplitude and phase for an amplitude mode matrix made using three Omni-Spectra 180° couplers type 2031-6335-00.

This matrix design is one of a family. Figure 4.5 shows the 8 x 8 Butler matrix. If the 90° couplers in the shaded areas are removed and replaced by coaxial lines to give the correct delay, the resulting matrix is an 8 x 8 amplitude mode matrix. Several workers have noted that amplitude modes are formed by combining the +m and -m phase modes. In fact the reverse is true; the +m and -m phase modes are formed by combining the cosine and sine amplitude modes in a 90° coupler. The amplitude mode matrix has several advantages over a Butler matrix (overleaf):

- Fewer components are required, just three couplers for a 4 x 4 matrix.

- The matrix is built from just one device; the 180° coupler.

- Amplitude modes of the same order are perfectly orthogonal. For phase modes exciting the +m mode results in a reflection at the -m mode port, unless the array elements are perfectly matched. For amplitude modes the reflections return to the same amplitude mode port.

- As demonstrated in chapter 3 amplitude modes can be impedance matched with an impedance-matching network at the mode port.

- Theoretical calculations using equation (4.2.4) showed that systematic errors in the phase and amplitude of the coupling sections cancel. Provided the coupling sections of the couplers in the second matrix have the same systematic errors as the first, the errors will cancel.

Systematic errors introduced by the Schiffmann section in one arm of the coupler remain, and do not cancel. The amplitude mode matrix has one major disadvantage over a Butler matrix. Davies (1965) has shown that directional patterns synthesised from a circular array can be electronically rotated by applying a linear phase progression to the phase mode inputs of the Butler matrix. This only applies to phase modes. Amplitude modes cannot be steered using a linear phase progression.

The amplitude mode matrix was constructed from the Butler matrix in the photograph of figure 4.6, with the quadrature coupler removed. Longer semi-rigid cables compensated for the removed coupler. The 180° coupler uses a stripline structure. Because the group velocity of this type of guide is different to the TEM mode of the semi-rigid cable, the relative phases of the 0^{th} and 2^{nd} order modes (generated by two couplers in sequence) is slightly

different to that of the C1 and S1 modes (generated by a single coupler). This error is minimised by adjusting the line stretchers, introducing a very small phase slope. Even with this error, the phase transmission characteristics of table 4.7 were realised to within ±10° and the amplitude transmission characteristics to within ±1 dB. The peak errors, compared with a Butler matrix are not reduced. The aim is to cancel them in the second matrix.

A second 4 x 4 amplitude mode matrix identical to the first was built to form the four beams. To evaluate this system the matrices were again connected directly together, as shown in figure 4.9. This time a wideband 180° phase shift in the 2nd order phase mode path was used to make the beamformer operation instantaneously wideband. Wideband 1 dB attenuators (Midwest type 444) were used in the C1 and S1 paths to compensate for the insertion loss of the second 180° coupler forming the 0th and C2 modes. Table 4.8 below gives the measured network analyser results for the beamformer.

Matrix parameter	Theoretical parameters for ideal system	Measured parameter
Transmission amplitude	0 dB	-4.0 dB @ 12 GHz
Output at quiescent ports	-∞ dB	-20 dB @ 12 GHz
Isolation between element ports (dB)	-∞ dB	15 dB @ 12 GHz
Return loss at element ports	-∞ dB	14 dB @ 12 GHz
Electrical length of matrix	$e^{-2jb\ln}$	2 x 7.33λ @ 10 GHz plus wideband phase compensation

Table 4.8 Network analyser measurements of the amplitude mode matrix pair.

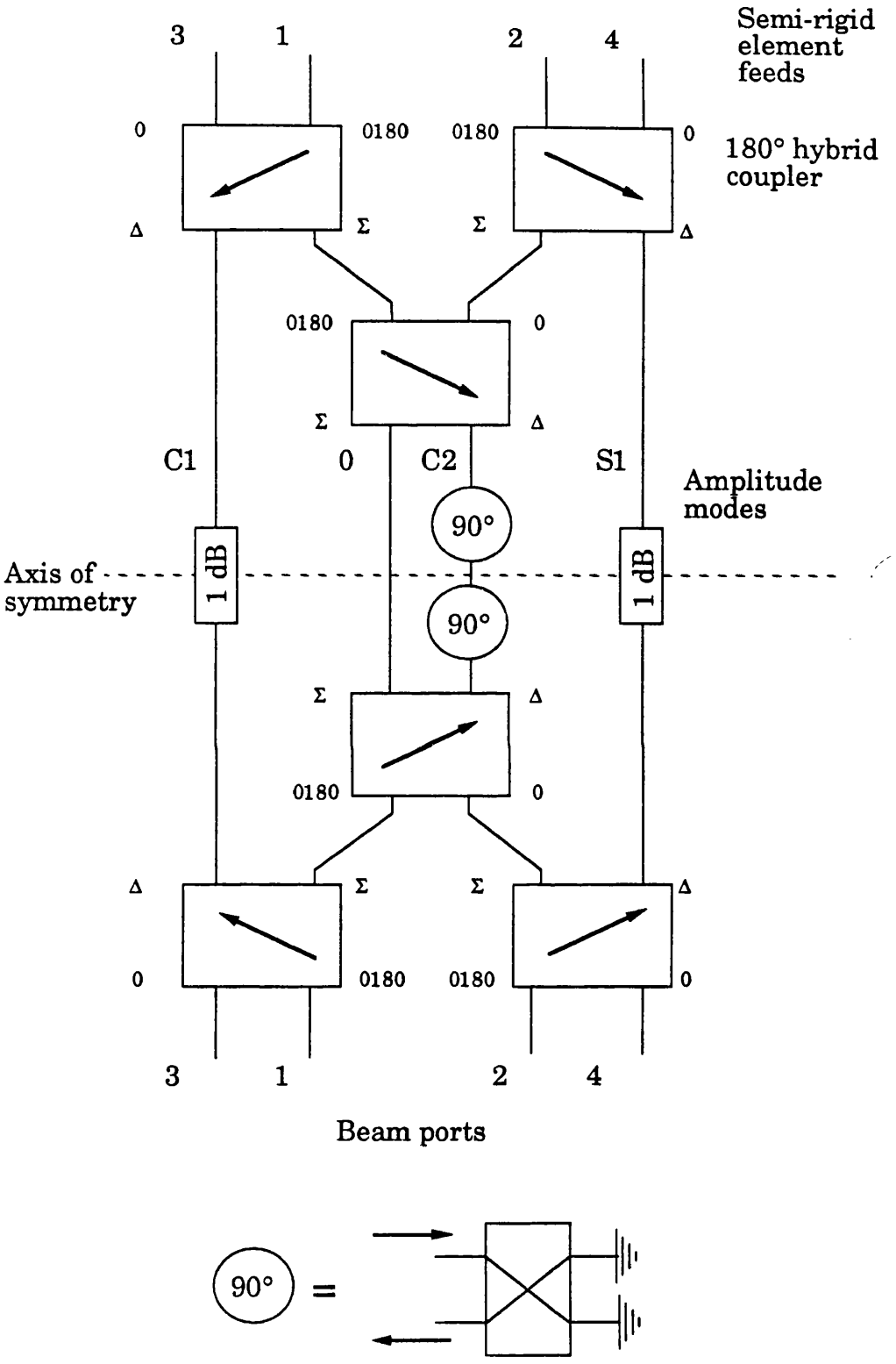

Figure 4.9 A pair of amplitude mode matrices connected together to form a wideband Fourier transform/inverse transform pair.

The signals at the three quiescent ports are at -20 dB at worst, 6 dB better than the Butler matrix beamformer. Several factors limited the improvement to 6 dB:

(i) Transmission errors in the Schiffmann section.

(ii) The 90° couplers used to form a 180° phase shift in the compensation of the 2nd order mode.

(iii) Phase and amplitude transmission errors caused by imperfect connectors and by reflections from mismatches within the matrix.

The level at the quiescent port is only -16 dB down on the (-4 dB) transmission amplitude. This resultant has the same effect on beams as the resultant R plotted in figure 4.2. The minimum sidelobe level will be -16 dB and the effect of this error on the -3 dB beamwidth will also be large. These results show that although the amplitude mode matrix is a considerable improvement (6 dB) over the Butler matrix, in terms of transmission errors, the results are not good enough for wideband synthesis of low sidelobe patterns. The predicted peak sidelobe level is in the region of -16 dB, and errors introduced by the frequency compensation networks have not even been considered yet. To achieve wideband patterns with low sidelobes, further work is required on the beamformer (section (4.3.3)).

Foti and Macnamara (1989) describe the design of hybrid 180° couplers with a transmission phase error of just ±1°, over a 26% bandwidth around 1 GHz. The amplitude errors are as large as those for the 50% bandwidth couplers used here, but these cancel in the amplitude mode matrix beamformer. At HF frequencies a symmetrical 180° coupling structure is used, based on a transformer with a centre-tapped secondary. There are no Schiffmann sections and no 180° wideband phase shift is required in the compensation, so errors (i) and (ii) above are eliminated. Phase errors introduced by connectors etc. are lower, so (iii) is reduced. The potential of the amplitude mode matrix at HF frequencies may well deserve further investigation.

Guy (1985) describes in principle a synthesis technique using a single Butler matrix with circulators placed in the element feeds. The compensation networks are terminated in short circuits, so the signals are reflected back through the lone matrix, forming beams at the 3rd port of the circulator. The network of figure 4.9 is perfectly symmetrical about the dotted line drawn through the centre of the compensation networks, so this approach could be applied to this network, where the transmission errors cancel. Unfortunately the four isolators available for this study had a peak isolation of just 17 dB, so the beam formed would here been the sum of a Chebyshev 30 dB sidelobe pattern with an omnidirectional monopole pattern, -17 dB down in amplitude.

4.3.3 **Exciting phase modes using weighted corporate feeds**

In the last two sections equation (4.2.4) was used to calculate the ideal transmission amplitude and phase for the beamforming network, but without any phase mode compensation. Let us now use this equation to calculate the theoretical transmission amplitude and phase, but with the compensation. Table 4.9 below calculates the amplitude mode compensation required to form a Chebyshev beam at 10 GHz. This amplitude taper forms a beam with a -3 dB beamwidth of 82° and -30 dB sidelobe levels, as depicted in figure 3.7.

Mode order	0	C1	C2	S1
Mode coefficients	0 dB, 0°	0 dB, +66°	-9.3 dB,+161°	0 dB, +66°
Mode compensation	-0 dB, 0°	-2.29 dB, -66°	-0.64 dB, -161°	-2.29 dB, -66°
Final mode weights	-0 dB, 0°	-2.29 dB, 0°	-9.94 dB, 0°	-2.29 dB, 0°

Table 4.9 The amplitude mode compensation used in the synthesis of a -30 dB sidelobe Chebyshev pattern.

The mode coefficients are taken from figure 3.17 - they are the same for phase modes and amplitude modes. To form four Chebyshev beams in the directions ϕ = 0°, 90°, 180° and 270° the element excitation is given in table 4.10 below. This was calculated using a computer model based on (4.2.4).

Element number	1	2	3	4
Beam 1 (0°)	-7.8 dB, 0°	-6.0 dB, +89°	-10.9 dB,+210°	-6.0 dB, +89°
Beam 2 (90°)	-6.0 dB, +89°	-7.8 dB, -0°	-6.0 dB,+89°	-10.9 dB, +210°
Beam 3 (180°)	-10.9 dB, +210°	-6.0 dB, +89°	-7.8 dB, -0°	-6.0 dB,+89°
Beam 4 (270°)	-6.0 dB,+89°	-10.9 dB, +210°	-6.0 dB, +89°	-7.8 dB, -0°

Table 4.10 The theoretical element amplitude and phase required to form four Chebyshev beams at 10 GHz.

For each beam the element facing the rear of the beam has the lowest amplitude: -10.9 dB. Inspection of the excitations for each beam show they are identical, with just the numbering of the elements transposed. Realising these transmission parameters with the amplitude mode matrix of figure 4.9 is described in the results section 5.2. This proved difficult, even at a single frequency, as predicted by the results of section 4.3.2.

As an aside, the excitation of table 4.10 resembles a beam cophasal excitation of the four-element array. To form a cophasal beam in the direction of element 1, the excitation is:

Element number	1	2	3	4
Beam 1 (0°)	-6.0 dB, 0°	-6.0 dB, +43°	-6.0 dB,+86°	-6.0 dB, +43°

Compared with this, the mode excitation applies a (small) amplitude taper and a more rapid phase progression. Of course, the modal analysis is superior, since it takes account of mutual coupling, and can be used to form low sidelobe patterns.

Provided the transmission amplitude and phase of table 4.10 is realised, the network used to form the beam is actually immaterial. Figure 4.10 depicts the substitution of a corporate feed for a Butler matrix feed. Although this network can only form one beam, the transmission errors are far less than those of the Butler matrix. The Wilkinson splitters used in this network are symmetrical devices, and the phase and amplitude balance between the outputs is very good. Network analyser measurements showed an accuracy of ±2° and ±0.1 dB. The excitation required changes with frequency. By repeating the calculations of table 4.9 across the frequency band the changes in the excitation were predicted. These are given in table 4.11 (overleaf), for a wideband beam in the direction $\phi = 180°$. This direction was chosen so the excitation of element 3 was the 0° phase reference. The reason for choosing element 3 as the phase reference will become clearer in section 4.4.3.

A beamformer where the phase modes are formed by a Butler matrix and beams formed by a second matrix

A weighted corporate feed to form a single beam

For a Chebyshev beam the amplitude and phase of W_1, W_2, W_3 and W_4 are given in table 4.10.

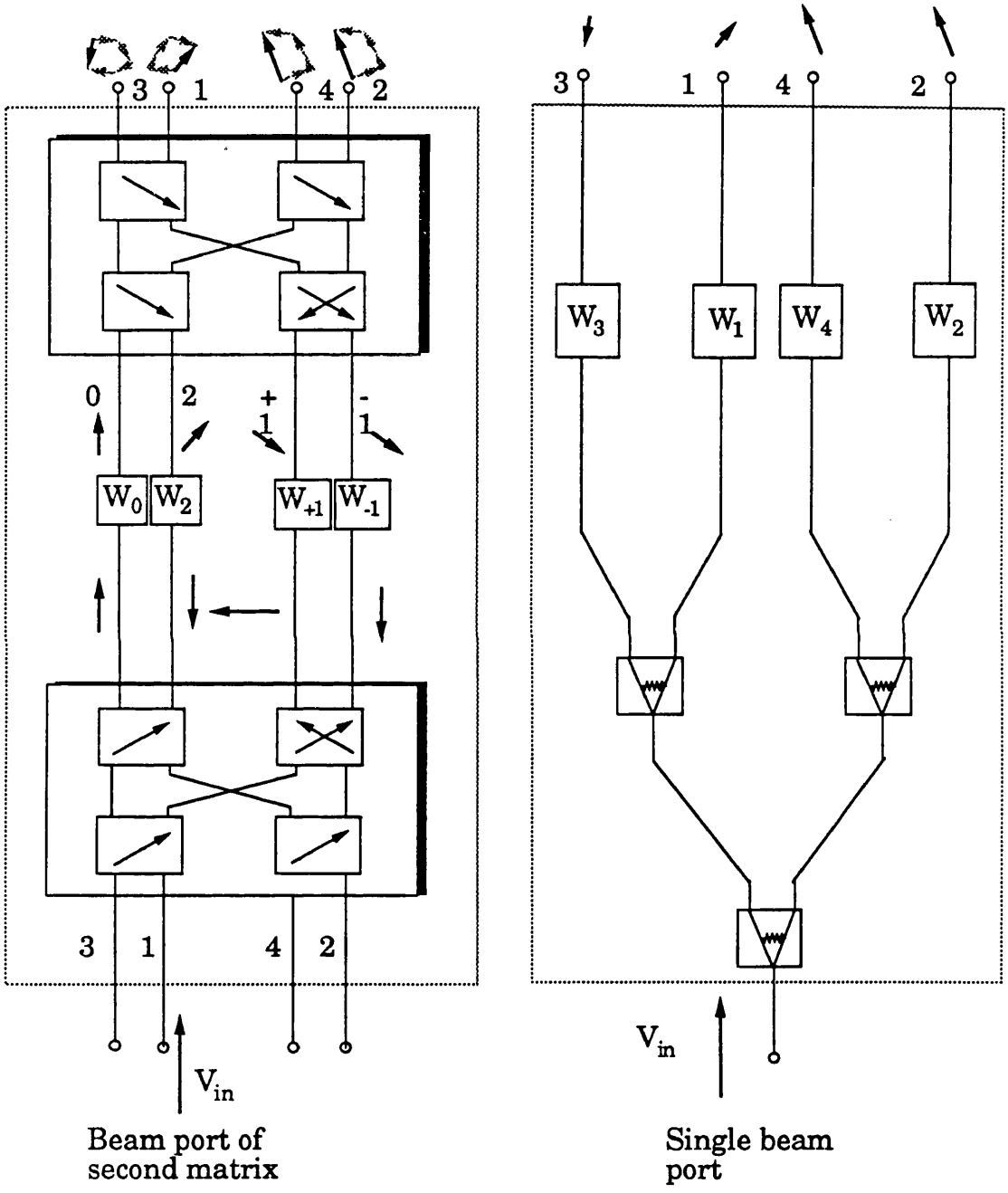

Figure 4.10 The replacement of a Butler matrix feed by a corporate feed to synthesise a single beam.

Element number	1	2	3	4
8 GHz	-8.6 dB, -102°	-6.0 dB, +134°	-9.2 dB, 0°	-6.0 dB, +134°
9 GHz	-9.4 dB, -128°	-6.0 dB, +105°	-9.3 dB, 0°	-6.0 dB, +105°
10 GHz	-10.9 dB, -150°	-6.0 dB, +89°	-7.8 dB, 0°	-6.0 dB, +89°
11 GHz	-11.9 dB,-160°	-7.1 dB, +84°	-6.0 dB, 0°	-7.1 dB, +84°
12 GHz	-11.6 dB,-166°	-7.8 dB, +79°	-6.0 dB, 0°	-7.8 dB, +79°

Table 4.11 The theoretical element amplitude and phase required to form a single wideband Chebyshev beam.

The peak transmission amplitude of the corporate feed is -6 dB. The results of table 4.11 have been normalised to this peak value. The change in the amplitude of the excitation with frequency is plotted in figure 4.11a. The non-linear responses are difficult to realise. By accepting a reduction in the peak gain at the ends of the frequency band, more realisable frequency responses can be plotted - figure 4.11b. Although the peak gain is reduced, the relative amplitude of the modes is unchanged, compared to figure 4.11a, so the shape of the beam is unchanged across the band.

The phase response of table 4.11 is plotted in figure 4.12a. The relative phases change monotonically with frequency. Linear phase responses are desirable, but unfortunately the change is not perfectly linear. Figure 4.12b plots the same relative phases at each frequency, but adjusted relative to the other frequencies to produce a more linear phase response.

The process used to determine the element excitation for a Chebyshev beam was also used to determine the excitation required to form a sin(x)/Nsin(x)

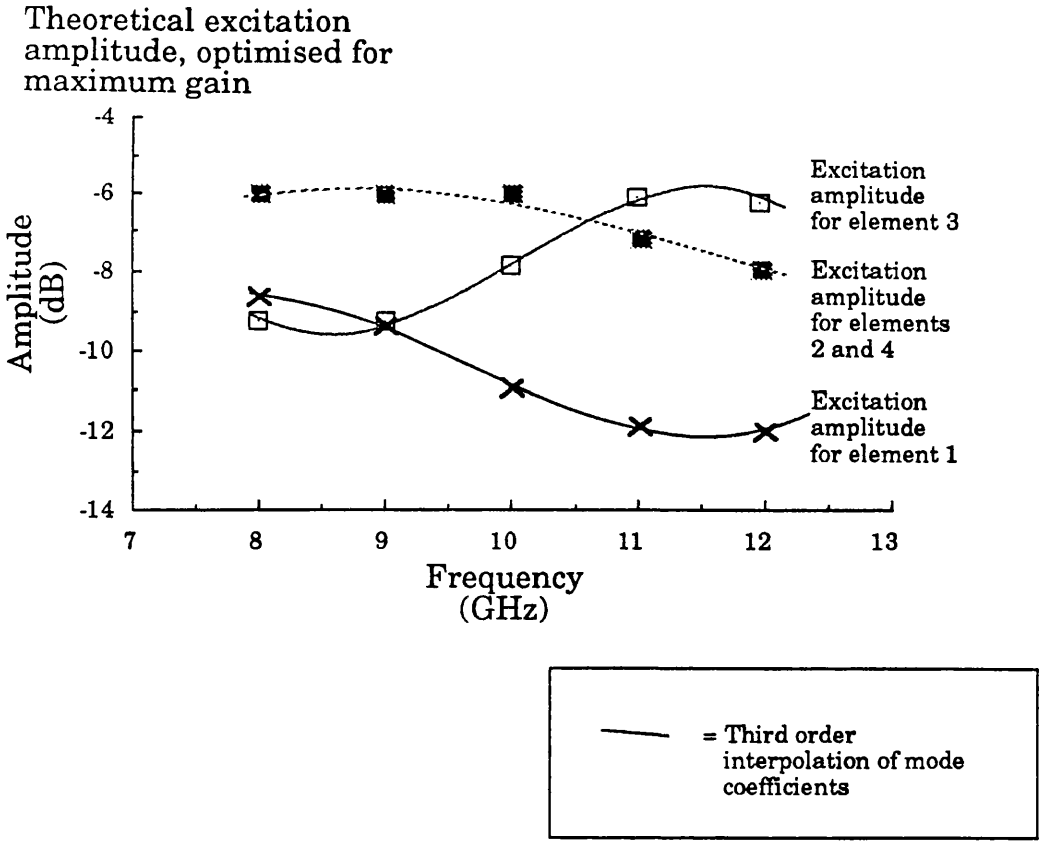

Figure 4.11 Amplitude of element excitation required to form instantaneously wideband -30 dB sidelobe Chebyshev beam:
(a) For maximum gain.
(b) For smooth amplitude responses.

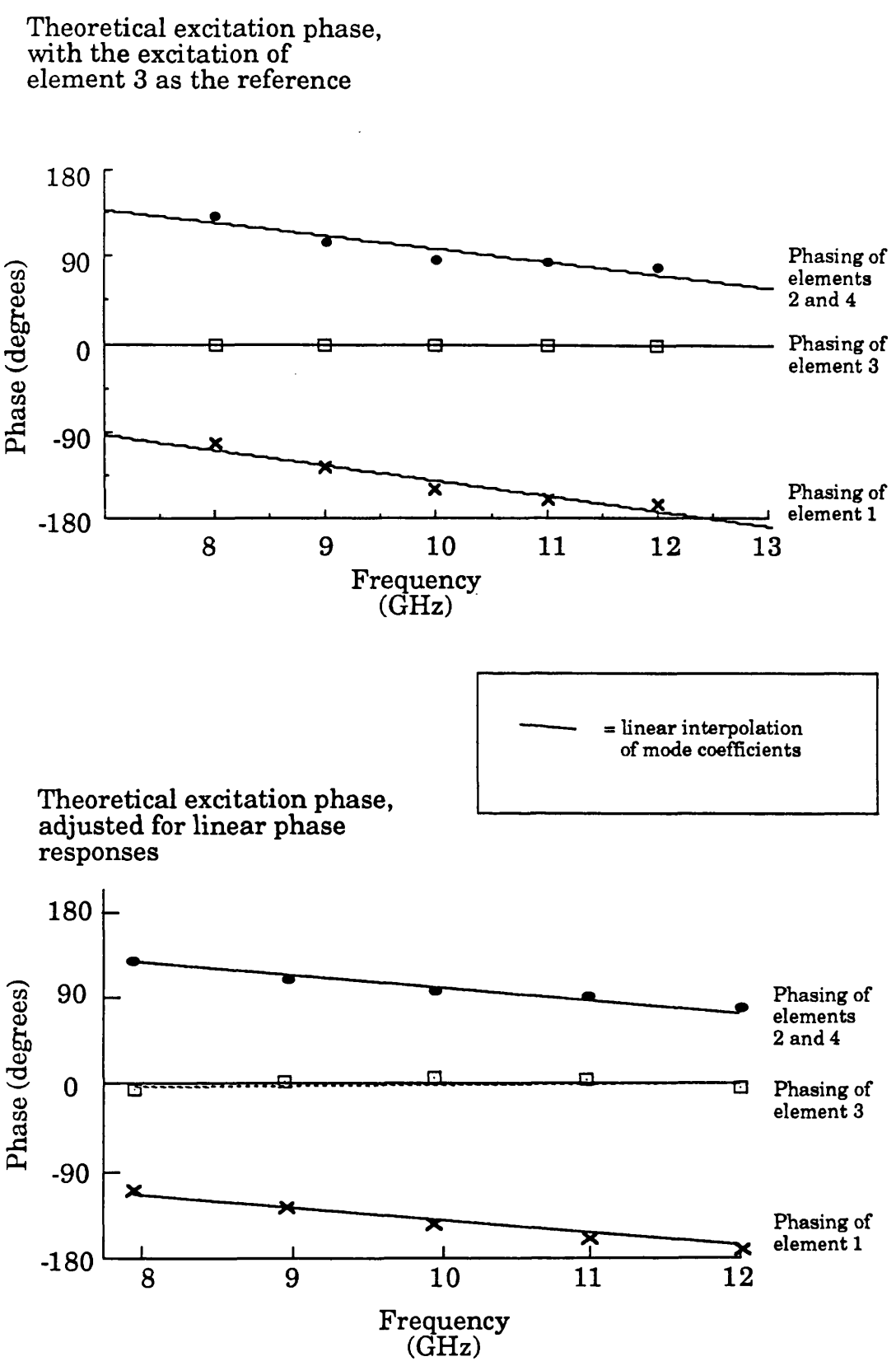

Figure 4.12 Phasing of array elements required to form instantaneously wideband -30 dB sidelobe Chebyshev beam:
(a) Element 3 phase as a reference.
(b) For linear phase responses.

beam. This excitation is plotted in figure 4.13. Again, reduction of gain at the ends of the band was necessary to produce a realisable amplitude response. While a sin(x)/Nsin(x) is not suitable for amplitude comparison DF, the demonstration of a second pattern was considered desirable to emphasise the versatility of this wideband synthesis technique. The next task was the design of the networks to realise the array excitations specified in this section.

4.4 The design of frequency-compensation networks

4.4.1 The principles used in building compensation networks

To synthesise a Chebyshev beam, the element excitation of figure 4.12 must be realised, using the weighted corporate feed of figure 4.10. To form the beam at a single frequency, say 10 GHz the amplitude weighing can be done using attenuation of 1.7 dB in the feed of element 3, and 5 dB in the feed of element 1. Delay lines can be used to realise the specified element phasing. The phase delay P introduced by a length of transmission line l is given by:

$$P = -\frac{2\pi l}{\lambda_g} \qquad (4.4.1)$$

where λ_g is the guide wavelength. The delay line does not affect the amplitude of the excitation significantly, but the physical length of the attenuator introduces an additional phase delay. This is corrected by reducing the length of the coaxial cable feeding the attenuator by a corresponding amount. While this technique cannot realise the wideband response of figures 4.11 and 4.12, some narrowband beams plotted in chapter 5 were formed using this simple technique.

For wideband synthesis of a Chebyshev beam, the frequency responses of figures 4.11 and 4.12 must be realised. The classical approach to realising a transfer function is to fit a polynomial to the voltage transfer function, express the function in terms of z (or y) parameters, then design a lumped

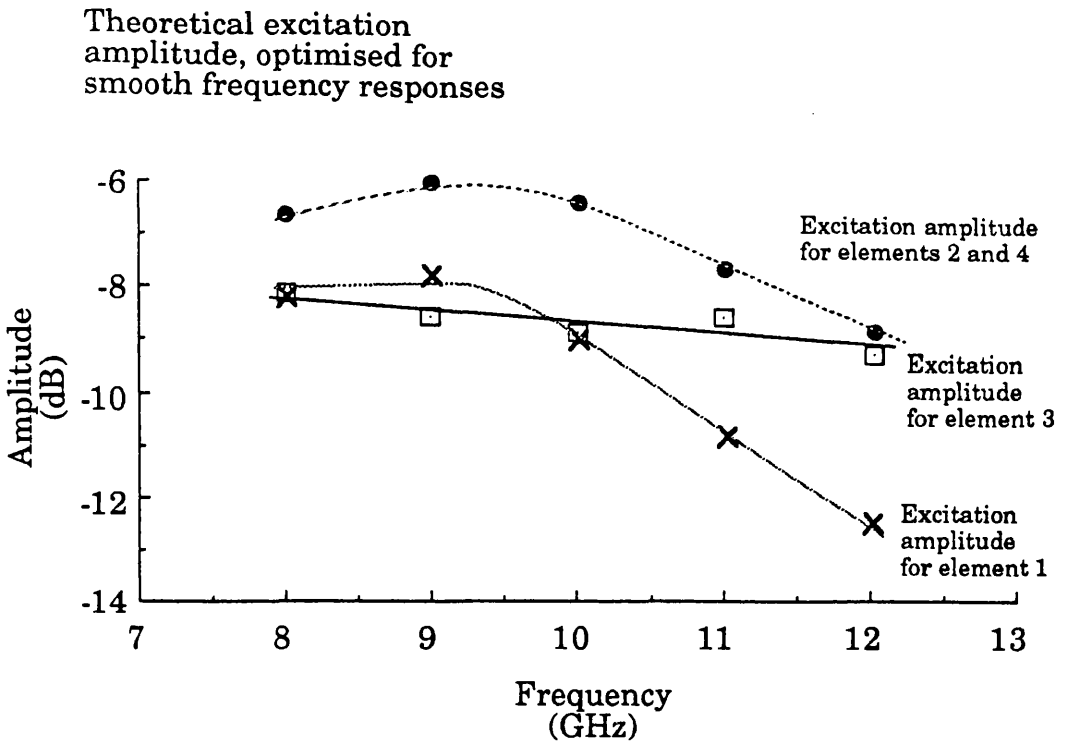

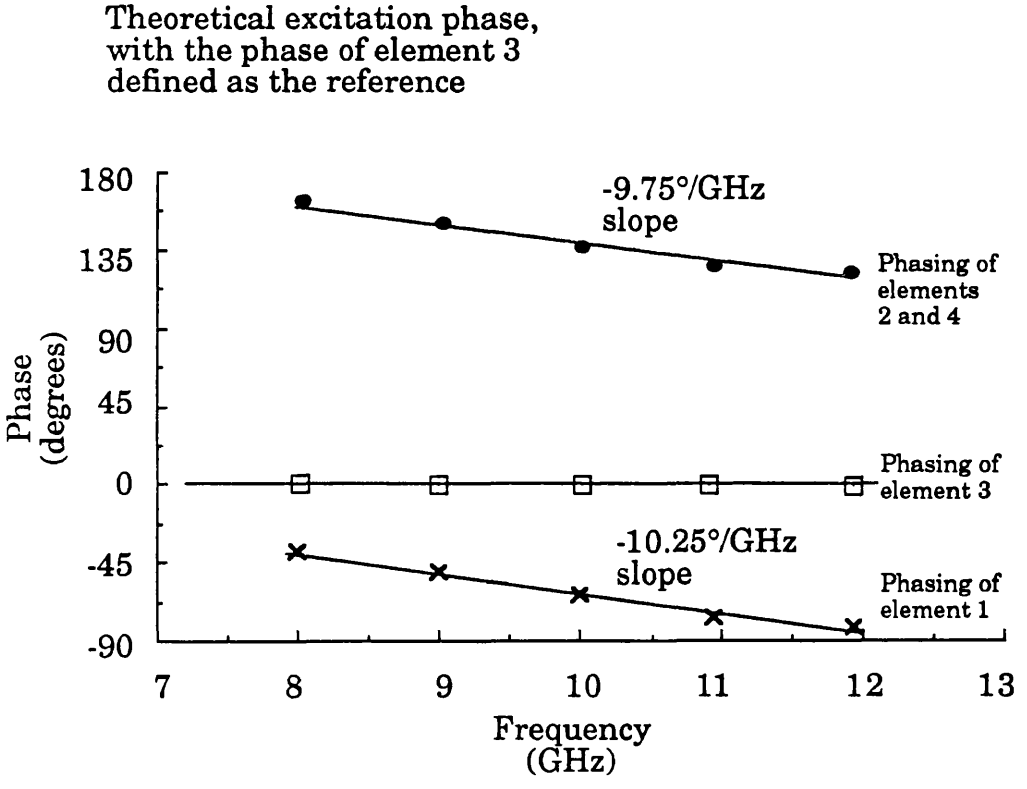

Figure 4.13 Amplitude and phase of element excitation required to form instantaneously wideband $\sin(5\phi/2)/\sin(\phi/2)$ azimuth pattern.

element network. It is difficult to apply this approach here, as the element excitation is rigidly specified in phase as well as amplitude across the frequency band.

Filters can be used to give amplitude responses that change with frequency. In figure 4.11 the compensation for element 3 requires a filter with a high pass characteristic, so there is greater attenuation at the bottom of the band. The other three elements require filters with a low pass characteristic. The required amplitude responses are shallow curves, similar to those at the 'knee' of a filter. The steepest response is that for element 1, with just a 5 dB roll-off from 8 to 12 GHz i.e. 10 dB per octave. In the stop band of a filter, the theoretical roll-off is 6N dB per octave, where N is the number of elements in the filter. For these shallow responses, filters with only one or two elements are required. Filters components can be selected so they present a 50 Ω match within the pass band, but most are unmatched within the stop band. These mismatches will lead to unwanted reflections in the compensation network.

Consider the phase response for elements 2 and 4 in figure 4.12, where the phase of element 3 is defined as the 0° reference. This has an (almost linear) slope of -42° across the half octave frequency range i.e. 10.25°/GHz. Phase slopes can be introduced by a length of delay line, as shown in figure 4.14. The phase slope dP/df introduced by a length of transmission line l is given by:

$$\frac{dP}{df} = -\frac{2\pi l}{V_g} \qquad (4.4.2)$$

where V_g is the group velocity for the transmission line. A positive phase slope can be applied by reducing the length of semi-rigid cable, compared with the reference path. A slope of -10.25°/GHz is obtained with 5.9 mm of UT 0.141 semi-rigid cable (V_g = 0.69c).

Producing a negative phase slope by increasing the length l of a transmission line

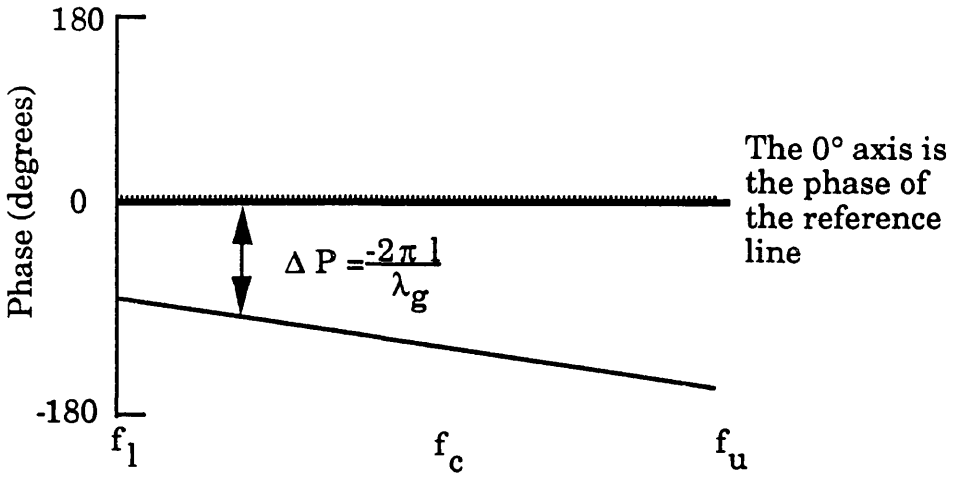

Producing a positive phase slope by reducing the length of a transmission line by l

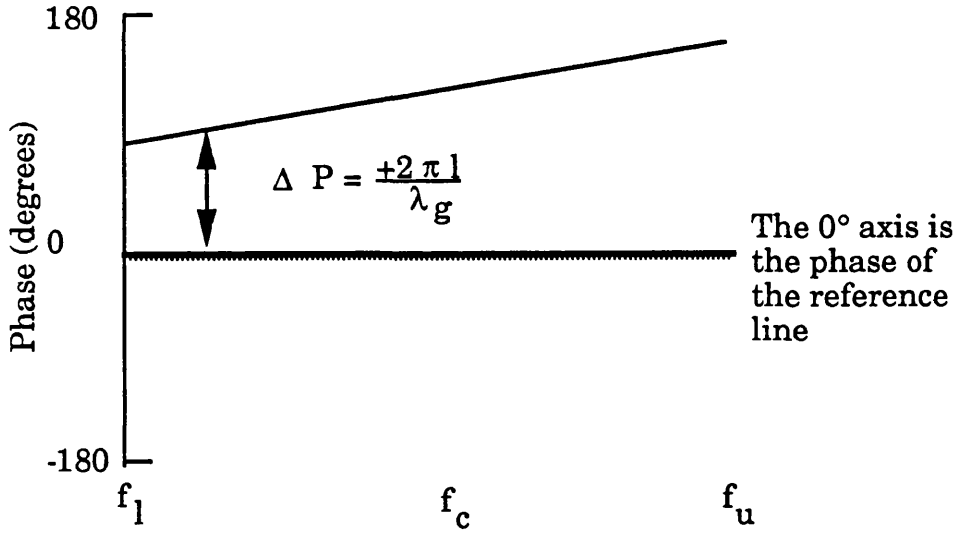

Figure 4.14 Introducing a phase slope by changing the length of a transmission line, compared to a reference line.

After insertion of the delay slope the phase of element 1 (relative to that of element 3) is -102.6° at 10 GHz, calculated using (4.4.1). The phase required by figure 4.12 is +89° at 10 GHz. A wideband phase shift of +191.6° is required in the path to element 3, without changing the phase slope. Substituting a directional coupler for one Wilkinson splitter in the corporate feed introduces a wideband phase shift. A 180° coupler splits the signal equally between the outputs, but with a relative phase shift of +180°. Now the path is only 11.6° in error. Using quadrature couplers as well, wideband phase shifts of 90°, 180° and -90° can be implemented. While this approach is useful for getting the coarse phase correct, components that can 'fine-tune' the wideband response are required. The design of microwave wideband phase shifters is considered in the next section.

Provided the delay lines and wideband phase shifts are well matched, they have no effect on the amplitude response. However the effect of amplitude compensation on the transmission phase must be considered. A filter has a phase response that changes with frequency, while the phase response (figure 4.12) required to form a Chebyshev beam is nearly linear. Generally, the steeper the response, the more rapid the change of phase with frequency. The Chebyshev filter, with a very sharp knee, has a less linear response than a Butterworth, while the Bessel filter is designed to produce a linear phase response. As described in section 4.3.3 the specifed amplitude response of figure 4.11 was adjusted to give a smooth change with frequency. Filters with an acceptably linear response over the half octave band can produce these very smooth responses.

As with all devices, the finite length of the filter introduces a phase slope. This is corrected by reducing the length of the coaxial cable feeding the filter by a corresponding amount. However this does not produce a phase of 0° across the band. The group delay of the filter acts as a wideband phase shift. This phase must be corrected using a wideband phase shift. Allowing for all the parameters, the wideband phase shift required ΔP is given by:

$$\Delta P = \Delta P_s + \Delta P_d - \Delta P_f - \Delta P_c \qquad (4.4.3)$$

where:

ΔP_s is the phase shift specified by figure 4.12 for the element excitation (for the Chebyshev beam).

ΔP_d is the (negative) phase shift introduced by the delay line to produce a phase slope.

ΔP_f is the phase shift introduced by the filter network, invariably positive.

ΔP_c is the coarse phase correction of +90°, 180° or -90° introduced by the substitution of a directional coupler for the Wilkinson splitter.

Let us consider the design of these compensation networks in the frequency band 8 to 12 GHz.

4.4.2 Components used in microwave compensation networks

Power splitters

The corporate feed of figure 4.10 requires three power splitters. Wilkinson splitters type PN2089-6204-00 were used. Measurements of these devices showed that the transmission phase balance was accurate to within ±2°

across the band, while the amplitude split was equal to within ±0.1 dB across the band. The return loss for these devices was better than 20 dB.

Directional couplers

As described in section 4.4.1, directional couplers can be used as phase shifts by substituting them for the Wilkinson splitter. Anaren quadrature couplers type 10018-3 were used to provide +90° phase shifts. The characteristics of this device are described earlier in table 4.2. Omni-Spectra 180° couplers type 2031-6335-00 were also available, but their use was avoided, as their wideband characteristics were not as good, with a higher VSWR and a greater change in coupling across the band. This is because they are constructed from a quadrature coupled section in tandem with a Schiffmann section, as described in section 4.3.1.

Delay lines

Section 4.4.1 describes the use of delay lines to introduce a phase slope. UT 0.141 semi-rigid cable was used to connect the microstrip networks to the isolators at the element feeds. Coarse delays were introduced by changing the length of the interconnecting cable. Fine adjustments were done using Midisco 1089-1 line stretchers with screw adjusters. The change in length was accommodated by a loop of semi-rigid cable.

Attenuators

Midwest wideband attenuators type 444 with values of 1, 2, 3 and 6 dB were available with a VSWR of less than 1.45. These coaxial devices had SMA connectors. The measured accuracy was within ±0.2 dB over the band 8 to 12 GHz. Variable attenuators were also available, but were not used as their wideband performance was not as good as that of the fixed attenuators, with a higher VSWR and a greater change in attenuation across the band. Fine tuning of the excitation amplitude was done by altering the microstrip compensation networks.

Isolators

The mismatch between the element and the feed reduces the efficiency of the system, and hence the received signal strength. In addition, if the components of the beamformer are not a perfectly matched to the characteristic impedance of the beamformer, the reflections from them are reflected again by the element mismatch, ultimately disturbing the transmission parameters. This error manifests itself as a ripple on the amplitude and phase response, when plotted as a function of frequency. This was discussed in section 4.2.4. Figure 4.11 depicts amplitude responses that roll-off by over -3 dB across the band. Since signals that are blocked by filters are reflected, a 3 dB return loss can be expected at some frequencies. Isolators were used in the element feed to reduce this problem. Omni-Spectra isolators type ML 3221 with a return loss of 17 dB were used.

Computer-aided design for microstrip filters and phase shifters.

At microwave frequencies filter designs are based on the same lumped-element models commonly used at lower frequencies. For example the Butterworth, Chebyshev or Bessel polynomials can be used to design filters. At microwave frequencies the filter elements (inductances and capacitances) are built using transmission line structures rather than true lumped elements. Matthaei, Young,and Jones, (1964) describe the structure of common transmission line filters. At UCL facilities were available for etching transmission line filters onto a microstrip substrate. The substrate used was R/T Duroid, with the characteristics of table 4.12 below. The filters were mounted on a jig with SMA to microstrip launchers, as shown in figure 4.15.

The performance of transmission line filters is not the same as that of filters built from true lumped-elements. To model these microstrip filters a computer-aided design package for microstrip circuits, called PUFF, was used. This package was developed by Compton and Rutledge (1987). In the

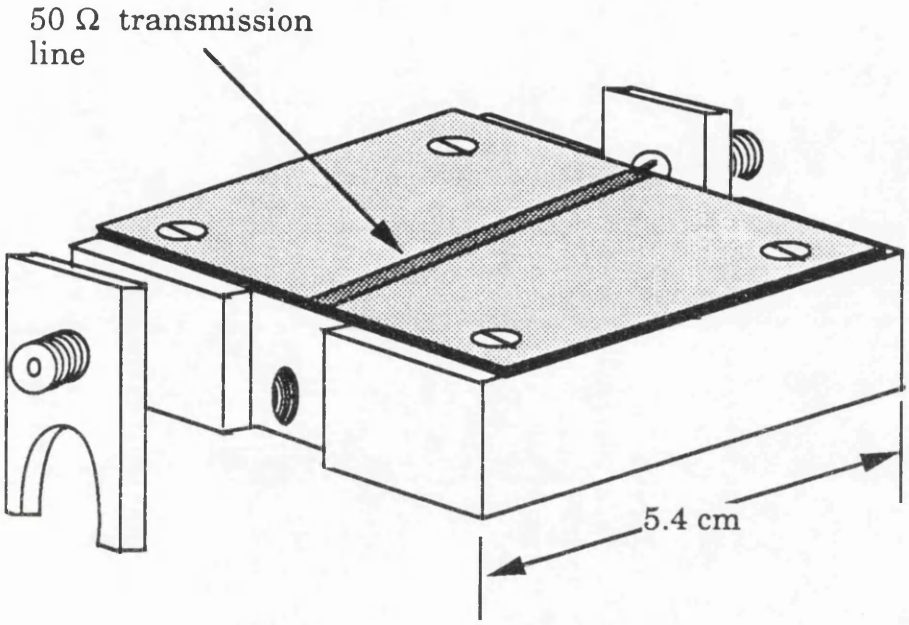

Specification for microstrip line on test fixture

Frequency range 8-12.4 GHz

Impedance 50 Ω

Insertion loss -0.5 ±0.3 dB

VSWR (max) 1.35

Figure 4.15 Mounting jig for microstrip components.

program, the user lays out microstrip (or stripline) circuits on the monitor screen. The circuits can be connected to output 'ports' and the program calculates the scattering parameters for these ports. The program 'menu' includes transmission lines, short circuits, lumped-elements and coupled lines. Corrections are made for RF effects such as the capacitive end correction at open circuits. User defined components, such as active devices, can be defined by a set of scattering parameters for the operating frequency range. This facility was used to model the attenuators, couplers isolators also used in the compensation network. Table 4.12 below gives a list of the input data used in the program.

Network type	Microstrip
Dielectric constant of substrate	2.2
Dielectric thickness	0.508 mm
Board size	50 mm
Circuit resolution	0.1 mm
Normalising impedance	50 Ω
Design frequency	10 GHz
Lower frequency	8 GHz
Upper frequency	12 GHz

Table 4.12 Data used in the computer-aided design of microstrip circuits with PUFF.

The microstrip artwork is output on a dot matrix printer. To illustrate the design of a filter figure 4.16 depicts the artwork for a six-element filter based on the Butterworth lumped-element model. The filter has shunt capacitors built using short lengths of wide (low-impedance) transmission line and series inductors formed from short lengths of narrow (high-impedance) transmission line. To test the PUFF prediction, this filter was etched onto a R/T Duroid substrate. The measured transmission response is plotted in figure 4.16, along with the PUFF prediction and also the lumped-element prediction for the amplitude response. Up to 12 GHz the

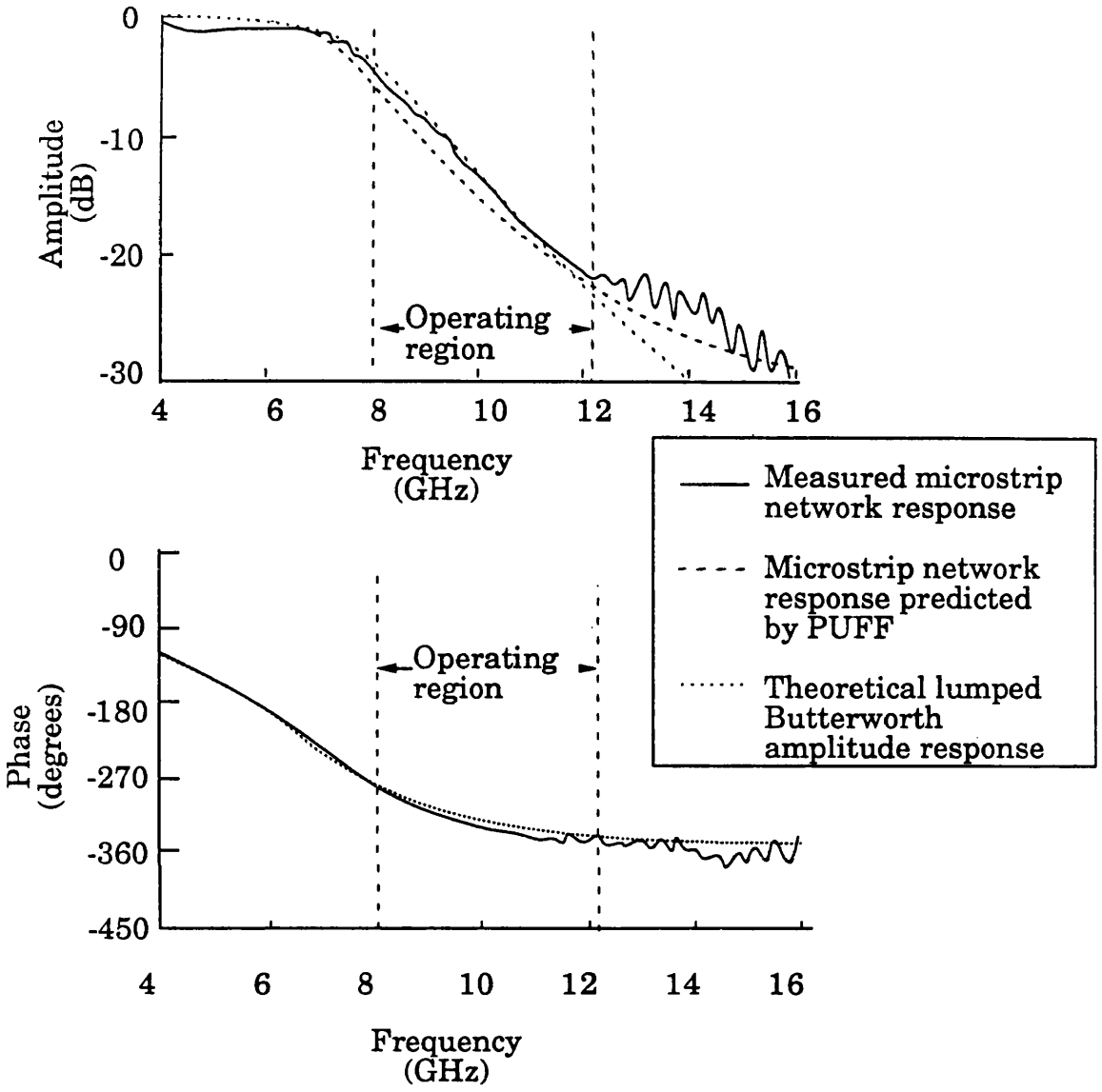

Artwork for six-element microstrip filter

Specification for microstrip six-element low pass filter

Impedance	50 Ω
-3 dB point	8.0 GHz
Roll-off (8-12 GHz)	36 dB/octave
Rejection (12-16 GHz)	<-22 dB
Pass band insertion loss	1.5 dB max
passband VSWR	1.5:1
Amp. error (8-12 GHz)	±1.5db
Phase error (8-12 GHz)	±10°

Figure 4.16 Measured response of microstrip six-element Butterworth filter, compared to the PUFF prediction.

agreement between the PUFF prediction and the measured results are good. Above 12 GHz more ripple is apparent - the SMA-to-microstrip launcher was badly matched at these frequencies.

The excitation of element 3 for the Chebyshev beam requires a high-pass response with greater loss at 8 GHz than at 12 GHz. The series capacitors and shunt inductors required for high pass networks cannot easily be realised on microstrip. Band pass filters can be realised on microstrip, the simplest example being a 50 Ω stub. If the length of the stub is λ/4 at 12 GHz, there is no transmission loss at that frequency, but at 8 GHz the loss is significant.

The design of microwave wideband phase shifts

The most commonly used microwave wideband phase shift is the coupled λ/4 section developed by Schiffmann (1958). The facilities required to build the coupled line structure of this device were not available at UCL. An alternative structure for producing wideband phase shifts is described in a paper by Wilds (1979). This circuit is an all pass network using both an open-circuit and a short-circuit stub. The change in impedance caused by the line discontinuity is corrected by reducing the line impedance along a λ/2 section. The paper predicts that wideband phase shifts from +15° to +135° can be obtained. This is satisfactory for our requirement, since phase shifts outside this range can be moved into it using the 90° and 180° phase shifts of directional couplers, as explained in section 4.4.1. This type of network can be constructed on the same Duroid substrate as the filter network and can be modelled using PUFF. Rather than use a true short circuit, one stub is connected to a patch that acts as a low-impedance capacitor to ground. Figure 4.17 shows the transmission parameters for a 40° wideband phase shift, designed with the aid of PUFF. The theoretical response is compared to the measured results for this device constructed on Duroid. This particular phase shifter was used in the compensation of element 3 to form a wideband sin(Nx)/Nsin(x) beam.

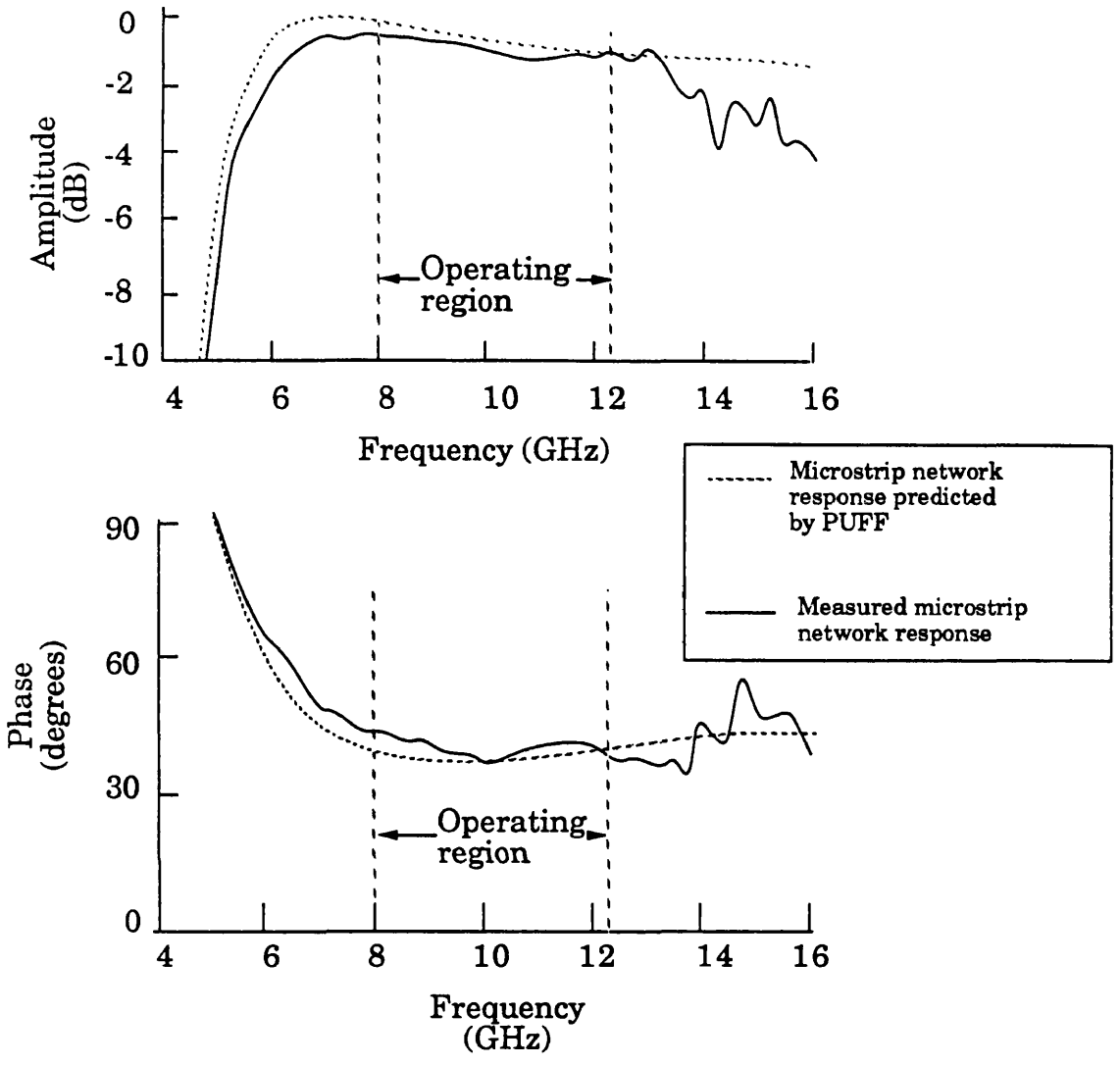

Scale: Full size

Microstrip artwork
for all pass network
100 Ω stubs
33 Ω main line section

Specification for microstrip
40° wideband phase shift

Impedance	50 Ω
Insertion loss (8-12 GHz)	-1±0.4 dB
VSWR	1.6:1
Phase Shift (8-12 GHz)	+40±4°
SMA connectors	

Figure 4.17 Measured response of a broadband 40° phase shift, compared to the PUFF prediction.

4.4.3 The compensation networks used for wideband pattern synthesis

The network used to form the -30 dB Chebyshev beam is depicted in figure 4.18. The same microstrip network is used for elements 2 and 4 as the specified excitation is identical. Figure 4.19 illustrates how this network progressively builds up the specified amplitude of figure 4.11 and realises the phase of figure 4.12. For clarity, this illustration works backwards from the beam port to the element port. Since $s_{21} = s_{12}$ (except for the isolators) this makes no difference. Some of the choices of component require explanation:

- The directional couplers of figure 4.19a apply wideband phase shifts to the elements, although the need for these only becomes apparent at the bottom of figure 4.19b.

- The excitation of element 1 is lower in amplitude than the other elements. Rather than using a 4 dB attenuator (3 dB and 1 dB) with a wideband +90° phase shift, a 1 dB attenuator in tandem with an extra quadrature coupler was used. The coupler path has 3 dB of loss.

- Figure 4.12 shows that the phase response required for elements 1, 2 and 4 has a slight curve. The wideband phase shifter of figure 4.17 has a similar curve, so this type of phase shifter was used in these paths to meet the phase response. This explains why the transmission phase for element 3 was defined as the phase reference, and hence did not require a wideband phase shift.

- There was a second reason for not using a microstrip phase shift in path 3. The phase shifter match was not perfect and adding this to the large mismatch of the band pass stub filter significantly altered the transmission responses of both. Although PUFF could predict this, the results were not satisfactory. The length of narrow transmission line spaced away from the main stub acted as a series

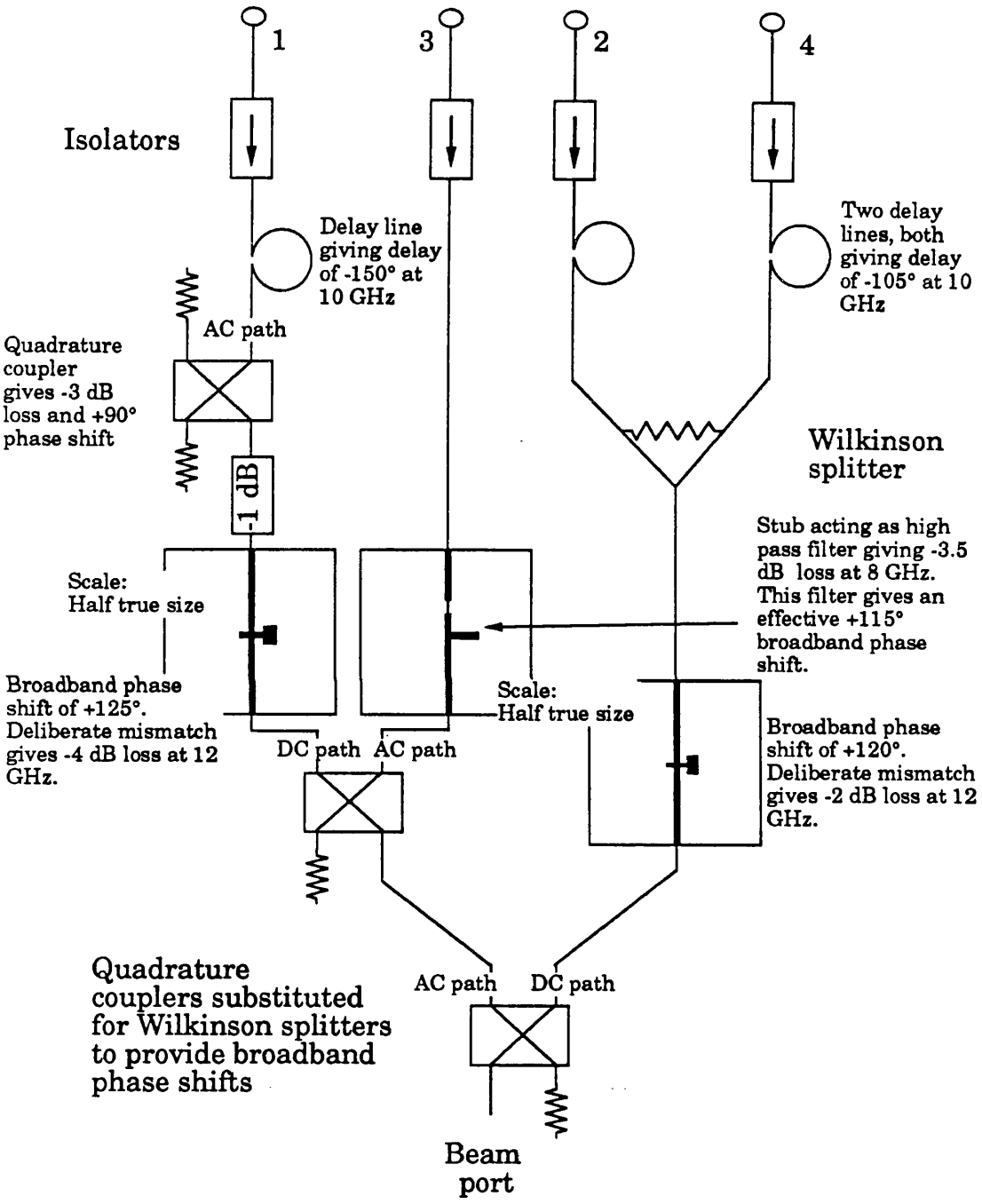

Figure 4.18 Corporate feed used to synthesise a wideband Chebyshev beam with low sidelobes. This network was developed with the aid of PUFF, used for the design of microstrip networks.

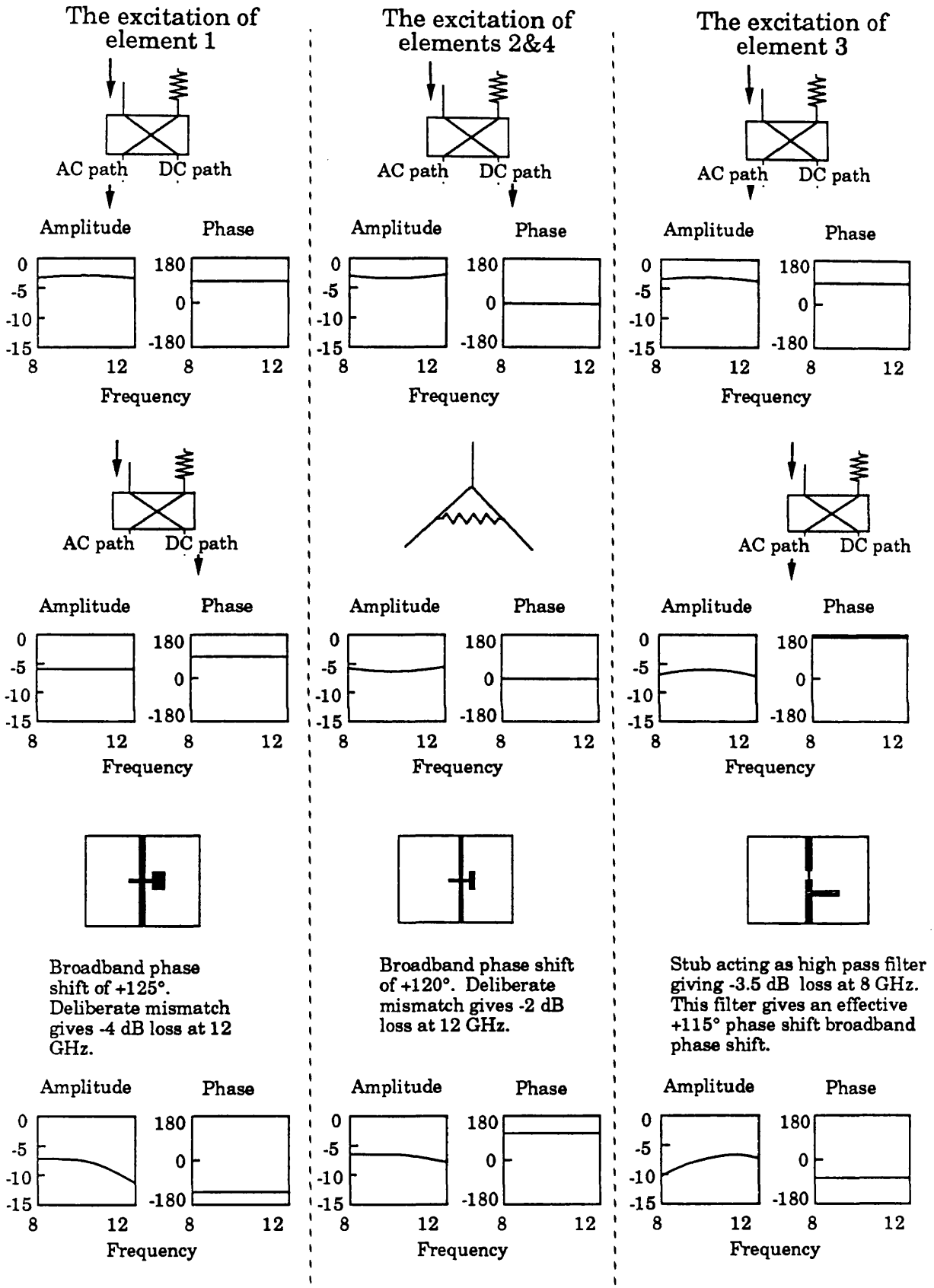

Continued on next page

Figure 4.19a A schematic illustration of how the network of figure 4.18 produces the array excitation of figure 4.20.

Continued from last page

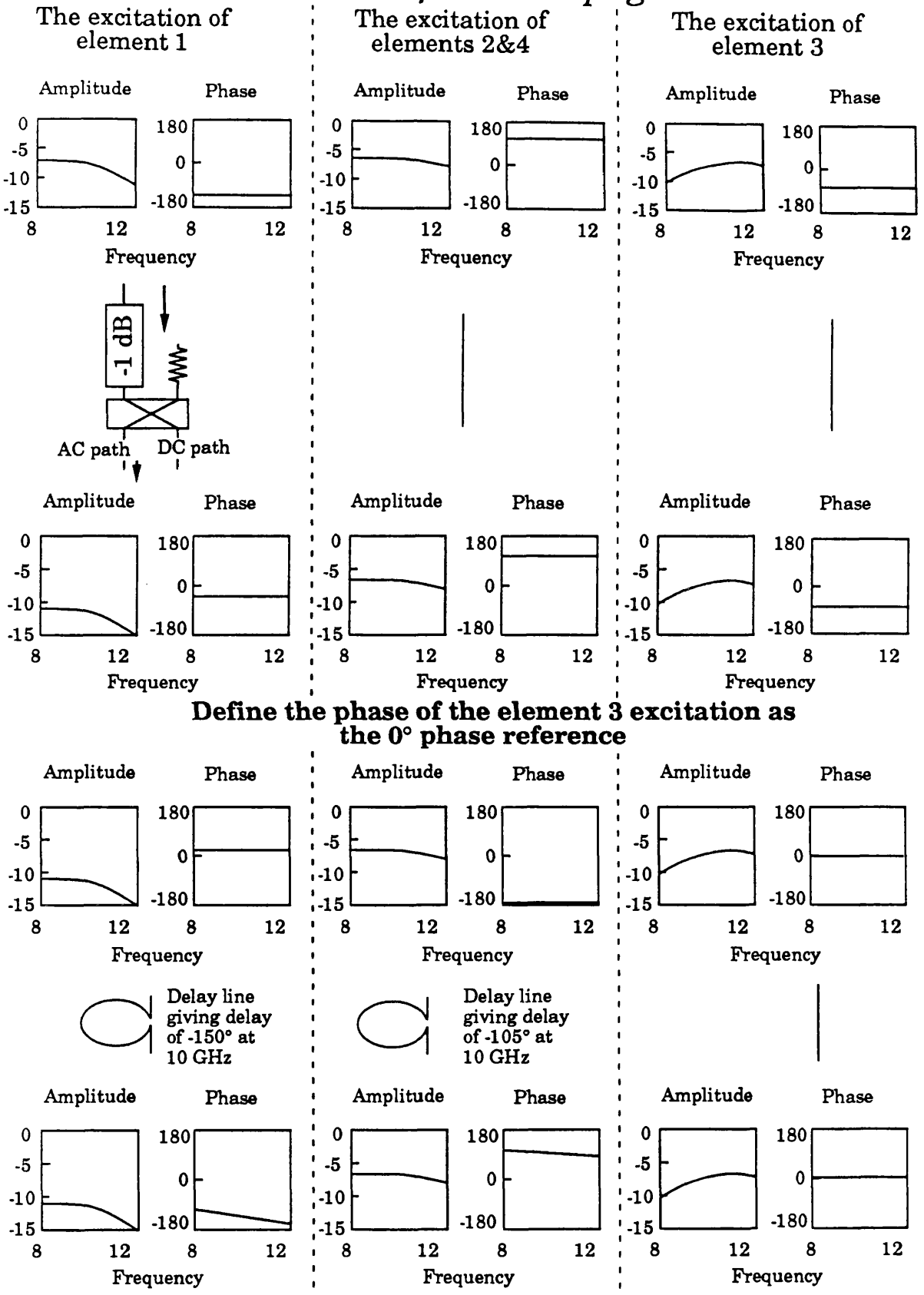

Figure 4.19b A schematic illustration of how the network of figure 4.18 produces the array excitation of figure 4.20. The isolators in the element feeds are not shown.

inductor that modified the stub response.

- For the same reason a filter was not used in tandem with the phase shifter in the path to element 1. Instead the phase shifter response was degraded so there was 4 dB of loss at 12 GHz, as required by figure 4.11. This was done with the aid of PUFF by altering the impedance of transmission line section away from the values recommended by Wilds (1979). Exactly the same approach was used to introduce 2 dB of loss at 12 GHz into the excitation of elements 2 and 4.

The measured response of the complete compensation network is plotted in figure 4.20. For comparison the PUFF prediction is also plotted, showing good agreement. The transmission amplitudes (specified at 1 GHz intervals across the band) are realised to within ±0.5 dB. The transmission phases are realised to within ±5°. For an excitation with this amplitude and phase error, a sidelobe level of -20 dB minimum is predicted by figure 4.2. The design sidelobe level of -30 dB will not be attained across the whole frequency band, although at some frequencies, (notably 9 GHz) sidelobes closer to -30 dB can be expected, as the phase and amplitude errors are smaller. The predicted variation in the -3 dB beamwidth is calculated with the aid of figure 4.3. The amplitude error will change the beamwidth by 2°, while the phase error introduces an additional 0.5°, giving a worst case error of 2.5°.

The combination of black isolators, black Duroid and a black baseplate was difficult to photograph, so an illustration of the beamformer layout is shown in figure 4.21.

The excitation is specified at 1 GHz intervals across the band. The plot of figure 4.11 and 4.12 uses interpolation to predict the excitation required at intermediate frequencies, such as 9.5 GHz. In chapter 5, measurements of the synthesised beam at intermediate frequencies are plotted to demonstrate that interpolation of the specified excitation is satisfactory.

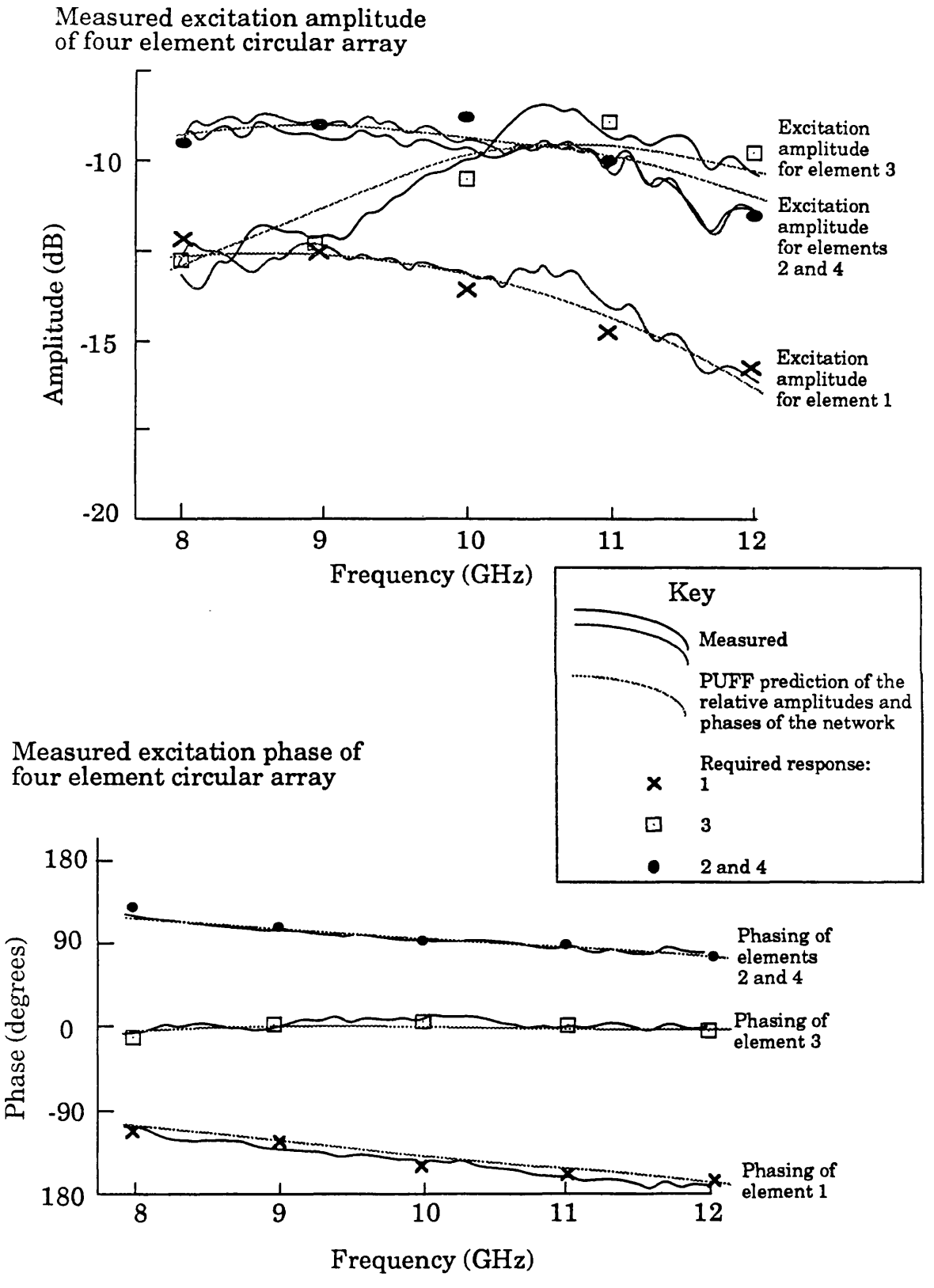

Figure 4.20 Measured excitation of circular array produced by the beamforming network. This excitation will form a wideband Chebyshev beam with a design sidelobe level of -30 dB.

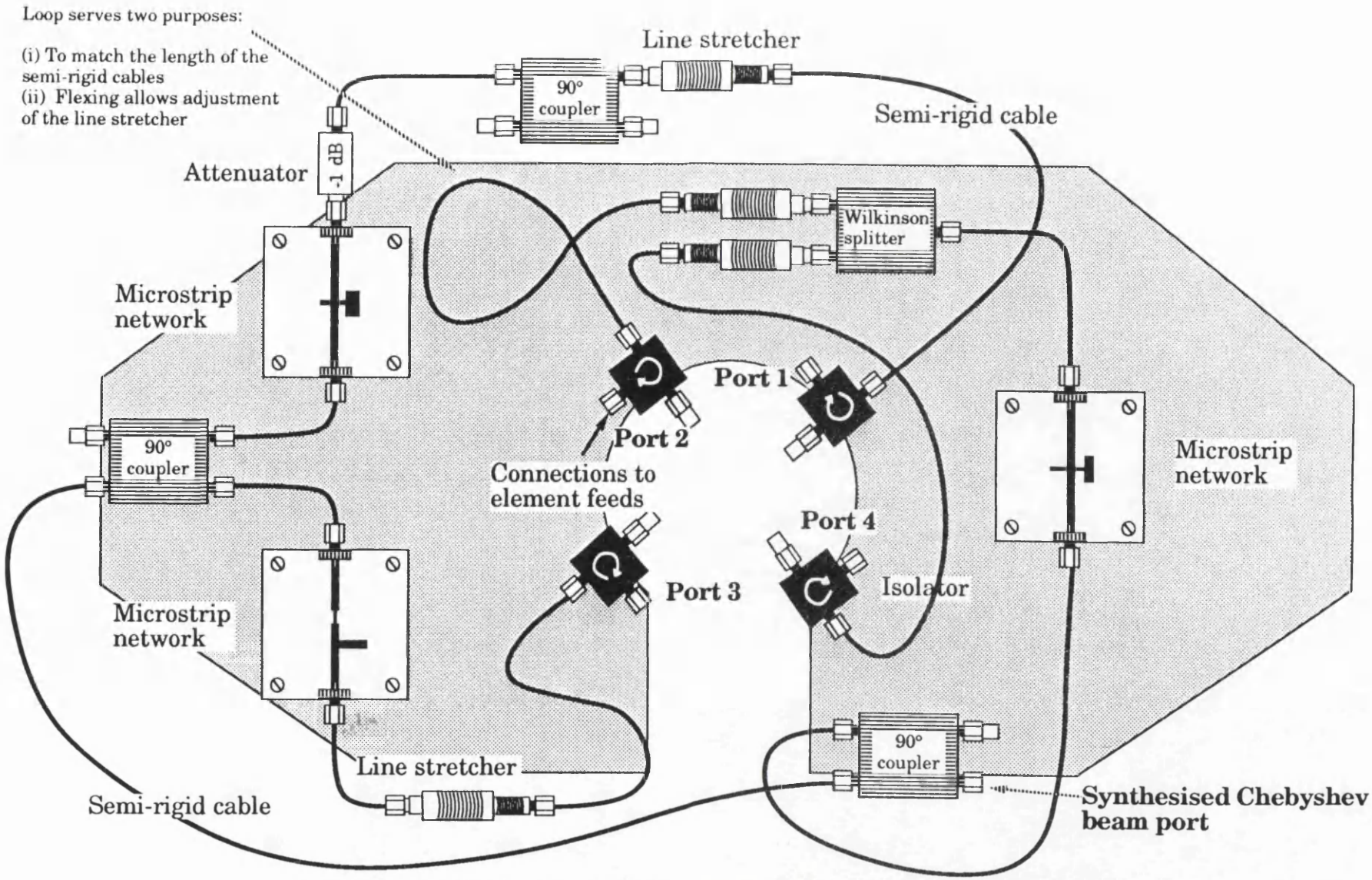

Figure 4.21 Illustration of the corporate feed designed to form a wideband Chebyshev beam over the frequency range 8 to 12 GHz.

Figure 4.22 shows the network used to form a $\sin(5\phi/2)5\sin(\phi/2)$ beam, formed by exciting the phase modes with equal amplitudes. This pattern, shown in figure 2.12 has a -3 dB beamwidth of 65° and a -12.1 dB sidelobe level. Again one microstrip network is used for elements 2 and 4, as the specified excitation is identical. The measured response of the complete compensation network is plotted in figure 4.23. For comparison the PUFF prediction is also plotted, showing good agreement. The transmission amplitudes (specified at 1 GHz intervals across the band) are realised to within ±0.5 dB and transmission phases are realised to within ±5°.

Semi-rigid feeds to monopole elements

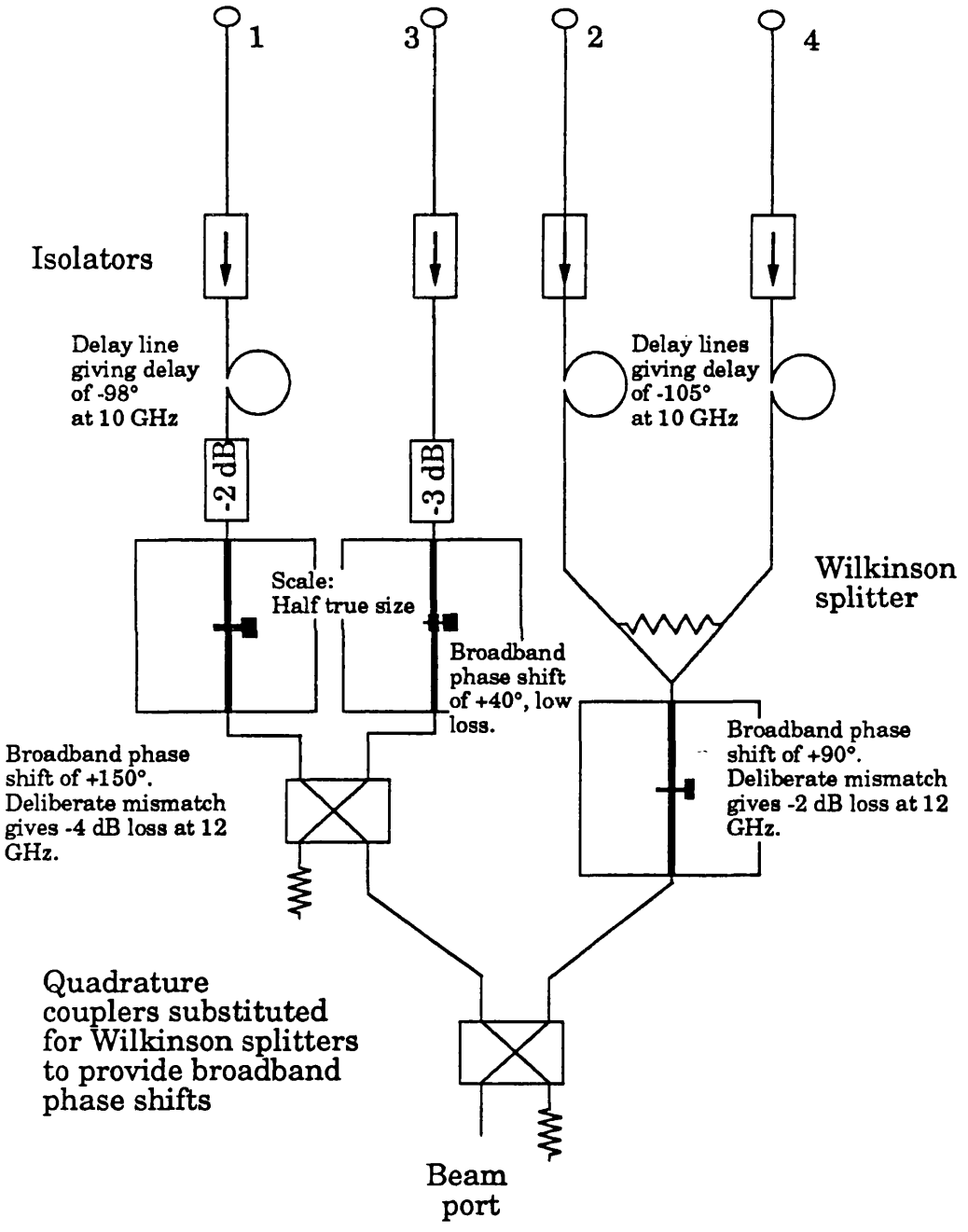

Figure 4.22 Corporate feed used to synthesise a wideband $\sin(5\phi/2)/\sin(\phi/2)$ beam with-12.1dB sidelobes. This network was developed with the aid of PUFF, used for the design of microstrip networks.

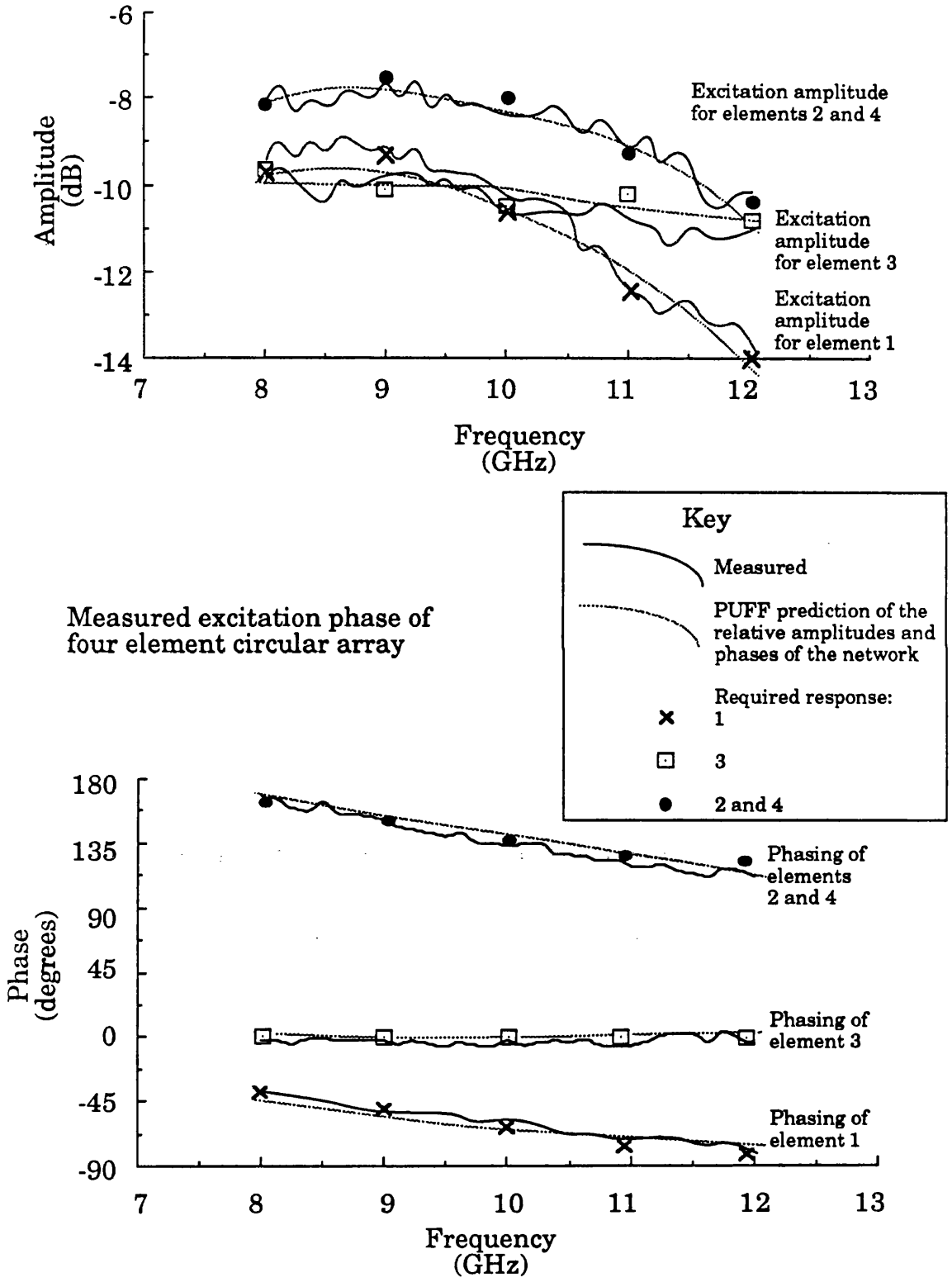

Figure 4.23 Measured excitation of circular array produced by the beamforming network. This excitation forms a wideband $\sin(5\phi/2)/\sin(\phi/2)$ azimuth beam.

Chapter 5

Measurements of synthesised beams

5.1 The radiation pattern measurement system

5.1.1 Anechoic chamber measurements

The measurement techniques described here were also used in measurements of individual monopoles, described in chapter three. A schematic diagram of the measurement system is shown in figure 5.1. The measurements were performed in a microwave anechoic chamber at UCL. The walls of the chamber were coated in a radar absorbent material supplied by Emerson and Cuming, Inc. The array was located about one metre from the back wall of the chamber, equidistant from the two side walls. For pattern measurements the array was illuminated by a microwave horn, located at the far end of the anechoic chamber. A Flann 20 dB standard gain horn model 1624 was used. For measurements of the radiation pattern in the 'far field' the distance between the source and receiving antenna must be greater than $2d^2/\lambda$, where d is the aperture of the larger antenna. This spacing is four times the Rayleigh displacement used in the optics field. For these measurements a calculated minimum spacing of 1 metre was required, based on the aperture of the illuminating horn. In fact the horn was 3 metres from the array.

The radiation pattern measurements were performed with an HP 8410B network analyser, in conjunction with an HP 8734B reflection/transmission test unit. An HP 8620C sweep oscillator was used as the microwave source. Half the source output was fed to the illuminating horn, while half was used to provide a reference signal for the network analyser. About +13 dBm of RF power reached the standard gain horn - losses in the long semi-rigid feed were significant. The RF signal received by the circular array was fed to the 'transmission return' port of the network analyser. This configuration ensured that an adequate dynamic range was available for

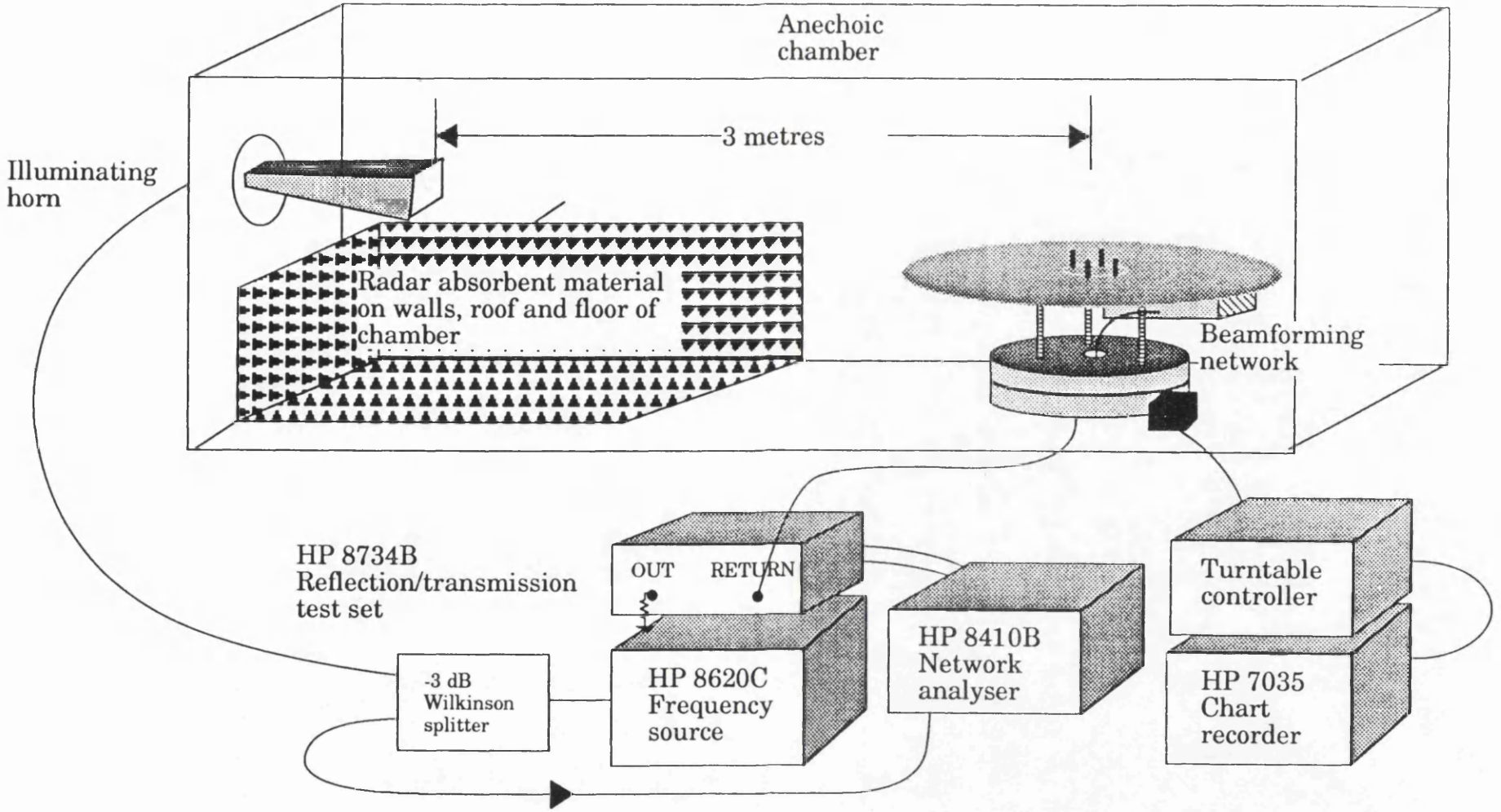

Figure 5.1 System for measuring radiation patterns in an anechoic chamber.

the accurate measurement of low sidelobes. By switching in attenuators during RF measurements on a single monopole element, it was verified that about 45 dB of dynamic range was available, sufficient for the target sidelobe level of -30 dB.

To measure azimuth radiation patterns the circular array was mounted on a turntable. The turntable was motor driven, rotating at 1/2 rpm. Radiation patterns of amplitude (Y axis) against azimuth (X axis) were plotted using an HP 7035 analogue chart recorder. The amplitude scale was checked using calibrated attenuators, registering a measurement accuracy of ±0.2 dB. An analogue voltage output proportional to the angle of rotation was fed to the chart recorder. The accuracy of the voltage output was checked using physical markers on the turntable circumference. The indicated angle was accurate to within ±1°. RF connection to the array used a microwave cable through the centre spindle of the turntable. A length of flexible RF cable, coiled like a watchspring, allowed free rotation. Measured changes in the transmission amplitude and phase of the flexible cable with azimuth angle were negligible. To reduce RF reflections, radar absorbent material was used to cover the turntable, ground plane supports and beamforming network.

Several types of measurement were performed using this basic set-up. The main ones are listed below, indicating the equipment settings and describing how calibration was performed.

5.1.2 **Azimuth radiation pattern measurements**

The microwave source was set to a fixed frequency for azimuth radiation pattern measurements. The frequency was checked using an HP 5342A counter. Calibration measurements of a standard gain horn with a known radiation pattern were made. This showed that the -3 dB beamwidth could be measured to within ±1°, and sidelobe levels to within 0.5 dB. The horn was oriented to produce vertically polarised radiation, co-polar to the vertical monopoles. To determine changes in the radiation pattern with frequency the pattern measurements were repeated at fixed frequencies

across the band 8 to 12 GHz.

5.1.3 Phase measurements

In chapter three (figure 3.18) the relative phases of the amplitude modes are plotted as a function of azimuth. The system of figure 5.1 was used, but with the vertical scale of the chart recorder connected to the phase output of the network analyser. To perform phase measurements on radiation patterns the array must be accurately centred on the turntable, otherwise the distance between the array and the illuminating source changes with the angle of rotation, introducing a sinusoidal phase modulation on measurements of the far field phase. By measuring the transmission phase to each array element in turn, the array was centred to within ±2° of phase at 10 GHz, corresponding to 0.16 mm. This precision was crucial to the accurate calculation of the phase mode coefficients described in section 3.5.

5.1.4 Changes in the azimuth radiation pattern with elevation

Amplitude comparison DF systems must operate above (and sometimes below) 0° of elevation. For accurate DF it is desirable that the azimuth pattern measured at, say, +20° of elevation is the same as that at 0°. Cuts of the azimuth radiation pattern at elevation angles above 0° were made to evaluate changes in the pattern. To do this the illuminating horn was raised up in height and tilted down to illuminate the circular array. The elevation angle of the illuminating horn could not be raised above 40°, as the top of the anechoic chamber was in the way. In any case, most microwave DF systems do not operate above +35° in elevation.

5.1.5 Cross-polar measurements

To determine the sensitivity of the array to cross-polar signals, the illuminating horn of figure 5.1 was placed on its side to give horizontally polarised radiation. Pattern measurements were then made using the system described in 5.1.2.

5.1.6 **Radiation pattern measurements in the elevation plane**

To take a section through the beam in the elevation plane the circular array was mounted on its side, with the ground plane vertical on the turntable. This was depicted earlier in figure 3.14, showing the plot of the elevation pattern of a monopole. RAM was packed around the 'rear' side of the ground plane to cover the beamformer. Since the monopole elements were horizontal, the illuminating horn was placed on its side to give horizontally polarised radiation.

5.1.7 **Swept frequency measurements of gain**

The HP 8620C source has an analogue voltage output proportional to the microwave frequency. This was connected to the X (horizontal) scale of the chart recorder. The Y (vertical) scale again measured the amplitude received by the circular array, with the peak of the synthesised beam facing the illuminating horn. This produced a plot of the received peak amplitude as the frequency was scanned. To provide a reference, a 10 dB standard gain horn was substituted in place of the circular array with its physical aperture coincident with the centre of the array.

5.2 Narrowband radiation pattern measurements

5.2.1 **Synthesis of a -30 dB sidelobe Chebyshev beam**

The beamforming network shown in figure 4.9 was mounted on the underside of the ground plane, as shown in figure 5.1. The monopoles were connected to the input ports of the first amplitude mode matrix using four semi-rigid cables of matched length. As discussed in section 4.3.2, the phase and amplitude errors introduced by the pair of matrices were too large to form instantaneously wideband beams, so the network was optimised to form beams at a single frequency: 10 GHz. Narrowband compensation was done using variable attenuators for amplitude weighting and delay lines for phase correction. Four beams were formed by the second matrix. The wideband compensation networks described in section

4.4 were not necessary for compensation at a single frequency.

The first radiation pattern demonstrated was a Chebyshev -30 dB sidelobe azimuth pattern, formed by exciting the zero, first and second order amplitude modes with a steep amplitude taper. This pattern has a theoretical -3 dB beamwidth of 82°. with the first sidelobes at a level of -30 dB, as calculated using the equations of section 2.1.4. This is close to the theoretical limit on sidelobes for this array, imposed by the presence of spatial harmonics with an amplitude close to -30 dB, relative to the fundamental modes. The calculated amplitude and phase of the mode compensation required was calculated in section 4.3.3:

Mode order	0	C1	C2	S1
Mode coefficients	0 dB, 0°	0 dB, +66°	-9.3 dB,+161°	0 dB, +66°
Mode compensation	0 dB, 0°	-2.29 dB, -66°	-0.64 dB, -161°	-2.29 dB, -66°
Final mode weights	0 dB, 0°	-2.29 dB, 0°	-9.94 dB, 0°	-2.29 dB, 0°

Table 5.1 The amplitude mode compensation used in the synthesis of a -30 dB sidelobe Chebyshev beam.

A second amplitude mode matrix was used to form the beams. For radiation pattern measurements one of the beam ports was connected to the network analyser 'transmission return' port, as described in section 5.1, while the unused beam ports were terminated in 50 Ω loads. The measured pattern did not resemble the theoretical Chebyshev shape. One sidelobe was at -15 dB, and the -3 dB beamwidth was 10° larger.

The complete beamformer was disconnected from the array and the transmission s parameters, between the beam port and the four-element ports was measured. As explained in section 4.2, a computer program had

been developed to calculate the theoretical transmission parameters for an error-free beamforming network. Table 5.2 below compares the theoretical s parameters to the measured parameters, for the beam port used first (port number 3). For clarity, path losses have been omitted. It is the relative amplitude and phase of the element excitation that determines the shape of the pattern.

Element number	1	2	3	4
Theoretical element excitation	-10.9 dB, +121°	-6.0 dB, 0° (reference)	-7.76 dB,-89°	-6.0 dB, 0°
Measured element excitation	-9.6 dB, +110°	-6.0 dB, 0° (reference)	-8.5 dB,-68°	-5.6 dB, +12°
Excitation error	+1.5 dB, -11°	0 dB, 0°	-0.74 dB, +21°	+0.4 dB, +12°

Table 5.2 A comparison between the measured and theoretical transmission parameters for the matrix beamformer (beam port 3).

The amplitude and phase errors introduced by the pair of matrices are very large. The amplitude of the excitation is wrong by 1.5 dB for element 1, and the phase of the excitation is wrong by 21° for element 3. Referring to section 4.2, errors of this magnitude will produce the measured increases in the beamwidth and sidelobe levels.

Fine adjustments to the amplitude and phase of the compensation were made to correct the errors in the transmission characteristics of the two matrices. Table 5.3 overleaf shows the measured transmission parameters after the adjustments were made.

Element number	1	2	3	4
Theoretical element excitation	-10.9 dB, +121°	-6.0 dB, 0°	-7.76 dB,-89°	-6.0 dB, 0° (reference)
Measured element excitation	-11 dB, +120°	-6.0 dB, +1°	-7.7 dB,-90°	-6.0 dB, 0° (reference)
Excitation error	-0.1 dB, -1°	0 dB, +1°	+0.16 dB, -1°	0 dB, 0°

Table 5.3 A comparison between the measured and theoretical transmission parameters for the beamformer after compensation adjustment (Chebyshev beam with -30 dB sidelobes).

Considerable time was spent fine tuning the compensation. The study of section 4.2 showed that even small phase and amplitude errors in the excitation increase the sidelobe levels above -30 dB. The transmission amplitude is within 0.2 dB of the specified values, while the transmission phase is within ±1° of the specified values. The beamformer was re-connected to the array and the azimuth measurement repeated. The measured Chebyshev beam is shown in figure 5.2. For comparison the theoretical radiation pattern is also plotted, showing good agreement. The -3 dB beamwidth of the measured pattern is within ±1° of the theoretical value of 82°, while the sidelobe level is within ±0.5 dB of the theoretical -28 dB. Note that the theoretical sidelobe level is -28 dB and not -30 dB; the effect of the third order harmonic of the pattern was included in the theoretical calculation using equation (2.3.1).

The absolute gain was about 0 dB ±0.5 dB, about 2.5 dB less than the theoretical value calculated using equation (3.5.6). This was due to losses in the network. As explained in section 4.3, each coupler introduced about 0.5 dB of loss and the connectors and cables contributed to the loss.

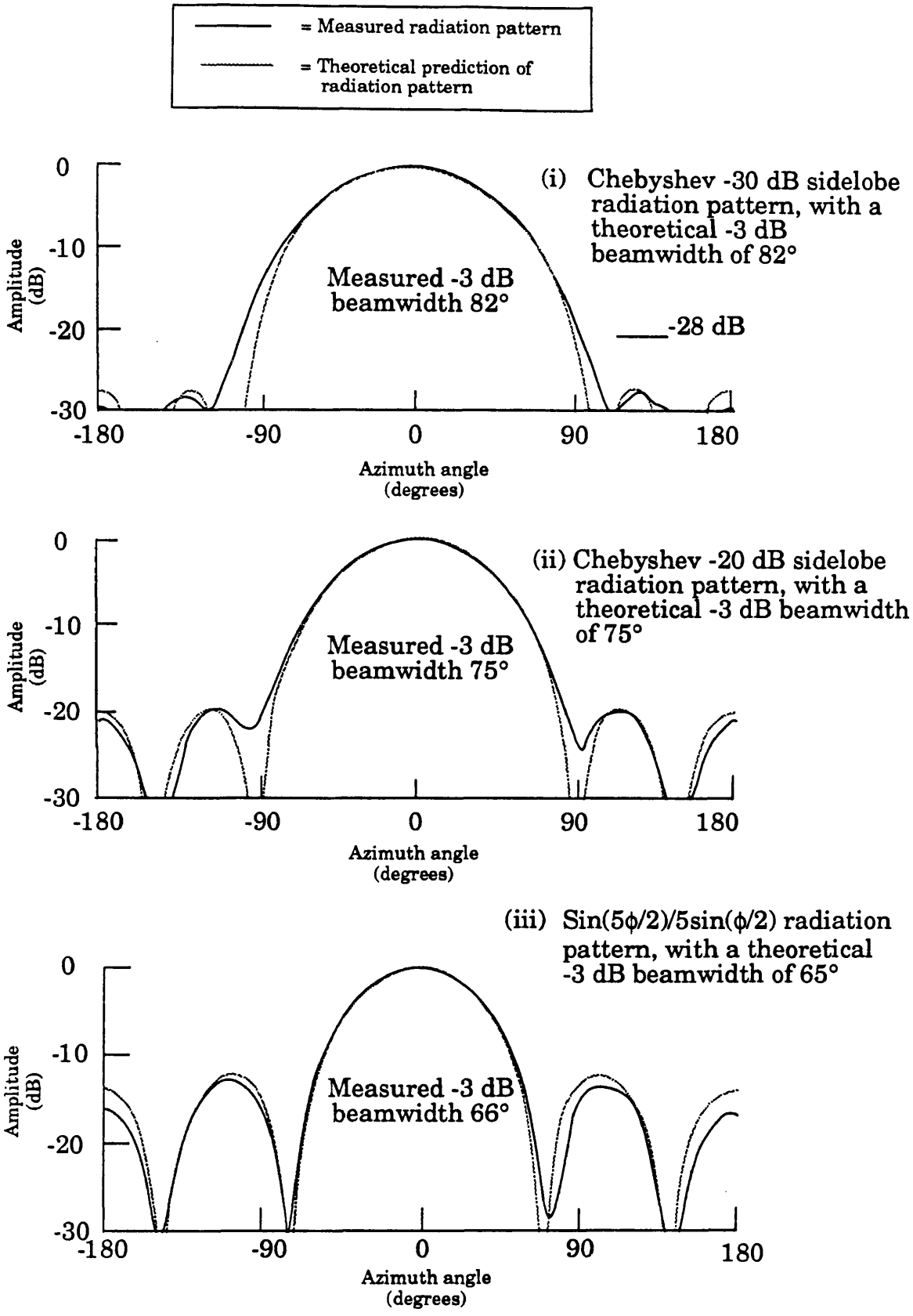

Figure 5.2 Measurements of beams synthesised using a matrix. to form the amplitude modes. The narrowband patterns were measured at 10 GHz in an anechoic chamber.

One of the main aims of this study was the formation of overlapping low sidelobe beams. Measurements were made of the synthesised beams at ports 1,2 and 4, (port 3 is shown in figure 5.2) but the results were unsatisfactory, showing patterns with sidelobes as high as -15 dB. The transmission parameters were measured for ports 1,2 and 4, revealing transmission errors as large as ±2 dB and ±20°, compared to the theoretical values. By adjusting the compensation networks, the errors for beam port 1 were reduced to less than ±2° and ±0.2 dB. The measured beam had the Chebyshev shape of figure 5.2, but pointing in the opposite azimuth direction. The sidelobe level was within ±0.5 dB of the theoretical -28 dB level and the -3 dB beamwidth was within ±1° of the theoretical 82°. Unfortunately the adjustment of the compensation severely degraded the measured pattern at beam port 3; it was only possible to obtain one beam at a time. Further analysis of the effect of beamformer errors on the synthesised beam will be carried out in section 5.5. Overlapping beams were demonstrated by Davies et al. (1984) using a very similar beamformer, but operating at UHF frequencies. Again only patterns with high sidelobes were demonstrated.

To conclude, it was not possible to produce a fan of overlapping low sidelobe beams, even at a single frequency, because of matrix errors.

5.2.2 **Synthesis of a -20 dB sidelobe Chebyshev beam**

To demonstrate the ease with which different patterns can be formed, the taper on the modes was reduced to produce a Chebyshev beam with -20 dB sidelobes. With this taper the theoretical beamwidth is decreased to 75°. The calculated amplitude and phase of the compensation required to form this beam is given in table 5.4 overleaf.

Mode order	0	C1	C2	S1
Mode coefficients	0 dB, 0°	0 dB, +66°	-9.3 dB,+161°	0 dB, +66°
Mode compensation	-3.58 dB, 0°	-5.17 dB, -66°	0 dB, -161°	-5.17 dB, -66°
Final mode weights (relative)	0 dB, 0°	-1.59 dB, 0°	-5.72 dB, 0°	-1.59 dB, 0°

Table 5.4 The amplitude mode compensation used in the synthesis of a -20 dB sidelobe Chebyshev beam.

To realise these weights additional attenuation was added to the 0^{th} and 1^{st} order modes. The theoretical transmission parameters for the beamformer were calculated using (4.2.4). The measured transmission parameters for the complete network are compared to the theoretical values in table 5.5 below. As for the -30 dB sidelobe Chebyshev beam, fine tuning of the compensation was necessary to eliminate the effect of matrix transmission errors.

Element number	1	2	3	4
Theoretical element excitation	-10.1 dB, +139°	-6.0 dB, 0°	-8.3 dB,-111°	-6.0 dB, 0° (reference)
Measured element excitation	-10.5 dB, +142°	-6.2 dB, +1°	-8.2 dB,-110°	-6.0 dB, 0° (reference)
Excitation error	-0.4 dB, +3°	-0.2 dB, +1°	+0.1 dB, +1°	0 dB, 0°

Table 5.5 A comparison between the measured and theoretical transmission parameters for the beamformer (Chebyshev beam with -20 dB sidelobes).

The measured radiation pattern is shown in figure 5.2. For comparison the theoretical radiation pattern is also plotted. The -3 dB beamwidth of the measured pattern is within ±2° of the theoretical value of 75°, while the first sidelobe level is within 0.5 dB of the theoretical -20 dB.

The theoretical directive gain of this beam is higher than that of the -30 dB sidelobe Chebyshev beam. The measured gain of this beam is 3.5 dB lower than that of the -30 dB sidelobe Chebyshev beam because the 0^{th} and 1^{st} order modes were attenuated to give the correct taper, as explained in section 3.5.

Again the amplitude mode compensation was adjusted to minimise the transmission errors for one beam port (number 3) alone. The synthesised beams at the other three ports had sidelobe levels as high as -14 dB.

5.2.3 **Synthesis of a sin(Nx)/Nsin(x) radiation pattern**

To demonstrate the versatility of this technique a $\sin(5\phi/2)/5\sin(\phi/2)$ pattern was formed by exciting the 0^{th}, 1^{st} and 2^{nd} order modes with equal amplitudes. This pattern has a theoretical -3 dB beamwidth of 65° with the first sidelobes at a level of -12.1 dB, determined using figure 2.2. The calculated amplitude and phase of the compensation required is given in table 5.6 below.

Mode order	0	C1	C2	S1
Mode coefficients	0 dB, 0°	0 dB, +66°	-9.3 dB,+161°	0 dB, +66°
Mode compensation	-9.3 dB, 0°	-9.3 dB, -66°	0 dB, -161°	-9.3 dB, -66°
Final mode weights (relative)	0 dB, 0°	0 dB, 0°	0 dB, 0°	0 dB, 0°

Table 5.6 Amplitude mode compensation used in the synthesis of a $\sin(5\phi/2)/5\sin(\phi/2)$ radiation pattern.

To realise these weights more attenuation was added to the 0^{th} and 1^{st} order modes. The theoretical transmission parameters for the beamformer were calculated using (4.2.4). The measured transmission parameters for the complete network are compared to the theoretical values in table 5.7 below. As for the -30 dB and -20 dB sidelobe Chebyshev beams, fine tuning of the compensation was necessary to eliminate the effect of matrix transmission errors.

Element number	1	2	3	4
Theoretical element excitation	-8.66 dB, +157°	-6.0 dB, 0°	-8.55 dB,-139°	-6.0 dB, 0° (reference)
Measured element excitation	-9.0 dB, +154°	-5.9 dB, 0°	-8.5 dB,-141°	-6.0 dB, 0° (reference)
Excitation error	-0.34 dB, -3°	+0.1 dB, +1°	+0.05 dB, -2°	0 dB, 0°

Table 5.7 A comparison between the measured and theoretical transmission parameters for the beamformer ($\sin(5\phi/2)/5\sin(\phi/2)$ beam).

The measured radiation pattern is shown in figure 5.2. For comparison the theoretical radiation pattern is also plotted. The -3 dB beamwidth of the measured pattern is within ±2° of the theoretical value of 65°, while the first sidelobe level is within ±1 dB of the theoretical -12.1 dB. The measured peak gain was -5.5 dBi, compared to a theoretical figure of -3 dB using (3.5.6) Although the directive gain of this beam is 7 dB, higher than that of the Chebyshev beams, the gain of this beam is lower because the 0^{th} and 1^{st} order modes are attenuated down to the level of the 2^{nd} order mode.

The Chebyshev beam of figure 5.2, with -28 dB sidelobes has the lowest sidelobes demonstrated using the phase modes of a circular array. Beams formed by Sheleg (1968) using a 32-element circular array demonstrated a sidelobe level of -19 dB in a (single-frequency) beam that was scanned using phase shifters. Results of Davies and Chow (1969) show 'ripple' at -23 dB on an electronically scanned pattern. However, the main aim of this study was the synthesis of instantaneously wideband patterns. Adjustment of the compensation to correct matrix errors across a wide frequency band was simply not feasible. A simpler corporate feed beamformer was developed to solve this problem, as described in sections 4.3.3 and 4.4. The next two sections present the results of measurements on instantaneously wideband beams formed using the same monopole array.

5.3 Synthesis of a wideband low sidelobe radiation pattern

5.3.1 **Introduction**

In section 4.4.3 the design of a corporate feed to form a single Chebyshev beam is described. The beamformer of figure 4.18 produces an array excitation where the 0^{th}, 1^{st} and 2^{nd} order phase modes have a taper calculated using the equations of section 2.1.4:

Mode order	-2	-1	0	+1	+2
Amplitude taper (dB)	-9.94	-2.29	0	-2.29	-9.94

With this taper the mainlobe has a theoretical -3 dB beamwidth of 82°, and equal level -30 dB sidelobes. The modes are excited with this taper instantaneously across the frequency band 8 to 12 GHz. The modes also had a linear phase progression applied to form the beam in the azimuth direction $\phi = 180°$, the direction of element number 3.

5.3.2 **Results of azimuth pattern measurements**

Azimuth radiation pattern measurements were done using the technique of section 5.1.2. First the source frequency was set to 10 GHz. The measured azimuth radiation pattern is shown in figure 5.3a. For comparison the theoretical beam shape is also plotted. The measured -3 dB beamwidth is within ±2° of the theoretical beamwidth. The sidelobe level is considerably higher than the theoretical level, at -20.5 dB.

The radiation pattern measurements were repeated across the frequency band 8 to 12 GHz, at 0.25 GHz intervals. Figures 5.3a and 5.3b show the plots taken at 8, 9, 10, 11 and 12 GHz. Since the beamformer was instantaneously wideband, only the RF source frequency was changed between measurements.

Figure 5.4 plots the change in the -3 dB beamwidth with frequency showing a variation of only ±3° over the half octave frequency range. Figure 5.4 also shows the change in the peak sidelobe levels with frequency. The sidelobe level is between -20 dB and the design figure of -30 dB. At two frequencies, 8.5 and 10. 25 GHz, the sidelobe level is within ±1 dB of the design sidelobe level: -28 dB. The reason for the increase in sidelobe levels is errors in the beamformer. As explained in section 4.4.3, the specified excitation could only be realised to within about ±0.5 dB, and ±5°. Inspection of figure 4.2 shows that for errors of this magnitude, a minimum sidelobe level of -20 dB can be expected. Further analysis of the effect of measured beamformer errors on these measured beams is done in section 5.5.

These results show that low sidelobe wideband patterns can be formed by a circular array. While at a single frequency it is possible to achieve sidelobe levels close to -30 dB, for wideband patterns errors in the wideband beamformer limit the sidelobe level to about -20 dB. Earlier studies of the phase mode excitation of circular arrays, for example by Sheleg (1969) have demonstrated the synthesis of directional beams at a single frequency, this Chebyshev beam was the first demonstration of an instantaneously wideband directional beam.

Chebyshev -30 dB sidelobe radiation pattern, with a theoretical -3 dB beamwidth of 82°

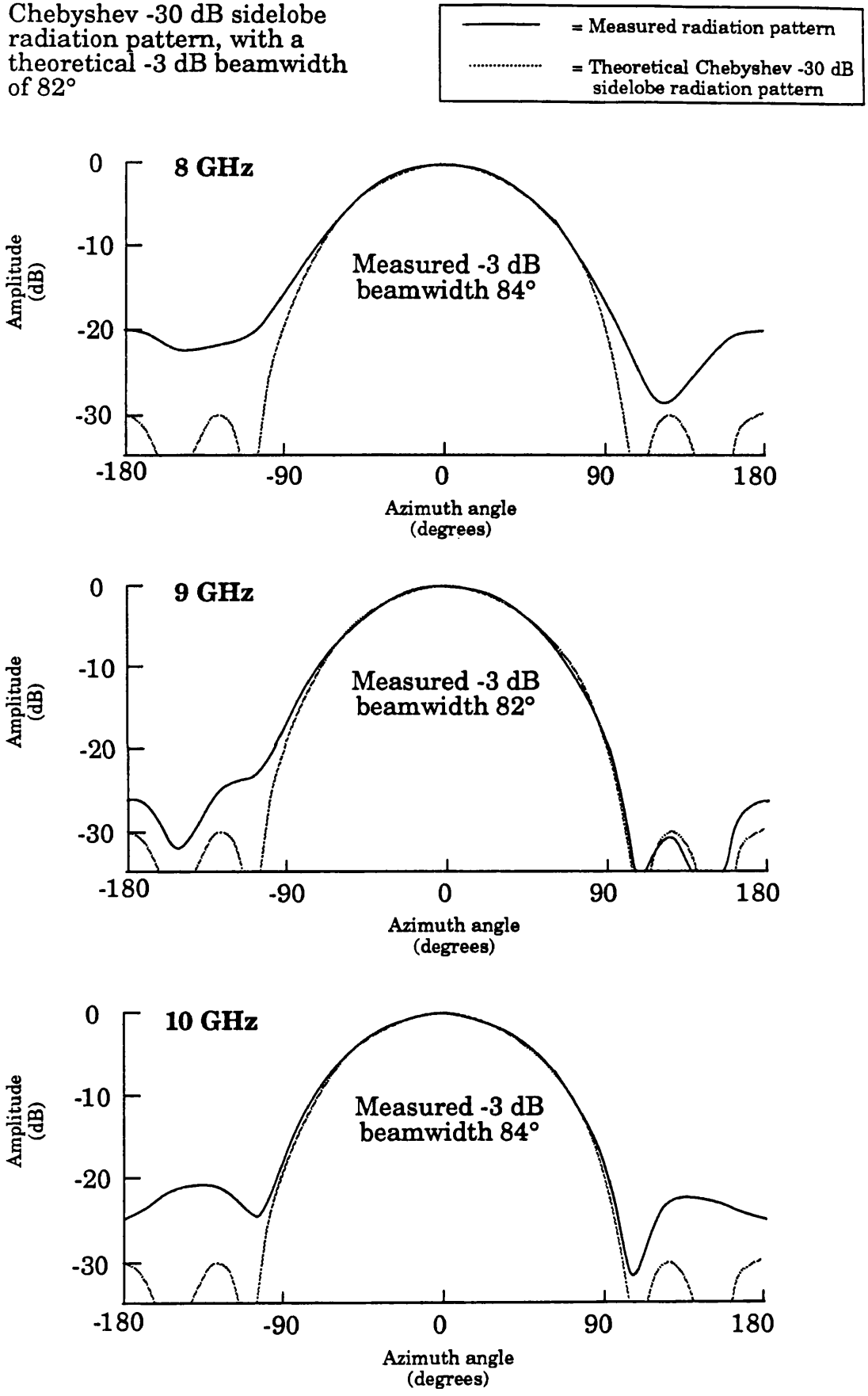

Figure 5.3a Measurements of a wideband pattern synthesised using a weighted corporate feed. These plots show the radiation pattern at 8, 9 and 10 GHz, at an elevation angle of +8°.

Chebyshev -30 dB sidelobe radiation pattern, with a theoretical -3 dB beamwidth of 82°

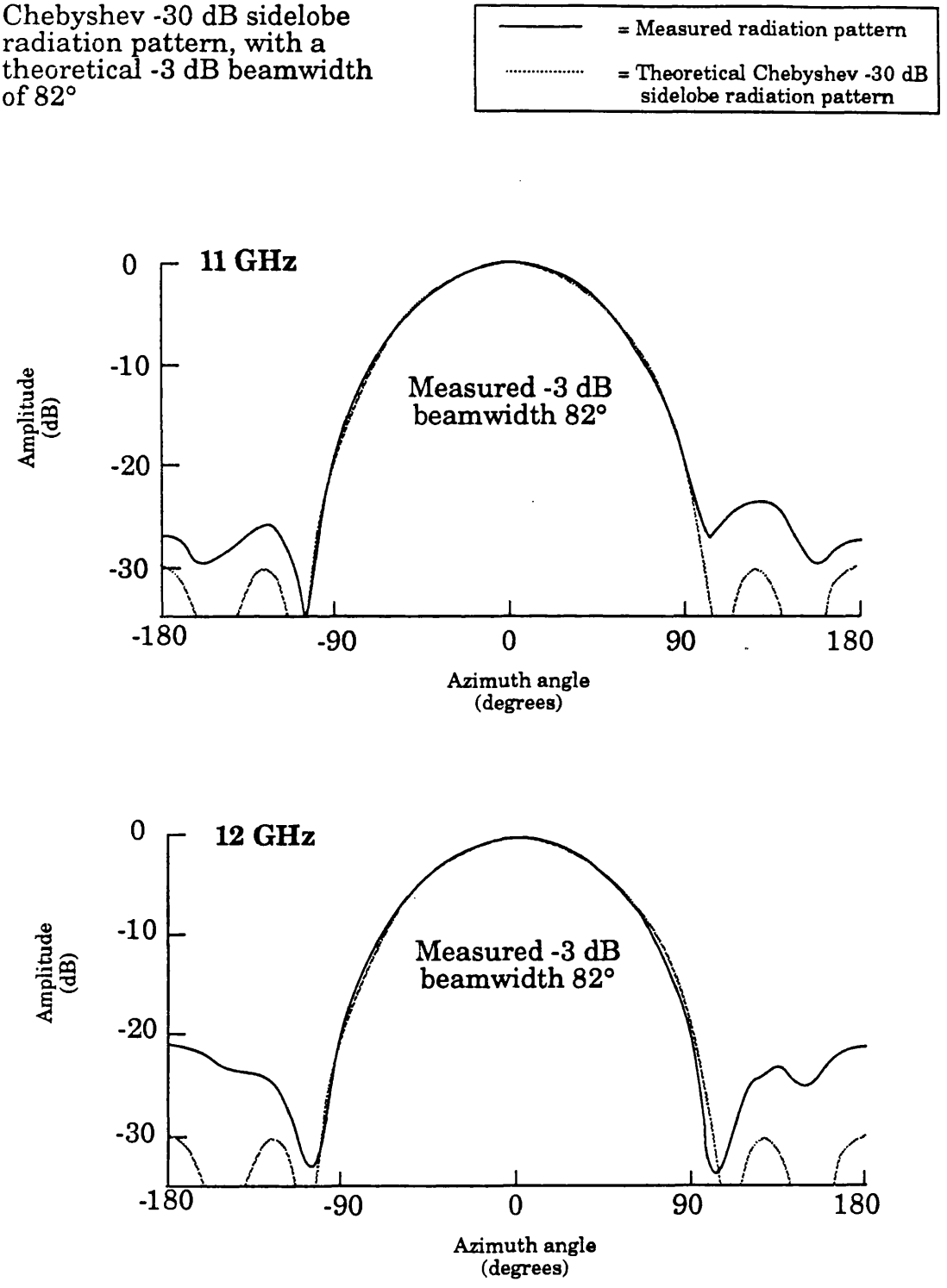

Figure 5.3b Measurements of a wideband pattern synthesised using a weighted corporate feed. These plots show the radiation pattern at 11 and 12 GHz, at an elevation angle of +8°.

Chebyshev -30 dB sidelobe radiation pattern, with a theoretical -3 dB beamwidth of 82°

Measured changes in the mainlobe -3 dB beamwidth with frequency

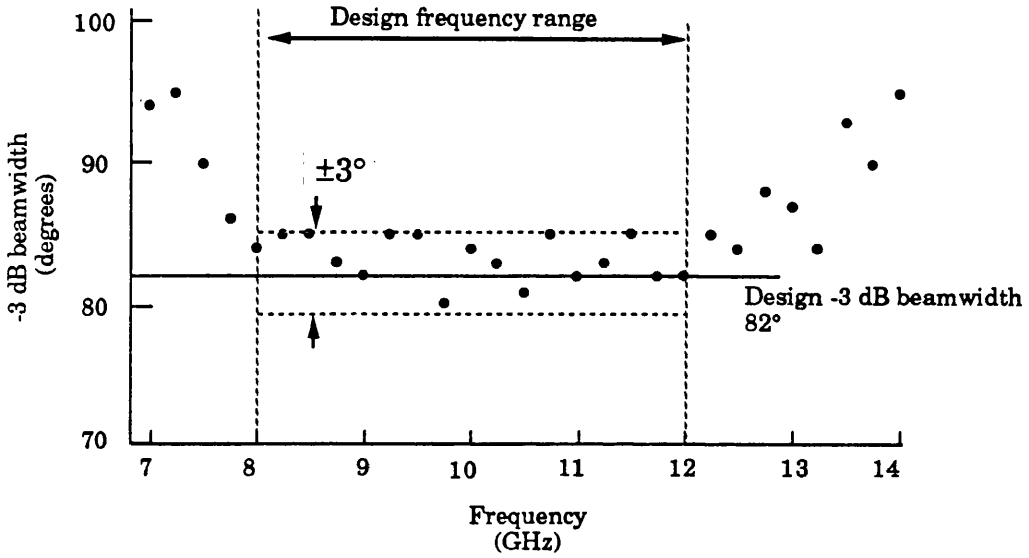

Measured changes in the peak sidelobe level with frequency

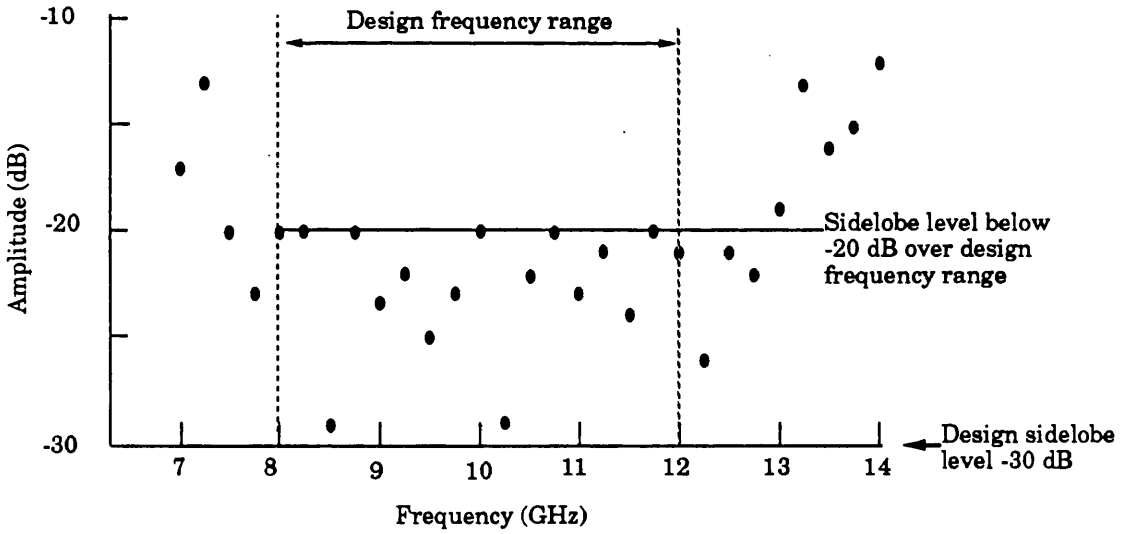

Figure 5.4 Measured changes in the -3 dB beamwidth and sidelobe levels of the Chebyshev beam as a function of frequency. The measurements were made at a fixed elevation angle of +8°.

Plots were also made of the synthesised beam outside the band 8 to 12 GHz. Figure 5.4 plots the beamwidth from 7 to 14 GHz; an octave of bandwidth. The beamwidth changes by ±7.5° across this frequency range. The sidelobe level increases up to about -10 dB at the ends of the frequency range. This deterioration is to be expected, as no attempt to optimise the characteristics of the microstrip networks outside the range 8 to 12 GHz was made, and most of the beamformer components were only rated for operation over a half octave band. With wider bandwidth beamformer components, a low sidelobe pattern could have been demonstrated over an octave of bandwidth. The gain would have been lower at the ends of the bands, due to the use of monopole elements.

5.3.3 **Changes in the azimuth pattern with elevation**

Measurements of the azimuth pattern were repeated at fixed elevation angles from 0° to +40°, using the technique of section 5.1.4. Figure 5.5a and 5.5b shows the measured change in the azimuth pattern with elevation, with the source set to 10 GHz. There is an increase in the -3 dB beamwidth with elevation, clearly illustrated in figure 5.6, showing the change in -3 dB beamwidth with elevation at 8, 9, 10, 11 and 12 GHz. At 0° of elevation the beamwidth is 82±3° (across the band), increasing to 92±2° at an elevation angle of +40°. This is a percentage change of 12%.

Inspection of figure 5.5, showing the change of the pattern with elevation at 10 GHz shows that the sidelobe level remains fairly constant up to about +16° of elevation, and then the peak sidelobe level drops to -25 dB at 32° of elevation. At 40° of elevation the peak sidelobe level has increased to -20 dB again. Inspection of figure 5.7 shows that this effect is repeated across the band, with an initial drop in sidelobe level, followed by an increase at higher elevations. The only exception is at 8 GHz, where the sidelobe level remains fairly constant, before increasing to -15 dB at +40° of elevation.

These results are in good agreement with the theoretical analysis of section 2.4. As the elevation angle increases, an increased taper is applied to the higher order modes, relative to the zero order mode. This taper increases

Chebyshev -30 dB sidelobe radiation pattern, with a theoretical -3 dB beamwidth of 82°

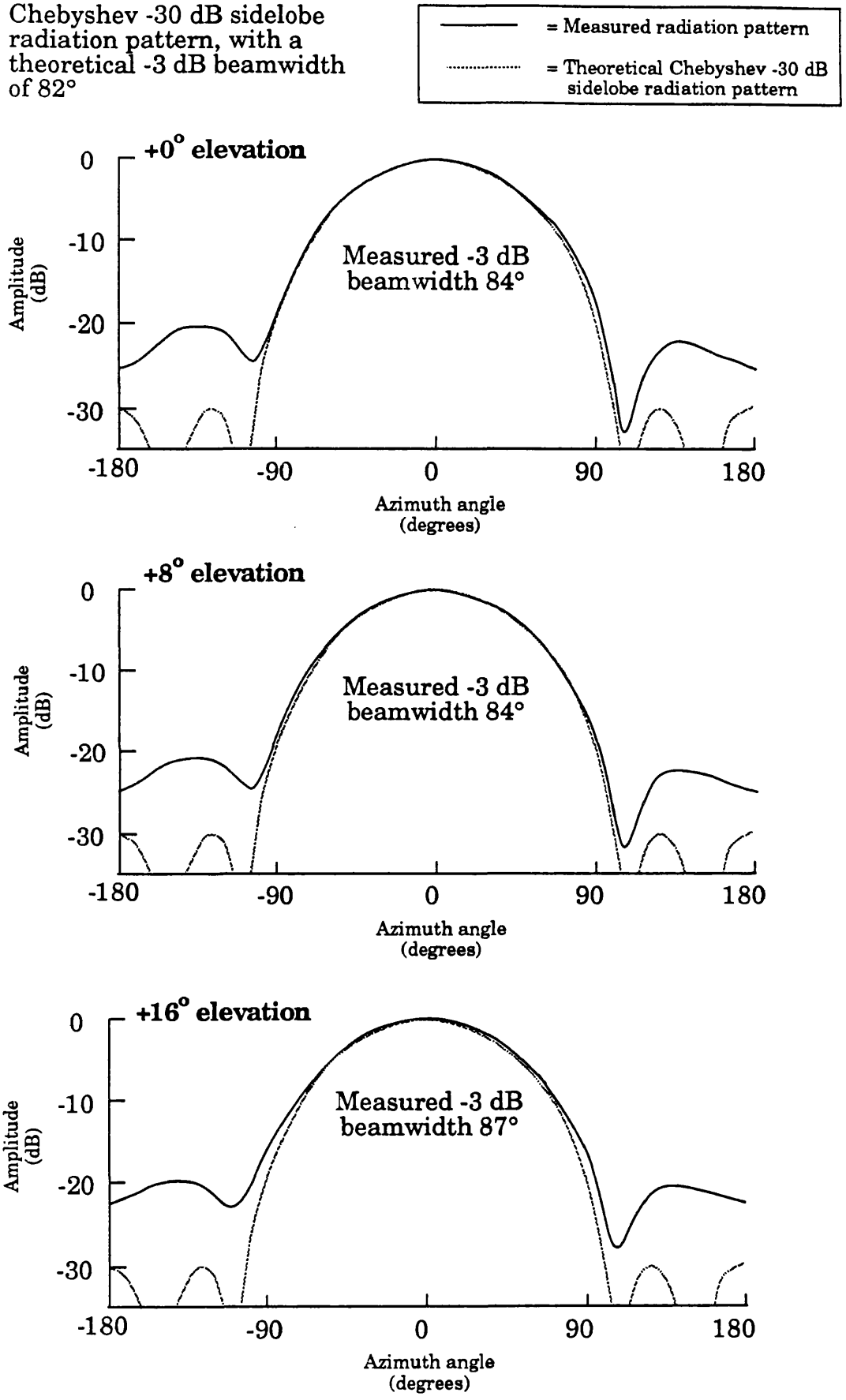

Figure 5.5a Measurements of a wideband Chebyshev beam synthesised using a weighted corporate feed. These plots show the radiation pattern at elevation angles of 0°, 8° and 16°, at a fixed frequency of 10 GHz.

Chebyshev -30 dB sidelobe radiation pattern, with a theoretical -3 dB beamwidth of 82°

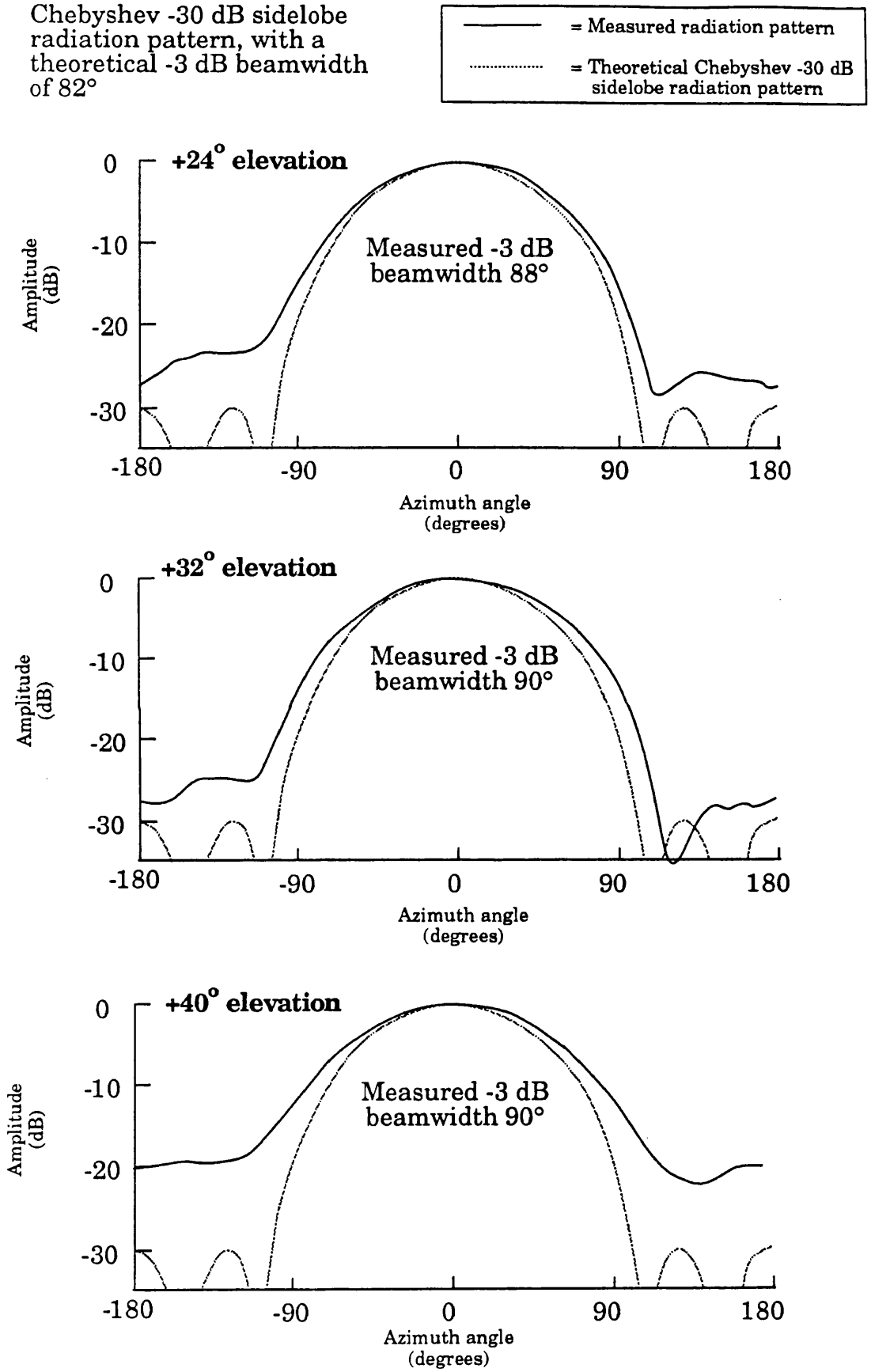

Figure 5.5b Measurements of a wideband Chebyshev beam synthesised using a weighted corporate feed. These plots show the radiation pattern at elevation angles of 24°, 32° and 40°, at a fixed frequency of 10 GHz.

Chebyshev -30 dB sidelobe radiation pattern, with a theoretical -3 dB beamwidth of 82°

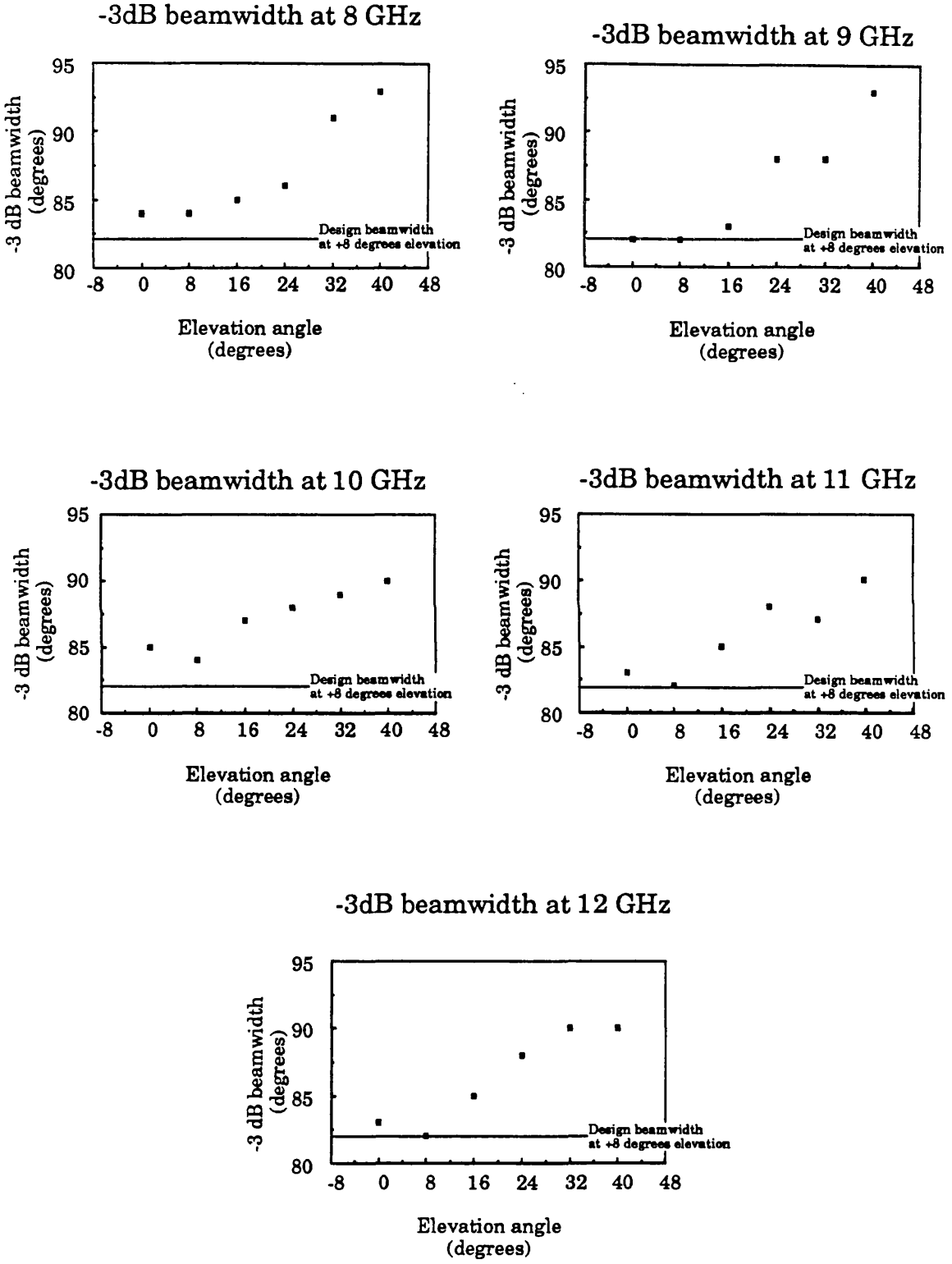

Figure 5.6 Measured changes in the azimuth -3 dB beamwidth of the synthesised Chebyshev beam as a function of elevation.

Chebyshev -30 dB sidelobe radiation pattern, with a theoretical -3 dB beamwidth of 82°

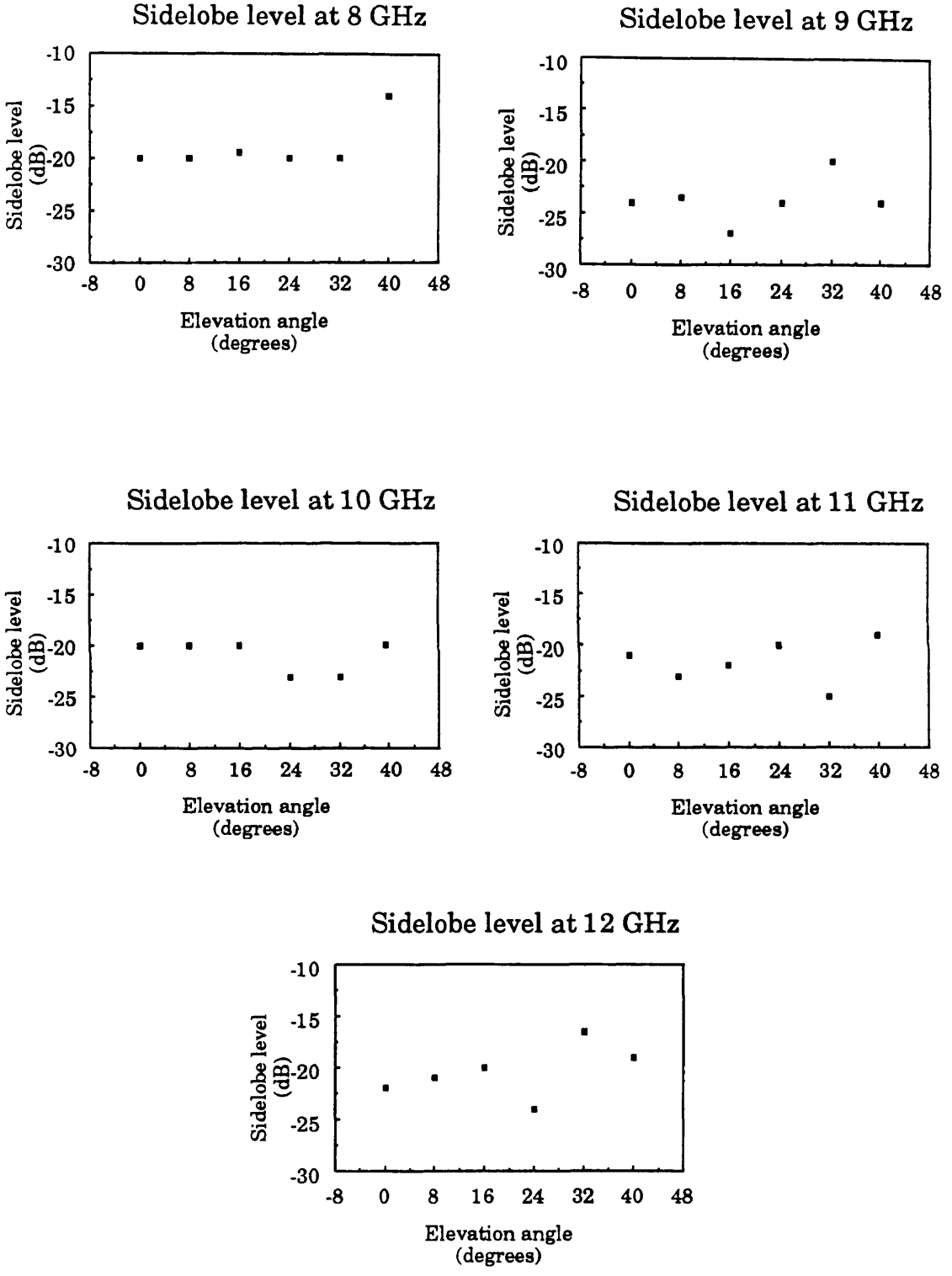

Figure 5.7 Measured changes in the peak sidelobe levels of the synthesised Chebyshev beam as a function of elevation.

the -3 dB beamwidth and reduces the average sidelobe level. However, as the elevation angle increases to 40° the average sidelobe level increases, and the set of four nulls disappears. This can be explained if we consider the relative phase of the phase modes on the position of the nulls, using the Schelkunoff unit circle analysis of section 2.1.3. As the elevation angle increases, the phases of the phase mode coefficients change so the modes move out of alignment. The zeros in the pattern move away from the unit circle and the nulls become shallower. The nulls also change their azimuth angle. For the -30 dB sidelobe Chebyshev beam the nulls either side of the backlobe move away from each other, so the backlobe becomes larger, at the expense of the two sidelobes. This effect was predicted in section 2.4, which considered the change with elevation for a -20 dB sidelobe Chebyshev beam.

None of the azimuth plots showed a significant squint in the direction of the beam with elevation.

5.3.4 **The elevation pattern of the synthesised beam**

Next the array was mounted on the turntable with the ground plane vertical, as described in section 5.1.6. By rotating the turntable a measurement of the elevation pattern for the beam was made. Figure 5.8 shows the measured elevation pattern of the Chebyshev beam at 10 GHz. The elevation pattern of the monopole element is also plotted, showing that the elevation beamwidth of the synthesised beam is the same as that of the monopole element. The pattern has the same amount of ripple, the result of using a finite ground plane, as discussed in section 3.5. The main difference between the two plots is in the backlobe - the taper applied to the phase modes produces a low backlobe in the $\theta = 180°$ direction. For monopole array elements, the pattern has the same intensity at $\theta = 0°$ and $\theta = 180°$, on the azimuth horizon.

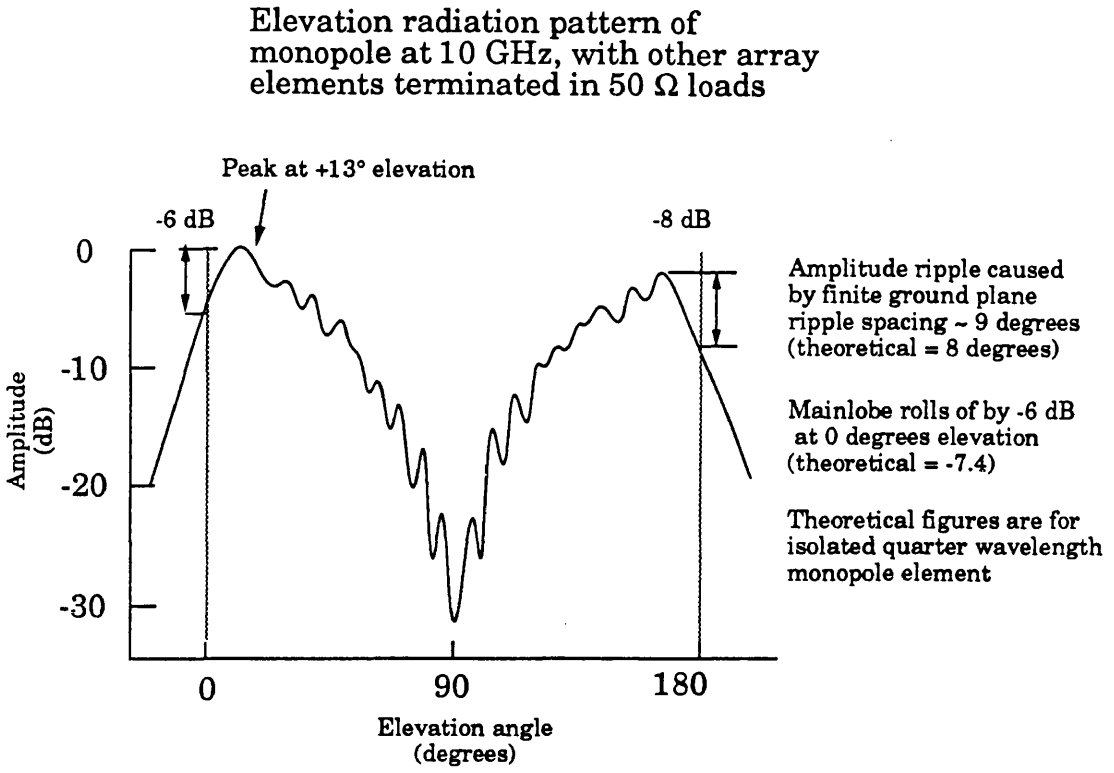

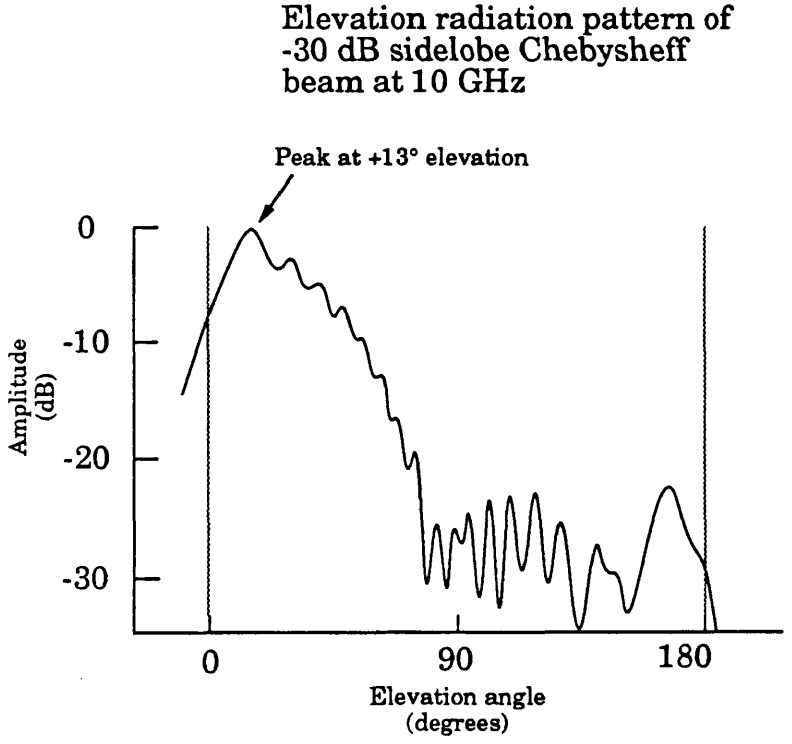

Figure 5.8 A comparison between the radiation pattern of the monopole element and that of the synthesised beam in the elevation plane. Both measurements were made in an anechoic chamber at 10 GHz.

5.3.5 **The gain of the synthesised beam**

Figure 5.9 shows the measured peak gain across the frequency range 8 to 12 GHz. This was done using the technique of section 5.1.7, with the ground plane returned to the horizontal plane. For comparison the theoretical gain, calculated in section 3.5 is also plotted in figure 5.9. The gain is close to 0 dBi at the centre of the band, dropping off at the ends because of the drop in the monopole gain. The gain is about 2 dB less than the theoretical gain. This can be attributed to losses in the beamforming network: ideally the peak transmission amplitude should have been -6 dB. In fact the measured amplitude was closer to -8.5 dB. The peak gain is about the same as that of a typical cavity-backed spiral antenna, as shown in figure 3.2.

5.3.6 **Cross-polar response of the synthesised beam**

The cross-polar response was plotted using the technique of section 5.1.5, with the illuminating horn rotated through 90° to produce horizontally polarised radiation, perpendicular to the vertical monopoles. Figure 5.10 plots the cross-polar response at 10 GHz, with the co-polar mainlobe also plotted to provide an amplitude reference. The cross-polar gain is very low, about -30 dB down on the co-polar response, with a weak mainlobe in the same azimuth direction as the co-polar mainlobe. Because the monopoles are thick ($\lambda/30$) a small horizontal component is picked up directly. In addition, reflections from the walls of the chamber can have a horizontal component.

Gain of the Chebyshev beam relative to isotropic

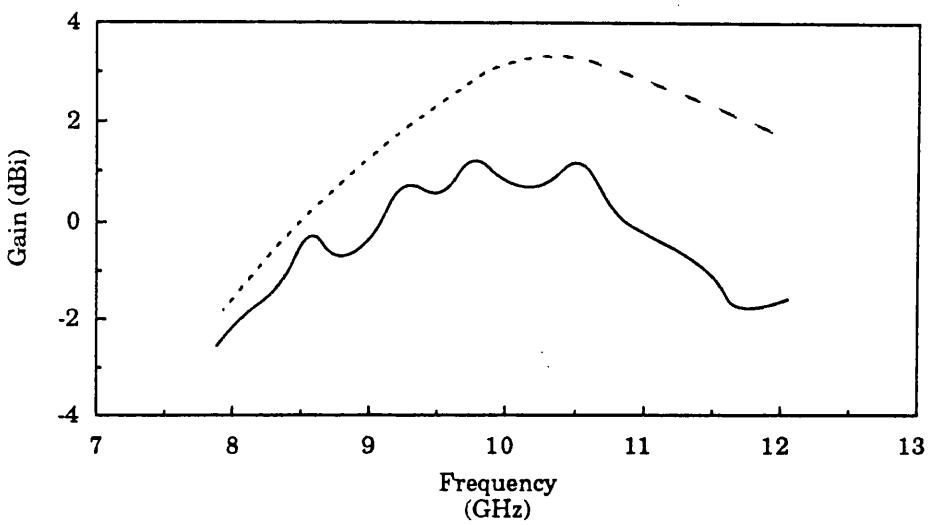

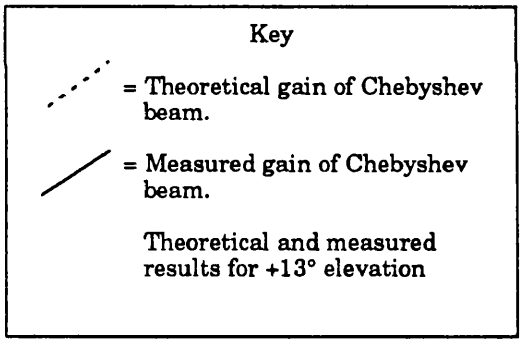

Reasons for differences between theoretical and measured results:

- Measured monopole gain lower than the theoretical gain - see figure 3.15.
- ±0.75 dB ripple due to mismatches between components of beamforming network.
- Losses in the network, 1.5 dB at the centre of the band.

Figure 5.9 A comparison between the measured gain of the Chebyshev beam and the theoretical gain.

Chebyshev -30 dB sidelobe radiation pattern (for vertically polarised signals) with a theoretical -3 dB beamwidth of 82°

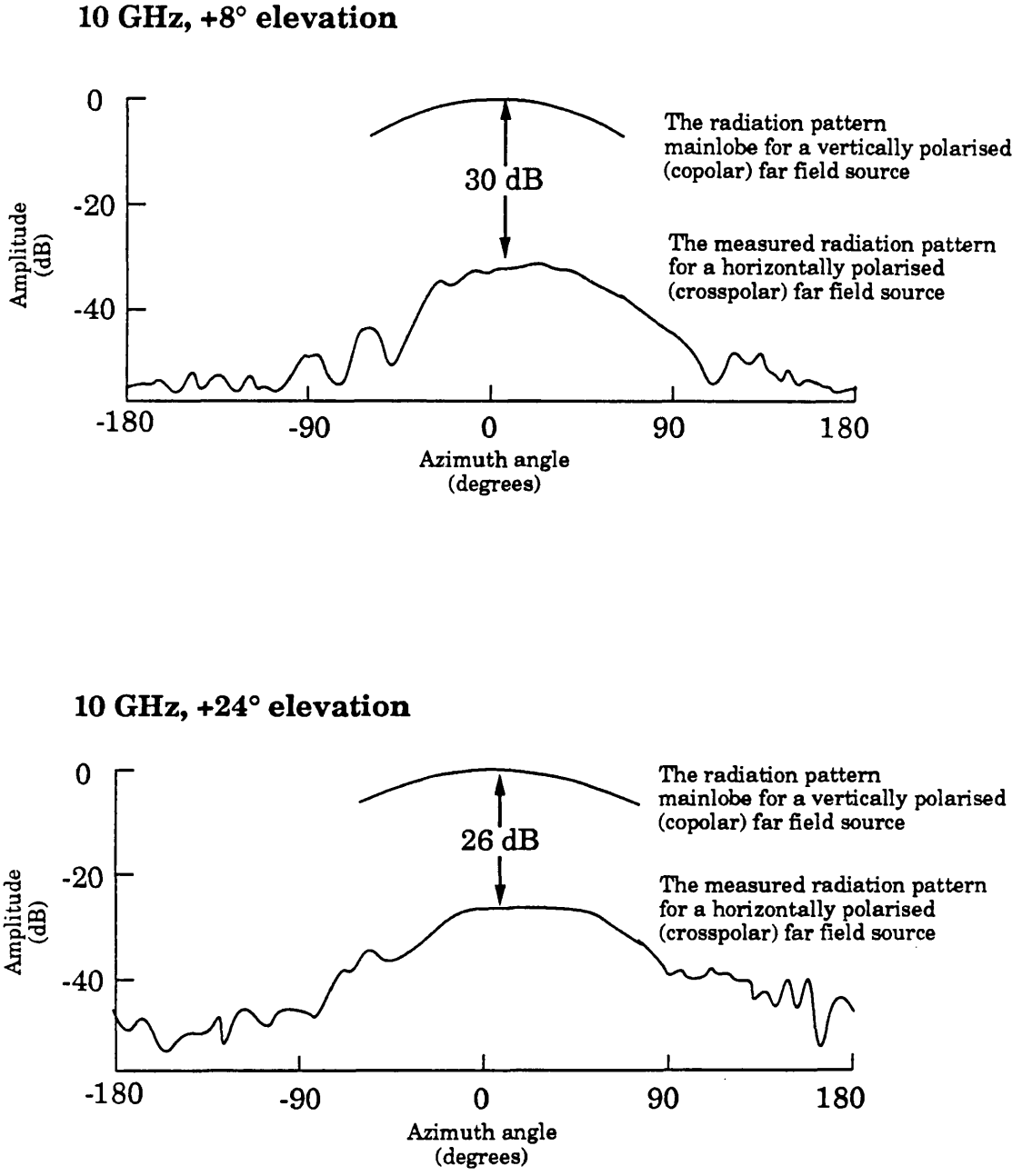

Figure 5.10 The sensitivity of the synthesised beams to horizontally polarised (crosspolar) signals, compared with that for vertically polarised signals. The 10 GHz measurements were made at +8° and +24° elevation.

5.4 Synthesis of a wideband sin(5ϕ/2)/5sin(ϕ/2) radiation pattern

5.4.1 **Introduction**

Figure 4.22 shows a beamformer designed to form a single wideband sin(5ϕ/2)/5sin(ϕ/2) beam. This beamformer produces an array excitation where the 0^{th} 1^{st} and 2^{nd} order phase modes are excited with equal amplitude, instantaneously across the frequency band 8 to 12 GHz. The mainlobe has a theoretical -3 dB beamwidth of 65°, and first sidelobes at -12.1 dB. There is also a single backlobe at -14 dB. The modes had a linear phase progression applied to form the beam in the azimuth direction ϕ = 180°, the direction of element number 3.

5.4.2 **Results of azimuth pattern measurements**

Azimuth radiation pattern measurements were made using the technique described in section 5.1.2. First the source frequency was set to 10 GHz. The measured azimuth radiation pattern is shown in figure 5.11a. For comparison the theoretical beam shape is also plotted. The measured -3 dB beamwidth is within ±1° of the theoretical value, while the first sidelobes are within ±1.5 dB of the theoretical -12.1 dB level. The synthesised pattern is almost identical to that produced at 10 GHz using a matrix type feed. Although the beamformers are completely different, the excitation of the circular array is the same.

The radiation pattern measurements were repeated across the frequency band 8 to 12 GHz, at 0.25 GHz intervals. Figures 5.11a and 5.11b show the plots taken at 8, 9, 10, 11 and 12 GHz. Since the beamformer was instantaneously wideband, only the source frequency was changed between measurements.

Figure 5.12 plots the change in the -3 dB beamwidth with frequency; it is constant to within ±2° over the half octave frequency range. Figure 5.12 also shows the change in the first sidelobe levels with frequency. They are

Sin(5ϕ/2)/5sin(ϕ/2) radiation pattern, with a theoretical -3 dB beamwidth of 65°

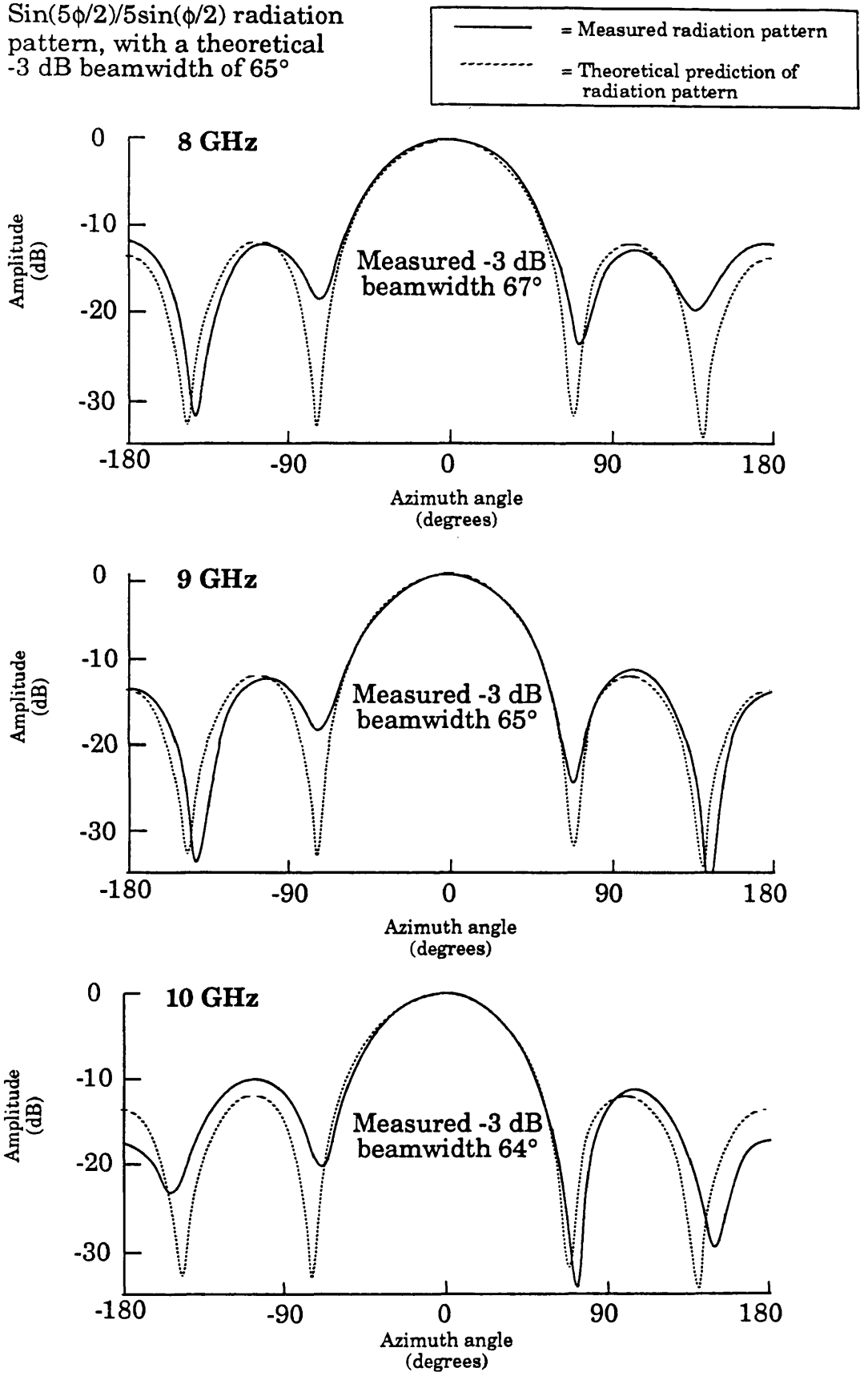

Figure 5.11a Measurements of a wideband sin(5ϕ/2)/5sin(ϕ/2) pattern synthesised using a weighted corporate feed. These plots show the radiation pattern at 8, 9 and 10 GHz, at an elevation angle of +8°.

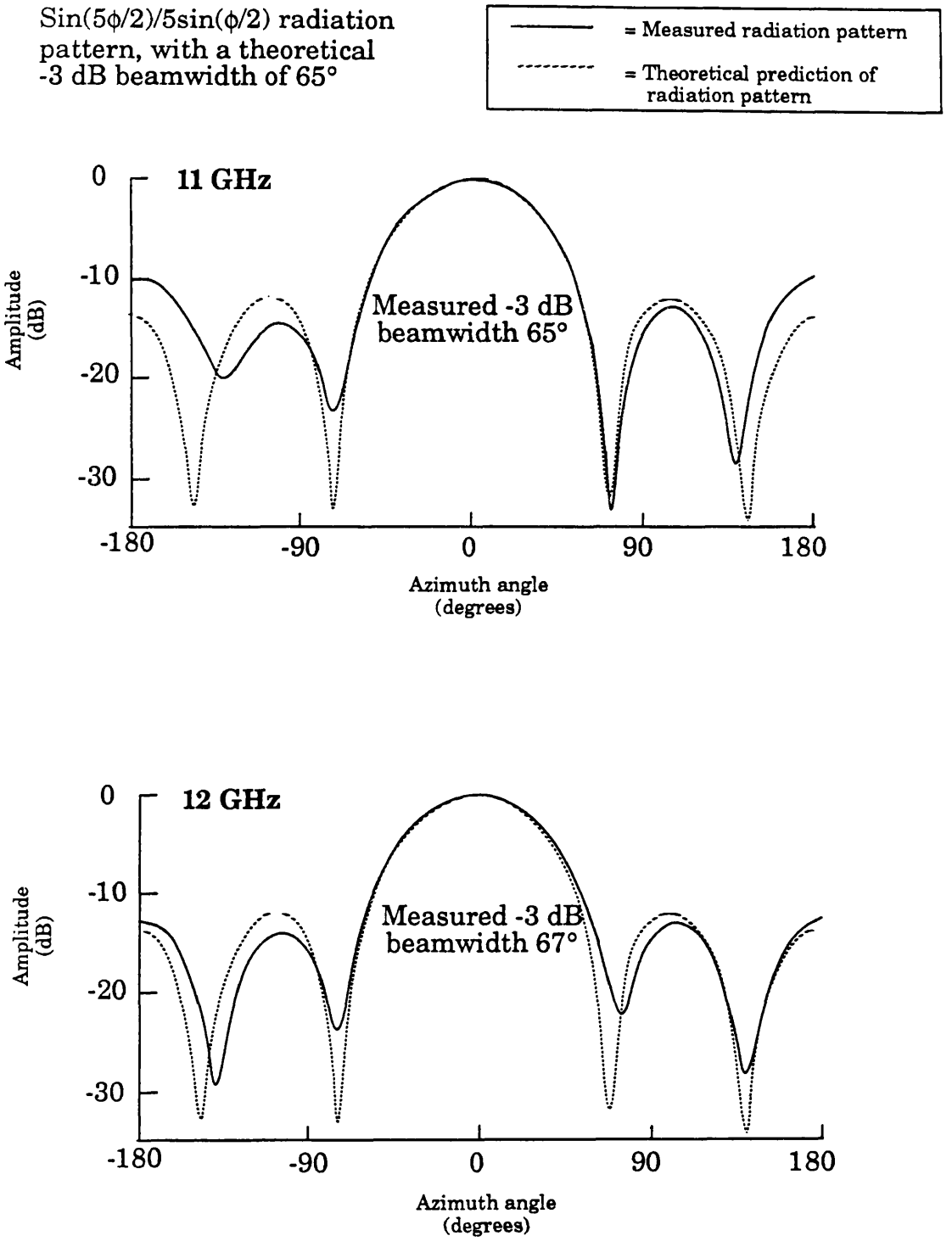

Figure 5.11b Measurements of a wideband sin(5ϕ/2)/5sin(ϕ/2) pattern synthesised using a weighted corporate feed. These plots show the radiation pattern at 11 and 12 GHz, at an elevation angle of +8°.

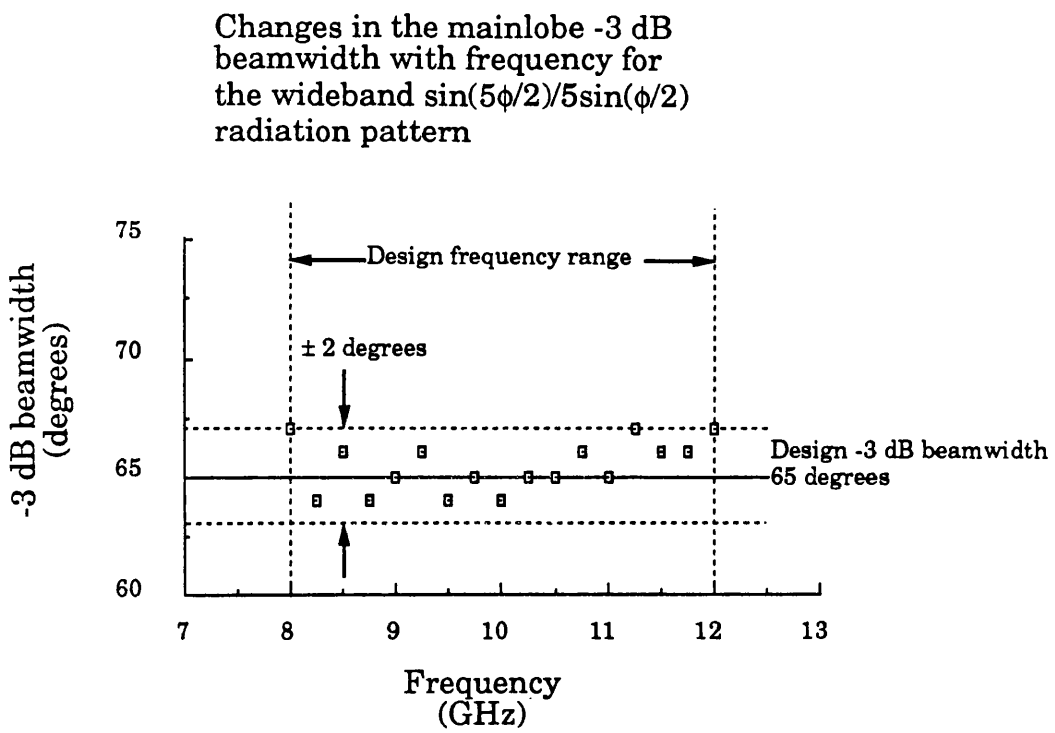

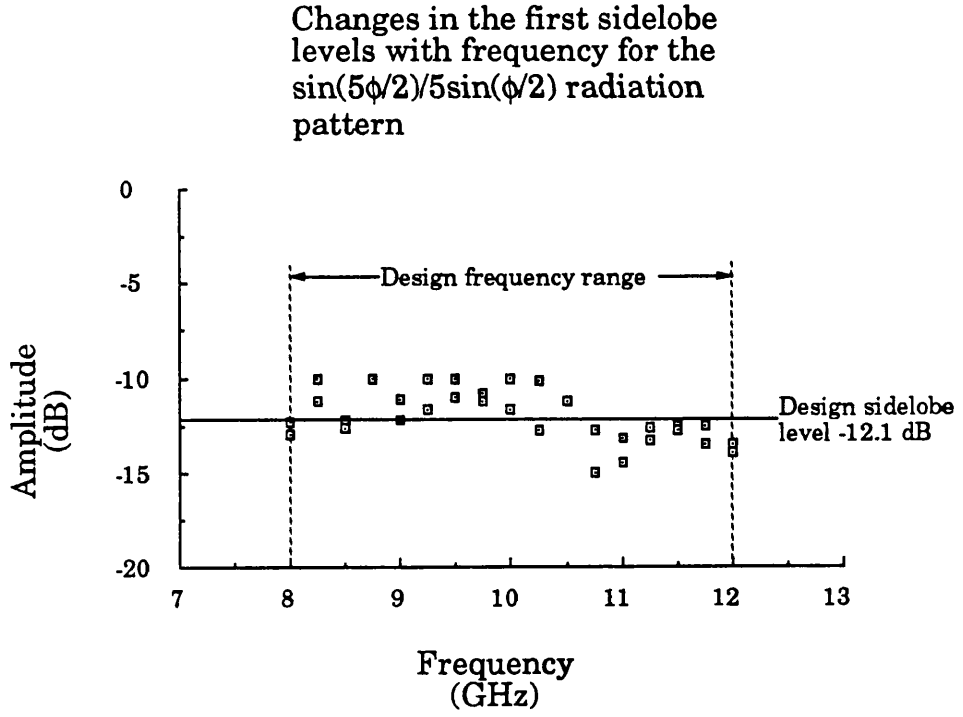

Figure 5.12 Measured changes in the -3 dB beamwidth and sidelobe levels of the sin(5ϕ/2)/5sin(ϕ/2) beam as a function of frequency. The beam was measured at a fixed elevation angle of +8°.

within ±2 dB of the theoretical -12.1 dB level across the band. As for the Chebyshev beam, the changes in the -3 dB beamwidth and sidelobe levels are due to errors in the array excitation, considered further in section 5.5.

5.4.3 **Changes in the azimuth pattern with elevation**

Measurements of the azimuth pattern were repeated at fixed elevation angles from 0° to +40°, using the technique of section 5.1.4. Figure 5.13a and 5.13b show the changes in the measured azimuth pattern with elevation, with the source set to 10 GHz. There is an increase in the -3 dB beamwidth with elevation, clearly illustrated in figure 5.14, showing the change in -3 dB beamwidth with elevation at 8, 9, 10, 11 and 12 GHz. At 0° of elevation the beamwidth is 65±2° (across the band), increasing to 72±2° at an elevation angle of 40°. This is a percentage change of 11%.

Inspection of figure 5.13 shows that there is a gradual drop in the level of the first sidelobes with elevation, from a peak level of -10.5 dB at +8° of elevation to -14 dB at +40°. This is more clearly illustrated in figure 5.15, where the drop in the first sidelobes is apparent across the band. For the single backlobe, pointing at 180° to the mainlobe there is a gradual increase in the level with elevation, from about -15 dB at 0° to -12 dB at 40°, although there are considerable variations across the frequency band.

As for the Chebyshev beam, these results are in good agreement with the theoretical analysis of section 2.4. As the elevation angle increases, an increased taper is applied to the higher order modes, relative to the zero order mode. This taper increases the -3 dB beamwidth and reduces the average sidelobe level. Because the modes move out of alignment in phase some lobes increase in height, as is the case for the single backlobe of this pattern. None of the azimuth plots showed a significant squint in the azimuth direction of the beam with elevation.

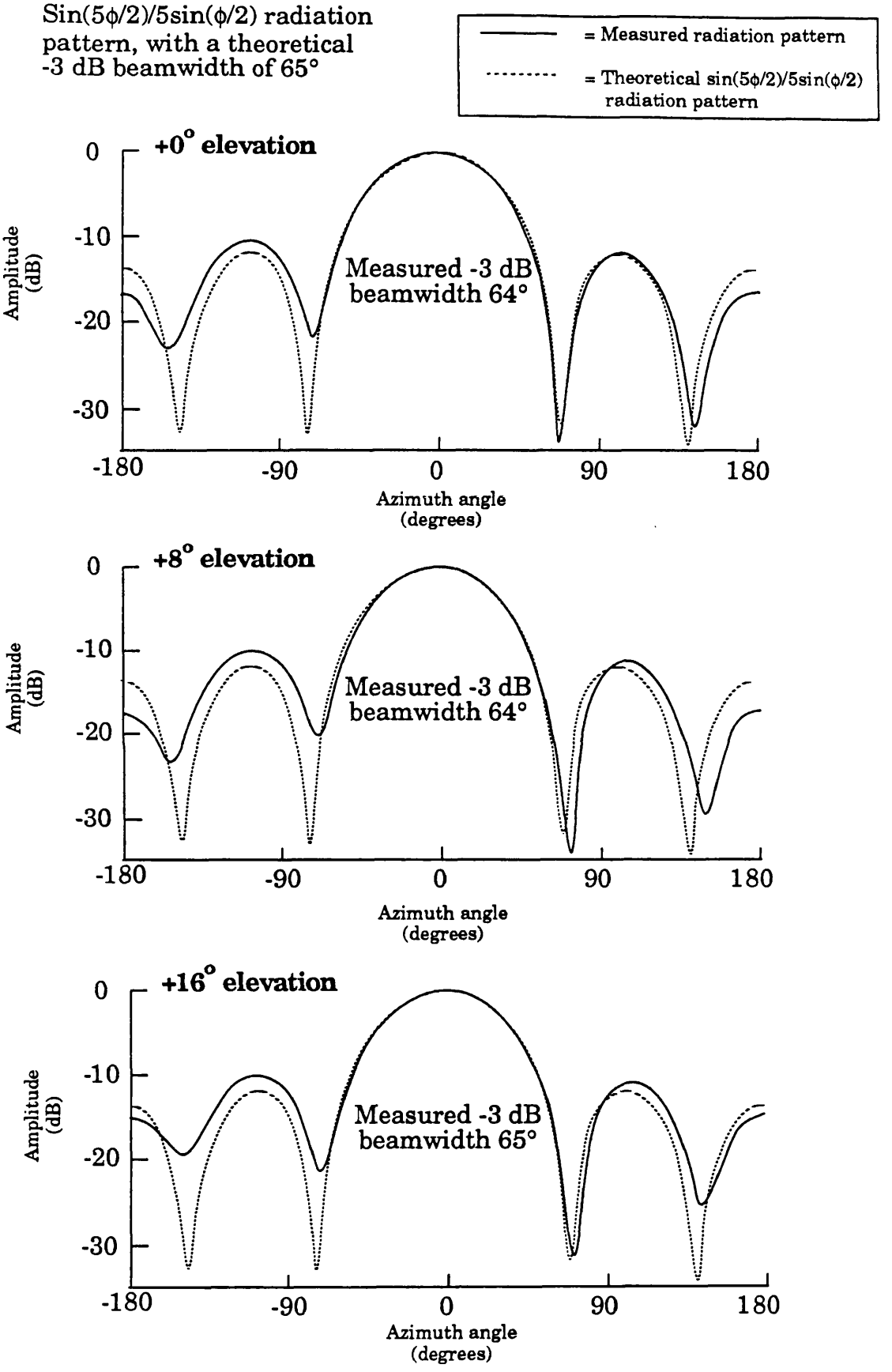

Figure 5.13a Measurements of a wideband sin(5ϕ/2)/5sin(ϕ/2) beam synthesised using a weighted corporate feed. These plots show the radiation pattern at elevation angles of 0°, 8° and 16°, at a fixed frequency of 10 GHz.

Sin(5ϕ/2)/5sin(ϕ/2) radiation pattern, with a theoretical -3 dB beamwidth of 65°

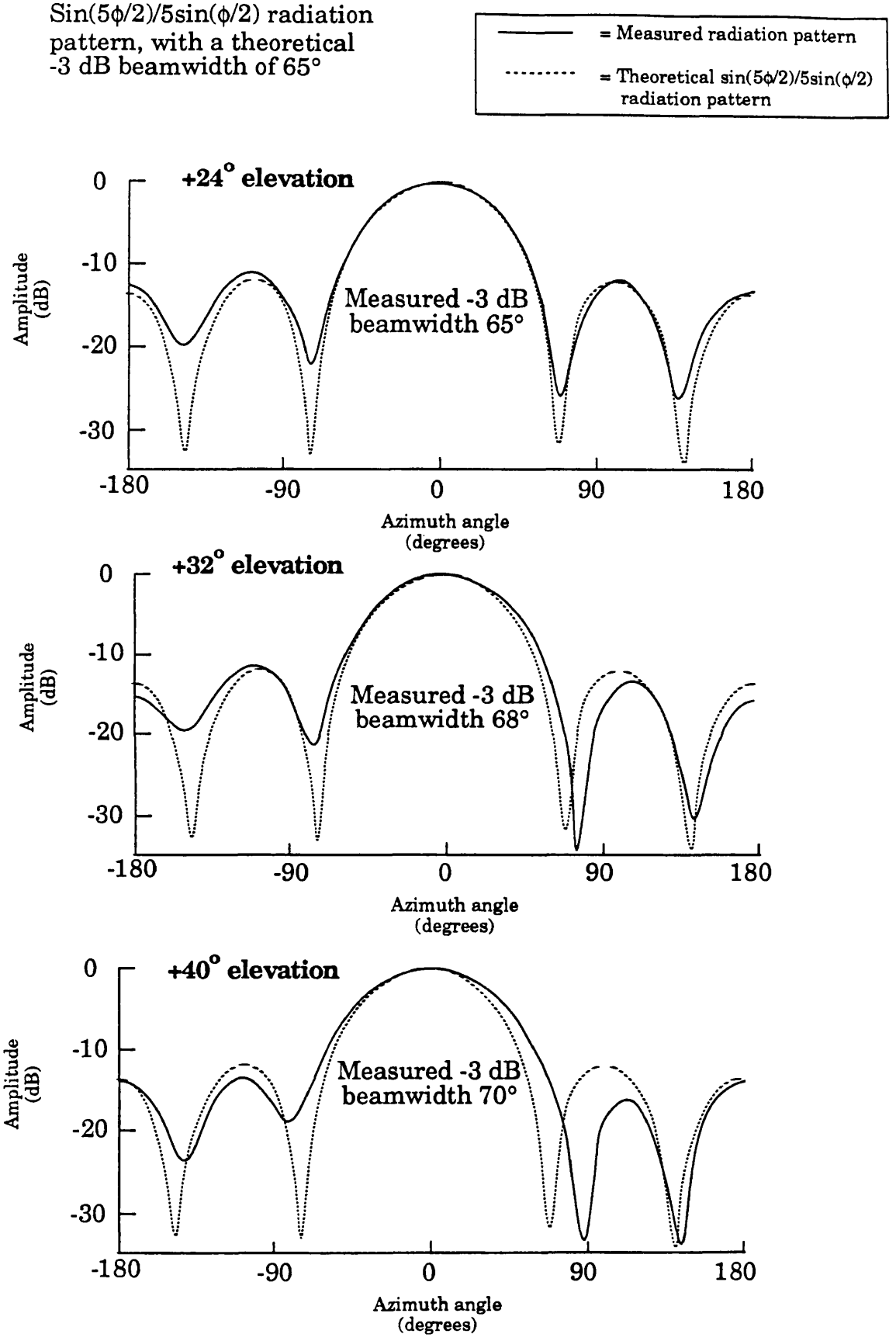

Figure 5.13b Measurements of a wideband sin(5ϕ/2)/5sin(ϕ/2) beam synthesised using a weighted corporate feed. These plots show the radiation pattern at elevation angles of 24°, 32° and 40° at a fixed frequency of 10 GHz.

Synthesised $\sin(5\phi/2)/5\sin(\phi/2)$
radiation pattern, with a theoretical
-3 dB beamwidth of 65°

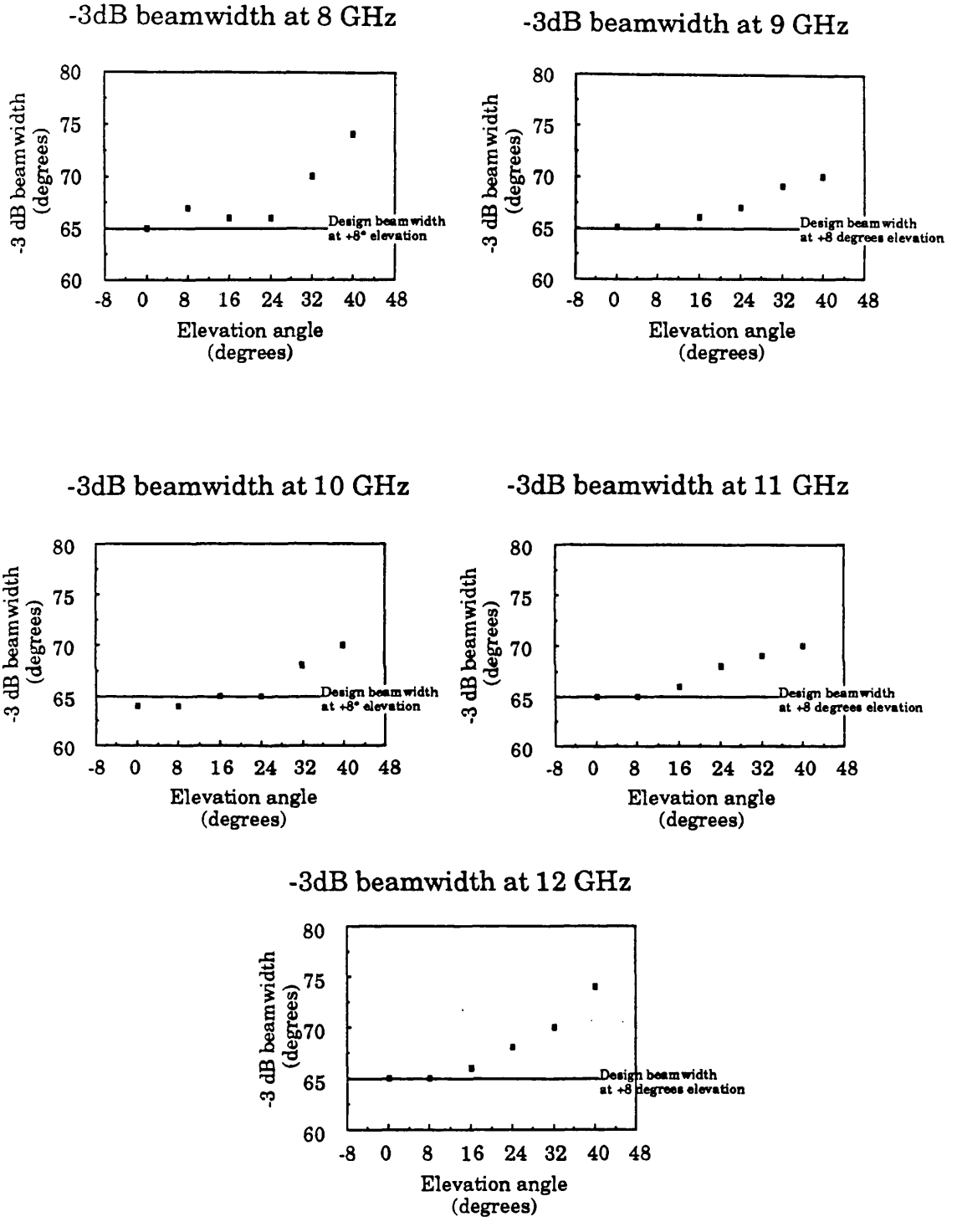

Figure 5.14 Measured changes in the azimuth -3 dB beamwidth of the $\sin(5\phi/2)/5\sin(\phi/2)$ beam as a function of elevation.

Synthesised $\sin(5\phi/2)/5\sin(\phi/2)$
radiation pattern, with a theoretical
-3 dB beamwidth of 65°

First sidelobe levels at 8 GHz

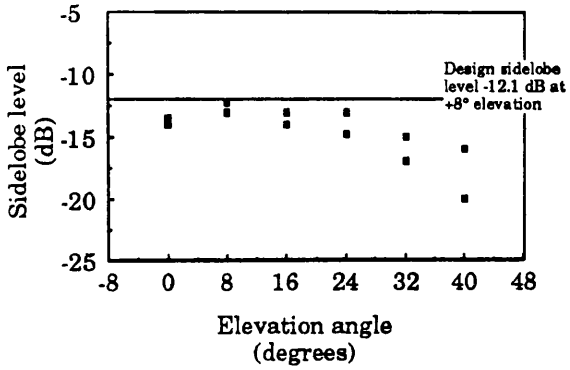

First sidelobe levels at 9 GHz

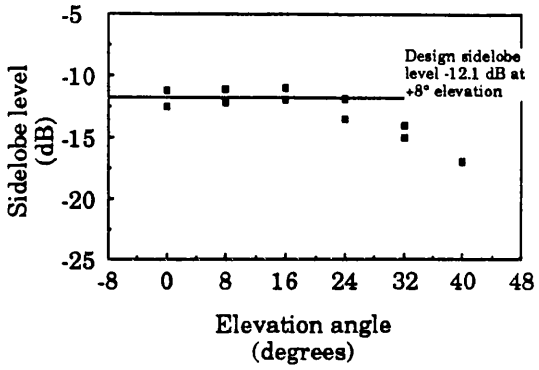

First sidelobe levels at 10 GHz

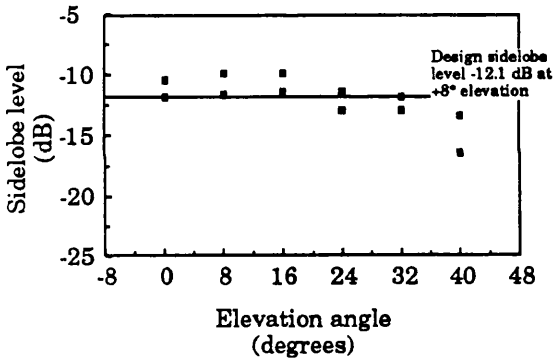

First sidelobe levels at 11 GHz

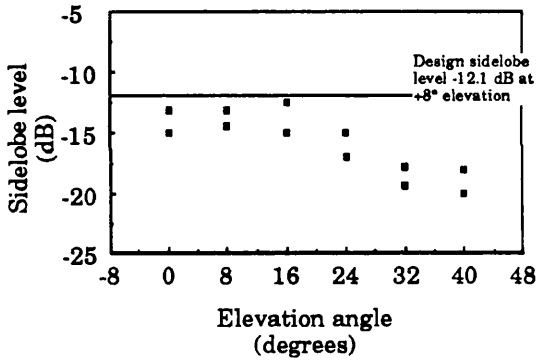

First sidelobe levels at 12 GHz

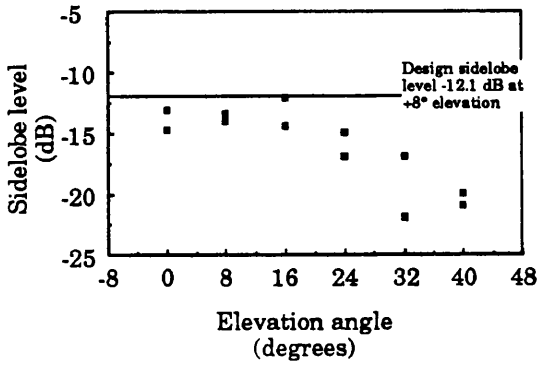

Figure 5.15 Measured changes in the first sidelobe levels of the $\sin(5\phi/2)/5\sin(\phi/2)$ beam as a function of elevation.

5.4.4 **The gain of the synthesised beam**

The peak gain of the beam was measured across the frequency range using the technique of section 5.1.7. The gain was -4 dBi at the centre of the band, compared to a theoretical figure of -3 dBi. As for the Chebyshev beam, the difference is attributable to losses in the beamformer. The theoretical gain of this beam is lower than that of the Chebyshev beam because the excitation attenuates the 0^{th} and 1^{st} order modes. The measured change in gain across the band was similar to that of the Chebyshev beam (figure 5.9).

5.5 Analysis and discussion of measured results

5.5.1 The effect of beamformer errors

The changes in the synthesised pattern caused by beamformer errors can be predicted using equation (4.2.6) from chapter 4:

$$A'_m(f) = \sum_{n=1}^{N} s'_{np}(f)\, e^{j2\pi(n-1)m/N} \qquad (5.5.1)$$

As an example, consider the measured characteristics of the Chebyshev beam at 10 GHz. The specified excitation of the elements is given in table 5.8 below. For comparison the measured excitation (with losses taken out) is also tabulated.

Element number	1	2	3	4
Theoretical element excitation	-10.9 dB, +121°	-6.0 dB, 0°	-7.76 dB,-89°	-6.0 dB, 0°
Measured element excitation	-10.5 dB, +117°	-6.6 dB, 0°	-7.3 dB,-88°	-6.6 dB, 0°
Excitation error	+0.4 dB, -4°	-0.5 dB, 0°	+0.46 dB, +1°	-0.5 dB, 0°

Table 5.8 A comparison between the measured and theoretical transmission parameters for the corporate feed (Chebyshev beam).

Using (4.2.6) the actual element excitation can be expressed as a mode excitation, as shown in table 5.9 overleaf. For clarity the linear phase progression used has been removed, and the taper is referred to the zero order mode.

Mode order	0	C1	C2	S1
Ideal mode excitation ($A_m K_m$)	0 dB, 0°	-2.29 dB, 0°	-9.94 dB, 0°	-∞ dB
Actual excitation ($A'_m K_m$)	0 dB, 0°	-1.09 dB, 0°	-10.05 dB, +2°	< -40 dB
Excitation error	0 dB, 0°	+1.2 dB, 0°	-0.11 dB, +2°	Negligible

Table 5.9 A comparison between the measured and theoretical mode amplitudes for the Chebyshev beam at 10 GHz.

The theoretical excitation produces a Chebyshev beam with -30 dB sidelobes. Since this pattern is oriented in the direction $\phi = 180°$, it does not contain a component of the S1 mode. If a significant S1 component was present, it would make this beam asymmetrical. The pattern excited by $A'_m K_m$, the actual mode excitation, is calculated using (4.2.3):

$$F(\phi) = \sum_{m=-M}^{M} A'_m(f)\, K_m e^{jm\phi} \qquad (5.5.2)$$

and plotted in figure 5.16. For comparison the measured pattern at 10 GHz is also plotted, showing good agreement. The main error is the amplitude of the 1st order mode. This is 1.2 dB higher, so the taper is reduced, This increases the sidelobe level to -20 dB and widens the -3 dB beamwidth. This is shown in both the calculated and measured plots of figure 5.16.

The theoretical plot predicts that two deep nulls should remain, while only one is lower than -30 dB on the measured plot. This particular error cannot be attributed to the beamformer, and may be due to element position errors or anechoic chamber reflections.

Chebyshev -30 dB sidelobe radiation pattern, with a theoretical -3 dB beamwidth of 82°

Mode weights for -30 dB sidelobe pattern

Mode	Amp.	Phase
0	0	0
1	-2.29	0
2	-9.94	0

Calculated mode weights produced by beamforming network

Mode	Amp.	Phase
0	0	0
1	-1.09	0
2	-10.05	+2

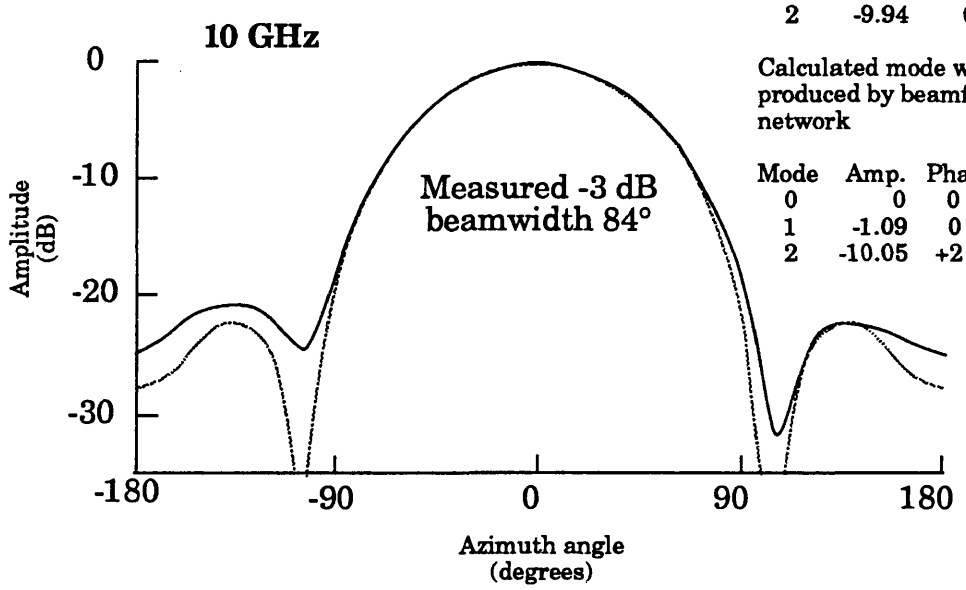

= Measured radiation pattern

= Theoretical prediction of radiation pattern

Mode weights for sin(5ϕ/2)/5sin(ϕ/2) radiation pattern

Mode	Amp	Phase
0	0	0
1	0	0
2	0	0

Synthesised sin(5ϕ/2)/5sin(ϕ/2) radiation pattern, with a theoretical -3 dB beamwidth of 65°

Calculated mode weights produced by beamforming network

Mode	Amp	Phase
0	0	0
1	-0.88	-11.5
2	-1.13	-15

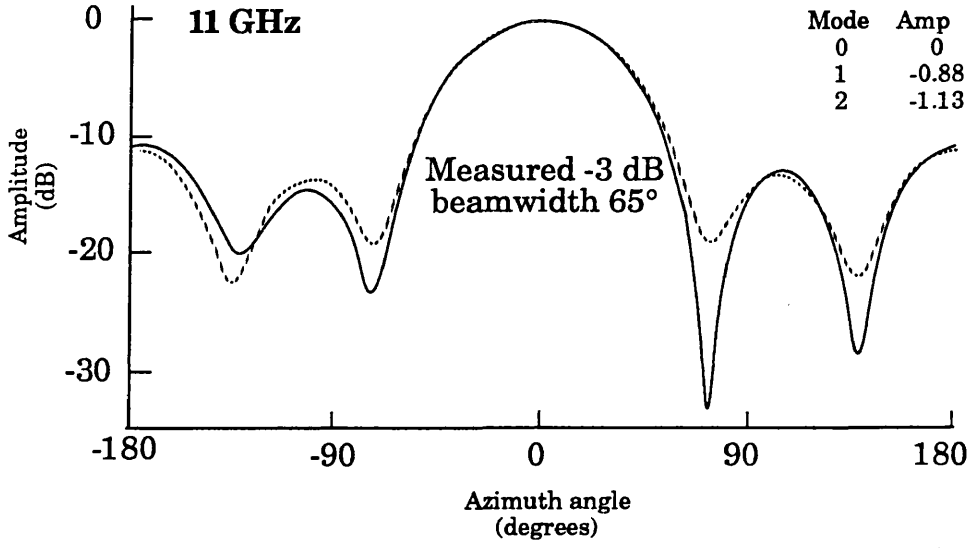

Figure 5.16 Theoretical prediction of the effect on radiation patterns of measured transmission errors in the beamformer .

Let us consider another example, where the error in the mode excitation is in phase, rather than amplitude. The $\sin(5\phi/2)/5\sin(\phi/2)$ pattern at 11 GHz had three nulls as high as -20 dB. Using the same calculations as for the Chebyshev beam, the error in the modal amplitudes and phase was calculated - see table 5.10 below.

Mode order	0	C1	C2	S1
Ideal mode excitation ($A_m K_m$)	0 dB, 0°	0 dB, 0°	0 dB, 0°	-∞ dB
Actual excitation ($A'_m K_m$)	0 dB, 0°	-0.88 dB, -11.5°	-1.13 dB, -15°	< -40 dB
Excitation error	0 dB, 0°	-0.88 dB, -11.5°	-1.13 dB, -15°	Negligible

Table 5.10 A comparison between the measured and theoretical mode amplitudes for the $\sin(5\phi/2)/5\sin(\phi/2)$ beam at 11 GHz.

The theoretical radiation pattern formed by this mode excitation is plotted in figure 5.16. For comparison the measured pattern is also plotted. There is good agreement between the two, both in sidelobe levels and the average level of null filling. Interestingly the -3 dB beamwidth is unchanged from the ideal case: the increase in width of the mainlobe caused by phase errors is cancelled by the increased amplitude taper of table 5.10. Agreement between theoretical and measured results cannot be perfect, as there are other sources of error present, as well as the beamformer. Nevertheless, these results clearly show that the main source of error is the beamformer. The patterns shown in figure 5.16 could have been improved by optimising the beamformer response at those frequencies, but only by degrading the pattern at other frequencies.

To conclude, for a linear array, the main limit on the attainable sidelobe level is mutual coupling, which modifies the excitation of the array. For circular arrays, the main limit is the errors introduced by the complex beamforming networks.

5.5.2 The implications of the measured results for an amplitude comparison DF system

Here the merits of the synthesised wideband beams results are compared with those of competing antennas, with emphasis on the amplitude comparison DF application.

Bandwidth

Compared with cavity-backed spirals the bandwidth of the beams formed with a circular array is lower. As discussed in section 3.2, cavity-backed spirals operate over a bandwidth close to a decade. The results here have a bandwidth of half an octave. The main limit on bandwidth is the components of the beamforming network. Even if these limits were relaxed by adopting wider bandwidth components, the bandwidth is limited to about an octave, as explained in section 3.5. Below 8 GHz, the amplitude of the second order mode is too low to form the Chebyshev beam with reasonable gain. Above about 15 GHz, the harmonic phase modes will increase the sidelobe level, however good the feed network is.

The mainlobe beamwidth

The -3 dB beamwidth of the synthesised Chebyshev beam is constant to within ±3° over the half octave bandwidth. This is better than most wideband elements, for example a cavity-backed spiral, with a change of ±11° (figure 3.2) over the frequency range 8 to 12 GHz or the 'Vivaldi Aerial' of Gibson (1979), with a change of ±4°. The DF error caused by a ±3° change in beamwidth is 4° maximum (see figure 3.4). The small change in the beamwidth of the Chebyshev beam with frequency is matched by very few antennas, although the Vivaldi Aerial comes close.

Squint

Within the limits of the measurement system (±1°) no squint was observed in the synthesised beam, either as a function of frequency, or with elevation.

Sidelobe level

At a single frequency (10 GHz) sidelobe levels of -28 dB were obtained (figure 5.2). This is the theoretical level for the given taper. While a steeper taper can theoretically give sidelobes below -30 dB, the practical difficulties involved in setting the phase and amplitude of the excitation are severe - even at a single frequency. Figure 4.2 shows that an accuracy of 0.2 dB and 1.5° is required for -30 dB sidelobes. Realising the (changing) element excitation over a half octave is more difficult. With the beamformers of figures 4.18 and 4.22 the excitation could only be realised to within ±0.5 dB and ±5°,across the band 8 to 12 GHz. Inspection of figure 4.2 shows that this will limit the sidelobe level to -20 dB minimum. This was indeed the case, as illustrated in figure 5.4, showing the measured sidelobe level of a Chebyshev beam over the frequency range 8 to 12 GHz. This is confirmed by figure 5.16, where theoretical predictions of the increase in sidelobe level is compared to the measured results. By comparison other wideband antennas, for example cavity-backed spirals (figure 3.2) or the Vivaldi Aerial also have sidelobe levels close to -20 dB.

Gain

The absolute gain of the -30 dB sidelobe pattern is very similar to that of a cavity-backed spiral with the same beamwidth. The gain of the wideband Chebyshev beam was similar to that of cavity-backed spirals; 0 dBi. For the $\sin(5\phi/2)/5\sin(\phi/2)$ beam the gain was 4 dB lower, a reversal of the situation found with linear arrays. The circular array radius was chosen to give a steep taper on the higher modes give low sidelobes and reduce ripple. If the main aim of this study had been to produce a -13 dB sidelobe beam by exciting the modes with equal amplitudes, an array radius close to $\lambda/2$ would have been chosen.

Multiple beams

In amplitude comparison DF systems a set of cavity-backed spirals are used to produce overlapping beams. Using a single circular array multiple overlapping beams can be formed using a pair of matrices, as demonstrated by Davies et al. (1984). However multiple low sidelobe beams could not be demonstrated in this study, even at a single frequency. Despite considerable effort applied to reducing the complexity of the matrices (see chapter 4) the cumulative effect of component errors degraded the synthesised patterns unacceptably. Possible solutions to this problem are discussed in section 6.3.

Cross-polar response

Cavity-backed spirals are circular polarised, while the monopole elements were sensitive to vertically polarised signals, as illustrated in figure 2.20. Rejection of the horizontal component reduces the system sensitivity, but can improve the DF accuracy, as the problems associated with a changing 'axial ratio' are eliminated.

Changes in the pattern with elevation

The measured wideband beams did not squint i.e. change their azimuth boresight direction as the elevation angle is increased from 0° to +40° of elevation. The sidelobe level of the wideband beams dropped as the elevation angle increased up to about 30°. As explained in section 2.4, at elevation angles above 0° an increased taper is applied to the modes. The gain of the measured beam drops as the elevation angle increases. Figure 5.8 shows that this reflects the shape of the monopole elevation pattern. This only affects DF sensitivity but not DF accuracy, as all four beams roll off in gain by the same amount for a signal incident at a given elevation angle.

Chapter 6

Summary and conclusions

6.1 Summary

6.1.1 **Introduction**

During the course of this study the synthesis of wideband radiation patterns using circular arrays has been investigated. The theoretical concept has been applied to the design, development and evaluation of a pattern synthesis system using a four-element circular array. The results obtained from this prototype have been used to determine the limits on the operating bandwidth, and also to compare the merits of this approach with those of existing wideband antennas.

6.1.2 **Linear array equivalence**

The radiation patterns formed by the phase modes of a circular array are similar to those formed by the elements of a half-wavelength spaced linear array. The radiation patterns of linear arrays are formed in sine(ϕ) half space, while phase mode radiation patterns are formed directly in ϕ space - around 360° of azimuth. Each phase mode can be thought of as an (omnidirectional) element of a linear array that radiates directly into ϕ space, with the 0^{th} order mode being the centre element. A discrete circular array of N elements can excite all the modes up to the order $\pm N/2$, and so is equivalent to a linear array with N + 1 elements. For the highest order mode the +N/2 and -N/2 modes are excited simultaneously, forming an amplitude mode with a cosinusoidal variation in amplitude with azimuth. The corresponding N/2 order sine amplitude mode cannot be excited by an N element circular array. While phase modes can be used in steered beams, amplitude modes can only be used in fixed beams.

For a linear array, a -13 dB sidelobe radiation pattern is formed by exciting all the elements with equal amplitude and phase. To radiate the phase modes of a circular array with equal amplitude the excitation must be compensated to correct for the phase mode coefficient - a complex term that determines the relative amplitudes of the modes. For a given mode order, the phase mode coefficient is determined by the array radius, mutual coupling and the radiation pattern of the circular array elements. Since the phase mode coefficient is complex, the relative phases of the modes must also be compensated. If the modes are visualised as the elements of a linear array (as shown in figure 2.12) the m^{th} phase mode coefficient corresponds to a passive two-port network with a complex transfer function located in each element feed. The input impedance of this network is the phase mode impedance (that is, the impedance of a circular array element when the array is excited by a phase mode).

One of the aims of this study was to produce low sidelobe beams for an amplitude comparison DF system. Cavity-backed spiral antennas commonly used in existing amplitude comparison DF systems have -20 dB sidelobe levels. Applying a taper to the phase modes reduces the sidelobe level of the synthesised beam. A Chebyshev taper (derived from linear array theory) was selected to form low sidelobe radiation patterns. A target sidelobe level of -30 dB was chosen; 10 dB better than that of cavity-backed spirals. As explained further on, both 'spatial harmonics' and errors in the array excitation (caused by the beamformer) set this limit on the sidelobe level.

A fan of overlapping beams is required for amplitude comparison DF. These are formed using a second Butler matrix connected to the (compensated) phase mode outputs of the first matrix. This was demonstrated over a narrow bandwidth by Davies et al. (1984). The orthogonal spacings (in ϕ space) for beams are the same as those for beams of the same shape formed by a linear array. With an N-element array, N overlapping beams can theoretically be formed. If the highest order amplitude mode is used, the fixed beams must be oriented in the azimuth directions of the N elements.

6.1.3 **Wideband pattern synthesis**

As stated in 6.1.2, the phase mode coefficient is determined by mutual coupling, the effective array radius (r/λ) and the radiation pattern of the circular array elements. These are all parameters that change with frequency. Patterns synthesised using phase modes will be narrowband unless changes in the phase modes with frequency are compensated. This can be done using RF networks with a reciprocal frequency response connected to the phase mode ports. Radiation patterns synthesised from compensated modes are instantaneously wideband, with a constant beamwidth and fixed sidelobe levels. The relative phases of the modes must also be held constant across the band, so the phase response of the RF compensation networks is also specified.

Accurate compensation requires precise information about how the phase modes change with frequency. This led to the development of a technique to determine the phase mode coefficient from measurements of the radiation pattern of a single element (located in the circular array). By repeating these measurements across the band, changes in the coefficients with frequency could be determined. This technique is discussed in greater detail in section 6.2.

During the course of this study the theoretical limits on the frequency band for pattern synthesis were investigated. The lower limit on the operating bandwidth is determined by the impedance of the array elements. When an array is excited by a mode of order m all the array elements have the same impedance, termed the m^{th} phase mode impedance. Due to mutual coupling the element impedance changes greatly as a function of the mode order. For an array of closely spaced elements the radiation resistance of the higher order modes is much lower than that of the 0^{th} order mode. The phase mode impedance also changes as a function of frequency. As the frequency falls, the real part of the radiation resistance drops towards zero, for the higher order modes. This is a classic example of a superdirective excitation.

The lowest operating frequency can be estimated from theoretical figures for the self and mutual impedances of the elements. In this study the phase mode impedances of a four-element monopole array were determined by two experimental methods, first from measurements of the self and mutual impedances of the array elements, and secondly by measuring the reflected signals from an array excited by a single phase mode. There was good agreement between the two sets of results.

For the four-element monopole array used in this study, the measured radiation resistance of the 2^{nd} order mode was about 2 Ω, so the efficiency with which this mode is radiated was an order of magnitude lower, compared with the 0^{th} order mode. This proved to be useful, since this mode required a taper of -10 dB to produce the Chebyshev radiation pattern. Below 8 GHz the 2^{nd} order mode could not be excited with the amplitude required for the Chebyshev beam, so 8 GHz was the lowest frequency at which the beam could be formed with reasonable gain, i.e close to 0 dBi.

In principle, impedance matching can improve the radiation efficiency by eliminating the mismatch between the element impedance and that of the feed network. Since all the elements have the same modal impedance, they can be matched by an impedance-matching network at the phase mode port of the matrix. This was demonstrated at a single frequency using a stub tuner. Because of the long electrical length between the phase mode port and the element feed point, this matching technique is fundamentally narrowband.

The upper frequency limit for beam synthesis is determined by spatial harmonics; when a mode is excited on a discrete array, harmonic modes are also excited. If the modes are visualised as the elements of a linear array, the harmonics correspond to additional elements connected to the same feed port as the fundamental mode - they cannot be excited independently. While additional elements with a 'built in taper' (provided by the phase mode coefficient) might appear desirable for low sidelobe patterns, these harmonics severely degrade both the sidelobe level and the mainlobe shape. The phase shift introduced by the phase mode coefficient

is generally in antiphase with that of the fundamental mode, a shift that cannot be corrected. In addition, the relative amplitudes of the two modes also change with frequency, resulting in a narrowband pattern.

The solution chosen in this study was to keep the inter-element spacing small, so the circular array was unable to excite or support the higher order harmonic modes. An inter-element spacing below $\lambda/4$ at the upper operating frequency was chosen in order to reach the target -30 dB sidelobe level. The inter-element spacing chosen was 5 mm, giving a theoretical upper frequency of 15 GHz, so the theoretical bandwidth is just under an octave. In this study the upper frequency limit was 12 GHz, determined not by ripple, but by the operating bandwidth of the beamformer components. At 12 GHz the 5 mm inter-element spacing was 20% below the $\lambda/4$ limit. The operating bandwidth of circular arrays is discussed further in section 6.2

6.1.4 **Array design**

At least five phase modes are required to synthesise a Chebyshev -30 dB sidelobe radiation pattern with a -3 dB beamwidth less than 90°, as required by amplitude comparison DF. Since a four-element circular array can excite five modes, and can form four overlapping beams, a circular array with four elements was adopted. Circular arrays with eight elements were also considered, because a fan of eight -30 dB sidelobe beams, each with a narrower -3 dB beamwidth, gives better DF accuracy. The sheer complexity of the 8 x 8 Butler matrices required ruled out this option. Even building 4 x 4 microwave Butler matrices with the required performance was difficult.

The next stage was to choose the type of array element. The bandwidth limits discussed above determined the 5 mm inter-element spacing. This corresponds to an array radius of 3.53 mm. Few antenna types can be fitted onto such a small array radius. The use of elements with a unidirectional $(1 + \cos(\psi))$ radiation pattern was desirable, as the phase mode amplitude changes less with frequency for directional elements, compared with

omnidirectional elements. The physical aperture of the directional elements considered was simply too large, so monopoles mounted on a large ground plane were adopted. Isolated monopoles have an omnidirectional radiation pattern in the azimuth plane. For the small array radius used, the changes in the relative amplitudes of the modes over the frequency band 8 to 12 GHz was tolerable. To maximise the gain, monopoles resonant at the centre of the band were used, with a length of 7.5 mm. To reduce the change in the reactance with frequency, thick monopoles were used. The elevation pattern of the $\lambda/4$ monopole in the elevation plane was suitable for the DF role. Beams synthesised with this array were sensitive to vertically polarised signals only.

6.1.5 **Butler matrix beamformer design**

Radiation patterns synthesised from compensated phase modes do not change shape as a function of frequency, but errors in practical beamformers will degrade their shape. Changes in the peak gain of adjacent beams and changes in the -3 dB beamwidth reduce the DF accuracy, while increases in the sidelobe levels and the filling in of nulls reduce the immunity to interfering sources, like jammers.

The main sources of error in the beamformers were:

- Errors in the transmission amplitude and phase of beamformer components.

- Imperfect isolation between coupler input ports.

- Reflections from imperfectly matched ports.

The theoretical effect of these errors on the shape of the -30 dB sidelobe beam was evaluated. The initial beamformer design, depicted in figure 4.1, used two Butler matrices in tandem with compensation networks in between.

A computer program was developed to predict the performance of the beamformer, specified in terms of the scattering parameters for the eight ports of the network. At that time, the compensation networks were not ready. In order to evaluate the matrix performance, the two matrices were connected together, thus forming a Fourier transform/inverse transform. The network analyser measurements were compared to ideal predictions for the transmission parameters. The results were disappointing, predicting that the measured transmission errors would limit the sidelobe levels to -14 dB - which was unacceptable.

Between the element port and the output beam port, a signal passes through four couplers. The computer model showed that for some paths the transmission errors add cumulatively, giving peak transmission errors of up to ±2 dB and ±20°. This was broadly in agreement with the measured results. A literature search showed that similar problems had been documented by Mosko (1984) in beamformers used to provide monopulse patterns simultaneously in the horizontal and vertical planes. The solution was to develop a 'symmetrical' beamformer, where the systematic transmission errors introduced by the first mode-forming network were cancelled by the systematic errors in the second beam-forming matrix. Since amplitude comparison DF does not use scanned beams, they can be formed from amplitude modes, rather than phase modes. A new matrix, termed an 'amplitude mode matrix', was developed to form a set of orthogonal amplitude modes. In addition to error cancellation, this matrix has three other advantages over the Butler matrix:

- The amplitude mode matrix uses only one type of component - the 180° coupler.

- It requires fewer couplers - three for a 4 x 4 matrix, as depicted in figure 4.8.

- If a single amplitude mode is excited, reflections from the mismatch of the elements is reflected back to the same amplitude mode port, so amplitude modes of the same order are isolated, unlike phase modes.

The theoretical analysis developed for phase modes is perfectly valid for amplitude modes: the phase mode coefficients, the phase modes impedance and the orthogonal relations of phase modes all apply to amplitude modes.

A pair of amplitude mode matrices were built, operating over the frequency range 8 to 12.4 GHz. Again the two matrices were connected together, forming an Fourier transform/inverse transform. The results predicted that beams sidelobes formed with this matrix would be limited to -20 dB. While this is a 6 dB improvement compared with the Butler matrix design, it is not good enough for our application. The theoretical analysis did not take into account the cumulative effect of random errors, for example the phase and amplitude errors introduced by the eight SMA connectors in each path between the element port and the beam ports. The cumulative effect of component mismatches was also severe, even though isolators were used at the element ports to eliminate the element mismatch. Even this improved matrix system was not satisfactory for low sidelobe pattern synthesis over a wide bandwidth.

6.1.6 **Measured narrowband radiation patterns**

Narrowband beams were formed using the pair of amplitude mode matrices, located underneath the ground plane of the four-element monopole array. Amplitude compensation was done using attenuators and phase compensation was done using delay lines. The beamformer was optimised to form a beam at the centre operating frequency for the matrix system, 10 GHz. Measurements were made of the synthesised radiation pattern using an anechoic chamber at UCL. Making use of the amplitude taper of the phase mode coefficients, a Chebyshev beam was formed with equal -28 dB sidelobes and a beamwidth of 82°. By reducing the taper a Chebyshev pattern with -20 dB sidelobes and a -3 dB beamwidth of 75° was formed. By radiating the five modes with equal amplitudes, a $\sin(5\phi/2)/5\sin(\phi/2)$ pattern was formed, with a -3 dB beamwidth of 65° and -12.1 dB sidelobes.

These radiation patterns demonstrated that linear array theory can be applied to the phase modes of circular arrays - at least at a single frequency. The ease with which the amplitude taper was changed demonstrates the versatility of pattern synthesis using orthogonal modes. No calculation of the effect of mutual impedances was necessary. Once the phase mode coefficients have been determined, mutual coupling plays no role in modifying radiation patterns synthesised using modes.

To optimise the performance of the matrix beamformer, the compensation was adjusted until the transmission parameters, between the beam port and the element ports, were close to the ideal values. These were calculated using a computer model of the complete beamformer, including the compensation networks. First, the network was corrected for the beam at port 3, but this severely degraded the pattern at ports 1, 2 and 4. Secondly, the network was corrected for the beam at port 1, but this degraded the pattern at ports 2, 3 and 4. Despite considerable efforts at improving matrix performance it was not possible to produce multiple low sidelobe beams with this beamformer - one of the main aims of this study. This is discussed further in section 6.2.

6.1.7 **The design of a corporate feed for wideband pattern synthesis**

As explained above, provided the specified transmission parameters between the beam port and the four element ports are accurately realised, the desired beam will be formed. This is irrespective of the type of beamformer used. A corporate feed is one of the simplest beamformers. For a four-element circular array it can be constructed from three Wilkinson couplers. The element excitation is equal in amplitude and phase. By inserting RF compensation networks into the corporate feed, however, the array excitation specified using phase mode theory can be realised. The excitation was calculated using a computer model of the Butler matrix beamformer. As the theoretical phase mode compensation in the ideal beamformer changes with frequency, so does the array excitation required to form an instantaneously wideband pattern.

A corporate feed cannot produce the fan of overlapping beams required for an amplitude comparison DF system. However, an experimental demonstration was carried out to demonstrate that wideband beams can be formed with a circular array. The array excitations required to form a wideband Chebyshev -30 dB sidelobe pattern and a $\sin(5\phi/2)/5\sin(\phi/2)$ radiation pattern were calculated. To realise the specified excitation, the design of microstrip compensation networks was investigated. Work on this area had already begun, as the weighting networks required for a corporate feed were similar in most respects to those required for phase mode compensation.

The transmission amplitude and phase of the compensation networks are both rigidly specified and both change with frequency. The networks should also be matched to reduce reflections within the feed. A microwave computer-aided design package (called PUFF) was used to model the microstrip components and optimise the design.

Coarse adjustment of the transmission amplitude was done using wideband attenuators. Simple low pass and band pass microstrip filters were used to realise the change in the transmission amplitude with frequency. The specified changes were only 2 to 4 dB across the frequency band. For frequencies where the filter mismatch was high, the VSWR was bad, so isolators were necessary to reduce the effect of the mismatch.

The wideband transmission phase of the compensation networks was also rigidly specified. Microstrip phase shifters designed to provide fixed phase shifts between 30° and 150° were constructed. If the required phase shift was outside this range, a 90° coupler was substituted for one of the cophasal Wilkinson splitters of the corporate feed, providing an additional phase shift. Linear changes in the transmission phase with frequency were realised using a simple delay line. Using these techniques, the specified transmission amplitudes and phases were realised to within ± 0.5 dB and $\pm 5°$.

6.1.8 **Measured wideband beams**

The corporate feed was configured to excite the phase modes with an Chebyshev amplitude taper to give -30 dB sidelobes. Anechoic chamber measurements of the wideband radiation pattern across the frequency band 8 to 12 GHz showed that the -3 dB beamwidth of the synthesised pattern was constant to within ±3° of the theoretical -3 dB beamwidth of 82°. The beam did not squint in azimuth. The measured sidelobe level was below -20 dB across the whole frequency band, so the peak sidelobe level was 10 dB higher than the target figure of -30 dB. Computer modelling showed that the increase in the sidelobe levels was due to beamformer excitation errors, of the order of ±5° and ±0.5 dB. This error also produced the ±3° change in the -3 dB beamwidth.

Measurements of the azimuth beam were made at fixed elevation angles up to +40°. The -3 dB beamwidth increased by about 10% between 0° and 40° of elevation. The sidelobe levels initially dropped, but increased again as the elevation angle approached 40°. The beam did not squint in azimuth with elevation. These results are in good agreement with a theoretical analysis of the changes in the synthesised beam with elevation (section 2.4). Since the monopole elements were vertical, the array was only sensitive to vertically polarised signals, with a -28 dB rejection of horizontally polarised signals. The radiation pattern in the elevation plane was also measured. As expected, the radiation pattern of the synthesised main beam in the elevation plane was very similar to that of the monopole element.

The absolute gain of the synthesised Chebyshev radiation pattern was about 0 dBi, comparable to that of cavity-backed spirals with similar directive gain, and in good agreement with theory. The variation in the gain was about ±2 dB across the band. While this gain variation could have been reduced by altering the compensation of the modes, the prime aim was to keep the relative amplitudes of the modes constant, so the beam did not change in shape with frequency.

The corporate feed was next configured to excite the phase modes with equal amplitudes to give a $\sin(5\phi/2)/5\sin(\phi/2)$ pattern. This pattern is unsuitable for amplitude comparison DF, as it has -12.1 dB sidelobes; the aim was to demonstrate the versatility of the wideband synthesis technique. Anechoic chamber measurements of the wideband radiation pattern across the frequency band 8 to 12 GHz showed that the -3 dB beamwidth of the synthesised pattern was constant to within ±2° of the theoretical -3 dB beamwidth of 65°. The first sidelobes were within ±2 dB of the design level of -12.1 dB. The elevation pattern and cross-polar characteristics of the beam were very similar to those of the Chebyshev beam, with the azimuth beamwidth increased by 11% at 40° of elevation. The first sidelobes dropped with increasing elevation, while the single backlobe increased to about -12 dB. The gain of the $\sin(5\phi/2)/5\sin(\phi/2)$ radiation pattern was lower than the Chebyshev beam, about -4 dBi. This was because the amplitude of the 0^{th} and 1^{st} order modes was attenuated to match that of the 2^{nd} order mode.

These results shows that instantaneously wideband patterns can be formed using a circular array, and excitations derived from linear array theory can be used to shape the wideband patterns.

6.2 Discussion of results

6.2.1 **Characterising the phase modes of circular arrays**

Davies and Chow (1969) plot the amplitude modes formed with a 16-element circular array at 427 MHz. For the array radius chosen the 2^{nd} order mode was not properly excited, and this led to difficulties in exciting efficient directional beams. This problem was only identified after the 16 x 16 matrix had been constructed and the mode amplitudes measured directly. The technique of Jones and Griffiths (1988) developed during this study accurately predicts the mode characteristics without using a matrix. Since most of the circular arrays developed at UCL have used 'off the shelf' array elements such as dipoles or monopoles, the performance of the system can be predicted at a much earlier time. This technique can also be used with directional elements such as loops.

The design of the signal processing networks, whether adaptive or fixed, can begin at an earlier date once the mode coefficients are known. The mode coefficients can vary quite widely from the theoretical values. For example, for the monopole array of this study, the 2^{nd} order mode is at an amplitude of -10 dB relative to the 0^{th} order mode at 10 GHz. The theoretical figure for omnidirectional elements is -20 dB (figure 2.9a). This discrepancy is explained by the measured element pattern in the array, which is more like a $\{1 + \cos(\psi)\}$ pattern than an omnidirectional pattern.

An additional bonus is that this technique predicts the mode coefficients for the harmonics, as well as the fundamentals. Previously only theoretical figures were available. This technique accurately predicted the increase in sidelobe level from -30 dB to -28 dB in the Chebyshev beam of figure 5.2.

In section 3.4 the impedance of the modes was predicted from measurements of the self and mutual impedances of the elements. From this the feed mismatch and hence the efficiency can be accurately predicted. Theoretical figures for the self and mutual impedance of elements provide only an approximate prediction of changes in the mode impedance with frequency.

6.2.2 **Limits on the frequency bandwidth for pattern synthesis**

The aim of this study was to form beams over a bandwidth exceeding a decade, corresponding to the bandwidth of antennas such as cavity-backed spirals. The phase comparison DF system of Cvetkovic et al. (1988) formed nulls over a 1.2 decade bandwidth using phase modes, so a similar bandwidth could be expected for beams formed with phase modes. His circular array operated at a maximum element spacing of 0.5λ at 30 MHz. A radius of 0.5λ could not be used in this study because a harmonic mode that applies a mild ripple to an omnidirectional pattern can produce a +15 dB increase in -30 dB sidelobes (see figure 2.17). The ripple on omnidirectional patterns can be adaptively corrected for the phase comparison DF rôle, but the sidelobe level of beams cannot be adjusted in this way.

The harmonic problem is not alleviated by increasing the number of elements, unless the inter-element spacing is reduced as well. Figure 2.17 shows the effect of the 3^{rd} order harmonic on a Chebyshev beam for a four element array. The sidelobes are increased by 15 dB. The effect of the 5^{th} order spatial harmonic on a Chebyshev beam formed from the modes of an eight-element array is very similar. For both four- and eight-element arrays, reducing the inter-element spacing reduces the ripple, but raises the lower operating frequency, as discussed next.

Cvetkovic's circular array operated at a minimum effective element spacing of 0.02λ, using the 0^{th} and 1^{st} order modes and terminating the 2^{nd} order mode unused. The lower operating frequency of the array in this study was 8 GHz, at an inter-element spacing of 0.13λ. This was the minimum inter-element spacing, since below this the 2^{nd} order mode could not be supported with an adequate amplitude. For low sidelobe beams, the 2^{nd} order mode is vital as it supplies two of the pattern nulls. For an eight-element array, similar problems would be encountered in exciting the 4th order mode with an inter-element spacing below 0.13λ.

Cavity-backed spirals and the Vivaldi Aerial of Gibson (1979) are wideband because the impedance and pattern properties of an antenna can be determined by its shape and dimension, expressed in wavelengths. If scaling the antenna (say, doubling its size) makes no difference to the shape of the radiating portion at a given frequency, then the antenna is wideband. The Vivaldi Aerial and the cavity-backed spiral meet this condition because their form can be specified by an angle variable alone. A circular array does not meet this condition. The effective array radius is a direct function of frequency. One solution to this problem is discussed in section 6.3.

6.2.3 **The difficulties encountered with Butler matrix feeds.**

The work described in section 6.2.1 solved the problem of ripple, but matrix errors played just as great a role in increasing sidelobe levels and deforming the main beam. Indeed, separating the two problems involved considerable work. This is not the first study in which the transmission amplitude and phase of the matrix severely affected the mode characteristics. Davies and Chow (1969) plot the amplitude modes of a 16-element circular array at 427 MHz. The peaks of the sinusoidal azimuth waveform should be at the same amplitude if the excitation is correct. In fact the level varies by ±1 dB for the 3rd order amplitude mode, ±4 dB for the 5th order mode and ±6 dB for the 7th order mode.

Why was so much difficulty encountered in forming beams with a Butler matrix when they have been successfully used in many applications, particularly phase comparison DF at HF frequencies ? Four main reasons can be identified:

(i) Microwave couplers are not as good as lower frequency couplers. The typical isolation between coupler ports is 17 dB for microwave couplers, compared with 35 dB for the Anzac HH-106 180° coupler over the frequency band 2 to 30 MHz. The return loss at a coupler port is 17 dB, compared with 23 dB for the Anzac coupler, so the reflections in the beamformer are 6 dB larger.

(ii) To synthesise a beam two matrices are used in tandem, while only one is used in a phase comparison system. The cumulative transmission amplitude and phase errors are doubled. By simplifying the matrix, a technique for cancelling systematic errors in the coupled sections was developed, but other transmission errors prevented this having a great effect. These errors are due to imperfect connectors and microstrip-to-coaxial transitions. Reflections from mismatches also introduce transmission errors, as described in section 4.2.

(iii) Phase comparison systems eliminate jammers by placing a single null in the azimuth direction of the jammer. The pattern is omnidirectional, except for a single null. In the Schelkunoff unit circle representation of the excitation, one null is located on the unit circle in the direction of the jammer, while the other independent nulls can be placed anywhere in imaginary space, provided they are not too close to the unit circle. To form the Chebyshev beam of figure 5.2, four nulls were placed on the unit circle at specified angular locations. Accurately placing four nulls (even though two are not independent) is more difficult than placing one.

(iv) To overcome ripple phase comparison DF systems form nulls adaptively at the frequency of the incoming jammer. This can also help to overcome matrix transmission phase errors at the frequency in question. The null formed is not instantaneously wideband, but this does not matter, as UHF jammers are generally narrowband. In the Schelkunoff unit circle representation, the null formed wanders with frequency. To form the wideband Chebyshev beam of figure 5.3, four nulls were located on the unit circle and maintained their positions (fairly well) across the frequency band 8 to 12 GHz.

The approach used here to deal with beamformer problems was to consider the RF network (Butler matrices and compensation) below the element feeds as a single beamformer. Using computer modelling, the characteristics of an 'ideal' beamformer could be compared with the measured characteristics. At a single frequency (10 GHz) the compensation was 'fine tuned' until the 'ideal' transmission amplitude and phases were realised to within about ±1° and ±0.1 dB. The beam thus formed had sidelobes of -28 dB, the limit determined by spatial harmonics, not the beamformer. This is the lowest sidelobe level attained using the phase mode analysis of circular arrays. The beamformer problem was now reduced to one of meeting the transmission amplitude and phase specified by the computer program. Working the program in reverse, by inserting measured transmission errors into it, allowed the prediction of the increase

in sidelobe level and the change in beamwidth.

To form the -28 dB sidelobe beam described above the compensation was adjusted to optimise beam 3 at the output of the second Butler matrix. Beams 1,2 and 4 had sidelobes as high as -15 dB. 'Fine tuning' worked for one beam port, but not for four. The formation of multiple low sidelobe beams, one of the main aims of this study, was not achieved. This was not done at a single frequency, let alone across the planned half octave bandwidth. Methods of overcoming this problem are discussed next.

6.3 Further investigations and applications

6.3.1 **Reducing beamformer errors**

In amplitude comparison DF systems a set of cavity-backed spirals are used to produce overlapping beams. Using a single circular array, multiple overlapping beams can be formed using a pair of matrices, as demonstrated by Davies et al (1984) at UHF. As in this study, multiple low sidelobe beams were not demonstrated, even at a single frequency. Despite considerable effort applied to reducing the complexity of the matrices in this study (see chapter 4, section 4.3) the cumulative effect of component errors degraded the synthesised patterns unacceptably.

Some of the problems with microwave matrices do not arise with HF matrices. The microwave 180° coupler is asymmetrical, with a single Schiffmann section in one arm. At HF a symmetrical 180° coupling structure is used, based on a transformer with a centre-tapped secondary. The isolation of HF couplers is much better (-35 dB rather than -17 dB) and connectors have a lower VSWR. The amplitude errors of the coupling structure are no better for HF couplers, but these are precisely the errors that cancel in the amplitude mode matrix pair, as described in section 4.3.2.

If it is possible to build HF amplitude mode matrices which are better than microwave matrices, it might prove feasible to mix down in frequency and

form beams at HF. The operating bandwidth of this technique is limited, as the fractional bandwidth of down-converted signals is larger. For example, to form wideband beams over the frequency range 9.75 to 10.25 GHz requires 500 MHz bandwidth directional couplers, whatever the centre frequency.

At microwave frequencies, integrating the complete beamformer and compensation networks onto a single substrate would reduce the number of connectors, reduce mismatches and make the structure smaller, hence reducing phase errors. Unlike the Butler matrix, the amplitude mode matrix beamformer does not have any cross-overs that are difficult to implement on microstrip or stripline. Microstrip CAD packages, such as Touchstone, can accurately model the compensation network components, as well as the matrix couplers. The computer program used in this study can calculate the ideal transmission parameters for each path between the beam ports and the element ports. For a four-element array this is a total of 16 paths. The design aim must be to realise these overall transmission parameters, rather than trying to optimise any particular component of the beamformer. Even with computer modelling, this problem is a formidable one, due to the complexity of the compensation networks. These networks must compensate for the mode amplitude, the mode phase, and changes in both with frequency.

Below microwave frequencies, signals from circular array elements could be sampled using an A to D converter, and processed using digital techniques to determine the frequency, amplitude and phase of the incoming signals. Beamforming could then be performed digitally, using phase mode theory to apply weights to the (digitised) element signals. Poulton, Corcoran and Hornak (1987) describe a flash A to D converter with a sampling rate of 1 gigasamples per second. This was achieved using four 250 megasamples per second A to D converters, interleaved using four sample and hold circuits controlled by the same clock. Waveforms with frequencies up to 500 MHz can be unambiguously resolved with six bit accuracy. For a DF system wideband amplifiers would be required to give the correct voltage (±0.64 V) at the input to the converter. For this A to D converter 500 MHz is the highest frequency at which pattern synthesis can

be done. For digitisation over the band 8 to 12 GHz, A to D converters with a sampling rate of 24 gigasamples per second are required, along with correspondingly fast signal processing. Even at the present rate of development, this level of performance is many years in the future.

6.3.2 **Arrays with odd numbers of elements**

Linear arrays with an odd number of elements are commonly used to form sum patterns, while arrays with an even number of elements are used to form difference patterns. To date. the phase mode analysis of circular arrays has concentrated on circular arrays with an even number of elements, as a Butler matrix was used to excite the phase modes. Circular arrays with an odd number of elements could be more useful in certain applications. As a simple example, consider a three-element circular array. Inserting N = 3 into equation (2.2.8) shows that this array excites the 0^{th}, +1 and -1 phase modes, with the 2^{nd} and higher order modes as harmonics. All three modes formed by a three-element array are phase modes, not amplitude modes, so all three can be used in steered beams or for phase comparison DF. Cvetkovic et al. (1988) use the 0^{th}, +1 and -1 phase modes for phase comparison DF, generated by a four-element circular array (the 2^{nd} order amplitude mode is terminated unused). Reducing the number of elements from four to three would reduce the cost of the array and eliminate the unused mode. This can be made into a general rule: *a circular array with N-elements (N even) can excite N - 1 phase modes and an amplitude mode of order N/2, while a circular array with N-elements (N odd) excites N phase modes.* Unfortunately the matrices required to excite odd arrays are difficult to realise. For a three-element array the matrix must have the transmission amplitude and phase of table 6.1 overleaf.

Phase mode	Element No. 1	2	3
0	1/√3	1/√3	1/√3
+1	1/√3	1/√3	1/√3
-1	1/√3	1/√3	1/√3

Transmission amplitudes for a 3 x 3 Butler matrix

Phase mode	Element No. 1	2	3
0	0	0	0
+1	0	+120	-120
-1	0	-120	+120

Transmission phases for a 3 x 3 Butler matrix

Table 6.1 The transmission characteristics required to excite phase modes on a three-element array.

Practical realisation of this matrix is difficult, ruling out a three-element array for a phase comparison DF system. However, as this study has shown, phase mode theory can be applied to circular arrays without using a Butler matrix. The phase mode impedances for a three-element array can be calculated from the self and mutual impedances of the array elements, as described in section 3.4, while the phase mode coefficients can be calculated from the element pattern, as described in section 3.5.

6.3.4 **Adopting wideband array elements**

This study used monopoles as elements for the circular array. It would be preferable to use truly wide bandwidth microwave elements, such as the Vivaldi Aerial. The phase centres for monopole elements are fixed, so as the frequency drops, the effective spacing becomes smaller and the higher order modes cannot be excited. For some elements, such as the Vivaldi Aerial, the phase centre moves out along the axis as the frequency drops. If the elements are arranged in a circle, facing outwards, then the effective array radius $r(f)/\lambda$ becomes a constant. For the Chebyshev beam a constant spacing in wavelengths ($r(f)/\lambda = 1/4$) for the phase centres would hold the

relative amplitudes and phases of the modes constant, allowing possibly a decade operating beamwidth. Some prototype Vivaldi Aerials were constructed for this study, but their physical size gave a minimum inter-element spacing of about 2 cm, so $r(f)/\lambda = 2/3$ at 10 GHz. For this spacing the harmonic ripple terms degrade the pattern unacceptably.

For an antenna facing an infinite flat reflector, the phase centre of the image lies behind the plane of the reflector. Figure 6.1 shows a circular array of Vivaldi Aerials used to excite a central reflector. Applying geometrical optics, this structure forms an array where the inter-element spacing of the radiating images can meet the wideband condition $r(f)/\lambda = 1/4$. While possibly worthy of further investigation, several fundamental problems, most relating to the position of the phase centre, can be identified:

- For some angles of elevation and azimuth the primary feed would radiate into free space, as well as the image.

- Even if the wideband elements themselves are well matched to free space (despite the close reflector), the 2nd order phase modes for a four-element array will have a low radiation resistance. Increasing the effective array radius increases the resistance, but the spatial harmonics then degrade the pattern.

- Realising the required change in the phase centre location with frequency for a Vivaldi Aerial may prove difficult.

- The depiction of a virtual image in figure 6.1 is a geometrical optics representation. This only applies to large reflectors where there is a large separation between the feed and the reflector. Alternative analyses of the structure could reveal a completely different location for the phase centre. Balanis (1982e) reviews the techniques used to determine the phase centres for antennas and concludes that the formulations are laborious. Indeed for many practical antennas a single phase centre valid for all θ and ϕ does not exist.

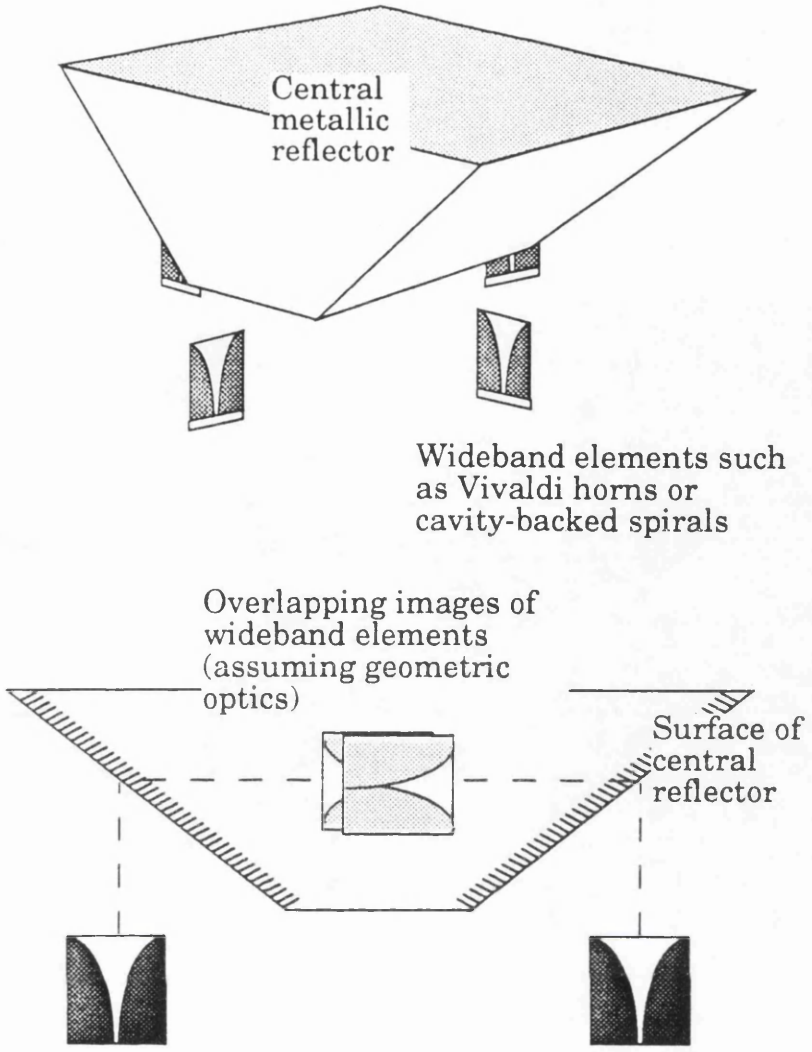

Advantages compared to monopole array

Truly wideband elements with up to a decade bandwidth can be used

The inter-element spacing of the 'images' can be very small, so the spatial ripple on the modes is small

Problems associated with this circular array design

At elevation angles above 0° the physical elements (as opposed to the images) also radiate into space

The nearby metallic reflector will alter the element impedance, affecting the wideband performance

For very close spacing of the "images" the phase mode impedance of the higher order phase modes will be small

Determining the phase centre of the image is difficult: the geometrical optics depiction above only holds for infinite metallic planes

Figure 6.1 Proposed circular array design using wideband elements facing a central reflector.

6.4 Conclusions

Using the phase mode analysis of circular array excitations, a technique has been developed for synthesising instantaneously wideband directional radiation patterns. Linear array theory was applied to the phase modes to form radiation patterns in ϕ space equivalent to those formed in $\sin(\phi)$ half space with a linear array. To form low sidelobe patterns, a Chebyshev taper was applied to the modes.

Methods of characterising the phase mode excitation of circular arrays from measurements of the element radiation pattern and mutual impedances were developed. This information was vital to the synthesis of low sidelobe patterns.

The beamformer design initially proposed for this study used a Butler matrix to excite the phase modes. By utilising microstrip compensation networks, the variation in phase and amplitude of these modes with frequency is corrected. Multiple wideband beams are formed from the compensated modes by a second matrix. Both theoretical and measured results showed that the cumulative effect of phase and amplitude errors introduced by this complicated network were unacceptable, so multiple beams could not be demonstrated. A simplified matrix design was developed to synthesised a low sidelobe (-28 dB) beam at 10 GHz. The beamformer was optimised for operation at that single frequency. Wideband low sidelobe beams could not be formed with a matrix-type beamformer.

A weighted corporate feed was developed to demonstrate instantaneously wideband pattern synthesis of a single beam. The element excitation required to form a low sidelobe pattern was calculated using phase mode theory. The RF networks developed for compensating phase modes proved suitable for realising the frequency-dependent element weights.

Measurements of wideband beams formed with the corporate feed had a constant beamwidth (82±3°) with sidelobes below -20 dB over the (half-octave) frequency band 8 to 12 GHz. Up to +32° of elevation the azimuth beams did not squint and the changes to the sidelobe levels and beamwidth were small. Theoretical predictions limit the bandwidth for this synthesis technique to about one octave.

In addition to a Chebyshev beam, a $\sin(Nx)/N\sin(x)$ wideband beam was formed with the same monopole array. This demonstrates the versatility of this synthesis technique.

References

Bach, H. and Hansen, J.E. (1969) "Uniformly spaced arrays", Chapter 5, Antenna Theory part 1, edited by Collin, R.E. and Zucker, F.J., McGraw-Hill, pp 163-172.

Balanis, C.A. (1982a) "Antenna Theory, Analysis and Design", Harper and Row, pp 304-321.

Balanis, C.A. (1982b) "Antenna Theory, Analysis and Design", Harper and Row, pp 57-59.

Balanis, C.A. (1982c) "Antenna Theory, Analysis and Design", Harper and Row, pp 229-231.

Balanis, C.A. (1982d) "Antenna Theory, Analysis and Design", Harper and Row, pp 254-256.

Balanis, C.A. (1982e) "Antenna Theory, Analysis and Design", Harper and Row, pp 587-589.

Baron, A.R., Davis, K.P. and Hofmann, C.P. (1982) "Passive direction finding and signal location", Microwave Journal, September, pp 59-76.

Bayliss, E.T. (1968) "Design of monopulse antenna difference patterns with low sidelobes", Bell System Tech. J., 47, pp 623-640.

Blass, J. (1960) "The multidirectional antenna: a new approach to stacked beams", IRE Convention Proc., Vol. 8, part 1, pp 48-51.

Borgiotti, G.V. (1983) "Conformal arrays", Chapter 11, Handbook of Antenna Design, Vol. 2,edited by Rudge, A.W., Milne, K., Olver, A.D. and Knight, P., published by Peter Peregrinus, pp 229-240.

Brown, G.H. and King, R. (1934) "High frequency models in antenna investigations", Proc. IRE, Vol. 22, No. 11, April, pp 475-480.

Butler, J. and Lowe, R. (1961) "Beam forming matrix simplifies design of electronically scanned antennas", Electronic Design, Vol. 9, April, pp 170-173.

Chow, P.E.K. and Davies, D.E.N. (1967) "Wide bandwidth Butler matrix network", Electronics Letters, Vol. 3 No. 6, June.

Compton, R. and Rutledge, D. (1987) "PUFF computer aided design for microwave integrated circuits", California Institute of Technology.

Cvetkovic, M., Davies, D.E.N., Griffiths, H.D. and Collins, B. S. (1988) "An HF direction finding and null steering system employing a four element circular array.", Proc. 4th IEE International Conference on HF Radio Systems and Techniques, IEE Conference Publication No. 284, pp 221-225.

Davies, D.E.N. (1965) "A transformation between the phasing technique required for linear and circular arrays", Proc. IEE, Vol. 112, No. 11, November, pp 2041-2045.

Davies, D.E.N., and Chow, P.E.K. (1969) "An experimental array with electronic beam rotation", Proc. European Microwave Conference, pp 129-132.

Davies, D.E.N. and Rizk, M.S.A.S. (1978) "A broadband experimental null-steering antenna system for mobile communications", The Radio and Electronic Engineer, Vol. 48, No. 10, October, pp 509-517.

Davies, D.E.N. (1983) "Circular arrays", Chapter 12, Handbook of Antenna Design, Vol. 2, edited by Rudge, A.W., Milne, K., Olver, A.D. and Knight, P., published by Peter Peregrinus, pp 305-314.

Davies, D.E.N., Griffiths, H.D., Karavassilis, N., and Jones, M.R. (1984) "Wideband UHF circular array study", Final report for Racal-Decca Advanced Development, October, pp 23-24.

Dolph, C.L. (1946) "A current distribution for broadside arrays which optimises the relationship between beamwidth and sidelobe level", Proc IRE, 34, pp 335-348.

Elliott, R.S. (1981a) "Antenna Theory and Design", Prentice-Hall, Chapters 4 and 5.

Elliott, R.S. (1981b) "Antenna Theory and Design", Prentice-Hall, pp 137-139.

Elliott, R.S. (1981c) "Antenna Theory and Design", Prentice-Hall, section 7.8, pp 297-305.

Foti, S.J. and Macnamara, T. (1989) "Design of wideband Butler matrices using Schiffmann sections", report for ERA Technology Ltd, pp 5/1-5/5.

Gibson, P.J. (1979) "The Vivaldi aerial", Proc. 9th European Microwave Conference, Brighton, U.K., pp 101-105.

Guy, J.R.F. and Davies D.E.N. (1983a) "Novel method of multiplexing radiocommunication antennas using circular array configuration", Proc. IEE, Vol. 130, part H, No. 6, pp 410-414.

Guy, J.R.F. and Davies, D.E.N. (1983b) "Studies of the Adcock direction finder in terms of phase-mode excitations around circular arrays", The Radio and Electronic Engineer, Vol. 53, No. 1., January, pp 33-38.

Guy, J.R.F. (1985) "Proposal to use reflected signals through a single Butler matrix to produce multiple beams from a circular array antenna", Electronics Letters, Vol. 21, No. 5, February, pp 209-211.

Hansen, R.C. (1983) "Planar arrays", Chapter 10, "Handbook of Antenna Design", Vol. 2, edited by Rudge, A.W., Milne, K., Olver, A.D. and Knight, P., published by Peter Peregrinus, pp 175-179.

Jones, M.R. and Griffiths, H.D. (1988) "Prediction of circular array phase mode characteristics", Electronic Letters, Vol. 24, No. 13, June, pp 811-812.

Karavassilis, N. (1984) "A study of circular arrays for HF direction finding", Ph.D thesis, University of London, November.

King, R.W.P. (1956) "The theory of linear antennas", part 1, Harvard University Press, Chapters II and III.

King, R.W.P., Mack, R. and Sandler, S. (1968) "Arrays of Cylindrical Dipoles", Cambridge University Press, pp 95-125.

Lipsky, S.E. (1987a) "Microwave Passive Direction Finding", John Wiley and Sons, pp 233-248.

Lipsky, S.E. (1987b) "Microwave Passive Direction Finding", John Wiley and Sons, pp 42-53.

Lipsky, S.E. (1987c) "Microwave Passive Direction Finding", John Wiley and Sons, pp 175-191.

Lipsky, S.E. (1987d) "Microwave Passive Direction Finding", John Wiley and Sons, pp 248-252.

Matthaei, G.L., Young, L. and Jones, E.M.T. (1964) "Microwave Filters, Impedance-Matching Networks and Coupling Structures", Chapter 7, McGraw-Hill.

Milne, K. (1987) "Synthesis of power patterns for linear array antennas", Proc. IEE, Vol. 134, part H, No. 3, June, 1987, pp 285-296.

Moncrief, F.J. (1978) "ESM improves fast patrol boat capabilities", Microwave Systems News, July, pp 64-66.

Mosko, J.A. (1984) "An introduction to wideband, two channel direction-finding systems: part II", Microwave Journal, March, pp 105-121.

Nystrom, L. (1987) "The analysis of a bearing discriminator with high accuracy", IEEE AP-S, Int. Symp. Digest, pp 552-555.

Poulton, K., Corcoran, J.J. and Hornak, T. (1987) "A 1 GHz 6-bit ADC system", IEEE Journal of Solid State Circuits, Vol. SC-22, No. 6, December, pp 962-970.

Rahim, T., Guy, J.R.F.and Davies, D.E.N. (1981) "A wideband UHF circular array", IEE conf. Publ. 195 part 1, pp 447-450.

Rahim, T. and Davies, D.E.N. (1982) "Effect of directional elements on the directional response of circular antenna arrays", IEE Proc., Vol. 129, part H. No. 1, pp 18-22.

Rehnmark, S. (1982) "2-18 GHz digital ESM receivers with 2° RMS bearing accuracy", Anaren publication M1830-28, presented at Military Microwaves, 1982.

Schelkunoff, S.A. (1943) "A mathematical theory of linear arrays", Bell System Tech. J., 22, pp 80-107.

Schiffmann, B.M. (1958) "A new class of broad-band microwave 90-degree phase shifters", IRE Trans, MTT-6, April, pp 232-237.

Sheleg, B. (1968) "A matrix-fed circular array for continuous scanning", Proc. IEEE, Vol. 56, pp 2016-2027, November, 1968.

Storer, J.E. (1952) "The radiation pattern of a monopole over a circular ground screen", J. Applied Physics,1952, Vol. 23, No. 5, pp 588-593.

Tai, C.T. (1961) "Characteristics of linear array antenna elements", Chapter 3, Antenna Engineering Handbook, edited by Jasik, H., McGraw-Hill, pp 3-1 to 3-24.

Taylor, T.T. (1955) "Design of line source antennas antennas for narrow beamwidth and low sidelobes", IRE Trans, AP-3, pp 16-28.

Titze, W. (1988) "The impedance matching of phase modes", Report for Racal-Decca Advanced Development, August.

Torrey, H.C. and Whitmer, C.A. (1948) "Crystal rectifiers", M.I.T. Rad. Lab. Series, Mcgraw-Hill Book Co., New York, Vol. 15.

Watson-Watt, R.A. and Herd, J.F. (1926) "An instantaneous direct-reading radiogoniometer", J. Inst. Elec. Engrs., Vol. 64, pp 611-622.

White, W.D. (1962) "Pattern limitations in multiple beam antennas", IRE Trans Vol. AP-10, pp 179-186.

Wilds, R.B. (1979) "Try $\lambda/8$ stubs for fast fixed phase shifts", Microwaves, December, pp 67-68.

Withers, M.J. (1969) "Frequency-insensitive phase-shift networks and their use in a wide-bandwidth Butler matrix", Electronics Letters, 5, No. 20, October, pp 496-497.

Woodward, P.M. (1947) "A method of calculating the field over a plane aperture required to produce a given polar diagram", Proc. IEE, Vol. 93, part III, pp 1554-58.

Appendix 1

A1 The excitation of a single circular array element expressed as a phase mode excitation

A1.1 **Introduction**

In chapter 3 section 3.5.2 the phase mode coefficients for a four-element array of monopoles are calculated from the measured radiation pattern of a single monopole element. This technique assumes that exciting a single array element is equivalent to exciting all four phase modes with equal amplitude. This appendix offers a proof that applies to four element circular arrays, but it is believed that a general proof could be given for arrays with 2^n equispaced elements. While the practical results of chapter 3 are for omnidirectional elements, this proof also applies to arrays of directional elements that are pointing radially outwards.

In section A1.2 the voltages at the four element ports are calculated, for the case where a single array element is excited by a source of voltage V_s and impedance Z_0, while the other element ports are terminated in loads Z_0.

In section A1.3 the voltages at the four element ports are calculated for the case where the array is modally excited by a Butler matrix feed. The four mode ports are excited by cophasal sources, of equal amplitude $V_s/2$ and impedance Z_0. The characteristic impedance of the matrix feed is also Z_0. The calculated voltages at the four element ports are shown to be the same as those calculated in section A1.2.

A1.2 **The excitation of a single array element**

The basis of this analysis are the z parameters defining the element self-impedance and the mutual coupling between the array elements. The voltages at the four element ports are given by:

$$V_1 = z_{11} I_1 + z_{12} I_2 + z_{13} I_3 + z_{14} I_4$$

$$V_2 = z_{21} I_1 + z_{22} I_2 + z_{23} I_3 + z_{24} I_4$$

$$V_3 = z_{31} I_1 + z_{32} I_2 + z_{33} I_3 + z_{34} I_4$$

$$V_4 = z_{41} I_1 + z_{42} I_2 + z_{43} I_3 + z_{44} I_4 \qquad \text{(A1.1)}$$

I_1, I_2 , I_3 and I_4 are the currents at the element drive points. The symmetry of a circular array allows us simplify this:

$$z_{11} = z_{22} = z_{33} = z_{44}$$

$$z_{12} = z_{21} = z_{23} = z_{32} = z_{34} = z_{43} = z_{41} = z_{14}$$

$$z_{13} = z_{31} = z_{24} = z_{42} \qquad \text{(A1.2)}$$

For the case where element 1 is excited by a source of voltage V_S, impedance Z_0, while the other elements are terminated in impedances Z_0 the excitation of (A1.1) becomes:

$$V_1 = \frac{z_{11}}{Z_0}(V_S - V_1) - \frac{z_{12}}{Z_0}V_2 - \frac{z_{13}}{Z_0}V_3 - \frac{z_{12}}{Z_0}V_4$$

$$V_2 = \frac{z_{12}}{Z_0}(V_S - V_1) - \frac{z_{11}}{Z_0}V_2 - \frac{z_{12}}{Z_0}V_3 - \frac{z_{13}}{Z_0}V_4$$

$$V_3 = \frac{z_{13}}{Z_0}(V_S - V_1) - \frac{z_{12}}{Z_0}V_2 - \frac{z_{11}}{Z_0}V_3 - \frac{z_{12}}{Z_0}V_4$$

$$V_4 = \frac{z_{12}}{Z_0}(V_S - V_1) - \frac{z_{13}}{Z_0}V_2 - \frac{z_{12}}{Z_0}V_3 - \frac{z_{11}}{Z_0}V_4 \qquad \text{(A1.3)}$$

By symmetry $V_2 = V_4$ so the fourth row can be eliminated. Rearranging these equations into a form suitable for matrix solution gives us the equation:

$$\begin{bmatrix} z_{11}+Z_0 & 2z_{12} & z_{13} \\ z_{12} & z_{11}+z_{13}+Z_0 & z_{12} \\ z_{13} & 2z_{12} & z_{11}+Z_0 \end{bmatrix} \begin{bmatrix} V_1 \\ V_2 \\ V_3 \end{bmatrix} = \begin{bmatrix} z_{11}V_S \\ z_{12}V_S \\ z_{13}V_S \end{bmatrix} \qquad \text{(A1.4)}$$

Using the substitutions:

$$A_1 = z_{11} + Z_0, \quad A_2 = z_{12}, \quad A_3 = z_{13}.$$

$$K_1 = z_{11}V_S, \quad K_2 = z_{12}V_S, \quad K_3 = z_{13}V_S. \qquad \text{(A1.5)}$$

we obtain the simplified form:

$$\begin{bmatrix} A_1 & 2A_2 & A_3 \\ A_2 & A_1+A_3 & A_2 \\ A_3 & 2A_2 & A_1 \end{bmatrix} \begin{bmatrix} V_1 \\ V_2 \\ V_3 \end{bmatrix} = \begin{bmatrix} K_1 \\ K_2 \\ K_3 \end{bmatrix} \tag{A1.6}$$

We can now solve for V using the matrix equation:

$$\frac{\left[A^T \right]\left[K \right]}{\mathrm{DET}\left[A \right]} = \left[V \right] \tag{A1.7}$$

The adjoint matrix $[A^T]$ is:

$$\begin{bmatrix} A_1(A_1+A_3)-2A_2^2 & 2(A_2A_3-A_1A_2) & 2A_2^2-A_3(A_1+A_3) \\ A_3A_2-A_1A_2 & A_1^2-A_3^2 & A_3A_2-A_1A_2 \\ 2A_2^2-A_3(A_1+A_3) & 2(A_2A_3-A_1A_2) & A_1(A_1+A_3)-2A_2^2 \end{bmatrix} \tag{A1.8}$$

The determinant for the matrix of (A1.6) is:

$$\mathrm{DET}[A] = A_1\left\{A_1(A_1+A_3)-2A_2^2\right\} - 2A_2(A_2A_3-A_1A_2)$$

$$+A_3\left\{2A_2^2-A_3(A_1+A_3)\right\}$$

$$=(A_1-A_3)\left\{(A_1+A_3)^2-4A_2^2\right\} \tag{A1.9}$$

Solving (A1.7) for V_1:

$$V_1 = \frac{K_1\left\{A_1(A_1+A_3)^2 - 2A_2^2\right\}}{(A_1-A_3)\left\{(A_1+A_3)^2 - 4A_2^2\right\}}$$

$$+ \frac{K_2\left\{2(A_2A_3 - A_1A_2)\right\}}{(A_1-A_3)\left\{(A_1+A_3)^2 - 4A_2^2\right\}}$$

$$+ \frac{K_3\left\{2A_2^2 - A_3(A_1+A_3)\right\}}{(A_1-A_3)\left\{(A_1+A_3)^2 - 4A_2^2\right\}}$$

Substituting for K_1, K_2 and K_3:

$$V_1 = V_S\frac{(A_1-Z_0)\left\{A_1(A_1+A_3)^2 - 2A_2^2\right\}}{(A_1-A_3)\left\{(A_1+A_3)^2 - 4A_2^2\right\}}$$

$$+ V_S\frac{A_2\left\{2(A_2A_3 - A_1A_2)\right\}}{(A_1-A_3)\left\{(A_1+A_3)^2 - 4A_2^2\right\}}$$

$$+ V_S\frac{A_3\left\{2A_2^2 - A_3(A_1+A_3)\right\}}{(A_1-A_3)\left\{(A_1+A_3)^2 - 4A_2^2\right\}}$$

This reduces to:

$$V_1 = V_S\left[1 - \frac{Z_0\left\{A_1^2 + A_1A_3 - 2A_2^2\right\}}{(A_1 - A_3)\left\{(A_1 + A_3)^2 - 4A_2^2\right\}}\right] \tag{A1.10}$$

Next solve (A1.7) for V_2:

$$V_2 = \frac{K_1(A_3A_2 - A_1A_2) + K_2\left(A_1^2 - A_3^2\right) + K_3(A_3A_2 - A_1A_2)}{(A_1 - A_3)\left\{(A_1 + A_3)^2 - 4A_2^2\right\}}$$

Substituting for K_1, K_2 and K_3:

$$V_2 = V_S\frac{(A_1 - Z_0)(A_3A_2 - A_1A_2) + A_2\left(A_1^2 - A_3^2\right) + A_3(A_3A_2 - A_1A_2)}{(A_1 - A_3)\left\{(A_1 + A_3)^2 - 4A_2^2\right\}}$$

$$V_2 = V_S\frac{Z_0A_2(A_1 - A_3)}{(A_1 - A_3)\left\{(A_1 + A_3)^2 - 4A_2^2\right\}} \tag{A1.11}$$

By symmetry V_4 is equal to V_2. Next solve for V_3:

$$V_3 = \frac{K_1\left(2A_2^2 - A_3A_1 - A_3^2\right) + K_2(A_2A_3 - A_1A_2) + K_3\left\{A_1^2 + A_1A_3 - 2A_2^2\right\}}{(A_1 - A_3)\left\{(A_1 + A_3)^2 - 4A_2^2\right\}}$$

$$V_3 = V_S\frac{Z_0\left(A_3^2 + A_3A_1 - 2A_2^2\right)}{(A_1 - A_3)\left\{(A_1 + A_3)^2 - 4A_2^2\right\}} \tag{A1.12}$$

A1.3 The excitation of an array element by phase modes

Now the element feed voltages for a modally excited array are calculated. The voltage seen at the n^{th} element feed of the four-element circular array is the linear superposition of the voltages at the phase mode ports:

$$V_n = \frac{V_n^{(0)} + \left(j^{(n-1)}\right)V_n^{(+1)} + \left(j^{-(n-1)}\right)V_n^{(-1)} + \left(j^{2(n-1)}\right)V_n^{(2)}}{2} \qquad \text{(A1.13)}$$

For a single mode excited with a source $V_s^{(m)}$ of impedance Z_0 the voltage seen at the element port is given by:

$$V_n^{(m)} = V_S^{(m)} \frac{Z^{(m)}}{Z^{(m)} + Z_0}$$

Where $Z^{(m)}$ is the 'phase mode impedance' of a circular array element, King, Mack and Sandler (1968) show, for a four-element array of dipoles, that the mode impedances are related to the open circuit z parameters by the equations:

$$Z^{(0)} = z_{11} + 2z_{12} + z_{13}$$

$$Z^{(+1)} = Z^{(-1)} = z_{11} - z_{13}$$

$$Z^{(2)} = Z^{(2)} = z_{11} - 2z_{12} + z_{13} \qquad \text{(A1.14)}$$

These equations apply to the monopole circular array elements. Equation (A1.13) can be written in the form:

$$V_n^{(m)} = \frac{V_S^{(0)}}{2}\frac{Z^{(0)}}{Z^{(0)}+Z_0} + \left(j^{(n-1)}\right)\frac{V_S^{(+1)}}{2}\frac{Z^{(+1)}}{Z^{(+1)}+Z_0}$$

$$+\left(j^{-(n-1)}\right)\frac{V_S^{(-1)}}{2}\frac{Z^{(-1)}}{Z^{(-1)}+Z_0} + \left(j^{2(n-1)}\right)\frac{V_S^{(2)}}{2}\frac{Z^{(2)}}{Z^{(2)}+Z_0} \qquad \text{(A1.15)}$$

We are interested in the case where the modes are excited by identical cophasal sources of voltage $V_s/2$. The voltage seen at the feed port of element 1 is then given by:

$$V_1 = \frac{V_S}{4}\left\{\frac{Z^{(0)}}{Z^{(0)}+Z_0} + \frac{Z^{(+1)}}{Z^{(+1)}+Z_0} + \frac{Z^{(-1)}}{Z^{(-1)}+Z_0} + \frac{Z^{(2)}}{Z^{(2)}+Z_0}\right\}$$

so

$$V_1 = \frac{V_S}{4}\left\{\frac{Z^{(0)}\left(Z^{(+1)}+Z_0\right)\left(Z^{(2)}+Z_0\right) + 2Z^{(+1)}\left(Z^{(0)}+Z_0\right)\left(Z^{(2)}+Z_0\right)}{\left(Z^{(0)}+Z_0\right)\left(Z^{(+1)}+Z_0\right)\left(Z^{(2)}+Z_0\right)}\right\}$$

$$+\frac{V_S}{4}\left\{\frac{Z^{(2)}\left(Z^{(0)}+Z_0\right)\left(Z^{(+1)}+Z_0\right)}{\left(Z^{(0)}+Z_0\right)\left(Z^{(+1)}+Z_0\right)\left(Z^{(2)}+Z_0\right)}\right\} \qquad \text{(A1.16)}$$

Using the same notation as for the single element excitation:

$$A_1 = z_{11} + Z_0, \quad A_2 = z_{12}, \quad A_3 = z_{13}$$

the denominator for V_1 simplifies to:

$$\left(Z^{(0)} + Z_0\right)\left(Z^{(+1)} + Z_0\right)\left(Z^{(2)} + Z_0\right)$$

$$= \left(A_1 + 2A_2 + A_3\right)\left(A_1 - A_3\right)\left(A_1 - 2A_2 + A_3\right)$$

$$= \left(A_1 - A_3\right)\left\{\left(A_1 + A_3\right)^2 - 4A_2^2\right\}$$

The denominator is the same as the determinant of (A1.9). Substituting for the numerator we obtain:

$$V_S = \frac{V_S}{4}\,\frac{\left(A_1 - Z_0 + 2A_2 + A_3\right)\left(A_1 - A_3\right)\left(A_1 - 2A_2 + A_3\right)}{\left(A_1 - A_3\right)\left\{\left(A_1 + A_3\right)^2 - 4A_2^2\right\}}$$

$$+ \frac{V_S}{4}\,\frac{2\left(A_1 - Z_0 - A_3\right)\left(A_1 + 2A_2 + A_3\right)\left(A_1 - 2A_2 + A_3\right)}{\left(A_1 - A_3\right)\left\{\left(A_1 + A_3\right)^2 - 4A_2^2\right\}}$$

$$+ \frac{V_S}{4}\,\frac{\left(A_1 - Z_0 - 2A_2 - A_3\right)\left(A_1 - A_3\right)\left(A_1 - 2A_2 + A_3\right)}{\left(A_1 - A_3\right)\left\{\left(A_1 + A_3\right)^2 - 4A_2^2\right\}}$$

$$= \frac{V_S}{4}\,\frac{4\left(A_1 - A_3\right)\left\{\left(A_1 + A_3\right)^2 - 4A_2^2\right\} - 4Z_0\left(A_1 - Z_0 - A_3\right)\left(A_1^2 + A_1A_3 - 2A_2^2\right)}{\left(A_1 - A_3\right)\left\{\left(A_1 + A_3\right)^2 - 4A_2^2\right\}}$$

So:

$$V_1 = V_S\left[1 - \frac{Z_0\left\{A_1^2 + A_1A_3 - 2A_2^2\right\}}{(A_1 - A_3)\left\{(A_1 + A_3)^2 - 4A_2^2\right\}}\right] \tag{A1.17}$$

This voltage at element port 1 is identical to that of (A1.10), where a single array element is excited.

For the excitation of (A1.15), where the phase modes are excited with equal amplitude and phase, the voltage seen at the feed port of element 2 is given by:

$$V_2 = \frac{V_S}{4}\left\{\frac{Z^{(0)}}{Z^{(0)} + Z_0} + j\frac{Z^{(+1)}}{Z^{(+1)} + Z_0} - j\frac{Z^{(-1)}}{Z^{(-1)} + Z_0} - \frac{Z^{(2)}}{Z^{(2)} + Z_0}\right\}$$

$$V_2 = \frac{V_S}{4}\left\{\frac{Z^{(0)}\left(Z^{(+1)} + Z_0\right)\left(Z^{(2)} + Z_0\right) - Z^{(2)}\left(Z^{(0)} + Z_0\right)\left(Z^{(+1)} + Z_0\right)}{\left(Z^{(0)} + Z_0\right)\left(Z^{(+1)} + Z_0\right)\left(Z^{(2)} + Z_0\right)}\right\}$$

Using the same substitution as for the single element excitation:

$$V_2 = \frac{V_S}{4}\frac{(A_1 - Z_0 + 2A_2 + A_3)(A_1 - A_3)(A_1 - 2A_2 + A_3)}{(A_1 - A_3)\left\{(A_1 + A_3)^2 - 4A_2^2\right\}}$$

$$-\frac{V_S}{4}\frac{(A_1 - Z_0 - 2A_2 + A_3)(A_1 - A_3)(A_1 - 2A_2 + A_3)}{(A_1 - A_3)\left\{(A_1 + A_3)^2 - 4A_2^2\right\}}$$

$$V_2 = V_S\frac{Z_0A_2(A_1 - A_3)}{(A_1 - A_3)\left\{(A_1 + A_3)^2 - 4A_2^2\right\}} \tag{A1.18}$$

This voltage at element port 2 is identical to that of (A1.11) for port 2, where a single array element is excited. By symmetry the voltage at element port 4 is identical to that at element port 2. Finally solve for V_3:

$$V_3 = \frac{V_S}{4}\left\{ \frac{Z^{(0)}}{Z^{(0)}+Z_0} - \frac{Z^{(+1)}}{Z^{(+1)}+Z_0} - \frac{Z^{(-1)}}{Z^{(-1)}+Z_0} + \frac{Z^{(2)}}{Z^{(2)}+Z_0} \right\}$$

$$V_3 = \frac{V_S}{4}\left\{ \frac{Z^{(0)}\left(Z^{(+1)}+Z_0\right)\left(Z^{(2)}+Z_0\right) - 2Z^{(+1)}\left(Z^{(0)}+Z_0\right)\left(Z^{(2)}+Z_0\right)}{\left(Z^{(0)}+Z_0\right)\left(Z^{(+1)}+Z_0\right)\left(Z^{(2)}+Z_0\right)} \right\}$$

$$+\frac{V_S}{4}\left\{ \frac{Z^{(2)}\left(Z^{(0)}+Z_0\right)\left(Z^{(+1)}+Z_0\right)}{\left(Z^{(0)}+Z_0\right)\left(Z^{(+1)}+Z_0\right)\left(Z^{(2)}+Z_0\right)} \right\}$$

Using the same notation as for the single element excitation:

$$V_3 = \frac{V_S}{4}\,\frac{\left(A_1 - Z_0 + 2A_2 + A_3\right)\left(A_1 - A_3\right)\left(A_1 - 2A_2 + A_3\right)}{\left(A_1 - A_3\right)\left\{\left(A_1 + A_3\right)^2 - 4A_2^2\right\}}$$

$$-\frac{V_S}{4}\,\frac{2\left(A_1 - Z_0 - A_3\right)\left(A_1 + 2A_2 + A_3\right)\left(A_1 - 2A_2 + A_3\right)}{\left(A_1 - A_3\right)\left\{\left(A_1 + A_3\right)^2 - 4A_2^2\right\}}$$

$$+\frac{V_S}{4}\,\frac{\left(A_1 - Z_0 - 2A_2 - A_3\right)\left(A_1 - A_3\right)\left(A_1 - 2A_2 + A_3\right)}{\left(A_1 - A_3\right)\left\{\left(A_1 + A_3\right)^2 - 4A_2^2\right\}}$$

$$V_3 = V_S\,\frac{Z_0\left(A_3^2 + A_3A_1 - 2A_2^2\right)}{\left(A_1 - A_3\right)\left\{\left(A_1 + A_3\right)^2 - 4A_2^2\right\}} \qquad \text{(A1.19)}$$

For all four elements the voltages calculated for the modal excitation are identical to those calculated for the excitation of a single array element.

To conclude, exciting all four phase modes of a four-element circular array with cophasal sources $V_s/2$, impedance Z_0 is identical to exciting array element 1 with a source V_s, impedance Z_0, while the other elements are terminated in loads Z_0. In both cases the voltages seen at the element feed ports are:

$$V_1 = V_S\left[1 - \frac{Z_0\left(z_{11}+Z_0\right)^2 + z_{13}\left(z_{11}+Z_0\right) - 2z_{12}^2}{\left(z_{11}+Z_0-z_{13}\right)\left\{\left(z_{11}+Z_0+z_{13}\right)^2 - 4z_{12}^2\right\}}\right] \qquad \text{(A1.20)}$$

$$V_2 = V_4 = V_S\left[\frac{Z_0 z_{12}\left(z_{11}+Z_0-z_{13}\right)}{\left(z_{11}+Z_0-z_{13}\right)\left\{\left(z_{11}+Z_0+z_{13}\right)^2 - 4z_{12}^2\right\}}\right] \qquad \text{(A1.21)}$$

$$V_3 = V_S\left[\frac{Z_0\left\{z_{13}^2 + z_{13}\left(z_{11}+Z_0\right) - 2z_{12}^2\right\}}{\left(z_{11}+Z_0-z_{13}\right)\left\{\left(z_{11}+Z_0+z_{13}\right)^2 - 4z_{12}^2\right\}}\right] \qquad \text{(A1.22)}$$